

From subduction to collision:
a combined metamorphic, structural and geochronological
study of polymetamorphic metasediments at the NE edge of
the Lepontine dome (Swiss Central Alps)

Inauguraldissertation

zur
Erlangung der Würde eines Doktors der Philosophie
vorgelegt der
Philosophisch-Naturwissenschaftlichen Fakultät
der Universität Basel

von
Michael Wiederkehr
aus Dagmersellen (LU)

Basel, 2009

Genehmigt von der Philosophisch-Naturwissenschaftlichen Fakultät
auf Antrag von

Prof. Dr. Stefan M. Schmid (Fakultätsverantwortlicher)
Geologisch-Paläontologisches Institut, Universität Basel

Prof. Dr. Romain Bousquet (Dissertationsleiter)
Institut für Geowissenschaften, Universität Potsdam/D

Prof. Dr. Roland Oberhänsli (Korreferent)
Institut für Geowissenschaften, Universität Potsdam/D

PD Dr. Alfons Berger (externer Experte)
Institut for Geografi og Geologi, Københavns Universitet/DK

Basel, den 24. März 2009

Prof. Dr. Eberhard Parlow
(Dekan der Philosophisch-Naturwissenschaftlichen Fakultät)

Abstract

This study analyses the tectono-metamorphic evolution of metasedimentary units belonging to the Valaisan and adjacent European domains at the north-eastern border of the Lepontine dome (Central Alps). The investigated area is characterized by a remarkable metamorphic gradient ranging from subduction-related HP/LT metamorphism in the NE to collision-related Barrovian overprint in the SW. Detailed structural fieldwork and petrological investigations including Raman spectroscopy of carbonaceous matter were carried out in order to reconstruct the tectono-metamorphic evolution on a larger scale. Furthermore, new $^{40}\text{Ar}/^{39}\text{Ar}$ dating of white mica and biotite reveal the timing of both subduction-related high-pressure metamorphism and collision-related Barrovian overprint. The combination of all these investigations allows for deciphering a complete P-T-d-t path (pressure, temperature, deformation and time) of an area that occupies a key position in the Alpine orogenic belt for understanding the transition from subduction to collision.

This study documents for the first time that relics of Fe-Mg carpholite indicating blueschist facies conditions occur also within metasedimentary units that are part of the north-eastern Lepontine dome where, so far, exclusively Barrovian assemblages were found. They occur in metasediments from both the Valaisan domain (Grava and Tomül nappes) and parts of the adjacent European domain (Peiden slices and Piz Terri-Lunschana unit). These high-pressure units were subsequently overprinted by a thermal event, as is documented by the growth of new minerals typical for Barrovian metamorphism.

The investigated metasediments provide clear evidence for a bimodal P-T path in the north-eastern Lepontine dome characterized by the following polyphase metamorphic evolution: (1) Subduction-related syn-D1 (Safien phase) HP/LT metamorphism under blueschist facies conditions (350-400 °C and 1.2-1.4 GPa) was established at 42-40 Ma, as revealed by $^{40}\text{Ar}/^{39}\text{Ar}$ dating of white mica associated with Fe-Mg carpholite; the early high-pressure event was followed by “cold” isothermal (or cooling) decompression during D2 nappe-stacking (Ferrera phase) for which an age of 36-33 Ma is inferred based on $^{40}\text{Ar}/^{39}\text{Ar}$ dating of white mica replacing Fe-Mg carpholite. (2) Early collision-related greenschist facies overprint (350-425 °C) post-dating substantial decompression and associated D2 deformation was established at 32-29 Ma and affected both HP and LP metasediments. This metamorphic event clearly predates D3 deformation (Domleschg phase, ~25 Ma) as is evidenced by folded isotherm contours. (3) Collision-related Barrovian overprint (500-590 °C and 0.5-0.8 GPa) represents a second and considerably younger (post 20 Ma) “isobaric” heating pulse only preserved in the SW part of the investigated area. Hence amphibolite facies metamorphism representing the mature stage of a colliding orogen is clearly separated by D2 and D3 deformations, as well as by an intervening greenschist facies event, from the D1 high-pressure stage. Amphibolite facies overprint occurred before and/or during the initial stages of D4 (Chièra phase), representing a second nappe-refolding event.

This investigation revealed a significant time gap in the order of some 20 Ma between subduction-related HP/LT metamorphism and collision-related MP/MT Barrovian overprint. This supports the notion of a polymetamorphic evolution associated with a bimodal P-T path. The results of this study argue that heat release from radioactive decay of vast amounts of accreted continental-derived basement nappes may play an important role in contributing much to heat production needed for amphibolite facies Barrow-type overprint. Based on field evidence, we conclude that heat transfer in the north-eastern Lepontine was essentially conductive during the latest stages of the thermal evolution.

Organization of the thesis

This thesis is organized as a “cumulative thesis” and consists of a series of seven chapters. Five of them (chapters 2-6) can be regarded as individual manuscripts to be published in international peer reviewed scientific journals. Chapters 2 and 6 have already been published while the remaining chapters have been, or in case of chapter 5, will be submitted soon. An outline of each of these chapters and the contributions of the individual co-authors is provided below.

Chapter 1:

Introduction

This chapter presents the scope and aims addressed by this thesis, and briefly provides the general geological background as well as an outline of the methodological approach.

Chapter 2:

From subduction to collision: Thermal overprint of HP/LT meta-sediments in the north-eastern Lepontine Dome (Swiss Alps) and consequences regarding the tectono-metamorphic evolution of the Alpine orogenic wedge

Wiederkehr, M., Bousquet, R., Schmid, S.M. & Berger, A.
published 2008: *Swiss Journal of Geosciences*

This chapter is devoted to the structural and metamorphic evolution of metasediments at the north-eastern edge of the Lepontine dome. In this area subduction-related HP/LT metamorphism and collision-related Barrovian overprint are spatially closely arranged next to each other. Based on extensive fieldwork a new model for the tectono-metamorphic evolution for the Valaisan domain and the adjacent European margin has been established. The area is characterized by a bimodal P-T path, whereby Barrovian overprint represents a separate heating pulse that follows isothermal decompression of an earlier HP/LT event. Furthermore, a qualitative discussion of the still open and debated question concerning the heat sources responsible for Barrovian metamorphism is given, based on the new field data.

The first author carried out all the fieldwork and was responsible for all the analytical investigations by electron microprobe and Raman spectroscopy. Furthermore he wrote a first version of the manuscript including figures and tables. The second, third and fourth authors (the thesis supervisors) helped with the discussions and interpretation of the data and the preparation of the final version of the manuscript.

Chapter 3:

3-D assessment of peak-metamorphic conditions by Raman spectroscopy of carbonaceous material: an example from the margin of the Lepontine dome (Swiss Central Alps)

Wiederkehr, M., Bousquet, R., Ziemann, M.A., Berger, A. & Schmid, S.M.
submitted to: *Contributions to Mineralogy and Petrology*

This chapter comprises a study that examines the evolution of carbonaceous matter recorded by Raman spectroscopy. Combined with metamorphic data, this method is a powerful tool for determining

accurate peak-metamorphic temperatures in low-grade metasedimentary units that generally are devoid of indicative mineral assemblages and in which the metamorphic zoning is only poorly constrained. Combined with detailed structural and metamorphic information the resulting temperature distribution pattern can be related to distinct thermal events established during the geodynamic evolution of the Alpine orogenic belt, namely during the transition from subduction to collision.

The first author wrote a first version of the manuscript including all figures and tables. He carried out the entire sample collection during fieldwork and carried out most of the investigations using Raman spectroscopy at the Raman Laboratory of Potsdam University. The second author provided logistical and advisory scientific help and assisted in finalizing the manuscript. The third author introduced M. Wiederkehr to the Raman Laboratory at Potsdam University and also performed some additional investigations by Raman spectroscopy. He also provided significant help in writing the related methodological part of the chapter and assisted in the general writing process. Furthermore, he provided substantial support and discussion during the data acquisition. The fourth and fifth authors helped with the discussions and interpretation of the data and carefully reviewed a first draft of the manuscript. The fifth author provided substantial help during the writing process and significantly improved the quality of the resulting manuscript.

Chapter 4:

$^{40}\text{Ar}/^{39}\text{Ar}$ dating of the subduction-collision transition in the Central Alps

Wiederkehr, M., Sudo, M., Bousquet, R., Berger, A. & Schmid, S.M.

submitted to: *Tectonics*

This chapter presents new $^{40}\text{Ar}/^{39}\text{Ar}$ ages for both metamorphic stages, i.e. a first subduction-related HP/LT event and the subsequent amphibolite facies Barrovian overprint. Based on microstructural observations several generations of white mica were identified inside Fe-Mg carpholite-bearing quartz-calcite veins. These were analyzed by *in situ* UV laser experiments. The recorded ages are interpreted to date the HP/LT event and subsequent stages along the retrograde evolution. Investigations focussing on biotite, whose occurrences are restricted to areas affected by pervasive amphibolite facies metamorphism, provided information on the timing of late-stage Barrovian overprint. These new isotopic ages complete the new tectono-metamorphic evolution presented in chapter 2 and provide important data concerning the temporal relationships between subduction and collision.

The first author collected most of the samples, performed mineral separation and all $^{40}\text{Ar}/^{39}\text{Ar}$ measurements at the argon laboratory of Potsdam University. He wrote a first version of the manuscript including all figures and tables. The second author introduced M. Wiederkehr to the $^{40}\text{Ar}/^{39}\text{Ar}$ dating technique and assisted in the $^{40}\text{Ar}/^{39}\text{Ar}$ laboratory and helped in the calculation of the ages and in the interpretation of the data. He also assisted during the writing process. The third author provided two samples from the Engadine Window for dating the HP/LT metamorphic event and assisted developing the concept of the investigations. He also reviewed the final version of the manuscript. The fourth author carefully reviewed and improved a first draft of the manuscript and helped with the discussion and interpretation of the results. The fifth author provided advisory scientific help and assisted with the preparation of the final version of the manuscript.

Chapter 5:

**Overprint of an earlier HP/LT metamorphic event by a later Barrow-type event:
Metamorphic evolution and geodynamic implications**

Wiederkehr, M., Bousquet, R., Schmid, S.M. & Berger, A.

This chapter comprises new petrologic data concerning progressive Barrow-type thermal overprint of HP/LT metasediments at the north-eastern border of the Lepontine dome obtained by P-T calculations. Furthermore, the relationships between the two contrasting types of metamorphic events and associated structures will be discussed in the framework of the results presented in the previous chapters, i.e. chapters 2-4 which, allows for reconstructing the geodynamic evolution of Valaisan- and Europe-derived metasedimentary units.

The first author performed the entire fieldwork and sample selection for the P-T investigations. He performed electron microprobe and X-ray fluorescence analyses and the P-T calculations. Furthermore he was responsible for a first version of the manuscript including all table and figures. The second, third and fourth authors (thesis supervisors) helped in the discussions and interpretations of the data and assisted during the writing process.

Chapter 6:

**Metamorphism of metasediments at the scale of an orogen: A key to the Tertiary
geodynamic evolution of the Alps**

Bousquet, R., Oberhänsli, R., Goffé, B., Wiederkehr, M., Koller, F., Schmid, S.M., Schuster, R., Engi, M., Berger, A. & Martinotti, G.

published 2008: *Geological Society Special Publications*

This chapter is devoted to metasediments and their potential in providing important information regarding the geodynamic evolution of the Alpine orogenic belt. Based on new data concerning the metamorphic evolution of metasediments this study presents the distribution of mineral assemblages at the scale of the entire orogen, related to either subduction-induced high-pressure metamorphism or collision-related Barrovian overprint. Their distribution and geodynamic significance is discussed.

The first and second author wrote a first version of the manuscript including all figures and tables. The fourth author (M. Wiederkehr) provided new data and first results concerning the north-eastern border of the Lepontine dome and easterly adjacent areas established during this thesis. Furthermore he reviewed a first version of the manuscript. All the other authors provided discussions and help in finalizing and improving an early version of the manuscript.

Chapter 7:

Summary and conclusions

This chapter presents the main summary and conclusions of the combined results of the entire thesis.

Acknowledgements

This thesis would not have been completed and much more difficult to finalize without the help and support of numerous people – Thanks to all of you!

First of all I would like to thank my supervisors, Stefan Schmid, Romain Bousquet and Alfons Berger for initiating this interesting and fruitful project – it was from the beginning thrilling!

The enthusiasm and passion for Alpine geology and the constant interest and thirst for knowledge of Stefan Schmid was a major driving force and motivation during the last years. His efficient work on numerous manuscripts significantly improved whatever I wrote and always within an amazingly short time. This efficiency proved extremely helpful during the last months while my thesis was rapidly developing.

From Romain Bousquet I learned to look closely at disgusting low-grade rocks which nobody likes to work with: the Bündnerschiefer! His passion for these rocks and, of course for carpholite, was the real driving force for this PhD study. His always positive perspective of all kinds of problems and his enthusiastic interest of metamorphic petrology was enormously motivating, especially during extensive and hard times in the laboratories at Potsdam University. Even in the hardest times and when problems appeared to be insurmountable, Romain still kept on saying “kein Problème”, a slogan which helped always to get through some tough periods during this PhD. I will always remember joint fieldwork (Avers, Luzzone and Engadine Window) and hospitality of his entire family in Potsdam.

This study benefitted a lot from the contribution by Alfons Berger. His profound knowledge in petrology and the tectono-metamorphic evolution of the Central Alps as well as in isotope geology was of great importance for the successful completion of the PhD thesis. His ability for reducing highly complicated problems to a rather comprehensive level was essential for isotopic and petrologic investigations. I profited a lot during fruitful discussions, constructive reviews of the manuscripts and his always friendly support during the last years.

I would especially like to thank Roland Oberhänsli from the University of Potsdam. He is one of the big shots concerning “carpholitology”, and his always open door and the fruitful discussions related to high-pressure metamorphism of Bündnerschiefer were very stimulating.

Martin Ziemann introduced me to the Raman Laboratory of the University of Potsdam and provided some additional measurements. His always perfectly organized lab and the excellent calibration of the Raman probe, as well his support during the writing of the Raman chapter are appreciated.

The introduction to and support in the $^{40}\text{Ar}/^{39}\text{Ar}$ Laboratory of Potsdam University by Masafumi Sudo, as well as his help for the interpretation of the data and substantial improvements in finalizing the manuscript on age dating are greatly acknowledged.

Willy Tschudin played a major role for the sample preparation of my thesis. Willy prepared almost uncountable numbers of thin-sections – most of them polished – very fast and always in excellent quality. This PhD thesis would not have been possible without his tireless service. I will never forget our highly stimulating morning coffee breaks – Thank you Willy!

I also would like to especially thank Senecio Schefer for his always open door for scientific discussions and advice and for the help with my numerous computer problems. Without him this PhD thesis would definitely look different!

I had the great luck that Guido Derungs performed his master thesis in the framework of my PhD study. The results of his thesis, as well as his supporting company during fieldwork including hauling masses of samples down the mountains were stimulating and provided substantial improvements for this study – Thank you Guido. I am also indebted to his parents, Vreni and Sigis Derungs for their hospitality and particularly for cooking large portions of traditional Grisons food!

Fruitful discussions on petrology and thermodynamics, as well as the performance of XRF analyses by Fred Gaides are very much thanked.

I am indebted to Jean-Pierre Hürzeler for his help with the SEM investigations.

This thesis benefited a lot from our thermodynamic and petrologic experts at the department of Basel University. I would like to thank Christian de Capitani for his help with DOMINO-THERIAK and Leander Franz for support and fruitful discussions regarding thermobarometry and metamorphic petrology.

Julien Allaz, Emilie Janots and Martin Engi are acknowledged for fruitful discussions related to metamorphism and geology of the north-eastern Lepontine dome as well as on the dating of mica and allanite/monazite. I also would like to thank Meinert Rahn for providing me his latest fission track results as well as some samples collected during the Greina mapping course.

For the help with microprobe analysis I am indebted to Oona Appelt and Dieter Rhede from the GeoForschungsZentrum Potsdam.

During my PhD I spent a considerable time at Potsdam University. For the friendly acceptance and fruitful discussions I would like to thank Uwe Altenberger, Andreas Möller, Manuela Borchert, Franziska Wilke, Henry Wichura and especially Astrid Riemann for her support during fieldwork and help during measurements in the labs as well as an unforgettable trip through the city of Potsdam. I am greatly indebted to Martin Timmerman for the help in sample preparation for $^{40}\text{Ar}/^{39}\text{Ar}$ *in situ* dating as well as to Christine Fischer for the careful and perfect preparation of the samples.

I also would like to especially thank the family Bousquet, namely Charlotte, Basile, Maëlys, Jonas and Felix. They provided a comfortable and very friendly “home” during my stays at Potsdam and improved my knowledge in French.

I thank Joëlle Glanzmann, Verena Scheuring and Susanne Tobler for administrative support and I am indebted to Heinz Hürlimann and Hans-Ruedi Rüegg for their help with technical issues. Koni Leu and Michael Meiling are thanked for computer support. Finally I would like to thank all other colleagues at the department of Basel University for their contribution to this thesis.

Special thanks go to Theresa and Koni Klingelfuss for lending me their comfortable caravan which provided a warm and dry “home” during fieldwork in the Valle di Blenio.

Finally, I would like to express my deep gratitude for the encouragement and infinite support in so many ways by my mother and by Richi Kern. Last but not least I thank Yvette for her understanding, patience and love.

Table of contents

Chapter 1:	1
Introduction	
1.1. Thesis motivation and outline of the incorporated projects	1
1.2. Methodological approach	3
1.3. Geological setting	4
Chapter 2:	7
From subduction to collision: Thermal overprint of HP/LT meta-sediments in the north-eastern Lepontine Dome (Swiss Alps) and consequences regarding the tectono-metamorphic evolution of the Alpine orogenic wedge	
Abstract	7
2.1. Introduction	8
2.2. Geological setting and major tectonic units	10
2.2.1. Sub-Penninic basement nappes	10
2.2.2. Sub-Penninic cover nappes and slices	13
2.2.3. Lower Penninic cover nappes (Valais Bündnerschiefer)	15
2.3. Structural evolution	15
2.3.1. First deformation phase (D1)	15
2.3.2. Second deformation phase (D2)	17
2.3.3. Third deformation phase (D3)	17
2.3.4. Fourth deformation phase (D4)	18
2.4. New data regarding the metamorphic evolution of the area	18
2.4.1. Spatial distribution of index minerals and mineral parageneses	18
2.4.2. Data on the earlier HP/LT metamorphic event	19
2.4.3. Data on the subsequent temperature-dominated event	21
2.4.4. Correlations between the structural and metamorphic evolution	23
2.4.5. Relations between HP/LT and MP/MT metamorphism: Significance of a metamorphic field gradient	25
2.5. Discussion and interpretation of the results	28
2.5.1. Regional correlations of the tectono-metamorphic evolution established in the working area and timing constraints	28
2.5.2. P-T-d-t path and reconstruction of the regional tectono-metamorphic evolution	31
2.5.3. Discussion of potential heat sources of Barrow-type overprint and thermal evolution	35
2.6. Conclusions	37
Acknowledgements	38

Chapter 3:	39
3-D assessment of peak-metamorphic conditions by Raman spectroscopy of carbonaceous material: an example from the margin of the Lepontine dome (Swiss Central Alps)	
Abstract	39
3.1. Introduction	40
3.2. Geological setting and sampling strategy	41
3.2.1. Tectono-metamorphic background	41
3.2.2. Sediments derived from the distal European margin (Sub-Penninic cover nappes and slices)	44
3.2.3. Sediments derived from the Valaisan Ocean (Lower-Penninic cover nappes and slices, Valaisan Bündnerschiefer)	44
3.2.4. Sampling strategy	44
3.3. RSCM method	46
3.3.1. Sample preparation	49
3.3.2. Raman spectrum of carbonaceous material	49
3.3.3. Analytical procedure: spectra acquisition and treatment	51
3.4. Results of the RSCM investigations	52
3.4.1. Overall evolution of Raman spectra with increasing metamorphic grade	52
3.4.2. Comparison between the available calibration methods	52
3.4.3. Mapping field thermal gradients in three dimensions	54
3.5. Discussion	62
3.5.1. Comparison of RSCM-derived maximum temperatures with temperatures inferred from other petrological data	62
3.5.2. Relationships between isotherm contours and the polyphase thermal evolution of metasediments	65
3.5.3. Inferences regarding the graphitization process along a metamorphic gradient	66
3.6. Conclusions	66
Acknowledgements	67
Chapter 4:	69
⁴⁰Ar/³⁹Ar dating of the subduction-collision transition in the Central Alps	
Abstract	69
4.1. Introduction	70
4.2. Tectono-metamorphic background and sampling strategy	71
4.2.1. Geological setting	71
4.2.2. Tectono-metamorphic evolution	73
4.2.3. Sampling strategy	74
4.3. Experimental procedure of ⁴⁰ Ar/ ³⁹ Ar dating	75
4.3.1. Sample preparation	75
4.3.2. Neutron activation by fast neutron	76
4.3.3. Ar isotopic analysis	76
4.4. Sample description and mineral chemistry	77
4.4.1. White mica	77
4.4.2. Biotite	80

4.5. Results of the $^{40}\text{Ar}/^{39}\text{Ar}$ measurements	81
4.5.1. <i>In situ</i> $^{40}\text{Ar}/^{39}\text{Ar}$ UV laser-probe ages on white mica	81
4.5.2. <i>In situ</i> $^{40}\text{Ar}/^{39}\text{Ar}$ UV laser-probe ages of biotite	83
4.5.3. $^{40}\text{Ar}/^{39}\text{Ar}$ CO_2 laser step-wise heating of biotite	88
4.6. Interpretations and discussion	90
4.6.1. Interpretation of individual age data	90
4.6.2. Correlation between isotopic data and microstructural features	91
4.6.3. Conclusions regarding the age interpretation	92
4.6.4. Comparison with previously published isotopic and fission track data	94
4.6.5. Implications regarding the tectono-metamorphic evolution	95
4.7. Conclusions	98
Acknowledgements	99
Chapter 5:	101
Overprint of an earlier HP/LT metamorphic event by a later Barrow-type event: Metamorphic evolution and geodynamic implications	
Abstract	101
5.1. Introduction	102
5.2. Geological background	104
5.3. Methods of investigations for P-T estimates	104
5.3.1. Mineral and whole rock chemistry	104
5.3.2. Methods used for P-T estimation	104
5.4. Metamorphic record of Valaisan and European margin derived metasedimentary units	105
5.4.1. Significance of the observed mineral assemblages	106
5.4.2. P-T estimates along a profile with increasing Barrow-type metamorphic grade overprinted onto earlier HP/LT metamorphism	111
5.4.3. Transition from subduction- to collision-related metamorphism	119
5.5. Deformation history and discussion of the regional variability regarding orientation and intensity of studied structures	121
5.5.1. Variability of the overall architecture of the study area	121
5.5.2. Variability of structural elements corresponding to distinct deformation events	121
5.5.3. Relationships between deformation and metamorphism	124
5.6. Interpretation and geodynamic implications	128
5.6.1. Timing constraints and metamorphic evolution of the study area	128
5.6.2. Implications for the exhumation of HP/LT units	130
5.7. Conclusions	131
Acknowledgements	132

Chapter 6:	133
Metamorphism of metasediments at the scale of an orogen: A key to the Tertiary geodynamic evolution of the Alps	
Abstract	133
6.1. Introduction	134
6.2. Metamorphic mineralogy of metasediments	136
6.2.1. Petrogenetic grids	136
6.2.2. Ambiguity of some mineral assemblages in the Alps	139
6.2.3. Ambiguity of some metamorphic facies	140
6.3. The metamorphic data in a geodynamic context	140
6.4. Subduction-related minerals and their distribution	141
6.5. Minerals related to collision processes and their distribution	145
6.6. Metamorphic structure of the Alps	147
6.7. Discussion	150
6.8. Conclusions	150
Acknowledgments	151
Appendix	151
Chapter 7:	
Summary and conclusions	153
7.1. Tectono-metamorphic evolution (P-T-d-t path)	153
7.2. Implications regarding the geodynamic evolution of the Alps	156
Bibliography	159

Chapter 1

Introduction

1.1. Thesis motivation and outline of the incorporated projects

This PhD thesis was carried out within the framework of the project “Tectono-metamorphic studies of the Alps”, a long lasting series of studies performed at the University of Basel and initially launched by the late Prof. M. Frey in 1992, financed by the Schweizerische Nationalfonds. The general goal of these series of former projects, and also for this study, is a better understanding of the tectonic and metamorphic evolution of the Alps in space and time and to get more insight in mountain building processes in general. The present study was initiated by Profs. Stefan M. Schmid and Romain Bousquet (Potsdam) and supported by PD Alfons Berger (Bern/Kopenhagen). It was financed by project NF-200020-113585 and precursor project NF-200020-103585.

This is a joint thesis (co-tutelle) amongst the Universities of Basel (Switzerland) and Potsdam (Germany). The study is devoted to the structural, metamorphic and geochronological evolution of metasedimentary units exposed in the Central Alps (northern Valle di Blenio and easterly adjacent areas in the Grisons) in order to reveal insights that are of fundamental importance for understanding the thermo-mechanical evolution of collisional orogens in general. Moreover, this work represents a case study that addresses the transition from subduction to collision in general and thereby provides important field and geochronological data for testing numerical models for the geodynamic evolution of orogenic belts (e.g. Bousquet et al. 1997; Jamieson et al. 1998; Roselle et al. 2002; Goffé et al. 2003).

The study addresses a key area for the reconstruction of the Alpine geodynamic evolution at the north-eastern margin of the Lepontine dome and easterly adjacent areas where pressure- and temperature-dominated metamorphic domains are found to be in close contact (Bousquet et al. 2002; Oberhänsli et al. 2004). The studied metasediments have a great potential to record the metamorphic evolution and can therefore be used for the geodynamic reconstruction of the Alpine orogenic belt. Moreover, these metasediments cover large areas and therefore enable observing and correlating the structural and metamorphic evolution continuously and over great distances.

The metamorphic structure of the Alps is the result of long lasting plate convergence and final collision between the European and Adriatic continental plates in Cretaceous to Cenozoic times (e.g. Trümpy 1960; Frisch 1979; Tricart 1984; Schmid et al. 1996). The geodynamic evolution and resulting metamorphic zonation related to Cenozoic orogeny can be subdivided into two distinct stages: (1) subduction-related pressure-dominated metamorphism and deformation of oceanic lithosphere formed during the opening of the Alpine Tethys, as well as parts of the immediately adjacent European lithosphere, and, (2) temperature-dominated Barrow-type metamorphism (Frey et al. 1980) related to collision between Europe and Adria, involving further accretion of massive volumes of crustal material (e.g. Lepontine dome and Tauern window; Bousquet et al. 1997; Goffé et al. 2003; Schmid et al. 2004) to the upper plate formed by the Austroalpine nappes and previously accreted high-pressure units.

Several pioneering studies on the spatial distribution of index minerals, as well as on different metamorphic facies types, resulted in the well established knowledge of the zoning of Alpine metamorphism, particularly within the Lepontine dome of the Central Alps (e.g. Wenk 1962, 1970; Niggli and Niggli 1965; Trommsdorff 1966; Frey 1969, 1978; Niggli 1970; Frey et al. 1980, 1999; Oberhänsli et al. 2004). However, the metamorphic zoning related to pressure-dominated metamorphism needs to be

discriminated from that related to Barrovian overprint in the Alps. While the pressure-dominated units (blueschists and eclogites) form an orogen-parallel belt, remnants of the temperature-dominated event are localized in the Lepontine dome and the Tauern window (e.g. Bousquet et al. 2008). From a geodynamic point of view only the Central Alps (Lepontine dome) and the Tauern window in the Eastern Alps reached the mature stage of a colliding orogenic belt that is characterized by pervasive Barrovian overprint.

Accordingly, the aims of the study can be summed up in terms of the following five main scientific questions:

- (1) What are the relationships between the two contrasting types of metamorphic events representing subduction-related HP/LT metamorphism and collision-related Barrov-type thermal overprint in respect to distinct deformation events? Thereby a well-defined relative geochronological sequence based on clear overprinting criteria of different deformation events combined with petrological investigations is of particular relevance for the reconstruction of the tectono-metamorphic evolution of the study area.
- (2) Which units show evidence for subduction-related high-pressure metamorphism and which do only show a collision-related metamorphic overprint? The identification of tectonic units affected by HP/LT metamorphism is of great importance for the reconstruction of the tectono-metamorphic evolution and for the location of the former Valaisan subduction zone located between the Briançonnais micro-continent and distal European margin. Furthermore, a precise recognition of subduction- and collision-related mineral assemblages is fundamental for the geodynamic reconstruction of the study area.
- (3) What is the timing of the subduction-related HP/LT metamorphic event of the Valaisan domain east of the Lepontine dome? Understanding the metamorphic evolution of orogenic belts requires well-constrained time data. Such data are of particular importance regarding the geodynamics of subduction, followed by unroofing in a collisional scenario later on. The timing of HP/LT metamorphism in the Valaisan high-pressure belt is not only very poorly constrained, the few available ages grossly scatter (see review given in Berger & Bousquet 2008). In this context this thesis provides important new timing constraints for the subduction-related metamorphic event, absolutely needed for the reconstruction of the geodynamic evolution of the Valaisan domain and the Central Alps in general.
- (4) What is the shape of the P-T path connecting both subduction-related high-pressure metamorphism and collision-related Barrovian overprint? Thereby it is essential to reveal if the P-T path is characterized by a bimodal shape whereby Barrovian overprint represents a separate heating pulse following isothermal decompression of the early HP/LT stage or, alternatively, if the metamorphic evolution is rather defined by a single clock-wise P-T loop. Answering this question is of fundamental importance for a better understanding of the transition from subduction to collision.
- (5) Which are the possible heat sources responsible for collision-related amphibolite facies metamorphism in colliding orogenic belts? This old question is of fundamental importance for the understanding of the formation of orogenic belts in general. Based on the new data provided by this study this question will be addressed qualitatively by the obtained field data in order to decipher the thermal evolution of the orogenic wedge during the geodynamic evolution of the Alpine belt.

All these questions were addressed using a multidisciplinary and integrative approach that combines structural, petrological and geochronological methods. This approach required intense scientific cooperation with a multinational team of specialists from the Universities of Basel and Potsdam.

The results of this thesis yield new implications regarding the regional tectono-metamorphic evolution of the north-eastern border of the Lepontine dome and easterly adjacent areas. Furthermore, the thesis contributes to a better overall understanding of geodynamic processes that occur during the progressive tectonic and metamorphic evolution of colliding orogens in general.

1.2. Methodological approach

In order to solve the above defined research questions a multidisciplinary approach including petrologic, structural and isotopic investigations was applied.

Petrologic investigations: Extensive fieldwork reveals the spatial distribution of mineral assemblages indicative for a specific geodynamic setting, i.e. subduction-related HP/LT metamorphism, or collision-related Barrovian overprint. This is of fundamental importance for the presented study, particularly the finding of occurrences of relics of the early high-pressure event. Identification and mapping of such indicative mineral assemblages allows for determining P-T paths which are essential for the metamorphic reconstruction.

Structural fieldwork: Detailed structural investigations allow for discriminating several discrete deformation events. They provide a relative chronology based on clear overprinting criteria. By combining the petrologic record with the structural data and deciphering the relationships between metamorphism and deformation the established relative chronology can be used for the tectono-metamorphic reconstruction. Structural measurements are of great importance for the construction of cross-sections showing the overall architecture of the study area. They also provide hints towards the tectonic reconstruction.

Raman spectroscopy of carbonaceous matter: The study area is characterized by a remarkable metamorphic field gradient ranging from amphibolite to blueschist facies conditions. The investigated low-grade (HP/LT and LP/LT) metasediments, the so-called “Bündnerschiefer”, commonly show a rather poor mineralogy devoid of indicative mineral assemblages needed for accurate P-T estimations. On the other hand carbonaceous material is ubiquitous in such metasediments, which can be used as a geothermometer by recording the degree of ordering in its crystallographic structure by Raman spectroscopy. This geothermometer always records peak-metamorphic conditions, it is very sensitive and allows for recording thermal gradients in the order of 10-15 °C. Consequently, this method provides important information for mapping the transition from subduction- to collision-related metamorphism.

$^{40}\text{Ar}/^{39}\text{Ar}$ isotopic investigations: Absolute dating of metamorphic events provides important information for the evolution of orogenic belts. Via $^{40}\text{Ar}/^{39}\text{Ar}$ dating of white mica the early subduction-related metamorphic cycle could be dated. Biotite, exclusively found in areas affected by pervasive Barrovian overprint, has been analyzed to date collision-related amphibolite facies overprint.

P-T modeling: The calculation of P-T conditions is important for unraveling the metamorphic record of a given rock sample. Thermodynamic modeling allows for constructing representative P-T paths and is therefore of great importance for the reconstruction of the geodynamic evolution.

1.3. Geological setting

The studied area is located at the north-eastern edge of the Lepontine dome that represents a dome both in a structural and thermal sense. Structurally, this dome consists of Europe-derived basement nappes (Sub-Penninic after Schmid et al. 2004) that represent the deepest exposures within the Central Alps (e.g. Froitzheim et al. 1996). These pre-Mesozoic basement nappes are tectonically overlain by Mesozoic-age metasedimentary units derived from both the distal European margin (Sub-Penninic cover nappes and slices) and the Valaisan Oceanic domain (Lower Penninic), separated from each other by the Penninic Basal Thrust. In the easterly adjacent areas the Mesozoic metasediments of the Valaisan domain build up an up to 15 km thick pile of metasedimentary cover nappes (Hitz & Pfiffner 1997; see crustal-scale transect in Schmid et al. 1996, their Plate 1). Due to the general axial plunge of the whole nappe stack to the E, these Valaisan-derived metasediments are seen to be tectonically overlain by nappes derived from the Briançonnais, Piemont-Liguria Ocean, and Austroalpine domain, respectively, still further to the east. Within the Engadine window the Valaisan Bündnerschiefer are again exposed within a local antiformal dome below the Austroalpine lid.

The sediments originally deposited on the former distal European margin include Urseren-Garvera Zone, Scopi unit and Peidener slices (together forming the so-called Gotthard Mesozoic), and additionally, the Piz Terri-Lunschana unit (Probst 1980; Berger et al. 2005, and references therein). In general, these sedimentary slices are made up of a Triassic sequence of quartzites, dolomitic marbles, evaporites, metapelites and metamarls followed by a lower to middle Jurassic sequence consisting of shales, sandstones, limestones, carbonaceous metapelites and calcschists, the latter often resembling the so-called Bündnerschiefer of the Penninic (Valaisan-derived) units (Baumer et al. 1961; Probst 1980; Etter 1987; Berger et al. 2005).

Sediments derived from the predominantly oceanic Valaisan realm form voluminous and rather monotonous sequences, predominantly consisting of calcschists (Bündnerschiefer) thrust along the Penninic Basal Thrust onto the sediments of the former European margin. These Valaisan Bündnerschiefer, flysch units, marbles and ophiolitic occurrences are subdivided into a number of slices. The largest are the Grava nappe (including the Prättigau Flysch) and the Tomül nappe, consisting of Cretaceous- to Eocene-age calcschists, limestones, shales, marls and sandy limestones (Nänny 1948; Ziegler 1956; Steinmann 1994a). The existence of mafic and ultramafic rocks (Nabholz 1945) indicates that at least parts of the Valaisan Bündnerschiefer were deposited on oceanic crust (Steinmann 1994a; Steinmann & Stille 1999).

The north-eastern rim of the Lepontine dome is the locus of several pioneering studies addressing fundamental principles related to the evolution of prograde Barrovian metamorphism (Chadwick 1968; Frey 1969, 1978; Niggli 1970; Wenk 1970; Fox 1975; Livi et al. 2002). The metamorphic conditions continuously increase from chloritoid-margarite bearing micaschists that are part of the greenschist facies area in the Urseren-Garvera Zone (Frey 1978; Livi et al. 2002) to staurolite-kyanite-garnet-biotite bearing metasediments indicating amphibolite facies conditions around the Lukmanier area and Pizzo Molare (Frey 1969; Chadwick 1968; Thakur 1971). Lower/middle amphibolite facies metamorphic conditions (0.5-0.8 GPa and 500-550 °C) have been estimated for Barrow-type metamorphism in the north-eastern Lepontine dome (Chadwick 1968; Frey 1969; Engi et al. 1995; Todd & Engi 1997; Frey & Ferreiro Mählmann 1999).

To the E low-grade metasediments predominate, but the metamorphic record is ill-constrained due to the scarcity of unambiguous mineral assemblages that generally only indicate “greenschist facies”

conditions. However, the recognition of Fe-Mg carpholite in the Valaisan-derived metasediments E of the Lepontine dome indicates that blueschist facies conditions around 1.2-1.4 GPa and 350-400 °C were established before late-stage greenschist-facies overprinting (Goffé & Oberhänsli 1992; Oberhänsli et al. 1995; Bousquet et al. 1998).

Chapter 2

From subduction to collision:

Thermal overprint of HP/LT meta-sediments in the north-eastern Lepontine Dome (Swiss Alps) and consequences regarding the tectono-metamorphic evolution of the Alpine orogenic wedge

This chapter is published as: **Wiederkehr, M.**, Bousquet, R., Schmid, S.M. & Berger, A. (2008): From subduction to collision: Thermal overprint of HP/LT meta-sediments in the north-eastern Lepontine Dome (Swiss Alps) and consequences regarding the tectono-metamorphic evolution of the Alpine orogenic wedge. In: Froitzheim, N. & Schmid, S.M. (Eds): Orogenic processes in the Alpine collision zone. Swiss Journal of Geosciences 101(Suppl), S127-S155.

Abstract

The Cenozoic-age metamorphic structure of the Alps consists of a through-going pressure-dominated belt (blueschists and eclogites) that strikes parallel to the orogen and was later truncated by two thermal domes characterised by Barrow-type metamorphism (Lepontine dome and Tauern window). This study documents for the first time that relics of Fe-Mg carpholite occur also within meta-sedimentary units that are part of the north-eastern Lepontine structural and metamorphic dome, where so far exclusively Barrovian assemblages were found. They occur in meta-sediments of both Valais Ocean-derived Lower Penninic Bündnerschiefer and structurally lower Europe-derived Sub-Penninic cover nappes and slices. These high-pressure units were subsequently overprinted by a thermal event, as is documented by the growth of new minerals typical for Barrovian metamorphism.

We present evidence for a two-stage metamorphic evolution in the northern part of the Lepontine dome: (1) Early subduction-related syn-D1 (Safien phase) HP/LT metamorphism under blueschist facies conditions (350-400 °C and 1.2-1.4 GPa) was immediately followed by “cold” isothermal (or cooling) decompression during D2 nappe-stacking (Ferrera phase). (2) Collision-related Barrovian overprint (500-570 °C and 0.5-0.8 GPa) postdates the D3 nappe-refolding event (Domleschg phase) and represents a late heating pulse, separated by D2 and D3 from the D1 high-pressure event. It occurred before and/or during the initial stages of D4 (Chièra phase) representing a second nappe-refolding event.

In discussing possible heat sources for the late Barrow-type heating pulse it is argued that heat release from radioactive decay of accreted material may play an important role in contributing much to heat production. Based on the field evidence, we conclude that heat transfer was essentially conductive during these latest stages of the thermal evolution.

2.1. Introduction

The zoning of Alpine metamorphism is rather complex, evolving over a very long period of time before, during and after the collision of Europe with Adria, i.e. from Late Cretaceous to Late Cenozoic times. Mapping of metamorphic facies in the Alps started with early pioneering studies based on the spatial distribution of index minerals and mineral assemblages (Wenk 1962; Niggli & Niggli 1965; Trommsdorff 1966; Frey 1969; Fox 1975; Frey et al. 1980). Metamorphic maps at the scale of the Alpine orogen, showing the spatial arrangement of the different metamorphic facies types, were repeatedly synthesised and improved (Ernst 1971; Niggli & Zwart 1973; Frey et al. 1999; Oberhänsli et al. 2004). The Cenozoic-age metamorphic pattern is characterised by a pressure-dominated belt (blueschists and eclogites) that strikes orogen-parallel but is interrupted by two thermal domes, the Lepontine dome in the Central Alps and the Tauern window in the Eastern Alps (Oberhänsli et al. 2004).

Our area of investigation is located at the NE border of the Lepontine thermal dome. There, along strike of the tectonic units, a remarkable metamorphic field gradient that ranges from pressure-dominated blueschist facies in the NE to temperature-dominated Barrovian metamorphism in the SW is observed within an amazingly short distance (< 10km, Figs. 2.1 & 2.2). This allows for a clear correlation between the two metamorphic events and structures that resulted from a polyphase deformation history. Hence, the area is well suited for studying spatial and temporal relationships between these two types of metamorphism, including their relative timing in respect to discrete deformation phases linked to particular geodynamical stages.

The availability of meta-sediments all along strike facilitates the reconstruction of the metamorphic and structural evolution in the working area. These meta-sediments contain widespread occurrences of Fe-Mg carpholite within an orogen-parallel HP/LT-metamorphic belt in eastern Switzerland (Grisons), characterised by blueschist facies conditions (Goffé & Oberhänsli 1992; Oberhänsli 1994; Oberhänsli et al. 1995; Bousquet et al. 2002). Approaching the Lepontine dome, the same meta-sediments become increasingly affected by a temperature-dominated, Barrovian metamorphic event, as is documented by amphibolite facies mineral assemblages characterised by garnet, biotite, staurolite and kyanite (Chadwick 1968; Frey 1969; Fox 1975; Engi et al. 1995; Frey & Ferreiro Mählmann 1999). No evidence is available, so far, that this part of the Lepontine dome, characterised by this Barrow-type MP/MT metamorphism, could have been previously also affected by HP/LT metamorphism.

This tectono-metamorphic study primarily aims to document this transition from HP/LT blueschist facies metamorphism in the east to amphibolite-grade Barrow-type metamorphism within the Lepontine dome further west. This will allow deducing whether these two contrasting types of metamorphism evolved at the same time but differently in the different parts of the study area, or alternatively, whether they evolved during consecutive stages of the evolution of the Alpine orogen. In the second case the pressure-dominated metamorphism represents an early stage related to subduction, followed by a temperature-dominated event, as proposed by Bousquet et al. (2008). The latter, i.e. a two-stage metamorphic evolution, was also proposed for more southerly located parts of the Lepontine dome. However, the question whether the Barrow-type overprint is associated with a second and discrete heating pulse that followed high-pressure metamorphism (e.g. Engi et al. 2001), or alternatively, simply represents a late stage during isothermal decompression (e.g. Nagel et al. 2002a; Keller et al. 2005a) is of fundamental importance from a geodynamic point of view. Furthermore, our study will address the important key question concerning the heat source of Barrow-type Lepontine metamorphism, debated since the pioneering metamorphic studies in the Alps. While Niggli (1970) concluded that regional metamorphism

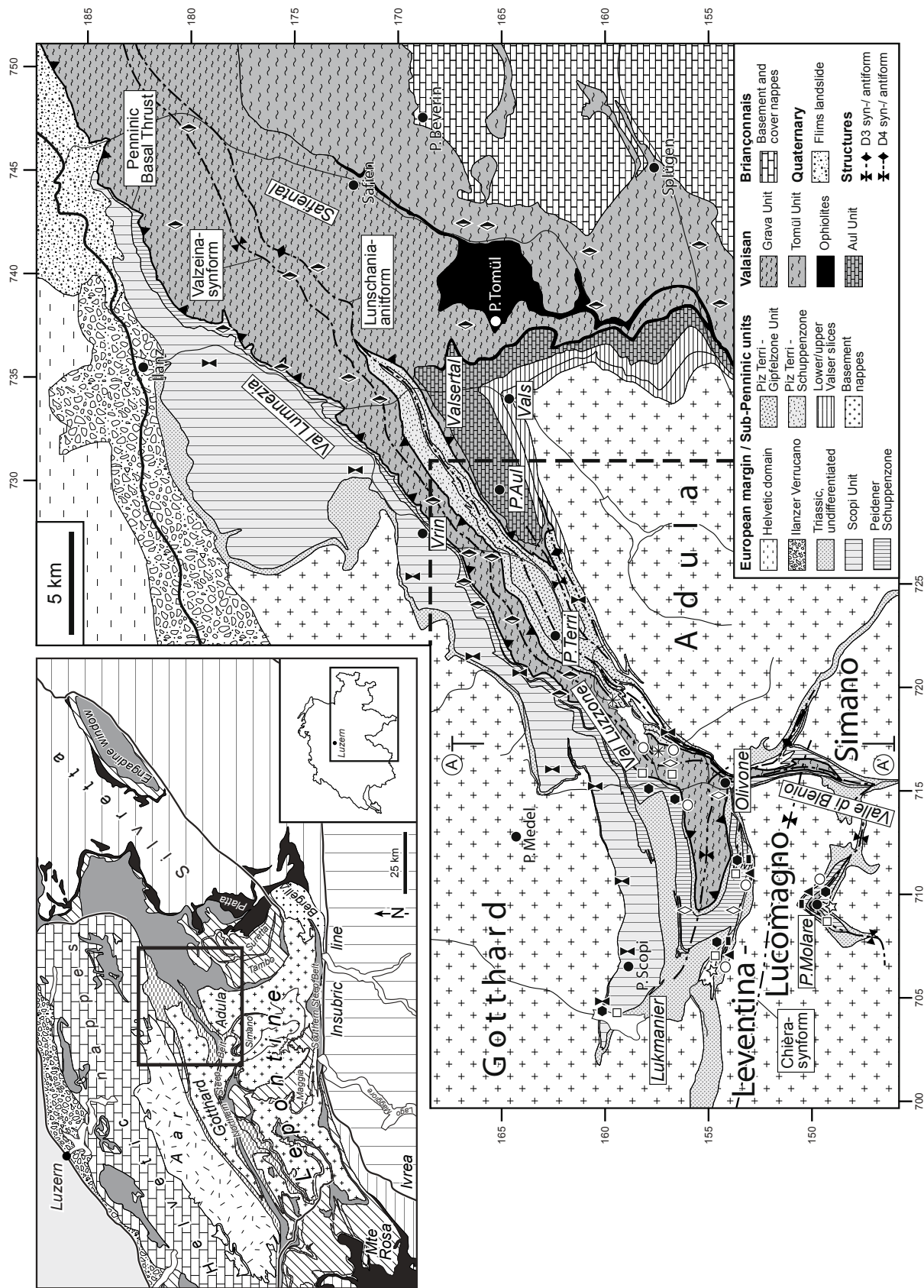


Fig. 2.1: Tectonic sketch map of the study area showing the main geographic localities mentioned in the text as well as traces of axial planes of major D3 and D4 folds, and the main occurrences of index minerals and mineral assemblages found in the meta-sedimentary units (light-grey: Sub-Penninic/European units, dark-grey: Lower Penninic/Valaisan units; symbols are explained in Figure 2.2). The tectonic map of the Central Alps in the upper left is after Schmid et al. (2004), the frame shows the location of the study area. Letters A-A' mark the trace of the composite cross section shown in Figure 2.3. The dashed line delineates the cut-out shown in greater detail in Figure 2.2.

in the Lepontine region is caused by tectonic burial during nappe stacking, Wenk (1970) proposed late-stage thermal doming induced by an additional (magmatic) heat source underneath a pre-existing overburden of nappes. The results presented in this study will provide insights that are of fundamental importance for understanding the thermo-mechanical evolution of collisional orogens in general.

2.2. Geological setting and major tectonic units

The investigated area is located at the north-eastern edge of the Lepontine structural dome and extends from the Lukmanierpass and Pizzo Molare areas in the west to the Safiental area in the east (Fig. 2.1). The Sub-Penninic nappes, interpreted as derived from the distal European margin (Milnes 1974; Schmid et al. 2004), originally occupied a lower tectonic position within the working area. Among these nappes are basement nappes that predominantly consist of pre-Mesozoic igneous and meta-sedimentary rocks, and cover nappes forming an orogen-parallel belt of Mesozoic meta-sediments. The cover nappes are not interrupted by oblique tectonic contacts (thrusts or faults) and they overlie the pre-Mesozoic basement units or nappes (Gotthard “Massif”, Leventina-Lucomagno and Simano nappes). These Sub-Penninic nappes are structurally overlain by Lower Penninic cover nappes that originated from the Valais Ocean, largely consisting of Mesozoic meta-sediments referred to as Bündnerschiefer. The front of the Adula nappe complex only reaches the southern rim of the working area. The occurrences of oceanic remnants that are imbricated with typical continental crustal rocks in the overlying Misox Zone (e.g. Partzsch 1998), and according to some authors also within the Adula-Cima Lunga nappe complex itself (e.g. Trommsdorff 1990, and references therein), indicate that the Adula nappe complex contains slivers from the continent-ocean transition between the European margin and the Valais Ocean (lithospheric mélange; Trommsdorff 1990). The Penninic Basal Thrust represents an early-stage first-order thrust along which the Valaisan Bündnerschiefer were originally thrust onto the Europe-derived Sub-Penninic units. However, this thrust was subsequently isoclinally refolded and hence penetratively overprinted by later structures. The tectonic units, subdivided following the schemes proposed by Schmid et al. (2004) and Berger et al. (2005), are mapped in Figures 2.1 and 2.2, as well as in cross section view (Fig. 2.3). In the following they are further described.

2.2.1. Sub-Penninic basement nappes

The Gotthard-“massif” is the lowermost thrust sheet of the Sub-Penninic nappe pile (Fig. 2.3) and represents a backfolded nappe front (Milnes 1974) rather than a par-autochthonous massif. This unit consists of pre-Mesozoic crystalline basement (Steiger 1962; Mercolli et al. 1994) overlain in stratigraphic contact only by an extremely thin veneer of Early to Middle Triassic quartzites, occasionally also containing dolomitic marbles and/or meta-evaporites (Frey 1967).

The Lucomagno-Leventina nappe structurally overlays the Gotthard-“massif”, from which it is separated by the Piora Zone, which represents an intervening Sub-Penninic cover nappe (Fig. 2.3). The southern realms of the Lucomagno-Leventina nappe predominantly consist of Variscan orthogneiss (Leventina gneiss; Casasopra 1939; Köppel et al. 1981; Rütli et al. 2008), forming the deepest outcropping parts of the Ticino sub-dome within the Lepontine dome (Merle et al. 1989). The northern part of the Leventina-Lucomagno nappe reaches the working area and consists of Pre-Mesozoic poly-metamorphic meta-sedimentary complexes (Lucomagno crystalline; Bossard 1925, 1929; Chadwick 1968).

The next higher Sub-Penninic basement nappe, i.e. the Simano nappe, contains Caledonian to Variscan orthogneisses and pre-Mesozoic poly-metamorphic pelitic to psammitic meta-sediments (Jenny et

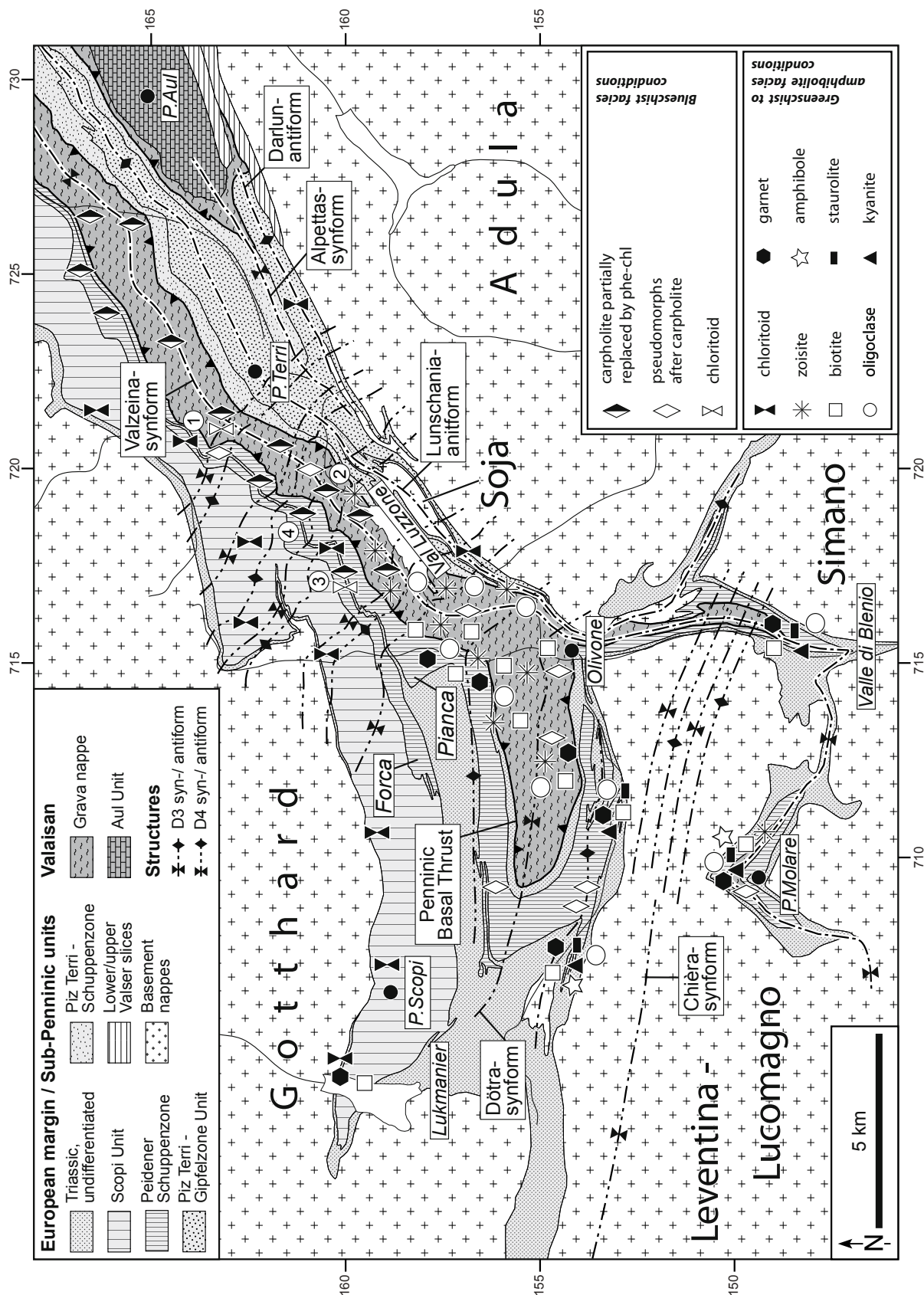


Fig. 2.2: Blow-up of the south-western part of the study area (bordered by the dashed line in Fig. 2.1) showing the traces of axial planes of major D3 and D4 folds, as well as the main occurrences of index minerals and mineral assemblages found in the meta-sedimentary units. Numbers 1 – 4 refer to the locations of the investigated samples presented in Table 2.1; coordinates are given in Swiss map coordinates (1: LUZ 0432, 720°938/162°275, 2600m; 2: LUZ 0416, 719°235/160°052, 1670m; 3: LUZ 047, 717°435/160°282, 1850m; 4: LAR 061, 718°531/160°727, 1960m).

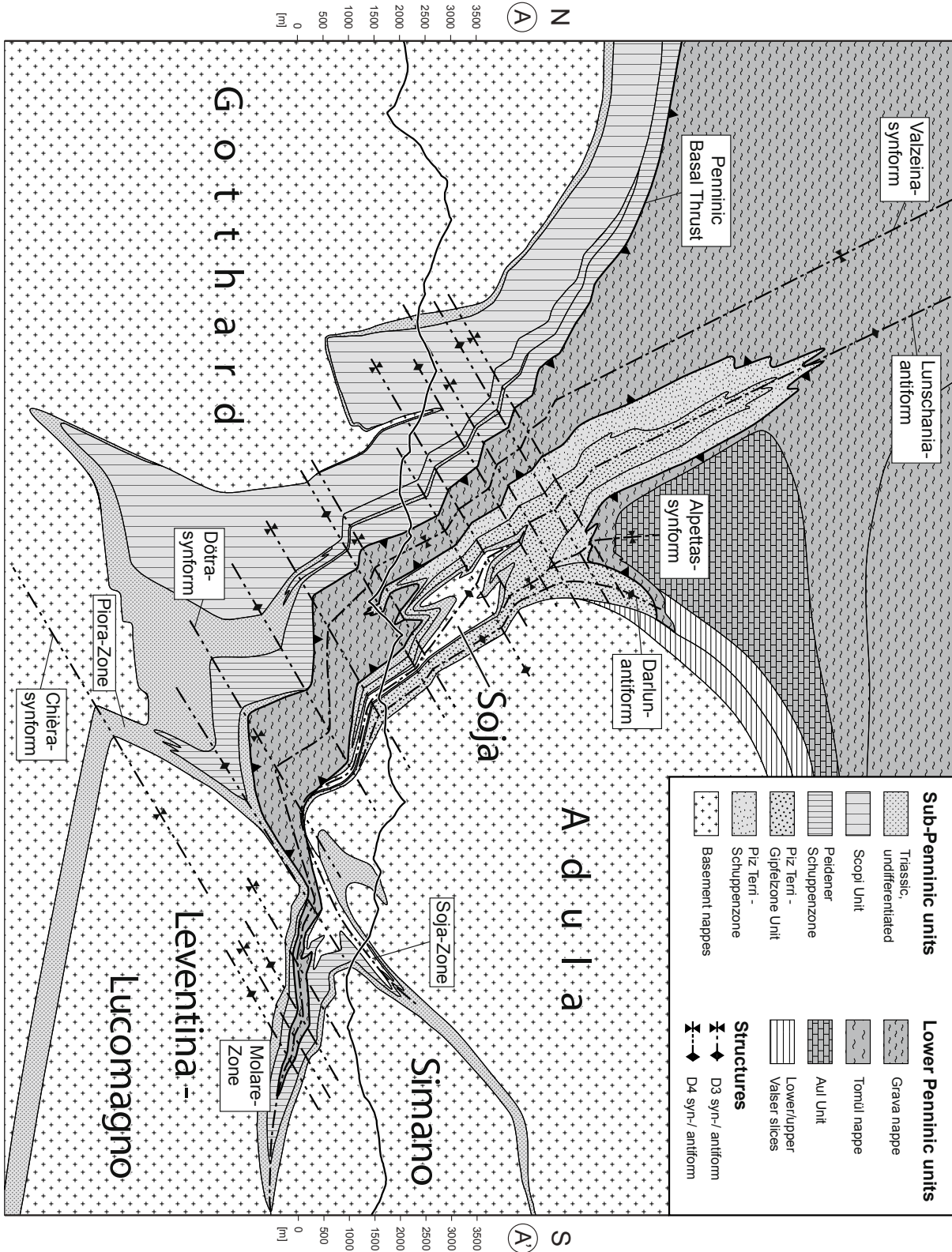


Fig. 2.3: Composite cross section, established on the basis of a series of cross sections by axial projection, showing the overall architecture of the working area (see Figure 2.1 for the trace of the cross-section into which laterally adjacent profiles were projected).

al. 1923; Niggli et al. 1936; Keller 1968; Köppel et al. 1981). It is separated from the underlying Lucomagno-Leventina basement nappe by the Molare Zone, again consisting of cover nappes (Fig. 2.3).

A thin sliver of pre-Mesozoic meta-sediments (locally Verrucano-type meta-conglomerates of presumed Permian age), that is part of the so-called Soja nappe (Jenny et al. 1923; Egli 1966) crops out in Val Luzzone at the front of the Adula nappe complex. This Soja nappe can be followed southwards where it is seen to separate the Simano nappe from the Adula nappe complex (Soja Zone of Fig. 2.3). Most authors correlate the Soja nappe with the Lebendun nappe west of the Lepontine dome (Burckhardt 1942; Egli 1966).

The Adula nappe complex represents the highest structural unit within the Sub-Penninic nappe pile. It is generally overlain by the Lower Penninic Bündnerschiefer, but in the working area the contact between the Adula and overlying units is sub-vertical due to a late stage tectonic event. This nappe complex is not a coherent basement sliver but consists of several thin basement slices, separated from each other by Mesozoic slivers (“internal Mesozoic”; Löw 1987) and thin sediment-bearing *mélange* units, including meta-basalts and ultramafics, i.e. remnants of oceanic (presumably Valaisan) crust (Jenny et al. 1923; Trommsdorff 1990; Berger et al. 2005). Since it predominantly consists of continental basement rocks, we attribute it to the Sub-Penninic nappe complex (Schmid et al. 2004).

The Adula nappe complex is well known for its high-pressure metamorphism, showing a progressive increase from blueschist facies conditions (1.2 GPa and 500 °C) in the north to eclogite facies conditions (800 °C and > 3 GPa) in the south (Heinrich 1982; Heinrich 1986; Löw 1987; Meyre et al. 1997; Nimis & Trommsdorff 2001; Nagel et al. 2002a). Slightly different P-T conditions are given by Dale & Holland (2003) who estimated 1.7 GPa and 640 °C in the north and 2.5 GPa and 750 °C in the south. High-pressure metamorphism is interpreted to be due to Eocene subduction of the distal European margin beneath the Adriatic continent (Becker 1993; Froitzheim et al. 1996; Schmid et al. 1996). A pressure-dominated upper blueschist facies event is also reported from the Simano nappe (1.2-1.4 GPa / 500°C; Rütli et al. 2005; Bousquet et al. 2008). Adula nappe complex and Simano nappe, together with the rest of the Sub-Penninic nappe stack from which so far no pressure-dominated metamorphism is reported, were overprinted by Barrow-type metamorphism reaching lower amphibolite facies conditions within the investigated area, i.e. 500-550 °C and 0.5-0.8 GPa (Engi et al. 1995; Todd & Engi 1997; Frey & Ferreiro Mählmann 1999).

2.2.2. Sub-Penninic cover nappes and slices

The sedimentary sequences found in these nappes and tectonic slices have strong affinities to non-metamorphic sequences of the southern Helvetic paleogeographic domain (Trümpy 1960). Hence, they are interpreted to represent the sedimentary cover of the most distal European margin (Froitzheim et al. 1996).

The Scopi unit represents a lowermost cover nappe and is characterised by a coherent sedimentary stack in an overturned position. It tectonically overlays a thin veneer of Lower and Middle Triassic stratigraphic cover (Melser Sandstone formation and Röti Dolomite formation) of the Gotthard-“massif” basement nappe (Fig. 2.3; Baumer et al. 1961; Jung 1963; Baumer 1964; Frey 1967; Etter 1987). The Scopi unit, together with the structurally higher Forca- and Pianca Zones (Fig. 2.4), forms what is often referred to as Gotthard-Mesozoic. These tectonic units are built up of sedimentary units detached along the evaporites of the Middle Triassic Röti Dolomite formation from their former crystalline substratum that has to be looked for south of the Gotthard “massif” (Etter 1987). The Scopi unit comprises a series of Late Triassic meta-pelites and meta-marls (Quartenschiefer), stratigraphically overlain by Jurassic sediments. The Lower to Middle Jurassic cover in Ultrahelvetic facies consists of carbon-

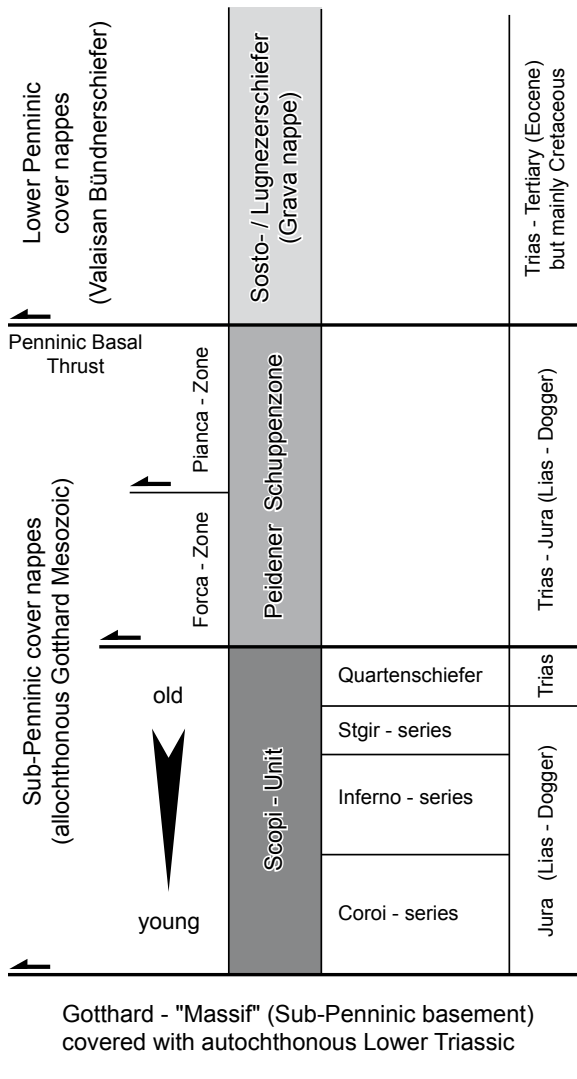


Fig. 2.4: Tectono-stratigraphic scheme of the Sub-Penninic – Lower Penninic transition after Etter (1987).

The Piz Terri-Lunschania unit is considered as Sub-Penninic because it is structurally in the footwall of the folded Penninic Basal Thrust. The Piz Terri-Lunschania unit originally represents the sedimentary cover of the basement of the Soja nappe and hence roots below the Adula nappe complex, i.e. also below the Penninic Basal Thrust (Figs. 2.1 & 2.3; Probst 1980). The structurally lower cover nappe, the so-called Piz Terri Gipfelzone unit, consists of thick and rather homogenous black and sandy calc-schists, which often resemble the Bündnerschiefer of the Lower Penninic units. The Piz Terri Gipfelzone unit was overlain by heterogeneous sedimentary slices consisting of dolomitic marbles, meta-pelites, black shales, quartzitic micaschists and layered shaly-sandy calcareous sediments (Piz Terri Schuppenzone). These are now found along both limbs of the Lunschania antiform. They have been interpreted as tectonic imbricates (Kupferschmid 1977; Probst 1980; Uhr unpubl.) and they are in direct tectonic contact with the Lower Penninic Grava nappe. The stratigraphy of the sediments of the Piz Terri-Lunschania unit is ill defined due to intense deformation and scarcity of fossils. A Triassic to Middle Jurassic age is inferred, based on lithological criteria and fossil record (Kupferschmid 1977; Probst 1980). So far little was known regarding the metamorphic overprint of this zone.

ates, calc-schists and meta-pelites that can be subdivided into three mappable formations, referred to as Stgir, Inferno and Coroi series (Baumer et al. 1961).

The Peidener Schuppenzone (imbricate zone), which tectonically overlies the Scopi unit, consists of incoherent and chaotic sedimentary slices. This imbricate zone can be further subdivided into two major parts (Forca and Pianca Zones, Fig. 2.4; Frey 1967). We interpret the Peidener Schuppenzone as a sedimentary accretionary complex, which contains lithologies that are identical with those of the Scopi unit, and they directly underlie the Lower Penninic cover nappes along the Penninic Basal Thrust (Figs. 2.3 & 2.4). The southern and western parts of the Gotthard-Mesozoic, which underwent metamorphism under lower to middle amphibolite facies conditions (0.5-0.8 GPa and 500-550 °C; Chadwick 1968; Frey 1969; Engi et al. 1995; Frey & Ferreiro Mählmann 1999), represent a classical area of regional Barrow-type metamorphism (Frey 1969; Niggli 1970; Wenk 1970; Fox 1975; Frey 1978).

Another pile of Sub-Penninic cover nappes and slices, referred to as Piz Terri-Lunschania unit, forms the core of a large isoclinal antiform (the so-called Lunschania antiform; Figs. 2.1 & 2.3), located in front of the Adula nappe complex.

2.2.3. Lower Penninic cover nappes (Valais Bündnerschiefer)

In the eastern part of the study area (Fig. 2.1) the lower Penninic cover nappes represent an up to 15 km thick volume of limestones, shales, marls and calc-schists originally deposited in the Valaisan Ocean. This thickness diminishes towards the west and around Olivone only very reduced series are conserved (Figs. 2.1, 2.2 & 2.3). Further to the east (Grisons area) the Lower Penninic Bündnerschiefer can be subdivided into, from top to bottom, the Tomül and Grava nappes, consisting of a Cretaceous- to Eocene-age sedimentary sequence (Nänny 1948; Steinmann 1994a, b), and three imbricate zones: Aul unit, Upper and Lower Valser Schuppenzone (Steinmann 1994a, b). In contrast to the Sub-Penninic cover nappes all these units are rooted above the Adula nappe (Probst 1980; Steinmann 1994a, b).

Only the Grava nappe reaches the Val Luzzzone and northern Valle di Blenio in the central and western parts of the working area, respectively, where the base of this cover nappe (here referred to as Sosto and Lugnez schists; Probst 1980) forms the Penninic Basal Thrust (Fig. 2.4). In the east, i.e. in the area around Vals, Jurassic-age (dating based on stratigraphic criteria; Steinmann 1994a) mafic and ultramafic rocks are associated with meta-sediments, both forming the Aul unit (Figs. 2.1 & 2.3). In some places the meta-basalts preserve pillow structures (Steinmann 1994a, b) and are locally associated with serpentinites (Piz Aul; Nabholz 1945). This indicates that parts of the Valais Bündnerschiefer were deposited on oceanic crust (Steinmann 1994a, b).

The metamorphism of the Valais Bündnerschiefer units is characterised by the occurrence of Fe-Mg carpholite (Goffé & Oberhänsli 1992; Bousquet et al. 2002), i.e. a typical index mineral for HP/LT conditions in meta-sediments (Goffé & Chopin 1986; Bousquet et al. 2008). Interestingly, Fe-Mg carpholite is described from both sides of the Lepontine dome, documenting blueschist facies conditions for the Petit St. Bernard area in the west (1.7 GPa, 350-400 °C; Goffé & Bousquet 1997) as well as in the Grisons including the Engadine window in the east (1.2-1.3 GPa, 350-400 °C; Bousquet et al. 1998). Both these high-pressure occurrences follow a northern suture zone between Briançonnais micro-continent and distal European margin that is formed by tectonic units attributed to the former Valais Ocean (Bousquet et al. 2002).

2.3. Structural evolution

In the following, we will first describe the four major deformation phases observed in the studied area. These are documented by clearly observable overprinting patterns. We will then correlate structural and metamorphic evolution in a second step and finally discuss and compare the results obtained in the working area with the large-scale geological context concerning the geodynamic evolution of the Alps.

2.3.1. First deformation phase (D1)

The first phase of deformation led to the formation of widespread, often carpholite-bearing calcite, quartz and quartz-calcite veins mainly found in calcareous schists in both the Sub-Penninic and Lower Penninic meta-sediments (Voll 1976). These veins represent oblique fibrous veins that opened in a transpressive manner by re-precipitation from hydrous solutions, which led to the growth of the fibres (Weh & Froitzheim 2001). The veins typically resemble fibrous carpholite pseudomorphs described in the literature (Fig. 2.5a; Goffé & Chopin 1986; Agard et al. 2001; Rimmelé et al. 2003a; Trotet et al. 2006). Such fibres of Fe-Mg carpholite, indicative of HP/LT metamorphic conditions, are typically found only within fibrous segregations and rarely in the surrounding rock matrix. Since no major folding structures

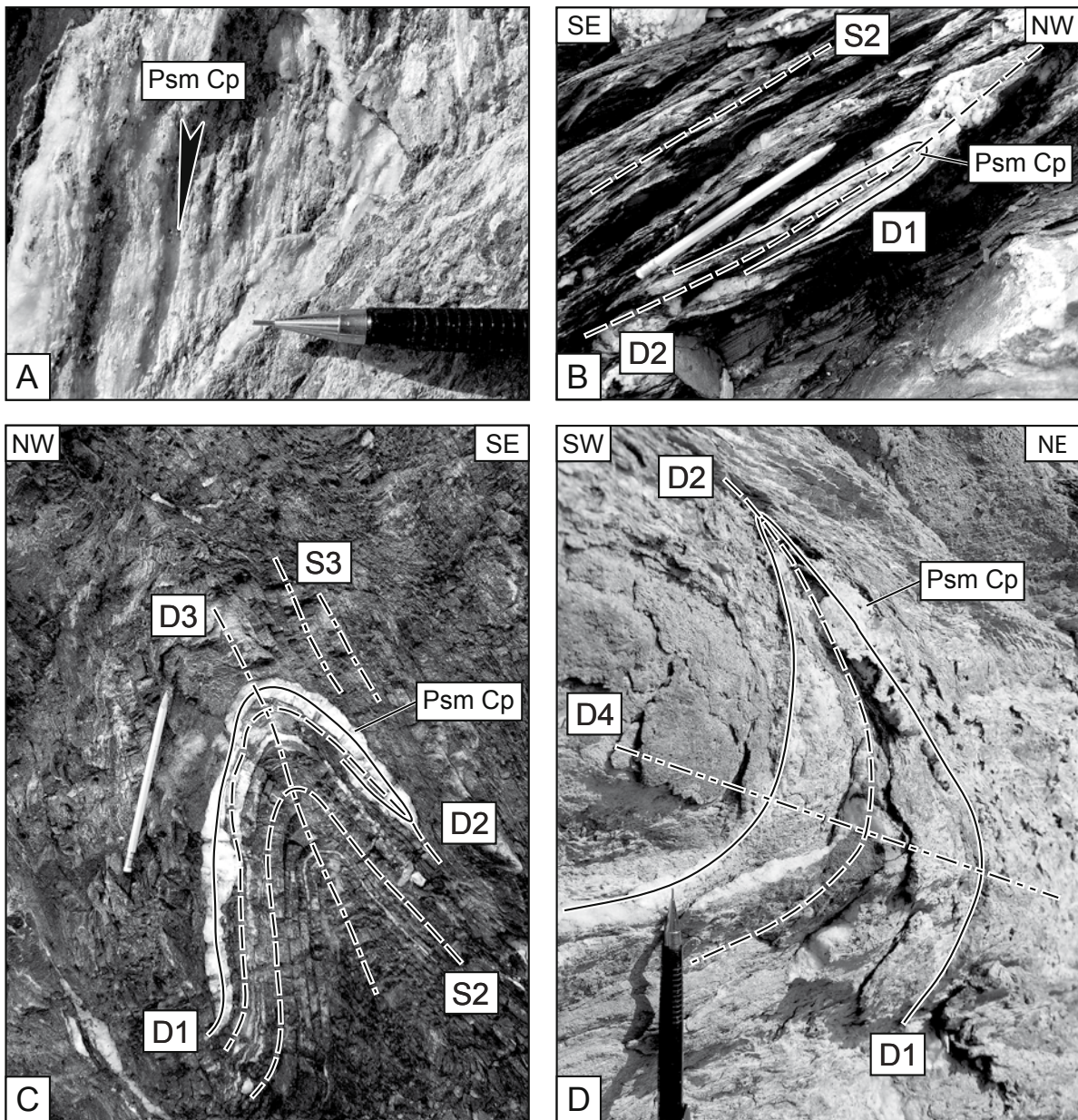


Fig. 2.5: Photographs of quartz-calcite veins representing pseudomorphs after Fe-Mg carpholite (Psm Cp). (A) Black arrow marks the orientation of characteristic fibrous growth of quartz, typical for pseudomorphs after Fe-Mg carpholite (Val Luzzzone, 716°865/158°363, 1780m). (B) Pseudomorphs after carpholite (related to D1 deformation, Safiental phase) are folded by D2 (Ferrera phase) and aligned parallel to the main foliation S2 in the fold limbs (Safiental, 739°942/160°530, 2350m). (C) Pseudomorph after carpholite, refolded by D2 and D3 (Domleschg phase; Valsertal, 738°292/174°969, 1580m). Generally a new axial planar schistosity S3 (“spaced cleavage”) evolved. In D3 fold hinges, S2 and S3 can easily be distinguished. (D) Pseudomorphs after carpholite, refolded by D2 (Ferrera phase) and D4 (Chièra phase; Val Luzzzone, 716°865/158°363, 1780m).

formed during D1 and since the surrounding rock matrix is occasionally found virtually undeformed (Fig. 2.6), we infer semi-ductile behaviour during D1, largely characterised by solution and re-precipitation processes.

Since the HP/LT mineral assemblage carpholite-chlorite-phengite-quartz±chloritoid is found in meta-sediments of both Lower Penninic (Grava and Tomül nappes) and Sub-Penninic units (Peidener Schuppenzone), the tectonic contact between the most distal European margin and the Valais Ocean, the Penninic Basal Thrust, must have already formed during D1. Although the more external Sub-Penninic units may also have been affected by D1, these units lack carpholite-bearing veins.

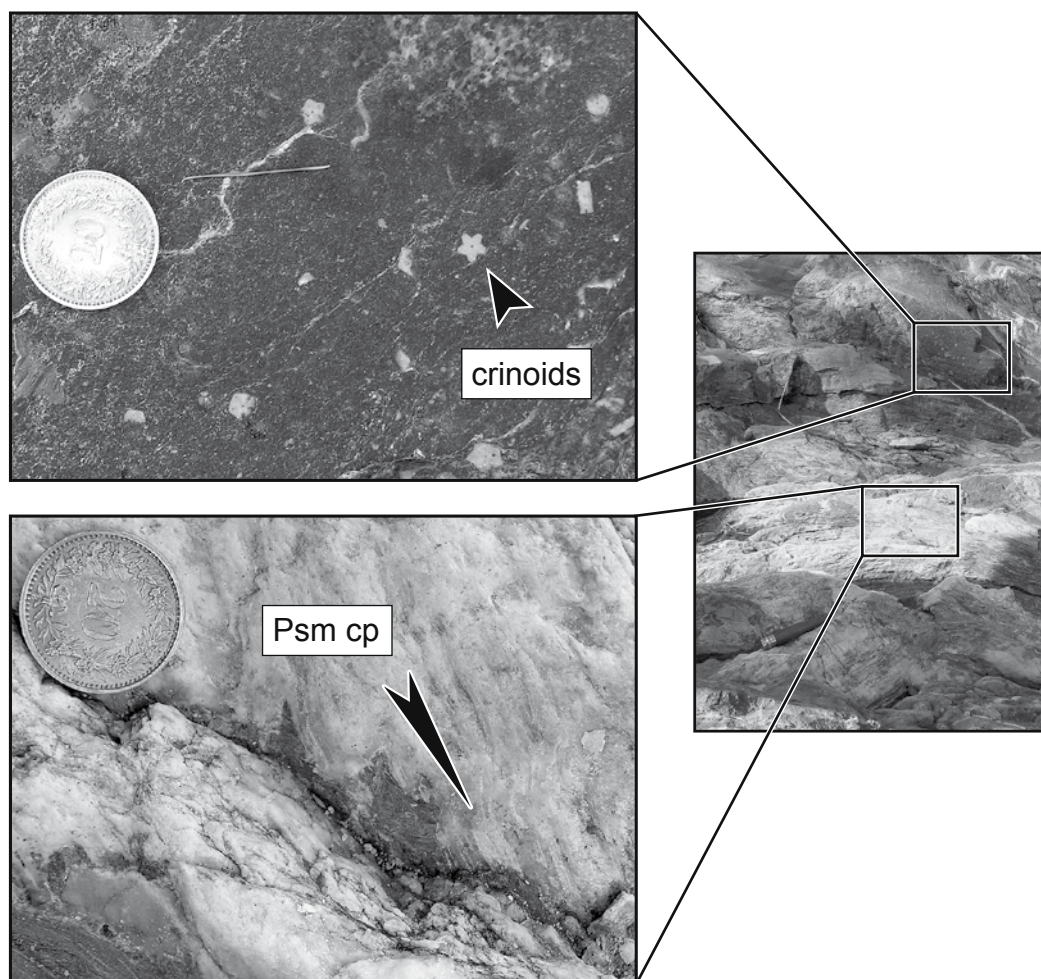


Fig. 2.6: Photograph showing pseudomorphs after carpholite, together with almost undeformed crinoids in the Forca slice of the Peidener Schuppenzone (Sub-Penninic sediments; Val Luzzone, 717°364/160°358, 1860m). The black arrow in the lower picture is oriented parallel to the quartz fibres.

2.3.2. Second deformation phase (D2)

This deformation post-dates D1, since the carpholite-bearing quartz-calcite veins are isoclinally folded and overprinted by the S2 penetrative main and axial planar schistosity (Fig. 2.5b). Due to poly-phase overprinting during later phases of folding, the orientations of D2 structures, such as fold axes and fold axial planes, show a large spread in orientation. The D2 schistosity completely transposes bedding, and possibly, relics of an earlier D1 schistosity that may have existed in pelitic lithologies.

This penetrative, main D2 foliation is largely formed by phengite and chlorite, which indicates greenschist facies conditions during D2 deformation. Hence D2 was associated with early exhumation of the blueschist-facies rocks. In analogy with the findings of Bucher & Bousquet (2007) and Bucher et al. (2003, 2004) in the Western Alps, we interpret this main phase of nappe stacking to be associated with the exhumation of high-pressure rocks. Thereby relatively more internal and higher-pressure units were thrust onto relatively more external and lower-pressure units.

2.3.3. Third deformation phase (D3)

D3 deformation produces tight mega-folds such as the Lunschania antiform (Figs. 2.1 & 2.3), as well as folds observable at the mesoscopic and microscopic scale. A second strong axial planar cleavage S3 is associated with D3 folding. However, the distinction between S2 and S3 can only be made in D3

fold hinges where S3 represents a spaced cleavage (Fig. 2.5c), while S3 completely transposes S2 in F3 fold limbs. In most places the main foliation represents a composite S2/S3 schistosity.

Due to D4 overprint in the western part of the working area, the D3 fold axes and fold axial planes often show variable orientations. Further east (east of Vrin), D3 fold axes strike SW – NE, plunging gently either NE or SW; fold axial planes steeply dip SE to SSE. There a crenulation is often associated with D3 deformation, the crenulation lineation being oriented parallel to D3 fold axes.

2.3.4. Fourth deformation phase (D4)

D4 deformation is only observed in the SW part of the investigated area (Figs. 2.1 & 2.2), strain intensity rapidly decreasing towards the NE. D4 deformation sets in east of Piz Terri while intensive folding affects the area around Pizzo Molare and between the southern Lukmanier area and Olivone (Figs. 2.2 & 2.3). D4 folds are open, often without an axial planar schistosity. They refold the S2/S3 composite schistosity (Fig. 2.5d). Typically, D4 folds have an undulating and wavy appearance, producing a staircase-like set of syn- and antiforms on the macroscopic scale, striking E-W to ESE-WNW (Figs. 2.2 & 2.3).

However, a new axial plane schistosity S4 locally evolves in fold hinges of tighter D4 folds and overprints the S2/S3 composite foliation. In such cases this new S4 foliation represents a pressure solution cleavage producing microlithons within which overprinting of the S2/S3 composite foliation is well preserved on a microscopic scale.

The E-W striking D4 fold axes dip moderately (20-40°) towards the E in most of the working area. Only around Pizzo Molare and south of Olivone the fold axes dip towards SE-ESE. It is important to note that the D4 fold axial planes generally plunge with 30-50° to the NE. Hence the D4 folds represent back-folds, which are typical for the so-called Northern Steep Belt at the northern rim of the Lepontine dome (Milnes 1974).

2.4. New data regarding the metamorphic evolution of the area

A remarkable metamorphic field gradient is deduced for the investigated area, ranging from low-temperature (≤ 400 °C) blueschist facies metamorphism in the east all the way to classical Barrow-type amphibolite facies overprint (up to 570 °C) further west (Figs. 2.1 & 2.2). Moreover, for the first time we are able to distinguish between two separate metamorphic stages in the Sub-Penninic and Lower Penninic meta-sedimentary units in the north-eastern Lepontine: an earlier HP/LT event is followed by a MP/MT Barrovian event.

2.4.1. Spatial distribution of index minerals and mineral parageneses

The HP/LT event is documented by the mineral assemblage Fe-Mg carpholite-chlorite-phengite-quartz \pm chloritoid, relics of which are widespread in the Lower Penninic Grava and Tomül nappes east of the Lepontine dome (Bousquet et al. 2002). Remnants of this assemblage, notably relics and/or pseudomorphs after Fe-Mg carpholite, are even found in the westernmost exposures of the Grava nappe as far as Pizzo Molare, hence in an area well inside the thermally overprinted realm of the Lepontine dome (Fig. 2.2). Relics and pseudomorphs after Fe-Mg carpholite were also found further north within the imbricated Sub-Penninic Peidener Schuppenzone. There, such pseudomorphs occur as fibrous quartz-calcite veins, which crosscut meta-sedimentary units containing almost undeformed crinoids (Fig. 2.6). This documents for the first time that HP/LT metamorphic conditions also affected Ultrahelvetic meta-

sediments, derived from the former distal European margin. This clearly points to the existence of a second and more northerly-located Alpine subduction zone with respect to the Upper Penninic Suture Zone, as pointed out by several authors (e.g. Stampfli 1993; Stampfli et al. 1998; Bousquet et al. 2002; Nagel et al. 2002a; Froitzheim et al. 2003; Pleuger et al. 2003).

The classical Barrow-type amphibolite facies overprint is associated with a pronounced metamorphic field gradient. Towards the south-west a gradual succession of newly growing minerals indicates an increase in temperature from greenschist to lower/middle amphibolite facies conditions. This is deduced from the progressive appearance of chloritoid, zoisite, plagioclase, titanite, biotite, garnet, staurolite, kyanite and finally amphibole (Fig. 2.2). Furthermore, in the south-western part of the working area around Pizzo Molare and between Olivone and the southern Lukmanier area, where pseudomorphs of Fe-Mg carpholite are also present, the mineral assemblage staurolite-kyanite-garnet-plagioclase-biotite-phengite±amphibole clearly indicates a thermal overprint under lower to middle amphibolite facies conditions (Chadwick 1968; Frey 1969; Thakur 1971; Engi et al. 1995). Towards the north-east the mineral parageneses chloritoid-phengite-chlorite-quartz and zoisite/clinozoisite-chlorite-phengite-quartz-calcite/dolomite indicate greenschist facies conditions related to the same Barrow-type event (Jung 1963; Frey 1967; Frey & Ferreiro Mählmann 1999). In contrast to the earlier HP/LT event, restricted to the Grava nappe and the Peidener Schuppenzone, the Barrow-type overprint affected all the units of the working area (Fig. 2.2). In the following the new data concerning the two metamorphic events will be described in more detail.

2.4.2. Data on the earlier HP/LT metamorphic event

Occurrences or relics of the HP/LT mineral assemblage Fe-Mg carpholite-chlorite-phengite-quartz±chloritoid are only found within quartz- and calcite-bearing veins or segregations. Fibrous mesoscopic appearance and characteristic light green silvery colour of such veins or segregations resemble the typical Fe-Mg carpholite pseudomorphs described in the literature (Fig. 2.5a; Goffé & Chopin 1986; Goffé et al. 1989; Fournier et al. 1991). It is important to emphasise that in the study area Fe-Mg carpholite was never found in the matrix of the rocks; it exclusively occurs within veins and/or segregations. This, together with the fact that undeformed crinoids are found in the neighbouring rocks next to these veins (Fig. 2.6), indicates that carpholite growth occurred in the context of veining and dehydration, i.e. probably during subduction.

However, Fe-Mg carpholite is only preserved in the form of microscopic-scale relics (Fig. 2.7a) within quartz-calcite segregations or veins that represent macroscopically visible pseudomorphs after large former Fe-Mg carpholite crystals (Fig. 2.5a). No Fe-Mg carpholite crystals preserved on a macroscopic scale, such as described from the Engadine window (Bousquet et al. 1998), were found. The macroscopic pseudomorphs are mainly built up by fibrous quartz (Fig. 2.5a). Its shimmering silver-green lustre is due to a thin layer of chlorite and phengite. In thin section, fibrous quartz is full of inclusions of chlorite, phengite and paragonite. This assemblage often forms needle-shaped pseudomorphs after Fe-Mg-carpholite (Fig. 2.7b). Rarely chloritoid has also been found as inclusions in such fibrous quartz-calcite veins.

In order to estimate peak-pressure conditions, the chemical compositions of HP/LT minerals were determined by wavelength-dispersive X-ray analysis (WDS) using a CAMECA SX-100 electron microprobe at the GeoForschungsZentrum (GFZ) Potsdam. The analytical conditions included an acceleration voltage of 15 kV, a beam current of 20 nA and beam diameters of 1-10 µm; PAP corrections were

applied. Natural and synthetic minerals were used as standards. Peak counting times were 10-20 s for major and 20-40 s for minor elements; backgrounds were counted for 5-20 s.

Relics of Fe-Mg carpholite are hair-thin micro-fibres (10 to 100 μm long, 0.5 to 10 μm wide) embedded in quartz (Fig. 2.7a) documented by Raman spectroscopy and microprobe analysis. In order to avoid the effect of contamination by the surrounding quartz, the chemical composition of Fe-Mg carpholite $[(\text{Mg,Fe,Mn})\text{Al}_2\text{Si}_2\text{O}_6(\text{OH,F})_4]$ was calculated on the basis of a fixed atomic number of cations (Goffé & Oberhänsli 1992). The value of X_{Mg} $[\text{Mg}/(\text{Mg}+\text{Fe}+\text{Mn})]$ is rather constant, ranging from 0.44 to 0.55 (mean value 0.49) in the Penninic Bündnerschiefer of the Grava nappe, and from 0.39 to 0.57 (mean value 0.49) in the Sub-Penninic Peidener Schuppenzone (Table 2.1). Generally the fluorine content is very low and varies from 0.0 to 0.99 wt %.

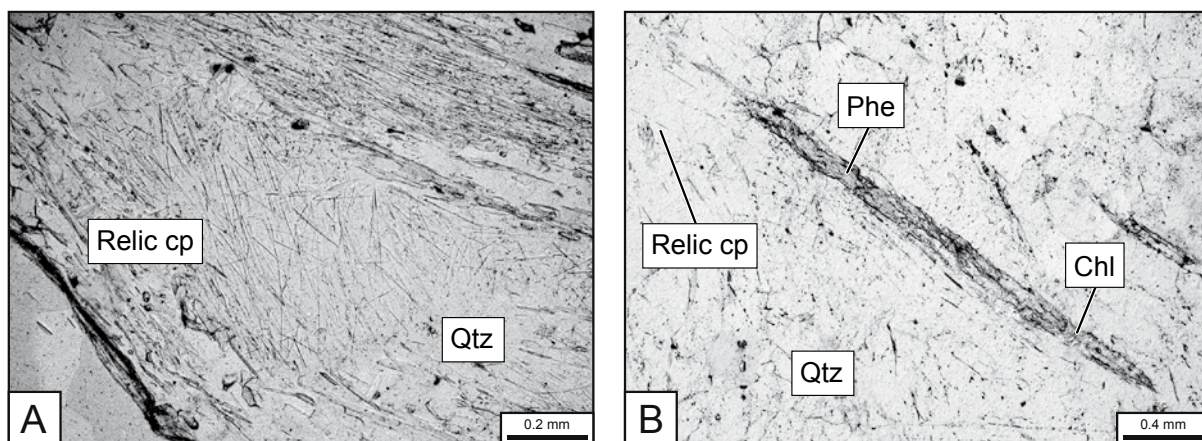


Fig. 2.7: Photomicrographs of thin sections showing mineral assemblages related to the HP/LT event, preserved as inclusions in quartz-calcite fibrous veins generally interpreted as pseudomorphs after Fe-Mg carpholite. (A) Hair-like fibres represent relics of Fe-Mg carpholite (cp) as inclusions in quartz (SW of Vrin, 723°990/166°197, 1890m). (B) Phengite, quartz and chlorite define a needle-shaped pseudomorph after carpholite. Still preserved relics of carpholite can be found as hair-like fibres (Val Luzzzone, 720°938/162°275, 2600m).

White mica is also found as inclusions in quartz grains. Both phengite and paragonite are present and associated with chlorite and quartz. They form also part of the pseudomorphs after Fe-Mg carpholite (Fig. 2.7b). There, phengite and paragonite occur as fine-grained flakes without any shape preferred orientation. The Si^{4+} content, reflecting the phengitic substitution in white mica replacing Fe-Mg carpholite, ranges from 3.24 in the Valais Bündnerschiefer to 3.12 p.f.u in the Sub-Penninic Peidener Schuppenzone (Table 2.1).

Chlorite occurs as randomly arranged grains, together with white mica and quartz, but also within pseudomorphs after Fe-Mg carpholite (Fig. 2.7b). In the Valais Bündnerschiefer the Tschermak substitution in chlorites is around 2.57 - 2.70 (Si p.f.u.), X_{Mg} ranging from 0.43 to 0.60. In the Sub-Penninic sediments between 2.52 and 2.61 Si p.f.u. and X_{Mg} from 0.44 to 0.48 were measured (Table 2.1).

Only in a few cases chloritoid was found inside quartz-calcite segregations containing relics of Fe-Mg carpholite. Such chloritoid forms small prisms with X_{Mg} -values varying between 0.12 in the Valais Bündnerschiefer and 0.20 in the Sub-Penninic meta-sediments (Table 2.1). This chloritoid is interpreted to have formed during prograde metamorphism by reaction from Fe-Mg carpholite, as shown by Vidal et al. (1992); i.e. during the high-pressure stage rather than during a greenschist facies event (see discussion in Oberhänsli et al. 2003).

Table 2.1: Representative microprobe mineral analyses of HP/LT assemblages found as inclusions in quartz-calcite veins, interpreted as pseudomorphs after carpholite of Valaisan (Grava nappe) and Sub-Penninic (Peidener Schuppenzone) meta-sedimentary units given in weight-percents. The locations of the samples are shown in Figure 2.2. The deviations from 100 % are mainly due to the OH-content not detected by microprobe analyses. The sums of Fe-Mg carpholite analyses have been corrected for fluorine content; the values given under “Total corr.” take into account that fluorine occupies an oxygen site. The structural formulae for carpholite were calculated by using 5 cations for Si and 3 cations for Al, Fe, Mn and Mg, following Goffé & Oberhänsli (1992). For chlorite we used 14 oxygens, for white mica 11 and for chloritoid 12, following Chopin et al. (1992). The following abbreviations have been used: Cp = Fe-Mg carpholite, Ctd = chloritoid, Chl = chlorite, Phe = phengite, Pg = paragonite.

Unit	Valaisan Bündnerschiefer (Grava nappe)									Sub-Penninic sediments (Peidener Schuppenzone)					
	LUZ 0432					LUZ 0416				Forca slice				Pianca slice	
	LUZ 0432					LUZ 0416				LUZ 047				LAR 061	
Sample	Cp	Ctd	Chl	Phe	Pg	Cp	Chl	Phe	Cp	Ctd	Chl	Phe	Cp	Chl	Phe
Minerals	Cp	Ctd	Chl	Phe	Pg	Cp	Chl	Phe	Cp	Ctd	Chl	Phe	Cp	Chl	Phe
Analysis (wt-%)	Cp828	Ctd215	Chl219	Phe221	Pg220	Cp849	Chl207	Phe224	Cp9B	Ctd16	Chl5	Phe1	Cp12	Chl4	Phe12
SiO ₂	37.40	24.46	25.36	49.46	48.43	37.63	25.30	48.60	37.85	25.32	23.17	47.18	38.00	23.63	47.20
TiO ₂	0.19	0.01	0.04	0.20	0.04	0.25	0.06	0.17	0.00	0.00	0.06	0.13	0.27	0.03	0.00
Al ₂ O ₃	31.11	39.36	22.91	33.52	40.30	31.31	22.40	34.08	32.41	38.80	23.57	35.94	30.02	22.60	36.34
Cr ₂ O ₃	0.03	0.00	0.00	0.00	0.00	0.00	0.00	0.00	0.00	0.00	0.00	0.00	0.03	0.00	0.00
FeO	11.44	25.42	27.37	1.34	0.20	12.64	26.51	1.24	10.92	22.55	27.27	0.81	13.90	27.05	0.49
MnO	0.25	0.06	0.02	0.00	0.01	0.30	0.05	0.00	0.06	0.27	0.01	0.00	0.03	0.08	0.01
MgO	6.32	1.85	12.73	1.39	0.12	5.68	13.39	1.20	6.27	2.83	11.98	0.85	6.49	12.62	0.62
CaO	0.00	0.00	0.00	0.00	0.07	0.02	0.01	0.00	0.01	0.00	0.00	0.00	0.04	0.03	0.02
Na ₂ O	0.00	0.00	0.04	0.67	7.26	0.00	0.00	0.76	0.01	0.00	0.01	0.84	0.04	0.03	0.92
K ₂ O	0.04	0.00	0.02	8.82	1.11	0.03	0.01	9.12	0.02	0.01	0.01	8.75	0.00	0.02	8.59
BaO	0.00	0.00	0.00	0.00	0.00	0.00	0.00	0.00	0.00	0.00	0.00	0.00	0.00	0.00	0.00
F	0.65	0.00	0.00	0.00	0.00	0.77	0.00	0.00	0.49	0.00	0.00	0.00	0.00	0.00	0.00
Total	87.43	91.15	88.48	95.39	97.54	88.64	87.72	95.16	88.03	89.78	86.07	94.50	88.76	86.08	94.19
Total corr.	87.17	91.15	88.48	95.39	97.54	88.32	87.72	95.16	87.83	89.78	86.07	94.50	88.76	86.08	94.19
Si	2.00	2.05	2.67	3.24	3.02	2.00	2.67	3.20	2.00	2.13	2.52	3.12	2.00	2.57	3.12
Ti	0.01	0.00	0.00	0.01	0.00	0.01	0.00	0.01	0.00	0.00	0.00	0.01	0.01	0.00	0.00
Al	1.96	3.90	2.84	2.59	2.96	1.96	2.79	2.64	2.02	3.85	3.02	2.80	1.86	2.90	2.83
Cr	0.00	0.00	0.00	0.00	0.00	0.00	0.00	0.00	0.00	0.00	0.00	0.00	0.00	0.00	0.00
Fe ²⁺	0.04	0.05	-	-	-	0.04	-	-	0.00	0.02	-	-	0.14	-	-
Fe ³⁺	0.47	1.74	2.41	0.07	0.01	0.52	2.34	0.07	0.52	1.56	2.48	0.04	0.47	2.46	0.03
Mn	0.01	0.00	0.00	0.00	0.00	0.01	0.00	0.00	0.00	0.02	0.00	0.00	0.00	0.01	0.00
Mg	0.50	0.23	1.99	0.14	0.01	0.45	2.11	0.12	0.49	0.35	1.94	0.08	0.51	2.04	0.06
Ca	0.00	0.00	0.00	0.00	0.00	0.00	0.00	0.00	0.00	0.00	0.00	0.00	0.00	0.00	0.00
Na	0.00	0.00	0.01	0.08	0.88	0.00	0.00	0.10	0.00	0.00	0.00	0.11	0.00	0.01	0.12
K	0.00	0.00	0.00	0.74	0.09	0.00	0.00	0.77	0.00	0.00	0.00	0.74	0.00	0.00	0.72
Ba	0.00	0.00	0.00	0.00	0.00	0.00	0.00	0.00	0.00	0.00	0.00	0.00	0.00	0.00	0.00
F	0.11	0.00	0.00	0.00	0.00	0.13	0.00	0.00	0.08	0.00	0.00	0.00	0.00	0.00	0.00
XMg	0.51	0.12	0.45			0.46	0.47		0.49	0.18	0.44		0.52	0.45	

2.4.3. Data on the subsequent temperature-dominated event

While remnants of the HP/LT metamorphic event are restricted to quartz-calcite segregations within the Lower Penninic Bündnerschiefer and the Sub-Penninic Peidener Schuppenzone, the temperature-dominated Barrovian event affected all tectonic units (Fig. 2.2). From north-east to south-west, i.e. from greenschist to lower/middle amphibolite facies overprint, the following mineral assemblages are described.

Greenschist facies: Chloritoid growing during the second metamorphic event and at the expense of pyrophyllite and chlorite can be texturally distinguished from that produced by the breakdown of Fe-Mg carpholite. Whereas the scarce occurrences of HP/LT chloritoid are restricted to microscopic-scale inclusions in quartz-calcite veins containing preserved relics of Fe-Mg carpholite, LP/LT chloritoid occurs in the rock-matrix as idiomorphic rosettes, bundles and prisms, together with quartz, white mica and chlorite. It is common in shaly formations of the Stgir and Coroi series of the Gotthard-Mesozoic (Scopi unit and Peidener Schuppenzone), as well as in quartzitic formations of the Piz Terri-Lunschana unit (Jung 1963; Frey 1967; Probst 1980; Fig. 2.2). The mineral assemblage chloritoid – white mica – chlorite – quartz is typical for the Sub-Penninic sedimentary units in the study area. The overlying Lower Penninic Bündnerschiefer are characterised by the mineral assemblage phengite-chlorite-quartz-calcite/dolomite. However, chloritoid has not been identified with the exception of rare occurrences in

quartz-calcite veins interpreted as relics of the HP/LT stage, as discussed above. The lack of chloritoid is most probably due to the bulk rock composition in the Lower Penninic Bündnerschiefer, which is generally Ca-rich and Al-poor.

Upper greenschist facies: In the Val Luzzone area, the mineralogical composition of the Lower Penninic Bündnerschiefer changes dramatically (Fig. 2.2). Newly formed zoisite/clinozoisite, plagioclase and titanite indicate an increase in temperature. This is corroborated by the mineral assemblage plagioclase – zoisite/clinozoisite – titanite – phengite – chlorite – quartz – calcite/dolomite found in marly or calcareous schists of the Grava nappe. When entering the upper greenschist facies stability field, zoisite/clinozoisite is the first newly grown mineral observed. Based on mineral shape and composition the following two zoisite/clinozoisite types are found within the same rocks (Frank 1983; Kuhn et al. 2005): (1) Fine-grained, needle-shaped, prismatic zoisite/clinozoisite, enriched in Fe^{3+} relative to Al^{VI} with an X_{Ep} [$\text{Fe}^{3+}/(\text{Fe}^{3+}+\text{Al}-2)$] of 0.15-0.20. Some grains show distinct compositional zoning, with cores being richer in Fe^{3+} compared to the rims (X_{Ep} core = 0.63; rim = 0.20), and, (2) an almost pure Al-end member with X_{Ep} of 0.03-0.05 forming relatively large crystals arranged as rosettes and sheaves, up to 5 cm in diameter (Fig. 2.8a). Plagioclase forming black plates up to several mm in size is present as oligoclase, with an An-content varying between 0.19 and 0.36. Titanite, another characteristic mineral of this zone, forms bi-pyramidal crystals up to 3 mm in size.

Upper greenschist to amphibolite facies transition: Biotite first appears west of the retaining wall of Lago di Luzzone within the Lower Penninic Bündnerschiefer (Fig. 2.2). This site roughly coincides with the north-eastern border of the Lepontine thermal dome as mapped by Spicher (1980). The assemblage biotite – plagioclase – zoisite/clinozoisite – titanite – phengite – quartz – calcite/dolomite \pm chlorite is characteristic for the upper greenschist to amphibolite facies transition. The Jurassic sediments of the Sub-Penninic units (Stgir series of the Peidener Schuppenzone) are less calcareous and more pelitic than the overlying Lower Penninic Bündnerschiefer (Fox 1975). This difference in chemical composition led to the formation of garnet in the Stgir series, which is absent in the Lower Penninic Bündnerschiefer in the study area. Garnet first appears north of Olivone (northern Valle di Blenio; Figs. 2.1 & 2.2) within the assemblage garnet – biotite – plagioclase – phengite – quartz \pm chlorite \pm zoisite/clinozoisite. The co-existence of garnet and biotite is typical for the upper greenschist to amphibolite facies transition (Bucher & Frey 2002). The almandine-rich garnets ($\text{Alm}_{0.71}\text{Prp}_{0.06}\text{Grs}_{0.21}\text{Sps}_{0.02}$) are chemically more or less unzoned and form crystals up to 1 cm in size.

Lower to middle amphibolite facies: Kyanite, staurolite and amphibole appear in addition further SW (Valle di Blenio, Pizzo Molare, and south of the Lukmanier pass; Figs. 2.1 & 2.2). Pelitic metasediments of the Sub-Penninic units are characterised by the mineral assemblage staurolite – kyanite – garnet – biotite – plagioclase – phengite – quartz (Baumer 1964; Chadwick 1968; Frey 1969; Thakur 1971; Fox 1975; Probst 1980), typically indicating lower to middle amphibolite facies conditions. In general, garnet is almandine-rich and shows a normal zoning pattern with increasing Mg- and decreasing Mn-content from core to rim. Garnets from the Pizzo Molare area yield $\text{Alm}_{0.62}\text{Prp}_{0.06}\text{Grs}_{0.23}\text{Sps}_{0.09}$ for the core and $\text{Alm}_{0.68}\text{Prp}_{0.12}\text{Grs}_{0.20}\text{Sps}_{0.00}$ for the rim. The An-content of plagioclase ranges between 0.16 and 0.30. The more calcareous chemistry of the Valaisan Bündnerschiefer does not allow for the growth of these new minerals; the assemblage biotite – plagioclase – zoisite/clinozoisite – titanite – phengite – quartz – calcite/dolomite \pm chlorite still persists in this metamorphic zone.

2.4.4. Correlations between the structural and metamorphic evolution

The early HP/LT event was associated with the formation of quartz-calcite veins containing pseudomorphs after Fe-Mg carpholite indicating blueschist facies conditions. We infer that these veins formed during D1 since they were folded by isoclinal F2 folds (Figs. 2.5b, c & d). These isoclinal folds are associated with a D2 penetrative axial planar foliation that formed under greenschist-facies conditions. From this we deduce that greenschist-facies conditions were already established during D2.

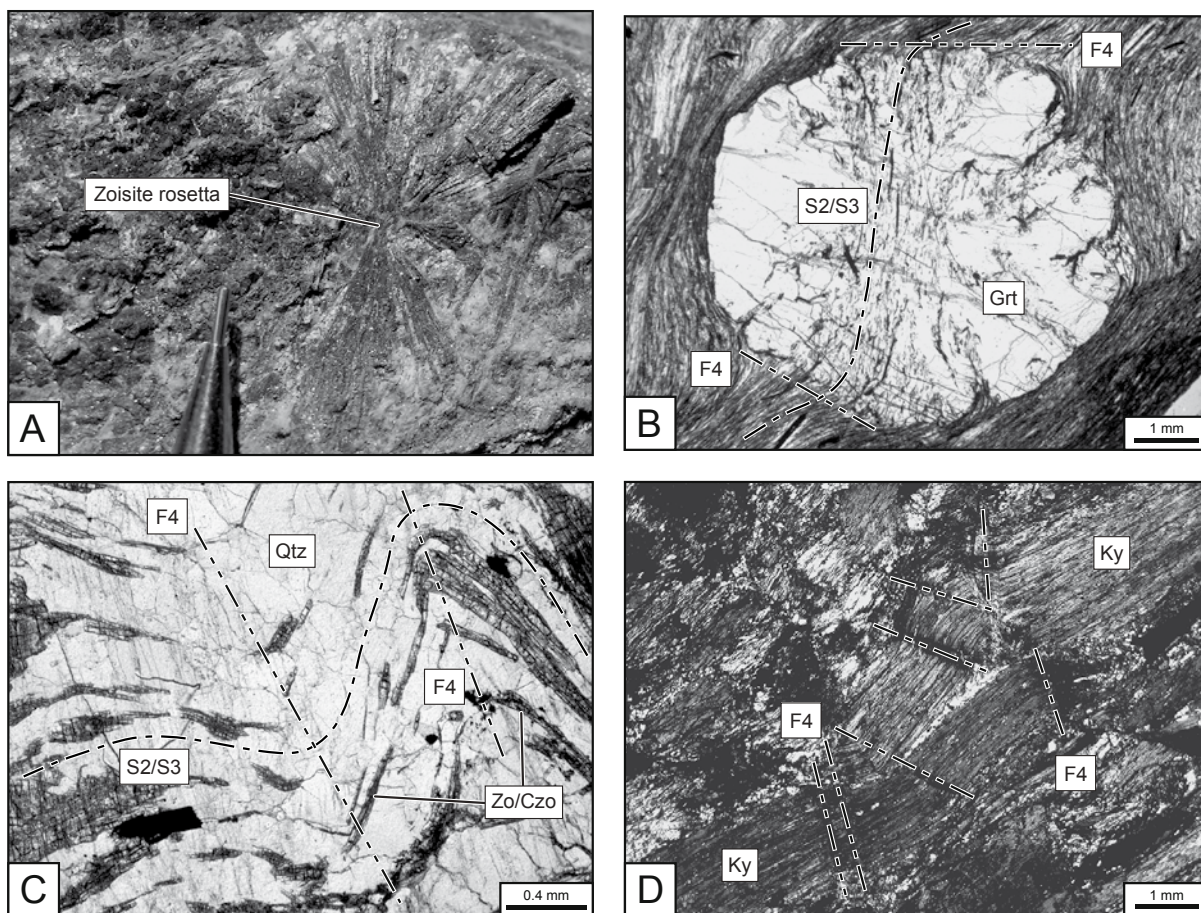


Fig. 2.8: Photographs showing microstructural relationships between porphyroblasts related to Barrovian overprint and deformation phases. (A) Rosetta of zoisite growing over the S2/S3 composite main foliation (Val Luzzzone, 716°469/158°124, 1450m). (B) Straight internal S2/S3 composite foliation inside a garnet porphyroblast (Grt), slightly curving at the rim; deflection of the S2/S3 foliation around the garnet and its relative rotation are the effects of subsequent D4 deformation (Val Luzzzone, 715°029/156°841, 1190m). (C) Zoisite/clinozoisite needles (Zo/Czo) oriented parallel to the S2/S3 composite main foliation are broken and bent by D4 deformation (Val Luzzzone, 716°093/157°771, 1390m). (D) Needles of kyanite (Ky) kinked by D4 folds (S of Pizzo Molare, 709°541/149°308, 2310m).

Porphyroblasts related to Barrow-type thermal overprint, such as chloritoid, zoisite/clinozoisite, titanite, plagioclase, biotite, garnet, kyanite, staurolite and amphibole, all clearly overgrow the S2/S3 composite main foliation and have no shape preferred orientation (Figs. 2.8a & b). Big flakes of biotite typically grow across the S2/S3 main foliation (“Quer-Biotit”). This implies a temporal hiatus between syn-D1 HP/LT metamorphism and post-D2/D3 Barrow-type overprint. Moreover, the random orientation of porphyroblasts related to Barrow-type thermal overprint, as well as the conservation of an unfolded internal S2/S3 compositional foliation in the cores of garnets (Fig. 2.8b), both indicate that at least the initial stages of the Barrovian overprint occurred under static conditions in most parts of the working area. The famous syn-D4 snowball garnets (Chadwick 1968; Fox 1975; Robyr et al. 2007) represent an exception and are restricted to a specific level of the Stgir series.

Deformation phases		D1 <i>Safien</i>	D2 <i>Ferrera</i>	D3 <i>Domleschg</i>		D4 <i>Chièra</i>	
Regional structures		formation of quartz-calcite veins	composite main foliation (S2/S3)			Chièra sf	
				Valzeina sf Lunschana af Alpettas sf Darlun af			
Crystallisation	Sub-Penninic metasediments (<i>Peidener Schuppenzone</i>)	Fe-Mg Carpholite Chloritoid Zoisite/Clinozoisite Plagioclase Biotite Garnet Kyanite Staurolite White mica Chlorite Quartz Calcite/Dolomite					
	Valaisan Bündnerschiefer (<i>Grava nappe</i>)	Fe-Mg Carpholite Chloritoid Zoisite/Clinozoisite Titanite Plagioclase Biotite White mica Chlorite Quartz Calcite/Dolomite					
Metamorphic facies		Blueschist		Greenschist	Amphibolite	Greenschist	
Major tectonic events		Accretion and subduction formation of the orogenic wedge	Nappe stacking decompression formation of the basal Penninic thrust	Nappe re-fold event formation of the Southern Steep Belt	Metamorphic crystallisation with minor or no deformation	Nappe re-fold event formation of the Northern Steep Belt	

Fig. 2.9: Summary of relationships between crystallisation and deformation in the Lower Penninic and Sub-Penninic metasediments; sf: synform, af: antiformal.

In most places the Barrovian mineral assemblages have been overprinted by D4 crenulation deformation; needles and prisms of chloritoid, zoisite/clinozoisite and kyanite are kinked, bent or broken (Figs. 2.8c & d). Most garnet porphyroblasts show some rotation of the internal S2/S3 foliation towards the rims (Fig. 2.8b), indicating that the last stages of the garnet growth occurred during D4. However the D2/D3 composite foliation is strongly crenulated in the rock-matrix outside of the garnet, indicating that most of the D4 crenulation post-dates the growth of garnet.

In summary (see Figs. 2.9 & 2.10), the Barrovian-type thermal overprint definitely post-dates D3 and started during a period without any significant deformation. The HP/LT event, however, was syn-D1 and terminated before D2. This implies that greenschist facies conditions were already established during decompression from the HP/LT stage and before the Barrow-type heating event.

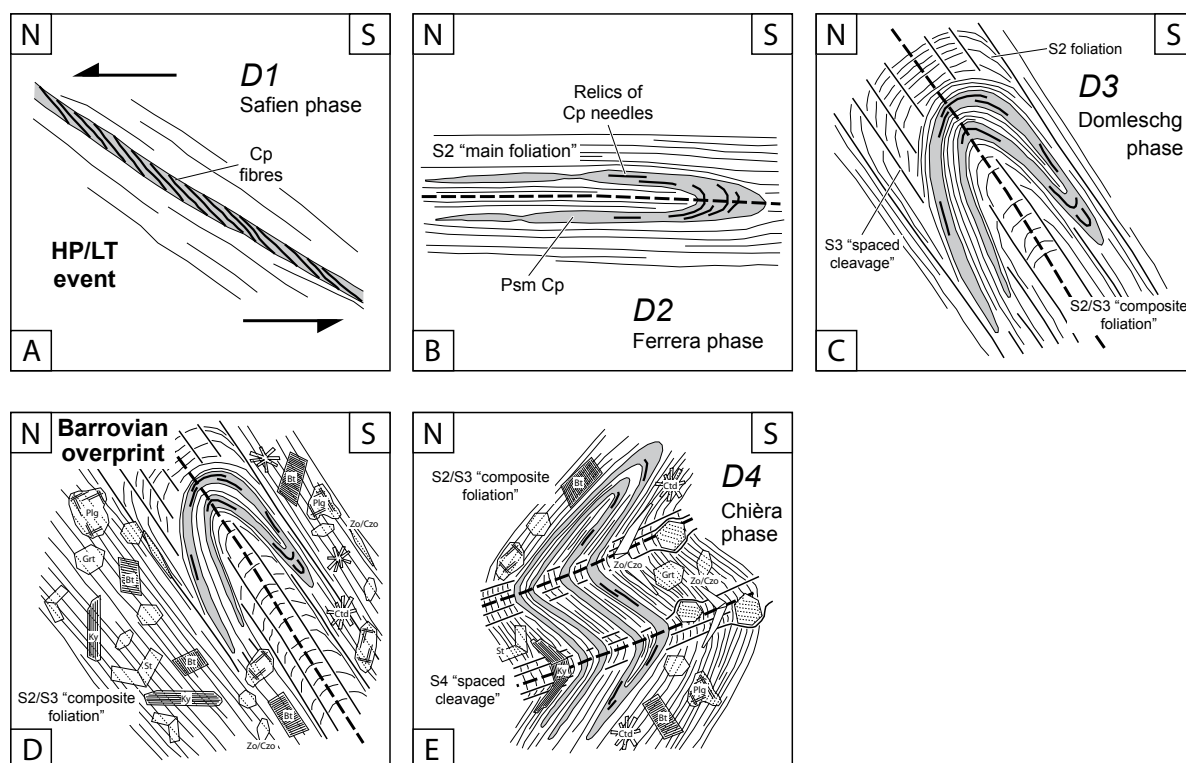
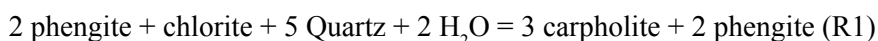


Fig. 2.10: Schematic sketches illustrating the tectono-metamorphic evolution in the study area. (A) Formation of fibrous quartz-calcite veins and Fe-Mg carpholite related to the HP/LT event, i.e. subduction (D1, Safien phase). (B) Pseudomorphs after carpholite, refolded by D2 (Ferrera phase), associated with the formation of the main penetrative foliation S2. (C) main foliation and earlier formed pseudomorphs after carpholite, refolded by D3 (Domleschg phase) and overprinted by a new spaced cleavage S3. (D) Amphibolite-facies Barrovian overprint leading to the growth of new porphyroblasts over the pre-existing S2/S3 composite foliation under static conditions. (E) D4 (Chièra phase), refolding the quartz-calcite veins a third time and deforming the amphibolite-facies mineral assemblages.

2.4.5. Relations between HP/LT and MP/MT metamorphism: Significance of a metamorphic field gradient

Pressure-dominated metamorphic event

Peak-pressure and -temperature conditions can be estimated from the composition of coexisting phengite, Fe-Mg carpholite, and chloritoid according to Bousquet et al. (2002). P-T calculations were carried out with the GEO-CALC software (Brown et al. 1988), by using the updated JAN92.RGB thermodynamic database (Berman 1988), Mg-carpholite data from Vidal et al. (1992), Mg-chloritoid data of B. Patrick (listed in Vidal & Theye 1996), and alumino-celadonite data from Massonne (1995). The mineral activities used are listed in Bousquet et al. (2002). In the working area, the measured mineral compositions of Fe-Mg carpholite, phengite, and chloritoid are similar to those described by Goffé & Oberhänsli (1992), Oberhänsli et al. (1995) and Bousquet et al. (2002). The pressure conditions for carpholite-bearing rocks are defined by the location of the equilibrium (Fig. 2.11):



while the stability field of Fe-Mg carpholite towards higher temperature is limited by the equilibrium: carpholite = chloritoid + quartz + 2 H₂O (R2)

From the mineral chemistry of the observed mineral assemblage and the position of the above-described equilibria, peak metamorphic conditions of 1.2-1.4 GPa and 350-400 °C are estimated for both Lower Penninic Bündnerschiefer and Sub-Penninic meta-sediments of the Peidener Schuppenzone (Fig. 2.11), similar to the P-T conditions estimated in the Safiental further to the east (Bousquet et al. 2002).

Most of the meta-sediments show retrogressed greenschist-facies assemblages documented by the widespread mineral assemblage phengite-paragonite-chlorite-quartz-calcite/dolomite. However, the preservation of Fe-Mg carpholite relics, as well as a retrograde path mainly characterised by the decay of Fe-Mg carpholite to chlorite and phengite (following R1; Fig. 2.11) forming pseudomorphs after

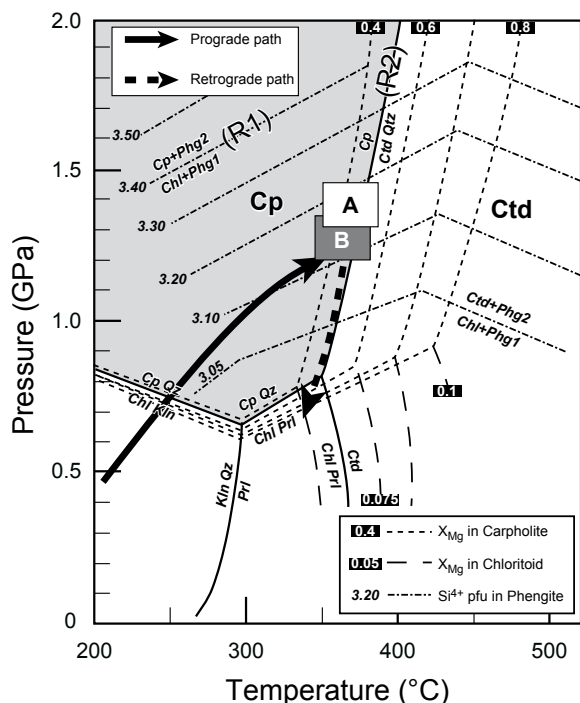


Fig. 2.11: Estimated P-T conditions for the Valaisan (Lower Penninic) Bündnerschiefer (A) and the European (Sub-Penninic) meta-sediments (Peidener Schuppenzone, B). P-T conditions have been estimated for Fe-Mg carpholite-phengite-chlorite-quartz±chloritoid assemblages (only preserved in quartz-calcite veins) using the chemistry of the different minerals (Table 2.1) according to reactions R1 & R2 (see explanations in the text). Peak-pressure conditions were established very close to the position of the reaction R2, as is documented by the scarce occurrences of chloritoid that formed by the breakdown of Fe-Mg carpholite along the prograde path, i.e. during the HP/LT stage. The preservation of both Fe-Mg carpholite and associated rare occurrences of HP/LT chloritoid imply near-isothermal decompression from the HP/LT stage (Bousquet et al. 1998). Petrogenetic grid for HP/LT metapelites after Bousquet et al. (2002, 2008).

is strictly irreversible (Pesquera & Velasco 1988) this geothermometer always records the peak temperature reached by a rock specimen along its P-T loop, with a relative accuracy in the order of 10-15 °C (Beysac et al. 2004). Here we only present the main results of this analysis of the “field thermal gradient” (Bollinger et al. 2004); details on method and results will be published elsewhere.

The peak temperatures derived from the Raman spectra obtained from over 140 samples collected between the Lucomagno/Pizzo Molare area in the west and Safiental in the east continuously increase from 350°C in Safiental to 570°C at the Pizzo Molare over an amazingly short distance along strike (Fig. 2.12). Most of this increase in temperature occurs in the Val Luzzzone, i.e. between Piz Terri and Olivone. Further east a fairly homogeneous temperature between 350 and 400 °C, with only a moderate gradient, has been deduced.

Comparison of the resulting temperature distribution pattern with the geological structures yields the following observation: In the south-west, the “isotherms” clearly cut all D2 nappe contacts und D3

carpholite, implies a cold (or fast) decompression path after the HP/LT metamorphic stage (Gillet & Goffé 1988). In the Engadine window and in Safiental, no re-heating during this decompression can be evidenced from the observed mineral assemblages (Bousquet et al. 1998).

Temperature-dominated, Barrow-type overprint: Results based on graphite-thermometry

The P-T conditions are only well constrained for the pelitic rocks of the Sub-Penninic sediments in the south-western part of the working area, around Pizzo Molare and the area between Olivone and southern Lukmanier. There, earlier investigations yielded 500-550 °C and 0.5-0.8 GPa (Frey 1969; Fox 1975; Engi et al. 1995; Todd & Engi 1997; Frey & Ferreiro Mählmann 1999). In order to provide more information on the temperature gradient from NE to SW associated with the Barrow-type amphibolite facies overprint, we performed graphite-thermometry following the procedure proposed by Beysac et al. (2002a). The method is based on the degree of crystallization of organic material, which is mainly temperature dependent (Buseck & Bo-Jun 1985). Relationships between grade of crystallisation and metamorphic conditions are empirically calibrated (Beysac et al. 2002a). Since graphitization of organic matter

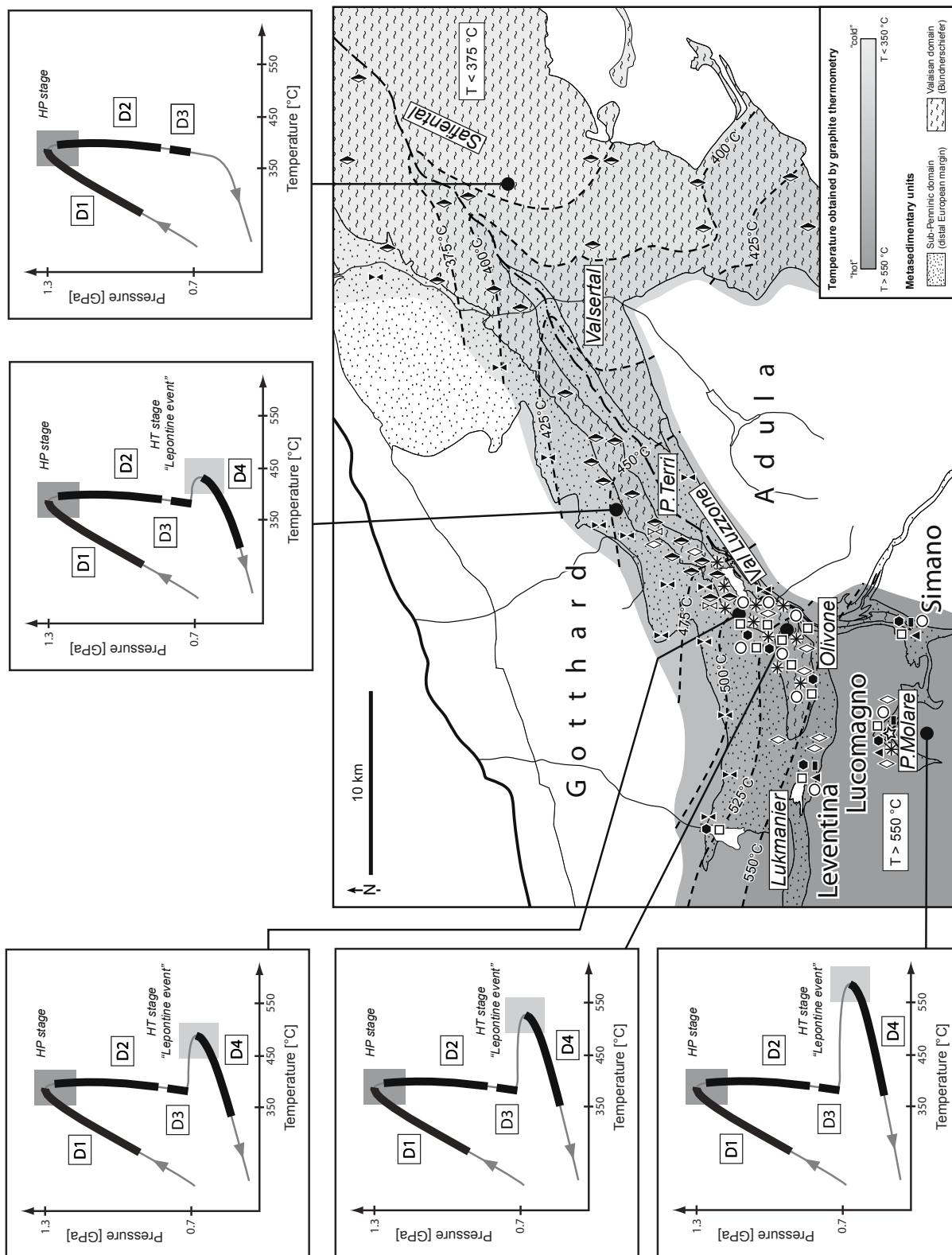


Fig. 2.12: Map of the temperature distribution obtained by graphite thermometry (Beysac et al. 2002), combined with the occurrence of index minerals. The temperature pattern in the west is young and cuts all nappe boundaries (D1 & D2) and the D3 mega-folds (Lunschania antiform). In the east, however, the temperature pattern is older and has been affected by the Lunschania antiform. The overall temperature distribution pattern results from the superposition of pressure-dominated metamorphism observed in the eastern part of the working area by a late thermal event, proposed to be caused by tectonically accreted or thickened heat-producing crustal material in the west. Five constructed P-T-d paths arranged from E to W are shown for illustrating the tectono-metamorphic evolution of the meta-sedimentary units at the north-eastern rim of the Lepontine dome.

post-nappe mega-folds, while in the north-east the “425 °C isotherm” is folded around the large scale D3 Lunschiana antiform (Fig. 2.12). This shows that the peak temperatures were reached at different times and under different metamorphic conditions in the east and west. The post-D3 temperature increase in the SW is related to the later Barrow-type overprint. The folded isotherms in the NE, however, indicate that the temperatures derived for this area are “older”, i.e. they pre-date the onset of the Barrovian overprint and are hence related to the high-pressure event and/or greenschist facies overprint that followed isothermal decompression. This in turn implies that a Barrow-type overprint possibly did not exist at all in the north-east, or was only associated with temperatures lower than 425 °C, i.e. temperature ranges previously reached during the blueschist and/or greenschist facies event.

The temperatures determined by Raman microscopy of carbonaceous rocks are in excellent agreement with previously published temperature estimates based on traditional methods in the SW part of the working area (500-550 °C; e.g. Frey & Ferreiro Mählmann 1999). They also indicate temperatures of 500-550 °C, reaching 570 °C in the Pizzo Molare area. In the north-east the inferred temperatures (<425°-375 °C) are near those inferred for the blueschist facies peak-pressure with traditional methods, ranging between 350-400 °C according to our study and that of Bousquet et al. (2002), as well as near those obtained for the greenschist facies overprint in the Grisons area (400 °C; Rahn et al. 2002).

The superposition of a Barrow-type over an earlier HP/LT evolution clearly indicates that the notion of a metamorphic field gradient can lead to misinterpretations. Strictly, a metamorphic field gradient primarily reflects the present-day distribution of pressure and/or temperature and cannot a priori be interpreted in terms of a particular geodynamic evolution.

2.5. Discussion and interpretation of the results

In the following we discuss the results obtained within the working area in a regional context and address the timing of the geodynamical evolution of the Alps. Then, in a qualitative way, we discuss possible heat sources that could be held responsible for Barrovian metamorphism in the north-eastern part of Lepontine thermal dome.

2.5.1. Regional correlations of the tectono-metamorphic evolution established in the working area and timing constraints

The D3 and D4 deformation phases led to the major features that are visible in map (Figs. 2.1 & 2.2) and cross-section (Fig. 2.3) view. D4 deformation resulted in the cascade-like geometry formed by a set of parasitic syn- and antiforms in the western part of the working area (Fig. 2.3), related to the formation of the Chièra synform which is well-developed only west of the working area (Milnes 1976; Etter 1987). There, the composite D2/D3 main foliation generally steeply dips northward and represents the overturned nappe-stack characterising the Northern Steep Belt. In our study area (Val Luzzone, Piz Terri, Val Lumnezia) the Chièra synform is only weakly developed, and instead, a series of cascade-like D4 syn- and antiforms overprint the D3 Lunschiana antiform; these gradually fade out further to the east. The overall geometry of the cross section in Figure 2.3 is characterised by progressive steepening of the main foliation from a sub-horizontal orientation in the south to a generally moderate southward dip in the north that is produced by this D4 folding; subvertical and overturned composite D2/D3 foliations and nappe contacts are restricted to the structurally lowest levels.

Our D4-event corresponds to the deformation event which is responsible for the so-called Chièra synform (Milnes 1976, Etter 1987) and will be referred to as Chièra phase. This phase can be parallel-

Table 2.2: Correlation of deformation phases defined in neighbouring tectonic units described in the literature. Grey shaded fields represent deformation events, which can be directly correlated. Note that the first and second deformation phase need not to be synchronous in all parts of the orogen, since deformation phases related to the accretionary stage migrated from internal to external. See text for further discussion of the timing constraints.

Correlation of deformation phases	<i>This study</i>		D1 <i>Safien</i>		D2 <i>Ferrera</i>			D3 <i>Domleschg</i>		D4 <i>Chièra</i>
	Major tectonic events		Accretion and subduction formation of the orogenic wedge		Nappe stacking decompression formation of the basal Penninic thrust			Nappe re-fold event formation of the Southern Steep Belt	Metamorphic crystallisation with minor or no deformation	Nappe re-fold event formation of the Northern Steep Belt
	Timing constraints						Bergell intrusion (32-30 Ma)		Metamorphic crystallisation (20-18 Ma) by mica (Ar-Ar), monazite (U-Pb)	
	Northern Steep Belt									
	Chadwick (1968)							Phase B		Phase V
	Thakur (1971)					F1		F2		F3
	Etter (1987)					D1		D2		D3
	Probst (1980)					B1, B2		B3, B4		B5
	Pennine									
	Schmid et al. (1996)	Avers			Ferrera		Niemet-Beverin	Domleschg		Chièra
Tambo/Suretta/Schams										
Milnes & Schmutz (1978)	Avers			Ferrera		Niemet	D3			
Schmid et al. (1990)				D1		D2	D3			
Prättigau Half-Window										
Weh & Froitzheim (2001)		D1a		D1b		D2	D3			
Northern Adula										
Löw (1987)		Sorreda	Zapport	Leis			Carassino ?			

ised with phase V of Chadwick (1968), D3 of Etter (1987) and Thakur (1971) and B₅ of Probst (1980), as is summarised in Table 2.2. Schmid et al. (1997a) estimated the Chièra phase to have been active during the 25-20 Ma age interval. However, new ages in the 20-18 Ma range, obtained on micas and monazite related to the Barrow-type overprint near our working area (Pizzo Molare and Val Piora area; Allaz et al. 2007; Janots et al. 2007), suggest a substantially younger, i.e. post-18 Ma age for this deformation event.

In Val Luzzone a set of D3 mega-folds was mapped. They are, from north to south: Valzeina synform, Lunschania antiform, Alpettas synform and Darlun antiform (Fig. 2.3). The profile construction of Figure 2.3 shows that we favour a correlation of the D3 Valzeina synform with the D3 Molare synform. The Lunschania antiform is cored by the basement of the Soja nappe, which can be traced southwards into the nappe boundary between the Simano nappe and Adula nappe complex. Alpettas synform and Darlun antiform were overprinted, deformed and cut out by late-stage faulting at the front of the Adula nappe complex.

Our D3 phase corresponds to the Domleschg phase of Pfiffner (1977), who defined this phase east of the study area. We emphasise, however, that D3 deformation in the working area is by far more pervasive in comparison to areas further east, i.e. at higher structural levels. An age of D3 between 30 and 25 Ma ago was inferred by Froitzheim et al. (1994) and Schmid et al. (1996), mainly based on the fact that this phase post-dates the Bergell intrusion. Its effects are widespread in the Lower and Middle Pennine nappes (Schmid et al. 1990; Baudin et al. 1993; Mayerat Demarne 1994; Marquer et al. 1996; Weh & Froitzheim 2001). To the west the D3 large-scale folds can easily be correlated (Table 2.2) with phase B of Chadwick (1968), D2 of Thakur (1971), B₃-B₄ of Probst (1980). Possibly, the Carassino phase of Löw (1987) represents a late stage of D3 deformation, as proposed by Etter (1987). This interpretation is mainly based on the fact that the axial planes of both Domleschg and Carassino phase steeply dip to the SSE. Parallelisation of the Carassino phase with the Domleschg phase implies that the Leis phase,

only affecting the Adula nappe complex, has to be older than the Domleschg phase, as is documented by clear overprinting criteria between Leis and Carassino structures (Löv 1987). This rules out the correlation between Domleschg and Leis phase proposed by Schmid et al. (1996) and favours a relatively older age for the Leis phase, as was already proposed by Pleuger et al. (2003, 2008).

The older deformation phases are more difficult to correlate at a regional scale. D2 can best be correlated with the Ferrera phase, defined in the Schams, Tambo and Suretta nappes (Milnes & Schmutz 1978; Schmid et al. 1990, 1996; Schreurs 1993), based on the fact that both these events are related to nappe stacking and that both are responsible for the formation of the first penetrative foliation. Weh and Froitzheim (2001) traced the Ferrera phase into the area of the Lower Penninic Bündnerschiefer (their D1a, b phase). It has to be emphasised, however, that the Ferrera phase was defined in a structurally higher level, i.e. the Middle Penninic Suretta nappe (Milnes & Schmutz 1978). Hence, the correlation with our D2 in a geometrical and kinematic sense does not imply that deformation in this structurally lower level was contemporaneous with the Ferrera phase, active during the 56-35 Ma age interval in the area of the Middle Penninic nappes (Schmid et al. 1996) as also documented by radiometric dating in the Suretta nappe (46 ± 5 Ma; Challandes et al. 2003). We emphasise that not all structural correlations presented in Table 2.2 imply that deformation producing these structures was contemporaneous at the scale of the Alps.

In the Lower and Middle Penninic units east of our area of investigation, the Ferrera phase has been severely overprinted by the Niemet-Beverin phase, which represents a first nappe refolding stage, resulting in large scale back-folding and inverting the nappe pile in the upper limb of the recumbent Niemet-Beverin mega-fold (Milnes & Schmutz 1978; Schmid et al. 1990; Schreurs 1993; Mayerat Dermanne 1994; Weh & Froitzheim 2001; Pleuger et al. 2003). Interestingly, no effects of this Niemet-Beverin phase (35-30 Ma; Schmid et al. 1996) were found in our area of investigation. Therefore, it is theoretically possible that the D2-event (Ferrera phase) could have lasted until some 30 Ma ago in our study area, i.e. at a much deeper structural level and in units occupying a more external paleogeographical position.

D1-deformation related to formation of quartz-calcite segregations, pre-dating D2 of the working area, corresponds to the sub-stage D1a of Weh & Froitzheim (2001; Table 2.2). These authors proposed that the formation of tight to isoclinal folds (their D1b; our D2) post-dates the formation of Fe-Mg carpholite-bearing veins associated with the formation of a penetrative foliation during their D1a (our D1). An estimate on the age of D1 in the working area may be obtained by considering the fact that D1 is linked with thrusting along the Penninic Basal Thrust, whose age is constrained by the age of the youngest sediments involved. Sedimentation in the Lower Penninic Bündnerschiefer realm lasted until Lowest Eocene times (i.e. some 50 Ma ago) according to Weh & Froitzheim (2001), but until Bartonian times (i.e. some 40 Ma) in the Sardona unit (Lihou & Allen 1996). The paleogeographical position of the Sardona unit is considered Ultra-Helvetic by some authors (e.g. Lihou & Allen 1996) but Penninic by others (mainly based on sedimentological and age criteria; e.g. Trümpy 1980; Hsü & Briegel 1991). Regardless of its precise paleogeographical position, it is extremely unlikely that the Sardona Flysch is of more external origin in respect to the Ultrahelvetic sediments of the Peidener Schuppenzone, given its high content of siliciclastic detritus partly shed from the “North Prättigau High” (Lihou & Allen 1996). Hence, D1-deformation, sediment-accretion and blueschist facies overprint are unlikely to have started before the Bartonian, i.e. before some 40 Ma ago.

Interestingly, the main nappe stacking Ferrera phase also post-dates an early thrusting event formed under HP/LT conditions, known as the Avers phase (Milnes & Schmutz 1978; Schmid et al. 1997b; Wiederkehr 2004) in the Briançonnais-Piemont-Liguria Ocean contact area in the Avers. However, since the Avers phase is related to the closure of the Piemont-Liguria Ocean during the Late Paleocene (Schmid et al. 1996), it must substantially pre-date the D1 event in our working area, which is related to the closure of the more northerly Valais Ocean.

In summary, this study could, for the first time in the investigated area, decipher the existence of an early blueschist-facies tectono-metamorphic event related to subduction and sediment-accretion. We refer to this event as the Safien phase (Table 2.2, Figs. 2.9 & 2.10). In contrast to Weh & Froitzheim (2001; their D1a and D1b), we emphasise a clear separation between the D1 and D2 events. This separation is supported by the fact that D2 formed under greenschist facies conditions. The age of the HP/LT Safien phase is constrained to post-date Bartonian times, i.e. 40 Ma. D2 deformation in our area is probably younger than the Ferrera phase in the Schams area; it probably lasted until the onset of D3-deformation, i.e. some 30 Ma ago. The onset of Barrow-type overprint, which post-dates D3 (i.e. 25 Ma according to the correlation of D3 with the age of the Domleschg phase; Schmid et al. 1996) is likely to be very much younger in respect of the high-pressure event. Given an almost static interval of mineral growth and the new radiometric dating of Barrow-type metamorphism in the area (Allaz et al. 2007; Janots et al. 2007), this heating pulse post-dates 20 Ma.

2.5.2. P-T-d-t path and reconstruction of the regional tectono-metamorphic evolution

The complex metamorphic evolution characterised by an early HP/LT stage (350-400°C, 1.2-1.4 GPa), later overprinted by a Barrow-type amphibolite facies event (500-570°C, 0.5-0.8 GPa) can be reconciled with either of two different P-T path trends: (1) A single P-T loop whereby the amphibolite facies overprint results from heating during decompression after HP/LT metamorphism, or alternatively, (2) a two-stage P-T evolution, whereby the amphibolite facies Barrovian overprint represents a separate heating pulse that follows earlier isothermal or cooling decompression from HP/LT conditions (Fig. 2.13). For the reconstruction of the regional tectono-metamorphic evolution and the interpretation of the geodynamic scenario, it is crucial to obtain constraints on the shape of the P-T path and its timing.

The following facts argue for isothermal or slightly cooling decompression of the Lower Penninic Valaisan Bündnerschiefer and the Sub-Penninic Peidener Schuppenzone after the HP stage: (1) very good preservation of Fe-Mg carpholite east of the study area (Engadine window), (2) its replacement exclusively by a lower pressure mineral assemblage (phengite-chlorite-quartz) within the studied area, and (3) the preservation of both pseudomorphs and relics of Fe-Mg carpholite within the north-

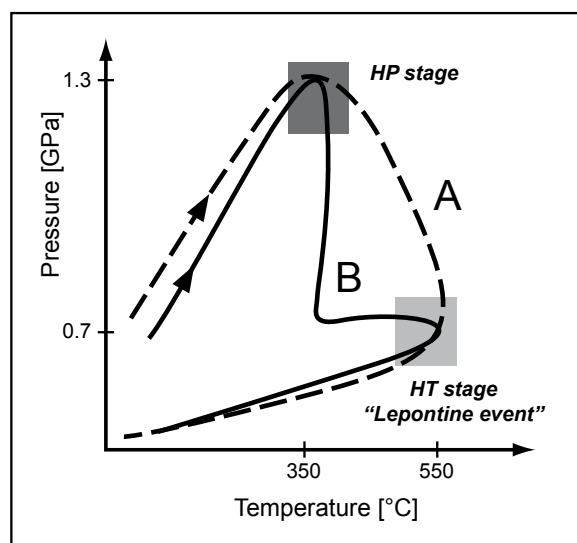


Fig. 2.13: Alternative P-T paths connecting the HP/LT event and the amphibolite-facies Barrovian overprint. Path A is a single P-T path, decompressional heating of the HP/LT stage leading to Barrovian overprint. Path B is characterised by a two-stage P-T path, Barrovian overprint represented by a separate heating pulse that follows isothermal or cooling decompression.

eastern Lepontine dome. Hence, the breakdown of carpholite in the Valaisan of the study area is entirely pressure-controlled and not associated with a temperature increase.

The analysis of the relationships between deformation and metamorphism and the timing constraints provide additional arguments in favour of a two-stage P-T-evolution characterised by a separate heating pulse that followed isothermal or cooling decompression from earlier HP/LT metamorphic conditions:

- (1) Both metamorphic events are separated from each other by two deformation phases implying a considerable time gap between them. The HP/LT event predates D2 and was estimated to have started ca. 40 Ma ago, certainly before 30 Ma (onset of D3-deformation). Barrow-type amphibolite facies overprint post-dates D2 nappe stacking and a first nappe re-folding event D3 (30-25 Ma), and hence, was younger than 20 Ma (Figs. 2.9 & 2.10).
- (2) Substantial decompression was associated with D2 nappe stacking and therefore predates the heating pulse that took place after D3.
- (3) The increase in temperature took place under more or less static conditions between D3 and D4.
- (4) Graphite thermometry documents a two-stage temperature distribution pattern. The D3 Lunschiana antiform folded an older HP/LT-related pattern and a younger, onion-shaped pattern cutting the D3 Lunschiana antiform was associated with Barrovian amphibolite facies overprint (Fig. 2.12).

We propose the following 5-stage scenario regarding the tectono-metamorphic evolution in the area (compare Figure 2.14):

(1) *Subduction and sediment-accretion stage (Safien phase)*: The Lower Penninic Bündnerschiefer of the Grisons area (mainly Grava and Tomül nappes) that today build up a 20 km thick accretionary wedge of meta-sediments (Hitz & Pfiffner 1997) formed during Cenozoic subduction of the Valaisan Ocean and the distal European margin beneath the Briançonnais micro-continent. Deeper parts of this sedimentary accretionary wedge experienced pressure-dominated metamorphism under blueschist facies conditions (350-400 °C, 1.2-1.4 GPa), including parts of the sedimentary cover in Ultrahelvetica facies (Peidener Schuppenzone), which were detached from their crystalline basement and incorporated into the HP/LT part of the accretionary wedge. The associated deformation (D1 Safien phase) was semi-ductile and led to the formation of shear fibre veins consisting of quartz, calcite and Fe-Mg carpholite. Exact timing of this HP/LT subduction and sediment-accretion stage is not yet possible. It is, however, constrained to have occurred during the Late Eocene (after 40 but before 30 Ma ago; see Berger & Bousquet 2008), hence substantially after similar but Late Paleocene to Middle Eocene high-pressure stages proposed for the Middle and Upper Penninic units (see overviews given by Froitzheim et al. 1996; Schmid et al. 2004; Berger & Bousquet 2008; Bousquet et al. 2008).

(2) *Nappe stacking and decompression stage (Ferrera phase)*: Nappe stacking was associated with substantial decompression of the blueschist-facies rocks. The presence of relics of Fe-Mg carpholite indicates decompression under isothermal or cooling conditions. This thermal regime, as well as ongoing accretion of the rest of the Sub-Penninic sediments (Scopi unit, Fig. 2.3), suggests that also European continental basement rocks, such as preserved in the Adula, Simano and Leventina-Lucomagno units, became involved in ongoing subduction and accretion during the Ferrera phase. We propose that the Ferrera phase in our working area may have outlasted earlier stages of the nappe-stacking Ferrera phase that affected the Middle Penninic units (e.g. Baudin et al. 1993), and probably was active until 30 Ma ago.

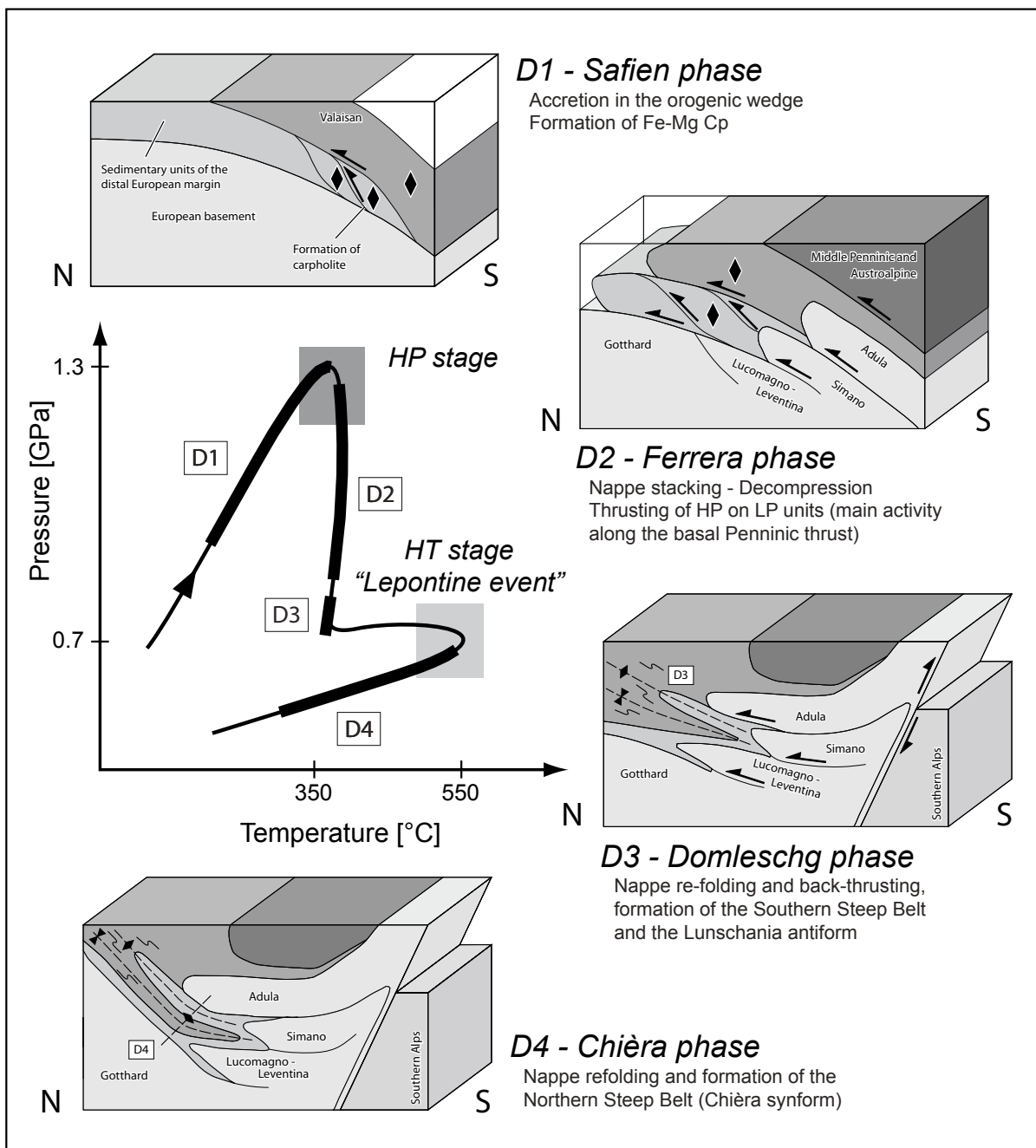


Fig. 2.14: P-T-d path for the Lower Penninic and Sub-Penninic (Peidener Schuppenzone) meta-sedimentary units and sketches of the geodynamic scenario during the various stages of the tectono-metamorphic evolution.

(3) *Nappe re-folding (Domleschg phase)*: This D3 nappe folding event substantially modified the Penninic nappe stack in the working area. It post-dates an earlier nappe re-folding phase established only within structurally higher North and Middle Penninic nappes east of the working area (Niemet-Beverin phase; e.g. Schreurs 1993; Baudin et al. 1993; Marquer et al. 1996; Weh & Froitzheim 2001). D3 deformation produced tight to isoclinal mega-folds with amplitudes up to some 10 km (Figs. 2.3 & 2.14): the most prominent Lunschiana antiform, but also the Valzeina and Alpettas synforms, as well as the Darlun antiform (Voll 1976; Kupferschmid 1977; Probst 1980; Steinmann 1994a, b; Weh & Froitzheim 2001; Uhr unpubl.; Figs. 2.1, 2.2 & 2.3). On the scale of the entire Alpine orogen the Domleschg phase, characterised by far less intense folding at higher structural levels, is interpreted as contemporaneous with back thrusting along the Insubric mylonite belt (Schmid et al. 1987), which occurred during the 30-25

Ma time interval (see discussion given in Schmid et al. 1997b). Note also that this phase is associated with ongoing accretion of continental basement (i.e. Lucomagno-Leventina nappe, Fig. 2.14). Regarding the eastern part of the investigated area, the tectono-metamorphic evolution essentially came to a halt after D3 deformation (Fig. 2.12). The following metamorphic and tectonic events only affected the western part of the working area.

(4) *Barrow-type thermal overprint*: This thermal pulse occurred during a tectonically quiescent phase within the working area (but not necessarily elsewhere, i.e. in the more external parts of the Alps), initiating shortly after some 20 Ma ago. Increasing temperatures led to the formation of porphyroblasts related to classical Barrow-type amphibolite facies overprint. This thermal overprint was sustained until the beginning stages of the last tectonic (D4) event (Figs. 2.12 & 2.14).

(5) *Back-folding in the Northern Steep Belt (Chièra phase)*: This second nappe re-folding event leads to back-folding within the Gotthard “massif” and adjacent areas. It is associated with the formation of the Northern Steep Belt of the Penninic realm that is well developed only west of our area of investigation (Milnes 1974). D4 deformation is intense in the south-west but gradually becomes weaker towards the north-east and, finally, fades out somewhere east of the Piz Terri-Vrin area (Figs. 2.2 & 2.3). A relatively tight synform, the Chièra synform (Milnes 1974; Milnes 1976; Etter 1987), brings the Lower Penninic and Sub-Penninic nappe stack into an overturned, steeply north dipping position (Northern Steep Belt) at the deepest structural levels. Within most of the working area, a set of parasitic syn- and antiforms develops, structurally located between the Chièra synform and the more northerly located corresponding Greina or Gotthard antiform (Thakur 1973) which brings the overturned nappe pile back into a normal position (Fig. 2.3). Hence, back-folding is much less pronounced in our working area compared to further west (Figs. 2.2 & 2.3). This folding outlasted Barrovian overprint (18-20 Ma; Allaz et al. 2007; Janots et al. 2007) and hence is very young (probably post-18 Ma) and contemporaneous with the N-directed thrusting in the Aar massif in the more external parts of the Alps (Grindelwald phase; Burkhard 1988; Schmid et al. 1996; Pfiffner et al. 1997) and movements along the Simplon line associated with back folding west of the Lepontine dome (Steck 1984, 1990; Marquer & Gapais 1985; Mancktelow 1992; Mancktelow & Pavlis 1994; Steck & Hunziker 1994; Keller et al. 2006).

We conclude that Barrovian overprint in the working area, representing a separate heating pulse (Fig. 2.14) is surprisingly young (18-20 Ma; Allaz et al. 2007; Janots et al. 2007) when compared to the timing of a similar separate heating pulse proposed for the Southern Steep Belt at around 30-27 Ma (Engi et al. 2001; Berger et al. 2005; Brouwer et al. 2005; Brouwer & Engi 2005). Barrow-type overprint at the western edge of the Lepontine dome, which occurred along a single continuous P-T path, occurred before some 20 Ma ago according to Keller et al. (2005a).

Barrow-type metamorphism in the Lepontine area is often referred to as the Lepontine metamorphic event. The term “event” is totally misleading since Lepontine Barrow-type metamorphism, rather than representing one single event, is diachronous; thermal overprint becomes progressively younger towards the north (Köppel et al. 1981; Engi et al. 1995). Consequently, different relations between deformation and crystallisation are commonly observed (Berger et al. 2005). We emphasise that the separate heating pulse described in this study is characteristic for the north-eastern part of the Lepontine dome only and that no direct inferences in terms of timing, geodynamic setting or nature of the heat source should be drawn regarding the rest of the Lepontine area, particularly its southern part.

2.5.3. Discussion of potential heat sources of Barrow-type overprint and thermal evolution

We now discuss possible heat sources that could potentially be responsible for Barrovian metamorphism in the north-eastern part of the Lepontine thermal dome. We do this in a qualitative way, being aware of the complexities of the subject. We first briefly introduce the presently known potential heat sources and then qualitatively discuss which of these heat sources could best explain the observations.

The existence of a separate heating pulse raises the old and still widely debated question after the heat sources for Barrovian overprint in collisional orogens (e.g. Jamieson et al. 1998). The following potential heat sources have been proposed for Barrow-type thermal overprint: (1) Shear or viscous heating (Burg & Gerya 2005). (2) Advective heat transfer by rising magma, i.e. plutons and dykes (Engi et al. 1995; Frey & Ferreiro Mählmann 1999), possibly induced by up-welling of hot asthenosphere due to slab break-off (von Blanckenburg & Davies 1995). (3) Advective heat transfer to the upper crust by exhumation of hot eclogitic slices within a subduction channel (Becker 1993; Engi et al. 2001), or alternatively, by extension-related exhumation of hot high-pressure rocks (Platt 1986; Ballèvre et al. 1990). (4) Accretion of continental crustal rocks characterised by high radioactive heat production (Chamberlain & Sonder 1990; Bousquet et al. 1997; Huerta et al. 1998; Roselle et al. 2002; Goffé et al. 2003).

Discussions on shear heating need to (1) evaluate the expected spatial and temporal distribution of shearing-induced heat and (2) quantify the amount of heat produced, which depends on strain-rates and deformation mechanisms (e.g. Peacock 1996). In the case of the Alpine orogen such shear heating would be expected to lead to a thermal zonation, which parallels the strike of the orogen, i.e. parallel to the strike of the potential high-strain zones (in general nappe contacts and shear zones associated with the formation of the nappe-stack) that produce this heat. This, however, is not the case within the study area since isotherms are perpendicular to important structural elements, such as the Penninic Basal Thrust and other nappe contacts (Fig. 2.12). Moreover, plate convergence rates in the Alps are considered too low (in the order of 1 cm per year; Schmid et al. 1996) to produce enough heat at a nappe or orogen-wide scale, while this heat source may play a role in case of localised shear zones. Hence, only at high convergence rates can shear heating be an important heat source at a large scale. This, however, is not the case regarding the thermal overprint that occurred at a very late stage, i.e. when the Alpine edifice was essentially established. Moreover microstructural observations of porphyroblasts related to Barrovian metamorphism indicate that thermal overprint took place under more or less static conditions and was not at all associated with deformation. Based on field evidence we conclude that shear heating probably had a rather limited influence on the thermal evolution in our working area.

The effect of advective heat transport by magma and/or local melt is also negligible during Barrovian overprint within our working area. While the intrusion of the Bergell pluton and segregating migmatitic melts (Berger et al. 1996, 2007; Burri et al. 2005) may additionally contribute to the heat budget in case of the Southern Steep belt, these effects can probably be ignored in case of our working area at the northern rim of the Lepontine dome.

Exhumation of hot eclogitic slices, combined with radioactive heat production by accreted continental crust, was proposed as a model for Barrow-type overprint within the Southern Steep Belt (Tectonic Accretion Channel model, e.g. Engi et al. 2001, Roselle et al. 2002). Rising high-temperature eclogites as a potential advective heat source are indeed available outside the working area, i.e. in form of the eclogite facies Adula nappe complex. Moreover, in the Western Alps, characterised by the occurrence of large volumes of high-pressure and ultra-high-pressure units, such as the Gran Paradiso and Dora-Maira

Internal Massifs, no Barrovian thermal overprint is observed (Oberhänsli et al. 2004). It seems that the rising of eclogites is not efficient enough to explain Barrovian overprint in our working area, since such eclogites are restricted to more southerly areas within the Lepontine dome, and also in view of the large temporal hiatus between high-pressure event and Barrovian overprint.

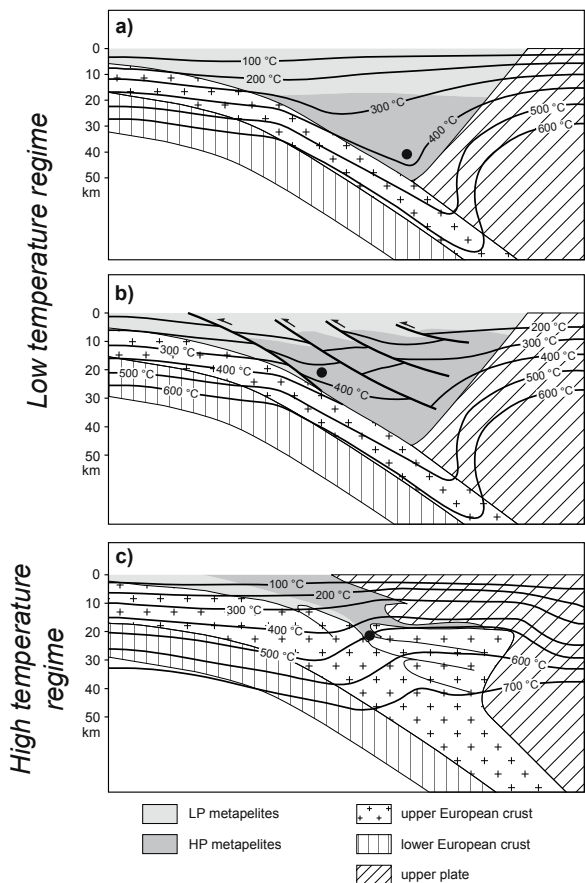


Fig. 2.15: Very schematic sketches, illustrating the evolution of isotherms in an orogenic wedge (inspired by Goffé et al. 2003) such as the Alps during three geodynamic stages of the orogen. Two strongly differing thermal regimes are distinguished: a low temperature (a & b) and a high temperature regime (c). The black dot represents the location of the meta-sediments of the study area. (a) Typical pattern of isotherms during the subduction stage. The wedge is dominated by accretion of large amounts of sediments. The deeper parts of the wedge are characterised by pressure-dominated metamorphism under blueschist facies conditions. (b) Isothermal or cooling decompression during nappe-stacking, bringing HP onto LP units; the isotherms remain down-bent. (c) Due to massive accretion of continental crustal material after collision, the rock composition within the wedge changes dramatically: Large amounts of upper-crustal European granitoid rocks were accumulated within the wedge (Sub-Penninic nappe stack). This accumulation of heat-producing crustal material is responsible for increasing temperatures by the up-bending of isotherms inducing the late-stage amphibolite-facies Barrovian overprint observed in the working area.

heat productions, see Jamieson et al. 1998). The most likely way to add such heat sources is the combination of subduction and subsequent thickening (e.g. Jamieson et al. 1998; Engi et al. 2001; Roselle et al. 2002; Goffé et al. 2003). Our field observations fulfil these prerequisites since subduction was followed by late-stage heating. Hence, we propose that the thermal regime during Barrovian overprint is

The strongest argument against advective heat transport by exhumation of eclogitic material in the northern Lepontine dome and the Tauern window is that the distribution of the HP/LT metamorphic units in the Alps is completely different from that of the areas characterised by a Barrovian overprint (Bousquet et al. 2008). The latter are restricted to dome-shaped areas, such as the Lepontine dome and the Tauern window (Bousquet et al. 2008). Both the Lepontine dome and the Tauern window are characterised by massive accretion of granitoid basement units derived from the distal European margin (Sub-Penninic nappe stack; Milnes 1974; Schmid et al. 2004). Hence, Barrovian overprint is spatially coupled with exposures of large nappe-stacks of continental material, characterised by high radioactive heat production. However, one might argue that, since both these domes represent structural highs, similar Barrovian-metamorphism would be expected at depth outside these domes. A simple consideration of the volume available between the earth's surface and the Moho, which is at approximately constant depth along strike (Waldhauser et al. 1998), excludes along-strike doming of the entire crust. Hence, this doming is related to the localised accretion of large volumes of upper European basement, as is documented by the stacking of the Sub-Penninic basement nappes; in other words, doming is the direct isostatic response of such localised accretion of European upper crust (see Bousquet et al. 2008 for a more detailed discussion).

The effect of radioactive heat production is only relevant if such material is accreted at certain depths (locations with primary lower radioactive

determined by the thermal structure during the final stages of subduction and the additional heat release from radioactive decay of accreted material. However, these considerations do not quantitatively explain the observed distribution of temperatures and additional model calculations to those of Bousquet et al. (1997), Roselle et al. (2002) and Goffé et al. (2003) are necessary.

Nevertheless the field data can be discussed within the frame of the thermal evolution of the Alpine orogenic wedge (see Fig. 2.15). The low-temperature regime is associated with an early subduction and sediment accretion stage and led to the formation of mineral assemblages that are typical for subduction processes and related down-folding of the isotherms (Fig. 2.15a). During ongoing subduction, deeper parts of the orogenic wedge were thrust onto lower pressure units, a process that is accompanied with nearly isothermal or cooling decompression (Fig. 2.15b). The high-temperature regime (Fig. 2.15c) occurs after the accretion of additional continental middle crust that led to the formation of the Sub-Penninic nappe-stack. This temperature regime leads to the up-doming of isotherms, which cut through nearly all the structural units (Fig. 2.12). Therefore, we infer that the observable crosscutting isotherms are most likely related to a late stage of purely conductive heat transfer. Note that these rising isotherms, in the absence of mass transport, elegantly explain the Barrow-type amphibolite facies overprint of HP/LT units that already experienced substantial decompression before, as is the case in our study area.

2.6. Conclusions

We provided evidence for a two-stage metamorphic evolution of meta-sedimentary units derived from the Valaisan Ocean (Grava nappe) and the distal European margin (Peidener Schuppenzone) in the north-eastern part of the Lepontine dome. A first HP/LT metamorphic event under blueschist facies conditions (350-400 °C and 1.2-1.4 GPa) was associated with subduction and sediment-accretion. It was immediately followed by “cold” isothermal or cooling decompression during nappe stacking. Continent-collision-related classical Barrow-type amphibolite facies overprint (500-570 °C and 0.5-0.8 GPa) represents a separate heating pulse that post-dates the D3 nappe-refolding event. It was induced by post-collisional accretion of continental crust, and it largely occurred under static conditions, partly during the initial stages of the D4 back-folding event that led to the formation of the Northern Steep Belt of the Penninic nappe pile. The two metamorphic events are separated by a time gap within our working area, estimated to be in the order of 20 Ma.

Amongst the various possible heat sources of Barrovian metamorphism we regard radiogenic heat production by accretion of continental crust during the collisional and post-collisional stages of Alpine orogeny, associated with rising isotherms, to be mainly responsible for this separate late-stage heating event at the north-eastern rim of the Lepontine dome. We propose that the Lepontine and Tauern thermal and structural domes both largely resulted from the local accretion of massive volumes of Sub-Penninic basement nappes derived from the distal European margin. This well explains the substantial Barrow-type thermal gradient observed at the north-eastern rim of the Lepontine dome, cutting across former nappe contacts almost perpendicular to strike. We emphasise, however, that in the southern parts of the Lepontine dome (Southern Steep Belt) other heat sources such as heat advection by rising eclogitic bodies and melts are probably also very important (e.g. Frey & Ferreiro Mählmann 1999; Nagel et al. 2002a; Keller et al. 2005a; Berger et al. 2007).

The new data from the north-eastern rim of the Lepontine dome provide strong evidence for the former existence of a contiguous HP/LT belt, representing a second northern suture zone associated with the closure of the Valais Ocean. Moreover, relative timing constraints indicate that both HP/LT meta-

morphism and Barrow-type overprint were diachronous at the scale of the Alpine orogen; hence all indicators of metamorphic zonation such as index mineral zone boundaries must be strongly diachronous.

Acknowledgements

Excellent preparation of numerous samples by W. Tschudin, as well as hauling masses of rocks down the mountains by G. Derungs, including great support in the field, are gratefully acknowledged. O. Appelt and Dr. D. Rhede from the GeoForschungsZentrum Potsdam are thanked for help with microprobe analyses. A supporting field visit of A. Riemann from the University of Potsdam is appreciated. Dr. M.A. Ziemann is thanked for the introduction and support in the Raman laboratory of Potsdam University. We also thank the two reviewers J. Pleuger and M. Janak for their constructive comments and suggestions for improving this paper, and the editor N. Froitzheim for his careful handling of the manuscript. Substantial funding by the Swiss National Science Foundation (project NF-200020-113585 and precursor project NF-200020-103585) is gratefully acknowledged.

Chapter 3

3-D assessment of peak-metamorphic conditions by Raman spectroscopy of carbonaceous material: an example from the margin of the Lepontine dome (Swiss Central Alps)

This chapter is under review as: **Wiederkehr, M.**, Bousquet, R., Ziemann, M.A., Berger, A. & Schmid, S.M. 3-D assessment of peak-metamorphic conditions by Raman spectroscopy of carbonaceous material: an example from the margin of the Lepontine dome (Swiss Central Alps). Submitted to *Contributions to Mineralogy and Petrology*.

Abstract

This study monitors the regional changes in the crystallinity of carbonaceous matter (CM) applying Raman spectroscopy to a total of 214 metasediment samples (largely so-called “Bündnerschiefer”) collected within the north-eastern rim of the Lepontine dome and easterly adjacent areas of the Swiss Central Alps ranging from blueschist to amphibolite facies conditions. The three-dimensional mapping of isotherm contours in map and profile view shows that the isotherm contours associated with the collision-related late-stage Barrow-type Lepontine event cut across nappe contacts and post-nappe stacking mega-folds, both along and across strike within the north-eastern rim of the Lepontine dome. Further to the NE the isotherm contours reflect temperatures reached during an earlier subduction-related blueschist facies event and/or subsequent near-isothermal decompression and are folded around large-scale post-nappe stacking folds. A substantial “temperature jump” across the tectonic contact between frontal Adula nappe complex and surrounding metasediments indicates that, in contrast to postulates raised by earlier studies, equilibration of temperatures during the late-stage Lepontine event is incomplete in this part of the investigated area.

3.1. Introduction

The metamorphic structure of the Alps is the result of long lasting plate convergence and final collision between the European and Adriatic continental plates in Cretaceous to Cenozoic times (e.g. Trümpy 1960; Frisch 1979; Tricart 1984; Schmid et al. 1996). The geodynamic evolution and resulting metamorphic zonation related to Cenozoic orogeny, which followed an earlier Cretaceous cycle (Froitzheim et al. 1994; Schmid et al. 2008) not addressed by this study, can be subdivided into two distinct stages: (1) subduction-related pressure-dominated metamorphism and deformation of oceanic lithosphere formed during the opening of the Alpine Tethys as well as small parts of the immediately adjacent European lithosphere, and, (2) temperature-dominated Barrow-type metamorphism related to collision between Europe and Adria, involving further accretion of massive volumes of crustal material (e.g. Lepontine dome and Tauern window; Bousquet et al. 1997; Goffé et al. 2003; Schmid et al. 2004; Bousquet et al. 2008) to the upper plate formed by the Austroalpine nappes and previously accreted high-pressure units.

Several pioneering studies on the spatial distribution of index minerals as well as on different metamorphic facies types resulted in a well established knowledge of the zoning of Alpine metamorphism, particularly within the Lepontine dome of the Central Alps (e.g. Wenk 1962, 1970; Niggli & Niggli 1965; Trommsdorff 1966; Frey 1969, 1978; Niggli 1970; Frey et al. 1980, 1999; Oberhänsli et al. 2004). However, the metamorphic zoning related to pressure-dominated metamorphism needs to be discriminated from that related to Barrovian overprint in the Alps: While the pressure-dominated units (blueschists and eclogites) form a belt striking orogen-parallel, remnants of the temperature-dominated event are localized in the Lepontine dome and the Tauern window (e.g. Oberhänsli et al. 2004; Bousquet et al. 2008). From a geodynamic point of view only the Central Alps (Lepontine dome) and the Tauern window in the Eastern Alps reached the mature stage of a colliding orogenic belt characterized by pervasive Barrovian overprint whereas the Western Alps never reached this mature stage and hence can be interpreted as a frozen-in subduction zone (Bousquet 2008).

This study addresses a key area for the reconstruction of the Alpine geodynamic evolution at the north-eastern margin of the Lepontine dome and easterly adjacent areas where pressure- and temperature-dominated metamorphic domains are found to be in close contact (Bousquet et al. 2002; Wiederkehr et al. 2008). The studied metasediments have a great potential to record the metamorphic evolution and can therefore be used for the geodynamic reconstruction of the Alpine orogenic belt (see also Wiederkehr et al. 2008). Moreover, these metasediments cover large areas and therefore enable observing and correlating the structural and metamorphic evolution continuously and over great distances. This is in contrast to work on blueschist- and eclogite-facies rocks that mainly investigates mafic systems (e.g. Evans 1990; Frey et al. 1991; Abbott 1992). Mafic rocks often only occur within dismembered and isolated bodies and hence do not allow for continuous mapping of metamorphic gradients.

Despite of the remarkable progress concerning the metamorphic evolution of low-grade (HP/LT and LP/LT) metasediments (see review given by Bousquet et al. 2008), accurate characterization of metamorphic gradients and P-T paths still remains problematic, mostly due to the absence of unambiguous mineral assemblages and to large uncertainties concerning thermodynamic data. Therefore, classical petrology reaches its limits under low-grade conditions and additional tools are needed for a precise determination of metamorphic conditions that form the basis for reconstructing the geodynamic evolution of the Alpine metasedimentary units. A potential tool amongst others is represented by investigating the evolution of carbonaceous material.

This study aims at demonstrating the great potential of using Raman spectroscopy of carbonaceous material for the investigation of particularly low-grade metamorphic metasediments. This method is, when associated with a detailed petrological and structural study, very powerful for the determination of maximum temperatures reached during the metamorphic evolution. Provided that the sampling uniformly and densely covers a large area this method also reveals three-dimensional information regarding temperature gradients. Carbonaceous material (CM) is ubiquitous in metasedimentary rocks in the area of investigation. The continuous transformation of the crystalline structure of CM from amorphous organic matter to fully ordered graphite (generally called graphitization process; e.g. Teichmüller 1987), on which the method is based, is mainly temperature dependent. Hence, the crystallinity of CM is expected to increase systematically with increasing temperatures and has recently been calibrated as a geothermometer by Beyssac et al. (2002a) and Rahl et al. (2005). It is widely accepted that graphitization is a thermal irreversible process, which is supported by the observation that, in contrast to metamorphic mineral assemblages, the degree of crystallinity of CM is not affected by retrogression (Beyssac et al. 2002a). Hence, this geothermometer always and reliably records the peak temperature reached by a rock specimen along its P-T loop (e.g. Beyssac et al. 2004; Bollinger et al. 2004; Rantitsch et al. 2004; Negro et al. 2006; Beyssac et al. 2007).

This study presents for the first time a systematic and comprehensive investigation of the evolution of CM using Raman spectroscopy in a large part of the Central Alps located near the north-eastern rim of the Lepontine dome and characterized by high topographic gradients. The peak temperature distribution maps and profiles cover a large volume of metasedimentary units (generally referred to as “Bündnerschiefer”) deposited onto basement belonging to the European continental margin and the adjacent Valaisan oceanic domain (Steinmann 1994a; Wiederkehr et al. 2008). The dataset comprises a total of 214 samples (Figs. 3.1 & 3.2, Tab. 3.1) and allows for high resolution mapping of maximum metamorphic temperatures in three dimensions. Two different calibrations, namely that of Beyssac et al. (2002a) and Rahl et al. (2005), were used, and they will be compared with each other. The peak temperature distribution will be discussed in terms of the P-T-paths associated with the high pressure and Barrow-type metamorphism, respectively.

3.2. Geological setting and sampling strategy

The analyzed metasediments of Mesozoic-age are located within the north-eastern rim of the Lepontine dome and in easterly adjacent areas (inset of Fig. 3.1), i.e. in an area that is ideal for studying the temperature gradients in a transition zone from subduction- to collision-related metamorphism. The area of investigation extends from the Garvera-Lukmanier-Pizzo Molare area in the W to the Prättigau half-window in the E and also includes the N-S oriented Misox Zone located between the Adula and Tambo nappes (Figs. 3.1 & 3.2). The same metasedimentary units can be observed continuously along strike from blueschist facies conditions in the E to amphibolite facies Barrovian overprint in the W (Fig. 3.1; Wiederkehr et al. 2008).

3.2.1. Tectono-metamorphic background

Pre-Alpine basement nappes dominate in the W and at deeper structural levels. The latter are formed by the so-called Sub-Penninic nappes (Trümpy 1960; Milnes 1974; Froitzheim et al. 1996), consisting of basement-dominated continental material scraped off the former European margin (e.g. Schmid et al. 2004) and accreted to the higher tectonic units during the latest stages of Alpine plate con-

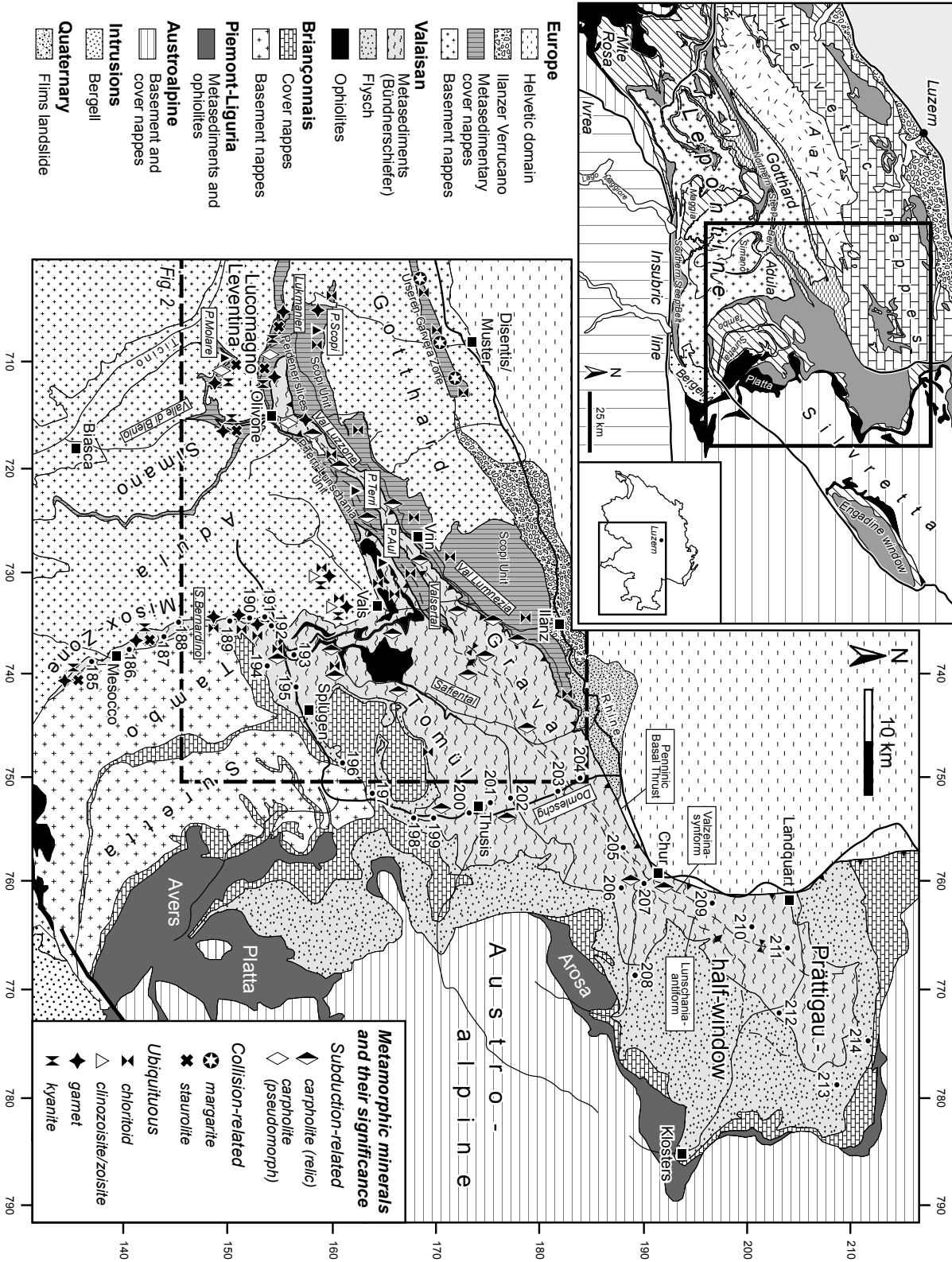


Fig. 3.1: Geological map of the investigated area indicating the main occurrences of minerals indicative for HP/LT metamorphism and Barrovian overprint, as well as the main geographical names mentioned in the text and giving the locations of specimen numbers 185-214; refer to Fig. 3.2 regarding the locations of all other samples and to Table 3.1 for exact location. The dashed line indicates the outlines of the more detailed map shown in Figure 3.2. The tectonic map of the Central Alps in the inset (upper left) is after Schmid et al. (2004). Coordinates given are those of the Swiss maps.

vergence. These nappes include, from bottom to top, the Gotthard, Lucomagno-Leventina, Simano and Adula nappes. These nappes form the bulk of the Lepontine structural dome that exposes the deepest tectonic units of the Alps. These basement nappes are overlain by thin slivers of Mesozoic metasediments, which originally were also part of the European margin (Europe-derived metasedimentary units of Figs. 3.1 & 3.2), often complexly folded and wrapped around the frontal parts of the Sub-Penninic basement nappes (e.g. Thakur 1973; Milnes 1974; Probst 1980).

The Penninic Basal Thrust separates the Europe-derived Sub-Penninic basement and cover units from the Lower Penninic cover nappes and thrust slices that originated from the Valais Ocean (Wiederkehr et al. 2008). These almost exclusively consist of Mesozoic metasediments referred to as Bündner-schiefer (e.g. Probst 1980; Steinmann 1994a; Berger et al. 2005; Figs. 3.1 & 3.2) and constitute a nappe stack occupying a structurally higher position that, due to the along-strike axial plunge, is found in the eastern parts of the studied area.

The north-eastern rim of the Lepontine dome is the locus of several pioneering studies addressing fundamental principles related to the evolution of prograde Barrovian metamorphism (Chadwick 1968; Frey 1969, 1978; Niggli 1970; Wenk 1970; Fox 1975; Livi et al. 2002). The metamorphic conditions continuously increase from chloritoid-margarite bearing micaschists that are part of the greenschist facies area in the Urseren-Garvera Zone (Frey 1978; Livi et al. 2002) to staurolite-kyanite-garnet-biotite bearing metasediments indicating amphibolite facies conditions around the Lukmanier area and Pizzo Molare (Fig. 3.1; Frey 1969; Chadwick 1968; Thakur 1971). Lower/middle amphibolite facies metamorphic conditions (0.5-0.8 GPa and 500-550 °C) have been estimated for Barrow-type metamorphism in the north-eastern Lepontine dome (Chadwick 1968; Frey 1969; Engi et al. 1995; Todd & Engi 1997; Frey & Ferreiro Mählmann 1999). A similar progressive increase of metamorphic conditions is also found in the Misox Zone further to the E (Thompson 1976; Teutsch 1982; Fig. 3.1).

To the E low-grade metasediments predominate, but the metamorphic record is ill constrained due to the scarcity of unambiguous mineral assemblages that generally only indicate “greenschist facies” conditions. However, the recognition of Fe-Mg carpholite in the Valaisan-derived metasediments E of the Lepontine dome indicates that blueschist facies conditions around 1.2-1.4 GPa and 350-400 °C were established before late-stage greenschist-facies overprint (Fig. 3.1; Goffé & Oberhänsli 1992; Oberhänsli et al. 1995; Bousquet et al. 1998). These findings document the existence of a northern HP/LT metamorphic belt, located between Briançonnais micro-continent and distal European margin (Goffé & Bousquet 1997; Bousquet et al. 2002; Bousquet et al. 2008). The Valaisan-derived metamorphic belt is separated from the well-documented southern HP-belt affecting Piedmont-Liguria-derived units by the Briançonnais-derived basement nappes, which partly lack such high-pressure overprint (Frey & Ferreiro Mählman 1999; Engi et al. 2004; Bousquet et al. 2008).

The subduction-related blueschist facies overprint found in the E, followed by greenschist facies retrogression, pre-dates a completely separate metamorphic event, namely collision-related Barrow-type amphibolite facies metamorphism only developed in the W (see Wiederkehr et al. 2008). Both events were diachronous at the scale of the Alpine orogen and hence all indicators of metamorphic zoning such as peak-metamorphic temperature inferred by the present study must be diachronous as well (Brouwer et al. 2005; Berger & Bousquet 2008; Janots et al. 2009). HP/LT metamorphism not only affected the metasediments of the Valaisan domain but also parts of the metasedimentary units derived from the European margin (i.e. Peidener slices and Piz Terri-Lunschania unit; Figs 3.1 & 3.2) and is

clearly separated by at least two deformation events from a MP/MT Barrovian overprint, as is documented by a typical bimodal P-T path (Brouwer et al. 2005; Zulbati 2008; Wiederkehr et al. 2008).

3.2.2. Sediments derived from the distal European margin (Sub-Penninic cover nappes and slices)

The sediments originally deposited on the former distal European margin include Urseren-Garvera Zone, Scopi unit and Peidener slices (together forming the so-called Gotthard Mesozoic), and additionally, the Piz Terri-Lunschana unit (Figs. 3.1 & 3.2; see Wiederkehr et al. 2008 for further details). In general, these sedimentary slices are made up of a Triassic sequence of quartzites, dolomitic marbles, evaporites, metapelites and metamarls followed by a Lower to Middle Jurassic sequence consisting of shales, sandstones, limestones, carbonaceous metapelites and calcschists, the latter often resembling the so-called Bündnerschiefer of the Penninic (Valaisan-derived) units (Baumer et al. 1961; Probst 1980; Etter 1987; Berger et al. 2005). Jurassic-age black shales, marls and calcschists were preferentially selected for sampling due to their high content in CM.

We also sampled Mesozoic metasediments found inside the northern basement-dominated Adula nappe complex (so-called “internal Mesozoic”; Löw 1987; sampling points depicted in Figure 3.2 located within the Adula nappe complex). In general these sediments consist of Triassic quartzites, dolomitic marbles and evaporites that were sliced and imbricated with the Adula crystalline basement. Kyanite-chloritoid-garnet-zoisite/clinozoisite bearing metamarls and calcschists of probably Lower Jurassic age are unambiguously associated with these Triassic sediments in some rare outcrops (Fig. 3.1; Jenny et al. 1923; Van der Plaas et al. 1958; Löw 1987; Thüring 1990; Wyss & Isler 2007). Due to the strong lithological affinities to the metasediments found in the Scopi unit, we also attribute these occurrences to have been derived from the distal European margin.

3.2.3. Sediments derived from the Valaisan Ocean (Lower-Penninic cover nappes and slices, Valaisan Bündnerschiefer)

Sediments derived from the predominantly oceanic Valaisan realm form voluminous and rather monotonous sequences, predominantly consisting of calcschists (Bündnerschiefer) thrust along the Penninic Basal Thrust onto the sediments of the former European margin. These Valaisan Bündnerschiefer, flysch units, marbles and ophiolitic occurrences are subdivided into a number of slices. The largest are the Grava nappe (including the Prättigau flysch) and the Tomül nappe (Figs. 3.1 & 3.2), consisting of Cretaceous- to Eocene-age calcschists, limestones, shales, marls and sandy limestones (Nänny 1948; Ziegler 1956; Steinmann 1994a). The existence of mafic and ultramafic rocks (Nabholz 1945) indicates that at least parts of the Valaisan Bündnerschiefer were deposited on oceanic crust (Steinmann 1994a; Steinmann & Stille 1999). Some samples analyzed originate from the Misox Zone, a narrow zone of Mesozoic metasediments that also includes ophiolitic slices, structurally located between the Adula nappe complex and the overlaying Tambo basement nappe (Gansser 1937; Strohbach 1965; Fig. 3.1) and representing the root zone of the Valaisan domain (Probst 1980; Steinmann 1994a).

3.2.4. Sampling strategy

The most densely covered area is that between Lukmanier and Pizzo Molare in the W to Safiental in the E, covered by a complementary study presented in Wiederkehr et al. (2008). Sampling is particularly dense between Olivone and Vrin (Fig. 3.2), where the lateral temperature gradient is pronounced

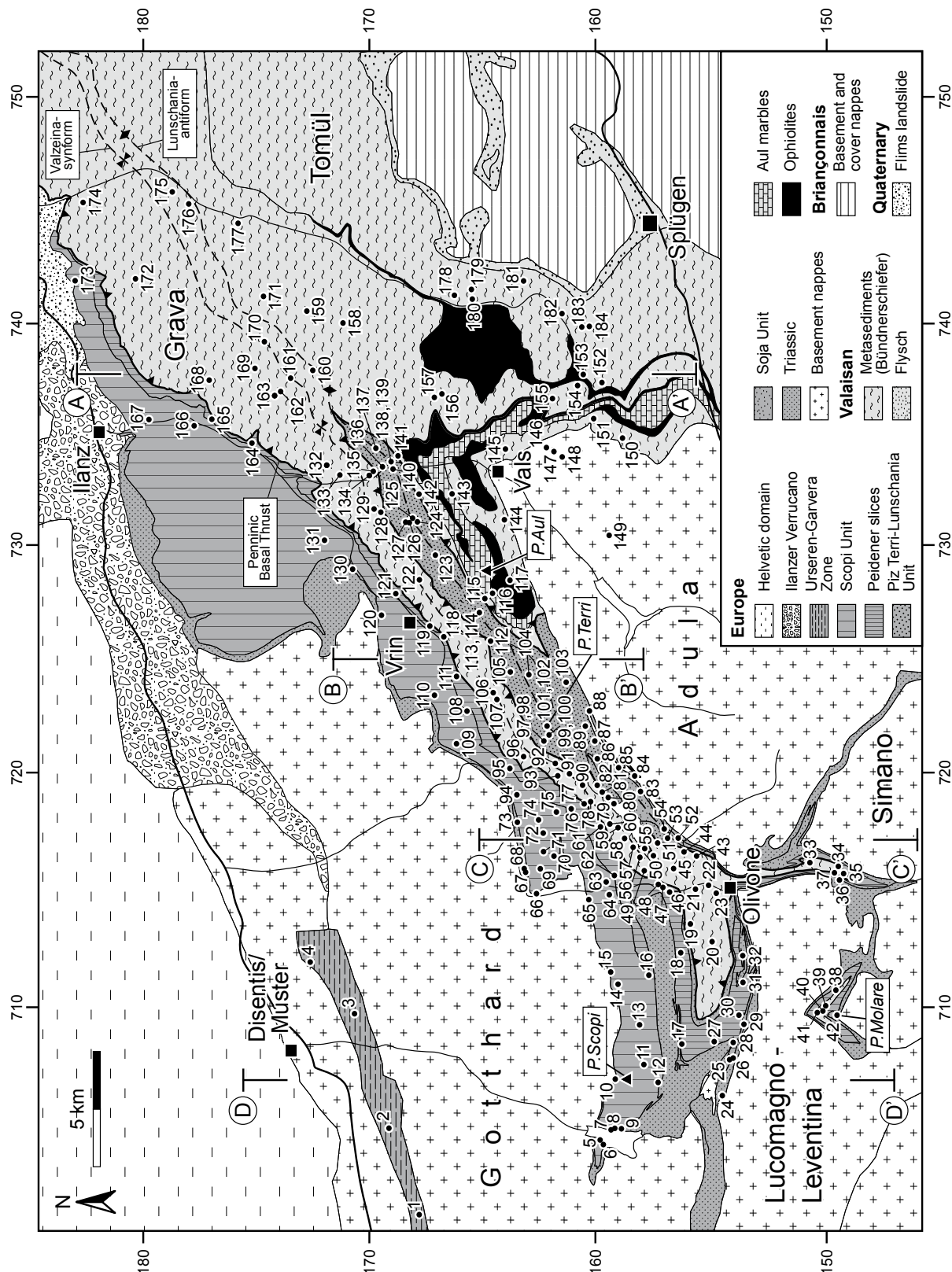


Fig. 3.2: Detailed geological map of the south-western part of the study area (see outlines of the map given in Fig. 3.1) showing the locations of specimen numbers 1-184; refer to Fig. 3.1 regarding the locations of all other samples and to Table 3.1 for exact location. The traces of cross sections shown in Figs. 3.8b, c, d & e are indicated by the letters A-A', B-B', C-C' and D-D', respectively. Coordinates given are those of the Swiss maps.

as indicated by the growth of new porphyroblasts related to Barrovian overprint, such as zoisite/clinozoisite, plagioclase, biotite and garnet, over an amazingly short distance along strike.

In order to include also additional samples taken at some further distance E and N from the closer area of investigation of Wiederkehr et al. (2008), and in order to increase the sample density, the data-set has been completed by reference samples used by previous studies. X-ray diffraction, combustion analysis, thermal analysis and vitrinite reflectance data (Petrova et al. 2002), as well as data from transmission electron microscopy (Ferreiro Mählmann et al. 2002), were collected along a profile that stretches from that part of the Misox Zone where amphibolite facies conditions prevail (southernmost sample points in Fig. 3.1) all the way to in the Prättigau half-window that was only affected by low-grade metamorphism (in the NE corner of Fig. 3.1). The samples previously used by these studies were included for the present study in order to spatially extend the data set, but also in order to compare these previous results with those of our own investigation. Furthermore, additional samples were taken from the collection of M. Frey (Basel University), samples that were subject of earlier investigations (Hoefs & Frey 1976; Frey 1978; Frey et al. 1982; Teutsch 1982; Thoenen 1989). These also include the Urseren-Garvera Zone (samples 1-4 in Fig. 3.2) and increase the sample density in the southerly adjacent Lukmanier area and in the Misox Zone.

3.3. RSCM method

The continuous transformation of the crystalline structure of CM from amorphous organic matter to fully ordered graphite (generally called graphitization process; e.g. Teichmüller 1987) is mainly temperature dependent, and hence the crystallinity of CM is expected to increase systematically with increasing temperatures and can therefore be used to estimate metamorphic conditions of a given rock sample (e.g. Quinn & Glass 1958; French 1964; Landis 1971; Grew 1974; Itaya 1981; Buseck & Bo-Jun 1985).

We monitor the regional changes in the crystallinity of CM by using Raman spectroscopy. The advantages of this method over others, such as X-ray diffraction, high-resolution transmission electron microscopy, isotope geochemistry or vitrinite reflectance measurements are (1) that Raman spectra show significant changes with increasing metamorphic grade (e.g. Wopenka & Pasteris 1993; Beyssac et al. 2002b), (2) that the method can be performed in a non-destructive way by *in situ* analysis and therefore permits the characterization of individual grains while preserving their petrological and textural relations, and (3) that the sample heterogeneity can be quantified thanks to a high spatial resolution and short spectrum-acquisition time, which allows for recording numerous spectra in a sample. Hence, Raman spectroscopy provides a powerful and very sensitive geothermometer (Pasteris & Wopenka 1991; Yui et al. 1996), especially since the relationships between the degree of crystallinity, as is expressed by the shape of the Raman spectra, and metamorphic conditions have been calibrated as a geothermometer over a wide temperature interval from 330 to 650 °C (Beyssac et al. 2002a). Recently, a new calibration extended the range of the geothermometer to temperatures as low as 100 °C and up to 700 °C (Rahl et al. 2005).

Several studies showed that Raman spectroscopy of carbonaceous material (RSCM method) is the best-suited method for *in situ* determinations of the crystallinity of CM in thin sections (e.g. Pasteris & Wopenka 1991; Wopenka & Pasteris 1993; Yui et al. 1996; Beyssac et al. 2002b, 2003a). The obtained spectra, empirically calibrated against independently determined temperatures (Beyssac et al. 2002a; Rahl et al. 2005) by now provide a reliable geothermometer. It is important to note that the thermally

Table 3.1: This list of samples also includes our own samples, completed by samples from the following studies: ⁽¹⁾ Frey (1978); ⁽²⁾ Hoefs & Frey (1976); ⁽³⁾ Thoenen (1989); ⁽⁴⁾ Petrova et al. (2002); ⁽⁵⁾ Frey et al. (1982). The specimens were taken from Valaisan- and Europe-derived metasedimentary units and analyzed by Raman spectroscopy of carbonaceous material in this study. The specimen numbers corresponds with those whose location is shown in map and profile view (Figs. 3.1, 3.2 & 3.8), the coordinates are the Swiss map coordinates. Elevation is given in meters. The origin of the samples (Tectonic unit) is also given, whereby: UG = Urseren-Garvera Zone, S = Scopi unit, PS = Peidener slices, TL = Piz Terri-Lunschiana unit, G = Grava nappe, T = Tomül nappe, M = Misox Zone, AV = Aul and Valser slices, PF= Prättigau flysch, AM = internal Mesozoic of the Adula nappe complex. Also listed are observed mineral assemblage, number of recorded Raman spectra (# sp.), R1 and R2 ratio (mean value and standard deviation SD), RSCM-inferred mean temperatures and uncertainties are given for the 95 % confidence interval (CI) for both calibrations. Temperature uncertainties were determined by dividing the standard deviation of the measurements by the square root of the number of measurements, multiplied by a parameter depending on the number of measurements as well as the chosen confidence interval. Samples highlighted by bold letters were not considered for the iso-temperature contours (see text for discussion).

#	Sample name	Swiss map coordinates		Elev. (m)	Tect. Unit	Mineral assemblage	# sp.	R1		R2		Beyssac et al. (2002)		Rahl et al. (2005)	
		X	Y					Mean	SD	Mean	SD	T (°C)	CI	T (°C)	CI
1	MF 856 ⁽¹⁾	700'800	167'700	2220	UG	Ctd-Mrg-WM-Chl-Qtz	25	0.60	0.08	0.43	0.03	452	5	446	4
2	MF 898 ⁽¹⁾	704'500	169'000	1580	UG	Ctd-Mrg-WM-Chl-Qtz	25	0.74	0.11	0.47	0.03	432	6	429	4
3	MF 120 ⁽²⁾	709'400	170'500	1420	UG	Ctd-Mrg-WM-Chl-Qtz	25	1.11	0.16	0.56	0.03	392	5	396	4
4	MF 922 ⁽¹⁾	711'600	172'400	2220	UG	Ctd-Mrg-WM-Chl-Qtz	25	1.76	0.13	0.63	0.01	359	2	376	4
5	MF 153 ⁽²⁾	704'000	159'800	1930	S	Bt-Mrg-WM-Qtz	25	0.19	0.04	0.24	0.04	534	8	539	14
6	LUK 066	703'915	159'784	1930	S	Gr-Bt-Mrg-WM-Chl-Qtz-Ce/Do	15	0.20	0.02	0.26	0.02	524	4	521	5
7	MF 951 ⁽³⁾	704'513	159'622	1960	S	Gr-Bt-Zo/Czo-WM-Qtz-Ce/Do	25	0.19	0.03	0.25	0.03	532	5	533	9
8	LUK 069	704'453	159'166	1970	S	Plag-WM-Qtz-Ce/Do	15	0.19	0.01	0.25	0.01	532	3	533	6
9	MF 944 ⁽²⁾	704'500	158'900	2000	S	Bt-Plag-Zo/Czo-WM-Qtz-Ce/Do	30	0.20	0.03	0.25	0.03	528	5	527	9
10	BOV 0612	706'656	158'772	3190	S	Ctd-WM-Chl-Qtz	45	0.29	0.07	0.31	0.04	502	6	491	9
11	BOV 064	707'305	157'857	2910	S	Plag-WM-Chl-Qtz-Ce/Do	15	0.21	0.03	0.26	0.03	524	7	522	11
12	MF 184 ⁽³⁾	706'577	157'426	2520	S	Gr-Bt-Zo/Czo-WM-Qtz	30	0.18	0.03	0.24	0.03	535	5	538	9
13	BOV 063	709'067	158'045	2580	S	Plag-WM-Qtz-Ce/Do	25	0.26	0.04	0.30	0.03	508	6	496	10
14	BOV 067	710'904	159'018	2350	S	Ctd-WM-Chl-Qtz	25	0.33	0.06	0.34	0.03	491	6	475	9
15	BOV 068	711'421	159'354	2380	S	Ctd-WM-Chl-Qtz	25	0.32	0.06	0.33	0.03	494	6	478	9
16	BOV 0611	711'277	157'680	1890	S	Gr-Bt-Plag-Zo/Czo-WM-Chl-Qtz	15	0.20	0.03	0.26	0.02	524	5	519	9
17	DÖT 063	708'208	156'187	2530	PS	Gr-Bt-Zo/Czo-WM-Chl-Qtz	21	0.17	0.02	0.23	0.02	538	4	542	7
18	DÖT 061	712'281	156'242	2100	PS	Gr-Bt-Ctd-Mrg-WM-Qtz	15	0.17	0.03	0.22	0.02	542	6	551	9
19	DÖT 052	713'556	155'867	2099	G	Bt-Plag-Zo/Czo-WM-Qtz-Ce/Do	10	0.19	0.03	0.25	0.03	529	10	528	17
20	DÖT 0510	712'890	154'745	1465	G	Gr-Bt-Plag-Zo/Czo-WM-Qtz-Ce/Do	10	0.17	0.03	0.25	0.03	529	9	522	16
21	BLE 0512	715'112	155'757	1090	G	Bt-Plag-Zo/Czo-WM-Chl-Qtz-Ce/Do	19	0.17	0.04	0.23	0.05	538	10	544	18
22	BLE 056	715'097	154'882	980	G	Bt-Plag-Zo/Czo-WM-Chl-Qtz-Ce/Do	10	0.18	0.05	0.24	0.05	534	16	537	29
23	BLE 052	714'864	154'466	910	G	Bt-Plag-Zo/Czo-WM-Chl-Qtz-Ce/Do	31	0.18	0.05	0.24	0.05	535	8	539	15
24	MF 1575 ⁽²⁾	705'900	154'400	1840	PS	Ky-Bt-WM-Qtz	20	0.15	0.02	0.20	0.02	550	5	567	8
25	LUK 0630	707'475	154'073	1790	PS	Gr-Bt-Plag-Zo/Czo-WM-Qtz-Ce/Do	36	0.14	0.03	0.20	0.04	552	5	567	10
26	MF 1581 ⁽²⁾	707'500	154'000	1780	PS	St-Ky-Grt-Bt-Plag-WM-Chl-Qtz	25	0.14	0.04	0.20	0.05	553	8	570	16
27	LUK 0644	708'402	154'680	1820	PS	St-Grt-Bt-Plag-Zo/Czo-WM-Qtz	20	0.14	0.05	0.19	0.05	557	11	579	21
28	LUK 0641	708'254	153'917	1590	PS	St-Ky-Grt-Bt-Plag-Zo/Czo-WM-Chl-Qtz	10	0.14	0.03	0.20	0.04	553	13	569	23
29	MF 1606 ⁽²⁾	709'100	153'500	1470	PS	St-Grt-Bt-Plag-Zo/Czo-WM-Chl-Qtz	25	0.13	0.03	0.18	0.04	561	8	585	14
30	LUK 0637	709'495	153'619	1520	PS	St-Grt-Bt-Plag-Zo/Czo-WM-Chl-Qtz-Ce/Do	10	0.16	0.03	0.22	0.03	544	10	553	18
31	LUK 0635	710'870	153'442	1430	PS	Gr-Bt-Plag-Zo/Czo-WM-Qtz	20	0.14	0.03	0.19	0.04	555	8	574	15
32	LUK 0646	712'242	153'582	1340	PS	Gr-Bt-Plag-Zo/Czo-WM-Qtz-Ce/Do	20	0.15	0.02	0.20	0.02	550	5	565	9
33	GRU 061	716'288	150'576	770	G	Bt-Plag-Zo/Czo-WM-Chl-Qtz-Ce/Do	21	0.14	0.03	0.19	0.03	556	6	577	11
34	GRU 062	716'156	149'270	760	G	Bt-Plag-Zo/Czo-WM-Chl-Qtz-Ce/Do	10	0.12	0.03	0.18	0.03	559	11	579	11
35	GRU 057	715'621	148'504	700	G	Bt-Plag-WM-Qtz-Ce/Do	10	0.13	0.03	0.19	0.04	558	11	578	21
36	GRU 053	714'990	149'545	630	PS	St-Ky-Grt-Bt-Plag-WM-Chl-Qtz	22	0.12	0.04	0.17	0.06	564	11	589	20
37	GRU 058	715'734	149'305	750	G	Bt-Plag-WM-Qtz-Ce/Do	10	0.13	0.02	0.18	0.02	560	6	582	11
38	MOL 051	710'270	149'696	2270	PS	St-Ky-Grt-Bt-Plag-WM-Qtz	10	0.12	0.02	0.19	0.03	557	8	574	15
39	MOL 055	709'715	149'780	2400	G	Bt-WM-Qtz-Ce/Do	10	0.12	0.02	0.17	0.02	563	7	587	13
40	MOL 062	709'617	150'119	2450	PS	St-Grt-Bt-Plag-Zo/Czo-WM-Qtz	10	0.12	0.02	0.18	0.03	560	8	582	15
41	MOL 058	709'468	150'172	2550	G	Bt-WM-Qtz-Ce/Do	10	0.13	0.02	0.19	0.03	557	9	576	16
42	MOL 061	709'541	149'308	2310	PS	St-Ky-Grt-Bt-Plag-WM-Qtz	10	0.12	0.02	0.17	0.02	563	6	588	12
43	CAR 0516	716'440	155'418	1570	G	Bt-Plag-Zo/Czo-WM-Qtz-Ce/Do	15	0.23	0.06	0.28	0.05	518	12	512	20
44	CAR 0515	716'834	156'093	1630	G	Bt-Plag-Zo/Czo-WM-Qtz-Ce/Do	16	0.14	0.07	0.19	0.08	558	19	580	34
45	SOS 051	716'092	156'428	2160	G	Bt-Plag-Ttn-Zo/Czo-WM-Qtz	15	0.25	0.05	0.30	0.03	506	7	490	11
46	BLE 0410	715'029	156'841	1190	PS	Gr-Bt-Plag-Zo/Czo-Mrg-WM-Qtz-Ce/Do	14	0.20	0.04	0.26	0.04	526	10	522	16
47	BLE 061	715'186	157'232	1210	PS	Gr-Bt-WM-Chl-Qtz	22	0.21	0.03	0.27	0.03	522	6	516	10
48	BLE 0413	715'346	157'292	1230	PS	Bt-Plag-Ttn-Zo/Czo-WM-Qtz-Ce/Do	13	0.22	0.05	0.27	0.04	519	11	512	19
49	LUZ 0442	716'017	157'831	1390	G	Bt-Plag-Zo/Czo-WM-Qtz-Ce/Do	15	0.25	0.09	0.29	0.07	513	18	506	29
50	CAR 0517	716'596	157'598	1650	G	Plag-WM-Qtz-Ce/Do	16	0.26	0.07	0.29	0.05	511	12	503	18
51	CAR 055	717'084	157'365	2030	G	Plag-Zo/Czo-WM-Chl-Qtz	16	0.20	0.06	0.25	0.04	532	9	536	15
52	CAR 052	717'226	156'393	1680	TL	WM-Qtz-Ce/Do	16	0.27	0.06	0.30	0.05	507	11	494	18
53	CAR 0510	717'901	156'992	2140	TL	Ctd-WM-Chl-Qtz-Ce/Do	17	0.31	0.11	0.33	0.07	496	15	482	23
54	CAR 059	717'906	157'007	2160	TL	WM-Chl-Qtz-Ce/Do	10	0.38	0.06	0.38	0.03	474	9	448	13
55	CAR 0519	716'835	157'783	1580	G	Plag-WM-Chl-Qtz-Ce/Do	10	0.26	0.05	0.30	0.04	508	11	496	17
56	LUZ 0456	716'469	158'124	1450	G	Plag-Ttn-Zo/Czo-WM-Chl-Qtz-Ce/Do	17	0.24	0.07	0.29	0.06	514	14	505	22
57	LUZ 055	716'865	158'363	1780	G	Plag-Ttn-Zo/Czo-WM-Chl-Qtz	10	0.35	0.05	0.36	0.04	480	11	451	15
58	CAV 054	717'107	158'540	1770	G	Plag-Zo/Czo-WM-Chl-Qtz-Ce/Do	16	0.35	0.08	0.34	0.04	490	10	475	14
59	LUZ 051	717'825	159'166	1850	G	WM-Chl-Qtz-Ce/Do	10	0.33	0.06	0.34	0.03	489	11	468	15
60	CAV 0520	717'808	159'311	1870	G	Plag-WM-Qtz-Ce/Do	15	0.35	0.07	0.36	0.04	481	10	457	15
61	CAV 0511	717'618	159'926	1820	PS	WM-Qtz	16	0.35	0.06	0.35	0.04	485	9	464	13
62	CAM 062	715'474	159'346	1430	PS	WM-Chl-Qtz	15	0.26	0.05	0.31	0.04	504	9	486	15
63	CAM 065	715'367	159'595	1400	S	Plag-WM-Chl-Qtz-Ce/Do	25	0.31	0.05	0.33	0.04	496	7	480	10
64	CAM 066	714'841	159'482	1380	S	Plag-WM-Chl-Qtz-Ce/Do	22	0.30	0.03	0.32	0.02	498	4	483	7
65	CAM 069	714'624	160'457	1470	S	Ctd-WM-Chl-Qtz	18	0.36	0.05	0.37	0.03	478	6	452	10
66	GRE 051	714'727	162'889	2000	S	Ctd-WM-Chl-Qtz	25	0.44	0.05	0.39	0.03	468	5	447	6
67	GRE 052	715'664	163'152	2310	S	Ctd-WM-Chl-Qtz	15	0.43	0.04	0.38	0.02	474	5	460	7
68	GRE 061	715'971	163'212	2370	S	Ctd-WM-Chl-Qtz	22	0.45	0.08	0.38	0.04	471	7	457	10
69	GRE 0610	715'985	162'527	2660	S	Ctd-WM-Chl-Qtz	22	0.41	0.05	0.36	0.02	479	5	465	6
70	GRE 069	716'552	161'946	2790	S	Ctd-WM-Chl-Qtz	22	0.43	0.05	0.38	0.03	471	5	453	7
71	GRE 068	716'779	162'403	2730	S	Ctd-WM-Chl-Qtz	22	0.41	0.07	0.37	0.04	477	7	461	9
72	GRE 067	717'565	162'430	2790	S	Ctd-WM-Chl-Qtz	22	0.43	0.06	0.38	0.03	473	6	457	7
73	GRE 062	718'047	163'562	2320	S	Ctd-WM-Chl-Qtz	20	0.48	0.05	0.39	0.02	466	5	451	7
74	GRE 065	718'180	162'606	2590	S	Ctd-WM-Chl-Qtz	15	0.48	0.08	0.40	0.03	462	7	444	10
75	LAR 0612	718'524	161'805	2050	S	WM-Qtz-Ce/Do	10	0.50	0.07	0.41	0.03	460	9	443	11
76	LAR 0614	718'722	160'899	1840	PS	WM-Qtz-Ce/Do	15	0.53	0						

Table 3.1: continued.

#	Sample name	Swiss map coordinates		Elev. (m)	Tect. Unit	Mineral assemblage	# sp.	R1		R2		Beysaet et al. (2002)		Rahl et al. (2005)	
		X	Y					Mean	SD	Mean	SD	T (°C)	CI	T (°C)	CI
84	SCA 051	720'104	158'455	2270	TL	WM-Qtz-Ce/Do	10	0.30	0.05	0.32	0.03	500	9	489	12
85	SCA 071	720'417	159'022	2540	TL	WM-Chl-Qtz-Cc/Do	20	0.43	0.04	0.40	0.02	465	5	437	8
86	GAR 053	720'863	159'895	2060	TL	Ctd-WM-Chl-Qtz-Cc/Do	10	0.29	0.04	0.32	0.02	499	8	485	12
87	GAR 052	721'604	160'190	2210	TL	Ctd-WM-Chl-Qtz-Cc/Do	12	0.44	0.11	0.40	0.05	465	14	440	17
88	VRI 0622	722'939	160'396	2940	TL	Ctd-WM-Chl-Qtz-Cc/Do	23	0.72	0.09	0.46	0.03	438	5	439	4
89	GAR 056	722'366	160'378	2600	TL	WM-Qtz-Cc/Do	11	0.46	0.07	0.40	0.02	461	7	435	8
90	MOT 0513	719'622	160'641	1790	G	WM-Qtz-Cc/Do	16	0.50	0.13	0.40	0.06	461	14	445	16
91	MOT 0512	720'114	161'192	2090	G	WM-Chl-Qtz-Cc/Do	15	0.49	0.09	0.41	0.04	460	10	440	12
92	LUZ 0425	720'598	161'470	2290	G	WM-Chl-Qtz	15	0.48	0.07	0.40	0.02	461	6	440	6
93	MOT 051	719'927	161'888	2210	G	WM-Chl-Qtz-Cc/Do	15	0.51	0.08	0.41	0.04	461	9	447	11
94	GRE 063	719'274	163'604	2250	S	Ctd-WM-Chl-Qtz	22	0.49	0.07	0.41	0.03	460	7	441	8
95	MOT 053	720'455	163'705	2420	PS	Ctd-WM-Chl-Qtz	22	0.50	0.10	0.40	0.04	464	8	452	9
96	MOT 059	720'730	163'126	2590	G	WM-Chl-Qtz-Cc/Do	16	0.62	0.11	0.44	0.04	445	8	435	7
97	TER 0511	721'621	162'296	2750	TL	Ab-WM-Qtz	16	0.25	0.05	0.27	0.03	521	8	525	11
98	TER 0510	721'682	162'126	2900	TL	WM-Qtz-Cc/Do	20	0.56	0.13	0.42	0.04	452	9	439	10
99	TER 058	721'830	162'118	2970	TL	WM-Chl-Qtz-Cc/Do	17	0.58	0.08	0.43	0.03	448	7	434	7
100	TER 057	721'991	162'147	3020	TL	WM-Chl-Qtz-Cc/Do	18	0.55	0.10	0.42	0.04	454	8	442	9
101	TER 056	722'082	162'198	3076	TL	WM-Qtz-Cc/Do	18	0.47	0.08	0.39	0.03	466	7	452	7
102	TER 051	722'245	162'212	3150	TL	WM-Qtz-Cc/Do	16	0.62	0.07	0.44	0.02	444	6	432	7
103	VRI 0618	724'214	161'412	2480	TL	WM-Qtz-Cc/Do	25	0.58	0.06	0.43	0.02	451	4	441	6
104	VRI 0616	724'498	162'815	1890	TL	WM-Qtz-Cc/Do	39	0.63	0.15	0.44	0.06	446	9	439	9
105	VRI 0629	724'661	163'907	2260	TL	WM-Qtz-Cc/Do	10	0.58	0.06	0.42	0.02	456	5	452	5
106	VRI 0630	723'747	164'637	2450	G	WM-Chl-Qtz	18	0.63	0.08	0.43	0.03	451	6	452	5
107	VRI 0633	723'227	164'617	2430	G	Ctd-WM-Chl-Qtz	22	0.59	0.12	0.43	0.04	450	9	439	10
108	VRI 061	722'919	165'841	2110	S	Ctd-WM-Chl-Qtz	20	0.65	0.08	0.43	0.02	450	5	453	4
109	VRI 064	721'495	166'274	2430	S	Ctd-WM-Chl-Qtz	17	0.64	0.17	0.42	0.05	454	12	458	11
110	VRI 0614	723'645	167'250	1870	S	Ctd-WM-Chl-Qtz	15	0.71	0.10	0.45	0.03	442	7	447	6
111	VRI 068	724'447	166'316	1630	PS	Ctd-WM-Chl-Qtz	15	0.67	0.08	0.45	0.02	442	5	437	6
112	VRI 052	726'018	164'498	1630	TL	WM-Qtz-Cc/Do	15	0.77	0.08	0.48	0.02	428	5	424	4
113	VRI 0636	727'363	165'266	2060	TL	WM-Qtz-Cc/Do	25	0.74	0.09	0.46	0.03	437	5	440	4
114	VRI 0637	727'363	165'266	2060	TL	WM-Qtz-Cc/Do	21	0.79	0.08	0.47	0.02	430	5	434	4
115	VRI 0638	727'890	165'007	2250	G	WM-Qtz-Cc/Do	18	0.58	0.07	0.40	0.02	461	5	464	6
116	VRI 0639	728'153	164'660	2520	AV	WM-Chl-Qtz	21	0.76	0.06	0.47	0.01	434	3	437	4
117	VRI 0640	728'577	164'644	2670	AV	Ab-WM-Chl-Qtz-Cc/Do	31	0.73	0.17	0.46	0.05	436	8	435	7
118	VRI 051	726'304	166'805	1420	G	WM-Qtz-Cc/Do	20	0.85	0.13	0.49	0.04	424	8	429	9
119	VRI 075	726'579	167'357	1400	PS	Ctd-WM-Chl-Qtz	25	0.72	0.10	0.46	0.02	436	4	435	3
120	VRI 073	727'048	169'497	1500	S	WM-Chl-Qtz-Cc/Do	25	0.95	0.12	0.52	0.02	408	4	411	2
121	VRI 0641	728'023	169'054	1280	PS	WM-Qtz-Cc/Do	22	0.80	0.19	0.47	0.04	431	8	436	6
122	VRI 0645	728'683	167'957	1570	G	WM-Chl-Qtz-Cc/Do	25	0.72	0.10	0.47	0.02	432	4	424	3
123	VRI 0649	729'844	167'225	2120	TL	WM-Qtz-Cc/Do	21	0.85	0.07	0.49	0.02	424	3	431	3
124	VAL 062	731'316	168'000	2420	TL	WM-Chl-Qtz	21	0.86	0.08	0.49	0.02	424	4	434	3
125	VAL 061	731'491	168'208	2270	TL	WM-Qtz-Cc/Do	26	0.95	0.16	0.52	0.03	410	6	412	8
126	VAL 063	731'289	168'354	2340	TL	WM-Chl-Qtz	24	0.76	0.09	0.48	0.02	426	4	419	4
127	VAL 064	731'289	168'557	2340	TL	WM-Chl-Qtz	18	0.74	0.07	0.46	0.02	437	4	440	4
128	VAL 066	731'805	169'620	2050	G	WM-Chl-Qtz-Cc/Do	20	0.84	0.12	0.49	0.03	421	6	422	6
129	VAL 065	731'823	169'913	2050	G	WM-Chl-Qtz-Cc/Do	19	0.90	0.11	0.50	0.02	418	5	425	5
130	VRI 072	729'104	170'789	1260	S	Ctd-WM-Chl-Qtz	25	1.00	0.13	0.53	0.02	405	4	409	4
131	VRI 0651	730'151	172'057	1370	S	Ctd-WM-Chl-Qtz	22	1.39	0.13	0.58	0.02	381	3	403	3
132	VAL 0546	733'770	171'970	1160	G	WM-Chl-Qtz-Cc/Do	16	1.21	0.08	0.57	0.01	389	4	402	4
133	VAL 0719	733'311	171'359	1020	G	WM-Chl-Qtz-Cc/Do	25	1.01	0.13	0.53	0.02	405	5	412	3
134	VAL 052	733'254	170'168	1050	G	WM-Qtz-Cc/Do	16	0.84	0.07	0.50	0.02	421	4	422	4
135	VAL 0720	733'422	169'874	1080	G	WM-Chl-Qtz-Cc/Do	27	0.88	0.13	0.51	0.03	416	6	416	5
136	VAL 057	733'765	169'471	1100	TL	Ab-WM-Qtz-Cc/Do	16	0.35	0.07	0.33	0.03	496	8	492	10
137	VAL 0624	734'691	169'923	1550	TL	WM-Chl-Qtz-Cc/Do	18	1.08	0.06	0.54	0.01	402	2	417	2
138	VAL 055	734'054	169'284	1100	TL	WM-Chl-Qtz-Cc/Do	17	0.88	0.12	0.50	0.03	417	7	418	5
139	VAL 056	734'054	169'284	1100	TL	Ab-WM-Qtz-Cc/Do	19	0.48	0.14	0.38	0.06	472	12	465	14
140	VAL 067	733'620	169'160	1100	TL	WM-Chl-Qtz-Cc/Do	21	0.67	0.09	0.44	0.02	444	5	444	4
141	VAL 0716	734'183	168'768	1180	G	WM-Chl-Qtz-Cc/Do	25	0.92	0.09	0.52	0.02	411	4	413	3
142	VAL 0714	732'470	167'831	2000	G	WM-Chl-Qtz-Cc/Do	25	0.93	0.13	0.52	0.03	411	5	412	3
143	VAL 0711	732'486	166'320	1950	AV	Ctd-WM-Chl-Qtz-Cc/Do	27	0.94	0.13	0.52	0.02	408	4	406	3
144	VAL 0710	731'370	163'971	1960	AV	Ctd-WM-Chl-Qtz-Cc/Do	25	0.87	0.09	0.51	0.02	416	4	415	3
145	VAL 0715	734'484	163'945	1750	AV	WM-Chl-Qtz-Cc/Do	26	0.94	0.07	0.52	0.02	410	3	414	3
146	VAL 079	734'426	161'844	1740	AM	Grt-Zo/Czo-WM-Chl-Qtz-Cc/Do	20	0.24	0.06	0.29	0.04	511	8	499	12
147	VAL 078	734'383	161'757	1790	AM	Grt-Ctd-Zo/Czo-WM-Chl-Qtz-Cc/Do	30	0.24	0.05	0.29	0.05	511	8	497	13
148	VAL 076	734'248	161'383	1920	AM	Grt-Ctd-Zo/Czo-WM-Chl-Qtz-Cc/Do	22	0.20	0.05	0.27	0.05	522	10	513	18
149	VAL 072	730'645	159'313	2540	AM	Ky-Grt-Ctd-Zo/Czo-WM-Chl-Qtz-Cc/Do	27	0.22	0.05	0.28	0.05	515	8	503	14
150	VAL 0724	734'965	158'690	2300	AV	Ab-WM-Chl-Qtz-Cc/Do	25	0.71	0.09	0.47	0.03	432	5	424	5
151	VAL 0722	735'836	160'005	1970	AV	Ab-WM-Chl-Qtz-Cc/Do	25	0.89	0.10	0.51	0.02	413	3	413	3
152	VAL 0618	737'462	159'815	2930	T	WM-Chl-Qtz	18								

Table 3.1: continued.

#	Sample name	Swiss map coordinates		Elev. (m)	Tect. Unit	Mineral assemblage	# sp.	R1		R2		Beysac et al. (2002)		Rahl et al. (2005)	
		X	Y					Mean	SD	Mean	SD	T (°C)	CI	T (°C)	CI
184	SAF 075	739'980	160'207	2490	T	WM-Chl-Qtz	26	1.07	0.09	0.53	0.02	404	3	419	3
185	MF 2141 ⁽⁴⁾	738'300	137'025	1200	M	Grt-Bt-Plag-WM-Chl-Qtz	35	0.17	0.04	0.23	0.05	541	7	548	13
186	MF 2042 ⁽⁴⁾	737'600	140'450	900	M	Grt-Plag-WM-Chl-Qtz	23	0.20	0.05	0.25	0.04	532	8	535	13
187	MF 1872 ⁽⁵⁾	736'300	143'800	1240	M	Mrg-WM-Chl-Qtz-Cc/Do	20	0.39	0.11	0.36	0.06	480	12	461	18
188	MF 1895 ⁽⁴⁾	734'900	145'325	1850	M	Grt-Plag-WM-Chl-Qtz	25	0.30	0.02	0.33	0.02	493	3	472	6
189	TP 32 ⁽⁴⁾	734'750	150'350	2220	M	Ctd-Zo/Czo-WM-Chl-Qtz-Cc/Do	23	0.31	0.04	0.34	0.02	490	4	467	5
190	TP 31 ⁽⁴⁾	734'600	152'200	2120	M	Grt-Ctd-Zo/Czo-WM-Chl-Qtz-Cc/Do	25	0.23	0.04	0.28	0.03	516	6	508	10
191	TP 34 ⁽⁴⁾	734'450	153'600	1840	M	Grt-Ctd-Zo/Czo-WM-Chl-Qtz-Cc/Do	25	0.23	0.03	0.29	0.03	512	5	498	8
192	TP 25 ⁽⁴⁾	735'325	154'200	1800	M	Ab-WM-Chl-Qtz-Cc/Do	17	0.49	0.04	0.41	0.01	460	3	441	4
193	TP 24 ⁽⁴⁾	738'125	156'475	1770	G	WM-Chl-Qtz-Cc/Do	25	0.70	0.10	0.46	0.03	438	5	437	4
194	HINT 079	739'193	153'874	1670	T	Cp-Ctd-WM-Chl-Qtz-Cc/Do	25	0.68	0.09	0.45	0.03	441	5	439	4
195	TP 22 ⁽⁴⁾	741'225	156'675	1620	T	Ab-WM-Chl-Qtz	25	0.96	0.07	0.52	0.02	409	3	416	4
196	TP 36 ⁽⁴⁾	748'700	161'350	2040	T	WM-Chl-Qtz	25	1.51	0.23	0.60	0.02	372	4	389	4
197	TP 37 ⁽⁴⁾	752'000	164'050	1000	T	WM-Chl-Qtz-Cc/Do	25	2.39	0.11	0.68	0.00	337	1	314	4
198	TP 20 ⁽⁴⁾	753'775	168'025	900	T	WM-Chl-Qtz-Cc/Do	20	1.99	0.08	0.65	0.01	351	2	360	4
199	TP 19 ⁽⁴⁾	753'800	169'925	870	T	WM-Chl-Qtz-Cc/Do	25	1.52	0.12	0.61	0.02	371	3	391	3
200	TP 15 ⁽⁴⁾	753'300	173'325	700	T	WM-Chl-Qtz	20	1.45	0.08	0.60	0.01	376	2	398	3
201	TP 39 ⁽⁴⁾	752'350	175'350	760	T	WM-Chl-Qtz-Cc/Do	20	1.53	0.16	0.60	0.01	374	3	397	3
202	TP 40 ⁽⁴⁾	751'850	177'300	670	T	WM-Chl-Qtz-Cc/Do	20	1.71	0.14	0.62	0.02	363	3	382	5
203	TP 12 ⁽⁴⁾	751'275	181'750	630	G	Ab-WM-Chl-Qtz-Cc/Do	21	1.63	0.10	0.62	0.01	364	2	382	3
204	TP 11 ⁽⁴⁾	750'150	183'600	680	G	WM-Chl-Qtz-Cc/Do	20	1.83	0.12	0.64	0.01	357	3	374	6
205	TP 9 ⁽⁴⁾	756'850	188'100	1030	G	WM-Chl-Qtz-Cc/Do	20	2.06	0.05	0.66	0.01	349	1	356	3
206	MW 9664 ⁽⁴⁾	760'650	187'870	800	G	WM-Chl-Qtz-Cc/Do	20	2.23	0.13	0.67	0.02	343	3	336	10
207	TP 42 ⁽⁴⁾	760'250	190'050	610	G	WM-Chl-Qtz-Cc/Do	15	2.09	0.19	0.66	0.01	346	3	345	8
208	Ps 7 ⁽⁴⁾	768'940	189'195	1200	PF	WM-Qtz-Cc/Do	10	1.24	0.12	>0.70		<330		255	5
209	TP 7 ⁽⁴⁾	762'125	196'500	970	G	WM-Chl-Qtz-Cc/Do	15	1.95	0.11	0.66	0.01	348	3	353	6
210	TP 5 ⁽⁴⁾	764'375	200'300	1060	G	WM-Chl-Qtz	22	1.42	0.17	0.59	0.02	378	4	398	4
211	Vs 3 ⁽⁴⁾	766'345	203'635	1250	G	WM-Qtz-Cc/Do	10	1.42	0.07	>0.70		<330		268	8
212	TP 1 ⁽⁴⁾	772'575	202'825	690	G	WM-Chl-Qtz-Cc/Do	12	1.47	0.06	>0.70		<330		266	6
213	MF 2987 ⁽⁴⁾	779'400	208'700	1830	PF	WM-Chl-Qtz-Cc/Do	10	0.56	0.02	>0.70		<330		131	5
214	MF 2986 ⁽⁴⁾	775'300	211'700	2150	PF	WM-Chl-Qtz-Cc/Do	10	0.55	0.02	>0.70		<330		135	6

induced graphitization process is strictly irreversible. Therefore the structure of CM solely depends on maximum temperatures reached along a given P-T path and is insensitive for detecting a polymetamorphic evolution and/or retrograde overprint (Wopenka & Pasteris 1993; Beysac et al. 2002a).

Since the 214 samples analyzed were collected in areas either dominated by subduction-related HP/LT metamorphism or by collision-related MP/MT Barrovian overprint (Figs. 3.1 & 3.2, Tab. 3.1) in terms of temperature, it is only the 3-D pattern of the temperatures derived by this method, combined with additional petrological data, which will be able to discriminate between these two events. All the results obtained by Raman spectroscopy were converted to peak-metamorphic temperatures by using both calibrations (Beysac et al. 2002a; Rahl et al. 2005). In order to obtain comparable results we strictly followed the analytical instructions given by Beysac et al. (2002a, 2003b).

3.3.1. Sample preparation

The Raman spectra were recorded *in situ* on conventional polished petrographic thin sections, allowing for the preservation of the textural relationship between CM and the surrounding mineral matrix. Additionally, the surrounding rock matrix facilitates the removal of laser-induced heat, which may affect the degree of organization due the extreme sensitivity of CM to laser-induced heating during spectra acquisition (Beysac et al. 2003b). Moreover, the recorded Raman spectra are highly sensitive to the orientation of CM due to its strong structural anisotropy, particularly in the case of well-crystallised graphite (e.g. Wang et al. 1989; Wopenka & Pasteris 1993). To avoid such variations the thin sections were cut perpendicular to the main foliation and, whenever possible also parallel to the stretching lineation, in order to consequently record Raman spectra in the same orientation, i.e. perpendicular to the expected mean stacking axis of the CM. Thereby it is possible to set the polarization of the laser beam perpendicular to the mean c-axis orientation of the CM.

3.3.2. Raman spectrum of carbonaceous material

In general, Raman spectra of CM can be decomposed into first-order (1100-1800 cm⁻¹) and second-order (2500-3100 cm⁻¹) regions (Tuinstra & Koenig 1970; Nemanich & Solin 1979; Fig. 3.3). It

has been shown by several studies that the first-order region is perfectly suited to record the degree of order/disorder of CM and thereby to determine peak-metamorphic temperatures (Pasteris & Wopenka 1991; Wopenka & Pasteris 1993; Yui et al. 1996; Beyssac et al. 2002a, 2002b; Rantitsch et al. 2004; Rahl et al. 2005). This first-order region includes up to four Raman peaks or bands (Fig. 3.3a; Tuinstra & Koenig 1970; Beyssac et al. 2002a, 2003a; Nasdala et al. 2004). The presence of the G band ($\sim 1580\text{ cm}^{-1}$), corresponding to the stretching vibration of aromatic carbon layers, is indicative for graphite crystals (e.g. Beyssac et al. 2003b). In perfect crystalline CM, i.e. graphite, this G band is the only feature of the first-order region. In poorly ordered CM, as a consequence of structural disorder, however, up to three additional bands (generally called D1, D2 and D3) are present in the first order region (Fig. 3.3a). These so-called defect bands are related to “physio-chemical defects” (Beyssac et al. 2003b; Negro et al. 2006). Whereas the D1 band ($\sim 1350\text{ cm}^{-1}$) is the most evident defect band and represents a separate peak, the D2 band ($\sim 1620\text{ cm}^{-1}$) is only visible as a shoulder on the dominant G band. Only in very poorly ordered CM does a third defect band D3 appear in the form of a very wide band located at $\sim 1500\text{ cm}^{-1}$. The degree of ordering is directly linked to appearance and intensity of the defect bands, and additionally, to position and peak width of the G band. The intensity of the defect bands decreases during progressive graphitization, thereby reflecting the increasing degree of organization (e.g. Pasteris & Wopenka 1991).

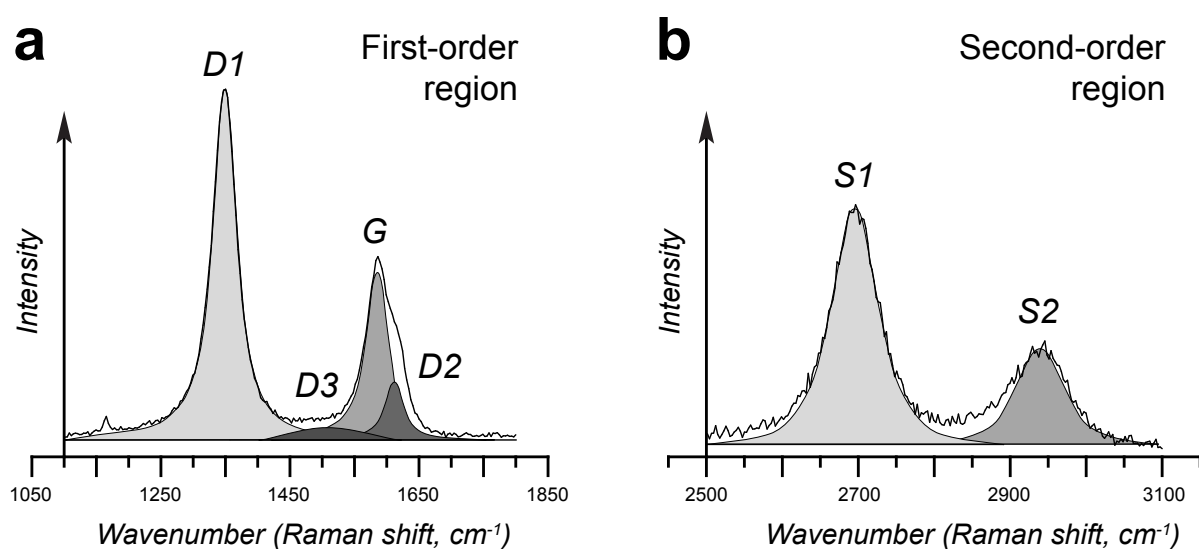


Fig. 3.3: Spectral deconvolution of the first- and second-order region of the Raman spectrum of CM, indicating a relatively disordered structure (sample Nr. 205 for which $350\text{ }^{\circ}\text{C}$ were inferred, see Table 3.1). (a) Position of the graphite G band and the D1, D2, D3 defect bands in the first-order region; (b) Position of the graphite S1 and S2 bands in the second-order region.

The second-order region is characterized by the appearance of two bands, S1 ($\sim 2700\text{ cm}^{-1}$) and S2 ($\sim 2900\text{ cm}^{-1}$), respectively, some minor features are also visible at $\sim 2400\text{ cm}^{-1}$ and $\sim 3300\text{ cm}^{-1}$ (Fig. 3.3b; Nemanich & Solin 1979; Wopenka & Pasteris 1993; Beyssac et al. 2003b; Lee 2004). As is the case regarding the first order-region there are also systematic changes within the second-order region due to increasing graphitization. While the intensity of the S2 band continuously decreases and finally completely vanishes, the S1 band becomes progressively narrower and asymmetric, ultimately splitting into two bands during the final stages of the graphitization process (e.g. Beyssac et al. 2002a). Such splitting is assumed to correspond to the establishment of a triperiodic order in the structure of the CM (Lespade et al. 1984).

During progressive temperature-induced ordering the Raman spectra of CM exhibit a characteristic evolution that is most obvious by looking at the intensities of bands related to disorder in the crystalline structure (D1, D2 & D3), but also evident from position and width of the characteristic G band in the first-order region and from width and asymmetry of the S1 band in the second-order region (Pasteris & Wopenka 1991; Wopenka & Pasteris 1993; Yui et al. 1996; Beyssac et al. 2002a, 2002b; Lee 2004). Beyssac et al. (2002a) showed that peak intensity ratio R1 ($R1 = D1/G$) and peak area ratio R2 ($R2 = D1/[G + D1 + D2]$), both part of the first-order region, are the most reliable indicators for the degree of ordering in CM. They found the following linear relationship between the R2 ratio and peak-metamorphic temperature in the range of 330-650 °C by calibration with other geothermometers:

$$T (\text{°C}) = -445R2 + 641$$

Recently, the following revised and slightly more complex calibration, involving both R1 and R2 ratios in a bivariate polynomial function, has also been presented (Rahl et al. 2005):

$$T (\text{°C}) = 737.3 + 320.9R1 - 1067R2 - 80.638R1^2$$

The R1 ratio, taken into account by this second calibration method, shows significant variations particularly under low- and very low-grade conditions: This contrasts with the R2 ratio, which is rather insensitive below 330 °C and above 650 °C. Therefore, this revised calibration potentially extends the temperature interval to the 100-700 °C interval (Rahl et al. 2005). However, due to uncertainties in the two calibration methods absolute temperatures can only be determined to ± 50 °C. It is important to note, however, that the relative accuracy is much better and allows for detecting inter-sample variations as small as ~ 10 -15 °C (Beyssac et al. 2004).

3.3.3. Analytical procedure: spectra acquisition and treatment

Micro-Raman spectroscopy was performed at the Raman Laboratory of the Institute of Geosciences at Potsdam University using a confocal, notch filter-based spectrometer (LabRam HR 800, HORIBA Jobin Yvon) equipped with an Olympus BX 41 microscope, an air-cooled Nd-YAG laser (Compass 315M, Coherent) for Raman excitation with the 532 nm line and a Peltier cooled CCD detector (Andor Technology). A Leica 50x magnification microscope objective was used for sample viewing under both reflected and transmitted light, as well as for the Raman measurements. The laser spot diameter at the sample surface was about 3 μm and the confocal pinhole was set to 200 μm . The laser power was reduced to 2-3 mW at the sample surface by a neutral D1 filter (transmission: 10 % of the laser power) in order to exclude effects due to sample heating. The LabSpec software of HORIBA Jobin Yvon has been used for data acquisition and estimation of the spectral parameters of the Raman bands. Before each session a silicon standard was used for checking the calibration of the spectrometer. Since thin section preparation, particularly polishing, induces mechanical damage to the structure of CM (Nemanich & Solin 1979; Beyssac et al. 2003b) we focussed the laser beam onto CM matter hiding beneath a transparent mineral within the section (Pasteris 1989; Beyssac et al. 2002a, 2003b), preferentially beneath quartz, but calcite, feldspar or chloritoid were also used.

The application of a grating of 300 lines/mm and a slit width of 100 μm resulted in the acquisition of Raman spectra in the range 175-3300 cm^{-1} with a spectral resolution of about 10 cm^{-1} . This configuration allowed for the registration of all first-order Raman bands of graphite in the region 1100-1800 cm^{-1} used for the estimation of the peak-metamorphic temperatures, and additionally the Raman bands of the covering transparent minerals, within a single spectral window. In each sample at least 10, but up to 45 independent spots were analyzed in order to gather insight regarding structural heterogeneities of

the CM within one and the same sample. Depending on the intensity of the Raman bands between two and four accumulations with an acquisition time ranging from 20 to 90 s were performed on each spot in order to improve signal to noise ratios of the spectra.

The Raman spectra were processed by using the program PEAKFIT 4.12 (Seasolve Software Inc.) with a Voigt function (combined Gaussian and Lorentzian profiles) and a linear background correction to determine the spectral parameters such as peak position, peak area, peak height and peak width FWHM (full width at half maximum).

Table 3.1 summarizes the results of spectrum decomposition for all 214 samples and gives the estimated peak-metamorphic temperatures based on both calibrations (Beyssac et al. 2002a; Rahl et al. 2005) in terms of mean values. Measurement-induced uncertainties regarding the derived temperatures are given as 95 % confidence intervals (CI).

3.4. Results of the RSCM investigations

3.4.1. Overall evolution of Raman spectra with increasing metamorphic grade

The change in metamorphic temperature over the entire area of investigation, ranging from lower/middle amphibolite facies conditions in the SW to lower greenschist facies conditions with occasional blueschist facies relics in the NE, is directly illustrated by the corresponding evolution of the Raman spectra of CM reflecting the degree of crystallization shown by Figure 3.4. This evolution shows all the typical features described in earlier studies (e.g. Pasteris & Wopenka 1991; Wopenka & Pasteris 1993; Yui et al. 1996; Beyssac et al. 2002b). The most obvious feature indicating the general trend towards increasing metamorphic grade in the area, by going from NE to SW and up-temperature, is the decrease in relative intensity of the D1 band (Fig. 3.4). This band is large and wide in the case of the low-temperature samples and decreases towards the SW and disappears almost totally in the highest-grade samples. The G band appears as a wide band occurring near 1600 cm^{-1} in very poorly organized samples where it is impossible to separate the contribution of the D2 component from that of the G band. From some inferred 335°C up-temperature (sample 197 of Fig. 3.4 & Tab. 3.1), this single and wide band splits up into the G and D2 bands. Still further up-temperature the D2 component decreases while the G band narrows (Fig. 3.4). In the second-order region, the S1 band represents the main spectral feature (Fig. 3.4). In poorly structured CM the second-order spectrum (2500-3000 cm^{-1}) is characterized by the presence of two very broad bands at ~ 2700 and ~ 2900 cm^{-1} , respectively. With increasing metamorphic grade, the S1 band becomes prominent over the S2 band. It finally takes on a slightly asymmetric shape at still higher grade which indicates incipient splitting of the S1 band into two components while the S2 band further decreases in intensity and disappears almost totally (Fig. 3.4).

3.4.2. Comparison between the available calibration methods

Given the exceptionally large number of measured samples and the large temperature interval covered by the area of investigation a comparison between the two available calibration methods by Beyssac et al. (2002a) and Rahl et al. (2005) is indicated. In this context it is important to note that the calibration of Beyssac et al. (2002a) is based on the R2 ratio only, a ratio that shows no change anymore below 330 °C and remains stable at ~ 0.75 (Beyssac et al. 2002a). In contrast, the R1 intensity ratio exhibits an ongoing evolution even towards low to very low metamorphic temperatures (Yui et al. 1996; Beyssac et al. 2002a; Rahl et al. 2005). The recent calibration by Rahl et al. (2005) is more complex and

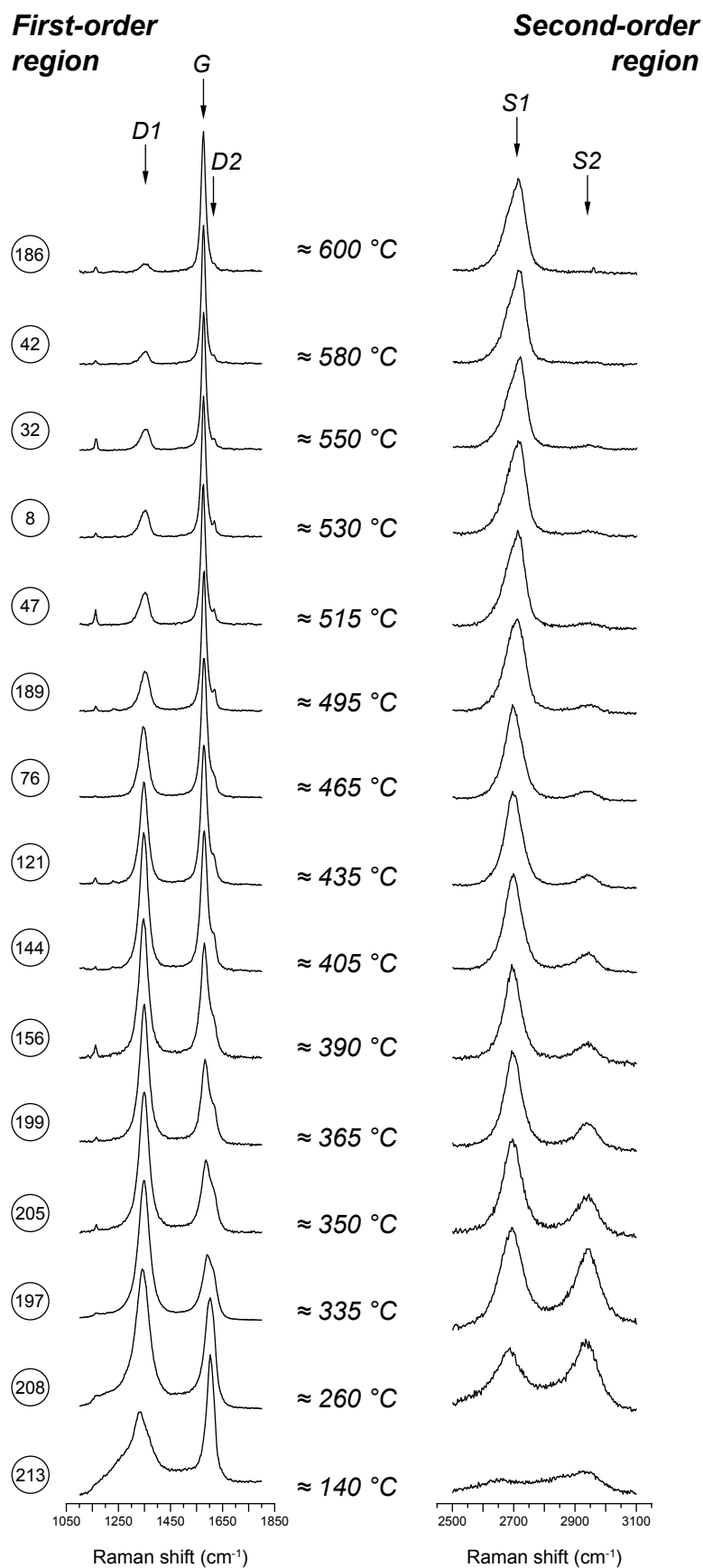


Fig. 3.4: Selection of representative first-order and corresponding second-order parts of the Raman spectra, arranged from bottom to top by increasing inferred temperatures and going from SW to NE across the area of investigation, respectively. The positions of the G, D1, D2, D3, S1 and S2 bands, as well as the estimated peak-metamorphic temperatures are indicated. The numbers on the left-hand side refer to the sample numbers listed in Table 3.1, for geographical locations see also Figs. 3.1 & 3.2. The small, narrow band at around 1160 cm⁻¹ in the first-order region is due to quartz as overlying transparent mineral; see text.

takes into account both ratios R1 and R2 (see section RSCM method for the two formulas used). Since R1 appears to be particularly sensitive under very low-grade metamorphic conditions, it was proposed that this new calibration has an extended application in the very low temperature domain, extending the lower temperature detection limit down to 100 °C (Rahl et al. 2005).

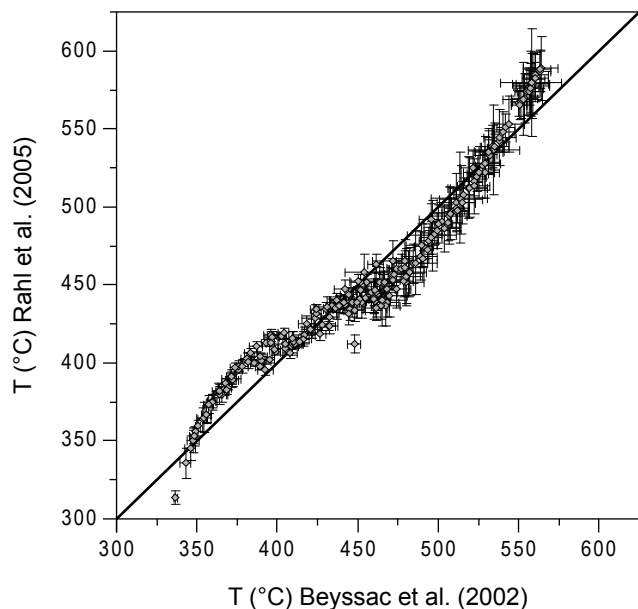


Fig. 3.5: Correlation of peak-metamorphic temperatures estimated based on the calibrations provided by Beyssac et al. (2002a) and Rahl et al. (2005), respectively, for all the analyzed samples. See text for details.

between 350-400 °C and from 550 °C upwards are relatively higher compared to those calculated according Beyssac et al. (2002a). The great advantage of the method of Rahl et al. (2005), however, is the possibility to estimate reliable metamorphic temperatures in low- to very low-grade metasediments, i.e. in the 100-330 °C temperature interval that cannot be handled with the calibration of Beyssac et al. (2002a). In general, the relative uncertainties of the temperatures derived by the calibration of Rahl et al. (2005) are higher, however, compared to those derived using Beyssac et al. (2002a), especially at temperatures higher than 480 °C (see Table 3.1 and Figure 3.5). In spite of these differences, both methods are characterized by a large relative accuracy. This allows to detect inter-sample variations in the order of ~ 10-15 °C and points out the powerful abilities of this geothermometer, as will be further demonstrated when discussing the recorded field thermal gradients.

3.4.3. Mapping field thermal gradients in three dimensions

Method used for contouring field thermal gradients in map and profile view

Based on the maximum temperatures obtained from the RSCM method we will present what we refer to as “isotemperature contours” in map and profile view. These contours simply represent lines that connect locations that reached a given maximum temperature in map or profile view, regardless of when these locations reached their maximum temperature and at which pressure. Note that these contours do by no means necessarily represent true isotherms at a given instant in time, since maximum temperatures could be reached at different times, given the complex metamorphic evolution of the studied area (Wiederkehr et al. 2008). Parts of the isotemperature contours reflect the temperatures reached during

Our dataset allows for comparing the estimated temperatures based on both calibrations. Figure 3.5 graphically correlates the temperature estimates based on Beyssac et al. (2002a) and Rahl et al. (2005), respectively. In general, the differences between the two calibrations are well inside the ± 50 °C uncertainty inherent in the empirical calibration of the temperatures, both methods provide similar temperature estimates, discrepancies being less than 30 °C (Fig. 3.5). At temperatures around 350, 425 and 530 °C both calibrations even yield exactly the same temperature estimates. In the intermediate temperature intervals some systematic differences are observed, however (Fig. 3.5). In the 450-525 °C range the temperatures calculated according to Rahl et al. (2005) systematically yield lower values, while the temperature estimates

the earlier HP/LT event, or its subsequent greenschist facies overprint during decompression, and will laterally connect with other parts that record the temperatures reached during a later distinct subsequent Barrow-type event, depending on which event was associated with the maximum temperature.

When attempting to construct such isotherm contours it soon became apparent that there is a rather small number of locations (16 locations out of a total of 214 measured) that obviously do not fit into a regional trend, neither in map nor in profile view, in that they exhibit exceptionally high temperatures in respect to neighbouring specimens. These are highlighted with bold letters in Table 3.1 and were not considered for constructing the isotherm contours. Three reasons are held responsible for such discrepancies.

Firstly, such heterogeneities may be caused by the fact that the graphitization process may not be solely temperature-dependent for a number of reasons. These include effects of pressure (Diessel et al. 1978; Teichmüller 1987), tectonic stress/strain (Bustin et al. 1986; Suchy et al. 1997; Ferreira Mähmann et al. 2002; Nover et al. 2005), duration of the thermal/metamorphic event (Itaya 1981; Okuyama-Kusunose & Itaya 1987), host-rock lithology (Grew 1974; Wopenka & Pasteris 1993; Wada et al. 1994), catalytic species/minerals (Bonijoly et al. 1982; Okuyama-Kusunose & Itaya 1987, and references therein), type of organic precursors (Kribek et al. 1994; Large et al. 1994; Bustin et al. 1995) and composition/activity of metamorphic fluids (Large et al. 1994; Guedes et al. 2005).

Secondly, depositional mixing of sedimentary detritus (e.g. Diessel et al. 1978; Itaya 1981) may yield peak temperatures valid for the source area rather than the metasediments sampled. We regard it more likely that such mixing is the most likely source of the scatter in case of the samples 44, 51, 84, 86, 97, 115, 136, 139, 140 and 210 (Tab. 3.1). A recent study performed along the metamorphic profile ranging from the Prättigau half-window to the Misox Zone provided evidence for the occurrence of detrital graphite in nearly all samples, as is documented by X-ray diffraction data (Petrova et al. 2002). Careful analyses of some of our samples showing anomalous peak-metamorphic temperatures (three samples originating from the Piz Terri-Lunschania unit; specimens 97, 136 and 139; Tab. 3.1) revealed that such depositional mixing of graphite of different degree of graphitization must indeed have occurred. These samples are characterized by the presence of large, randomly oriented, isolated flakes of white mica, unambiguously representing detrital white mica.

A third reason for such discrepancies applies to specimens 190 and 191 (Tab. 3.1) originating from the Misox Zone close to the contact with the Adula nappe complex, as well as to specimens 146, 147, 148 and 149 from within the Adula nappe complex. The temperatures recorded by these specimens are considered as being related to an upper blueschist/eclogite facies event (considerably higher tempered than the surrounding Fe-Mg carpholite bearing blueschist facies rocks) that only affected the Adula nappe complex and immediately adjacent parts of the Misox Zone, as will be discussed later.

The isotherm contours were drawn manually, based on the calibrations of Beyssac et al. (2002a) and Rahl et al. (2005), respectively in case of Fig. 3.6, and based on Beyssac et al. (2002a) in case of Figs. 3.7 and 3.8. We performed manual contouring, because we were also guided by keeping a more or less constant spacing between isolines, had to exclude some of the specimens (see below) and, in case of the Lunschania antiform, also used structural information. The resulting manually constructed peak-temperature contours were found to be close to those obtained by geostatistical methods using a kriging routine.

In case of the temperature vs. distance and temperature vs. altitude profiles presented in Figs. 3.7 and 3.8, respectively, and prior to the contouring within the plane of the section, the sample locations

were projected into the profile plane in a direction parallel to the isotherm contours, previously constructed in map view (Fig. 3.6) and from within a corridor whose width is given in the figure captions. The sample localities were projected horizontally in the case of Figs. 3.7 and 3.8a, and by using the angle of the local axial plunge specified in the figure caption in case of Figs. 3.8b, c, d and e.

Comparison of the field thermal gradients obtained with two alternative calibration methods

We first present the peak-metamorphic temperatures obtained by the RSCM method as a function of geographical location (see also Table 3.1). The two maps depicted in Figure 3.6, based on the two available calibrations, predict comparable and very reliable peak-metamorphic temperatures that vary from $<330^{\circ}\text{C}$ in NE (Prättigau half-window) up to $560\text{--}590^{\circ}\text{C}$ in the SW (Pizzo Molare, Lepontine thermal dome; Tab. 3.1, Fig. 3.6).

Both maps show similar shapes of the constructed isotherm contours, especially for the 425 and 525°C range, for which they are located exactly at the same place in both maps (compare Figs. 3.6a & b). It is also remarkable that in both maps the 375 , 400 and 425°C isotherm contours show the same characteristic excursion in map view towards the NE. As discussed in Wiederkehr et al. (2008), this feature is related to the fact that the 375 , 400 and 425°C isotherm contours (as well as those at $<375^{\circ}\text{C}$) record temperatures that were acquired during the earlier metamorphic evolution and were subsequently folded around a NE-plunging antiform (Lunschania antiform of Wiederkehr et al. 2008). This leads to a map pattern of folded isotherm contours, nicely illustrating the exceptional quality of both data sets. This excursion towards north-east is not shown by the isotherm contours in the $450\text{--}550^{\circ}\text{C}$ range that are aligned more or less parallel to a NW-SE-direction, i.e. perpendicular to the predominant metamorphic field gradient in the western part of the investigated area. There these isotherm contours are related to temperatures that prevailed during the Barrow-type event and that

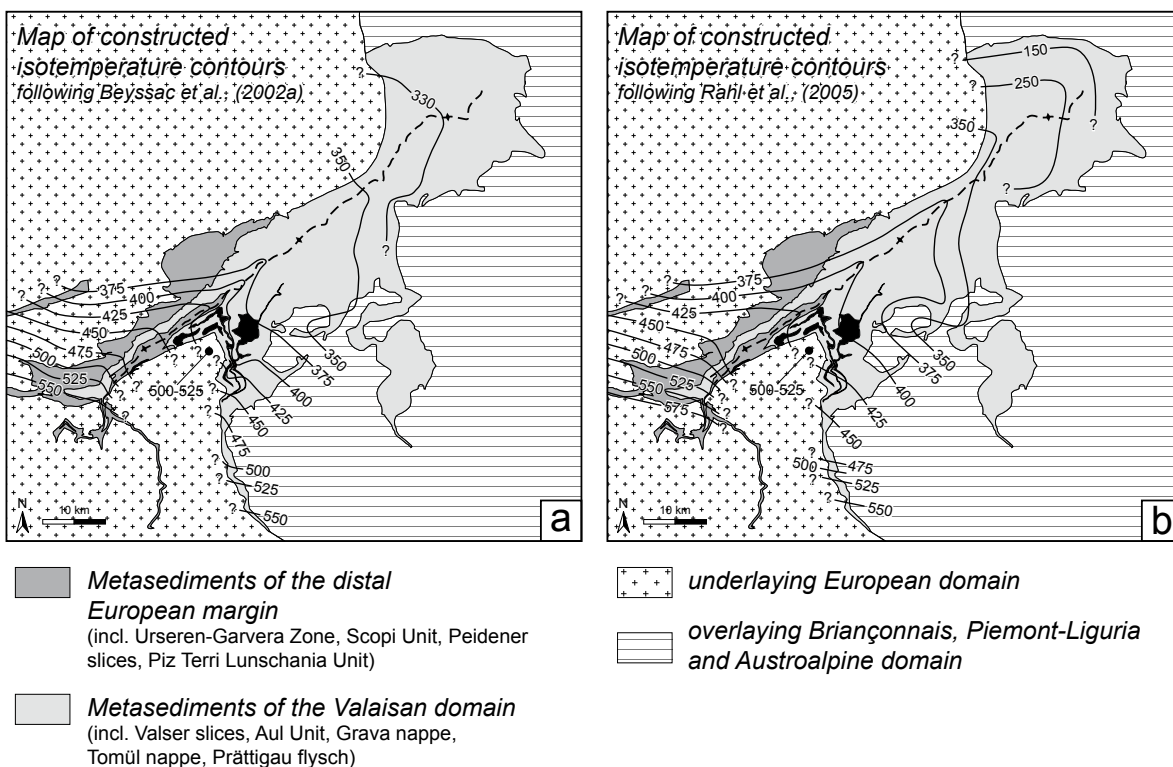


Fig. 3.6: Comparison of the estimated peak-metamorphic temperature distribution in map view in the form of isotherm contours (see text) derived from the samples listed in Table 3.1 using the calibrations given by (a) Beyssac et al. (2002a), and (b) Rahl et al. (2005). Temperatures are given in $^{\circ}\text{C}$. Stippled line indicates the trace of the axial plane of the Lunschania antiform.

are higher than those acquired during the earlier HP/LT stage and/or subsequent greenschist facies overprint. This Barrow-type event not only post-dates an earlier HP/LT event but also the subsequent folding of the earlier formed associated field temperature gradient.

The most obvious discrepancies between Figs. 3.6a and b, i.e. between the field temperature gradients derived from the two alternative calibrations, are found in the NE, i.e. at low temperatures. The temperature distribution pattern of Rahl et al. (2005; Fig. 3.6b) generally shows a stronger gradient, as is revealed by the contouring of additional isotherm contours down to 150 °C. This independently illustrates the advantages of using the Rahl et al. (2005) calibration at low temperatures. Minor discrepancies are also found in two other areas: In the intermediate-temperature domain above some 450°C the isotherm contours derived on the basis of Rahl et al. (2005) appear more closely spaced, which leads to a higher temperature gradient. Particularly the 450 °C isotherm appears relatively shifted to the W. Moreover, in the highest-temperature domain slightly higher temperatures are inferred and an additional isotherm contour at 575 °C had to be constructed when analyzing the temperatures obtained by the calibration of Rahl et al. (2005).

We conclude that despite minor discrepancies both calibrations essentially yield identical features above 330°C, features that are mainly characterized by a field temperature gradient that radially decreases away from the Lepontine dome in the SW towards the Prättigau half-window in the NE, superimposed with an excursion of the isotherm contours to the NE that coincides with the locus of an antiform which folds the isotherm contours below some 450°C. In the following, we present the peak-metamorphic temperatures obtained in more detail, and we will also present the field thermal gradients in profile view, thereby addressing the third dimension.

Peak temperatures along the Pizzo Molare-Domleschg profile

Along this SW-NE oriented profile (Fig. 3.7a) metasedimentary units derived from both the European margin and the Valaisan oceanic domain crop out in a continuous fashion. This allows for a clear correlation of deformation events and relative timing of metamorphic events along strike (Wiederkehr et al. 2008). These authors showed that both the metasediments of the Valaisan domain (Grava nappe) and parts of those derived from the distal European margin (so-called Peidener slices) are characterized by a bimodal P-T path whereby amphibolite facies Barrovian overprint represents a separate heating pulse that followed isothermal or cooling decompression of an early HP/LT blueschist facies event. Hence, a large part of the specimens analyzed derive from this profile that plots temperature versus horizontal distance, covering a temperature range from 560-590 °C in the SW down to 350-370 in the NE (Fig. 3.7a).

The highest temperatures were obtained at localities around Pizzo Molare and Grumo (northern Valle di Blenio; Fig. 3.2) which marks the north-eastern edge of the high-temperature part of the Lepontine thermal dome characterized by amphibolite facies Barrow-type metamorphism (e.g. Engi et al. 1995; Todd & Engi 1997; Frey & Ferreiro Mählmann 1999) and from where temperatures radially decrease towards the N and NE. The overall field thermal gradient along this SW-NE section at first exhibits a relatively high lateral field thermal gradient along Val Luzzzone, ranging from some 540 °C north of Olivone down to 430-450 °C around the Piz Terri, over a distance of only some 10 km (Fig. 3.7a). This portion with a high lateral gradient coincides with dramatic changes in the mineralogy of the metasediments (Wiederkehr et al. 2008) and is interpreted to represent the north-eastern edge of the Lepontine Barrow-type thermal dome. Further to the NE, between Vrin and Safiental/Domleschg (Fig. 3.1), the lateral field thermal gradient is significantly lower within the 450 to 350°C interval (Fig. 3.7a).

Interestingly, this change in the lateral field thermal gradient also coincides with a change in the inclination of the isotherm contours in a temperature versus altitude profile, as is seen from Figure 3.8a. This figure allows for a reliable construction of the steepness of the isotherm contours due to the high relief and the exceptionally dense network of sampling localities. Over Val Luzzzone the isotherm contours steepen up to some 30-45° inclination to the NE, but flatten out towards the E in the area of Piz Terri (Fig. 3.8a). The metamorphic field gradient (not necessarily equal to a geothermal gradient) amounts to some 14 °C/km perpendicular to the contours. Further, the change in inclination towards the moderate inclination observed NE of Piz Terri (Fig. 3.8a) coincides with a significant change in the trend of the isotherm contours in map view discussed before: in the SW (i.e. where the contours are steeply inclined in Fig. 3.8a) they cut across the Lunschania antiform while further to the NE

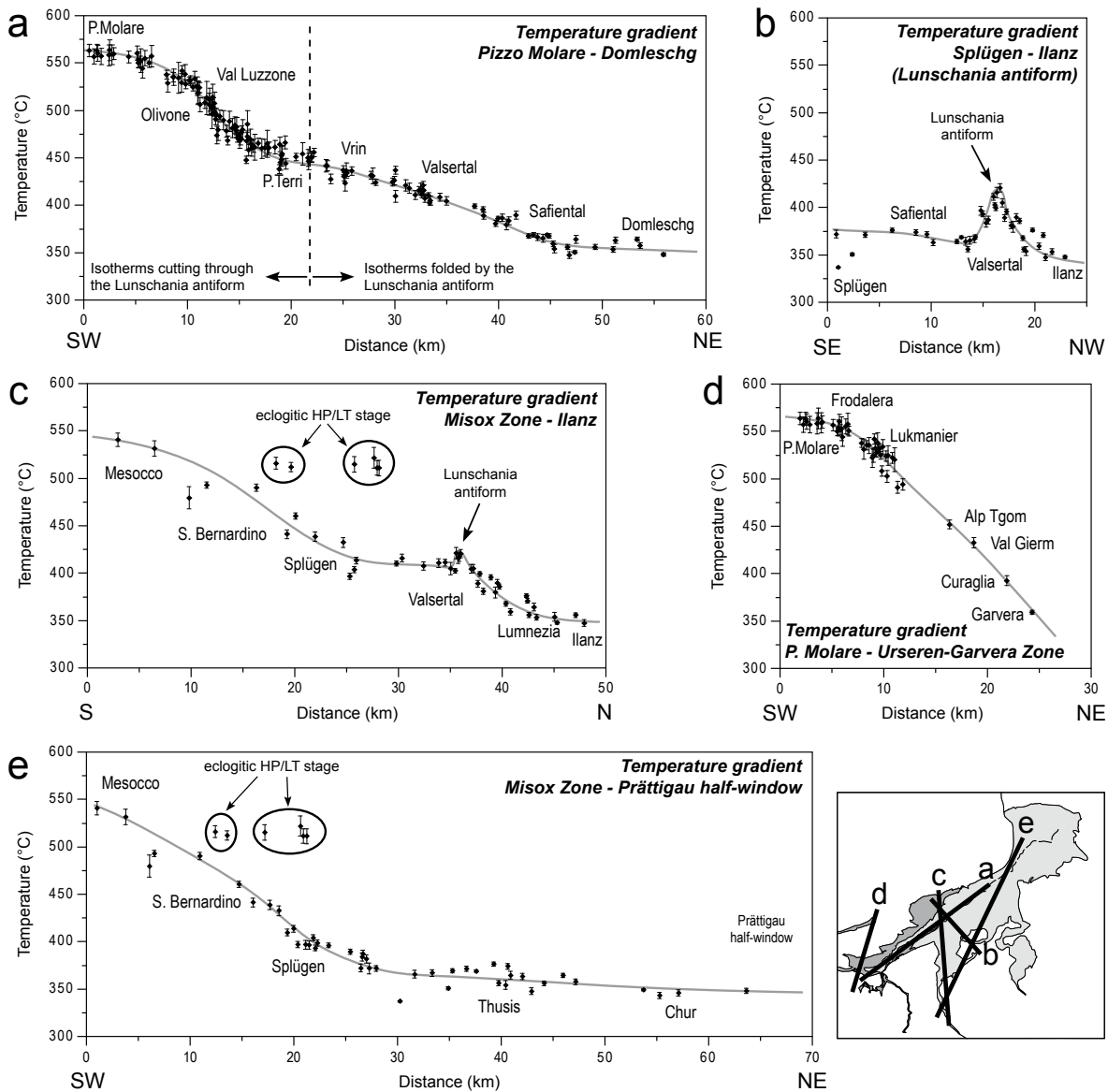


Fig. 3.7: Temperature-distance profiles summarizing the peak-metamorphic temperatures as inferred by the RSCM method using the Beyssac et al. (2002a) calibration along NE-SW to N-S trending profile traces, whose locations are indicated in an inset (lower right). The samples and inferred temperatures listed in Table 3.1 were projected into the cross-section plane perpendicular to the isotherm contours shown in Figure 3.6a from within a corridor of the following width: (a) 16 km for profile P. Molare - Domleschg; (b) 6 km for profile Ilanz - Splügen; (c) 10 km for profile Misox Zone - Ilanz; (d) 10 km to the WNW and 7 km to the ESE off the profile trace for profile P. Molare - Urseren-Garvera Zone; (e) 20 km for profile Misox Zone - Prättigau half-window. Line represents manual best-fit of the temperature-distance gradient. Encircled samples are from specimens that record temperatures related to an upper blueschist/eclogitic HP/LT stage (see text for discussion). See Fig. 3.1 for the location of geographic localities.

they are folded by this same antiform (Fig. 3.6). This supports the interpretation that the isotherm contours reflect the maximum temperatures reached during at least two separate metamorphic events, pre-dating and post-dating folding of the Lunschania antiform, respectively.

Peak temperatures along two profiles across folded isotherm contours

Effects interpreted to be due to the folding of isotherm contours (Wiederkehr et al. 2008) are visualized by two temperature-distance profiles oriented at a high angle to the fold axis of the Lunschania antiform depicted in Figures. 3.7b (Splügen-Ilanz) and 3.7c (Misox Zone-Ilanz). Both profiles show a localized temperature peak reaching some 425 °C in the Valsertal and coinciding with the core of the Lunschania antiform, superimposed onto the overall lateral field thermal gradient. This corroborates the idea of folded isotherm contours in the eastern part of the working area. Interestingly, the transition between folded and intersecting isotherms is located between 450 and 425°C (see Fig. 3.6) which is within the temperature interval where the steep lateral field thermal gradient becomes flatter towards the E (Figs. 3.7a & 3.8a). All this clearly indicates that the isotherm contours record the older HP/LT metamorphic event and/or immediately subsequent greenschist facies overprint in the NE while they record the younger Barrow-type event in the SW, where obviously the temperatures associated with the older LT event were reset by subsequent Barrow-type thermal overprint.

Peak temperatures along the Pizzo Molare-Urseren-Garvera Zone profile

Due to the lack of metasediments across the basement of the Gotthard unit this profile (Fig. 3.7d) is rather poorly constrained in its northern portion where only four samples (samples 1-4, Tab. 3.1 and Fig. 3.2) from a thin veneer of Mesozoic sediments belonging to the E-W striking Urseren-Garvera Zone are prone to analysis. Nevertheless, this profile provides important information concerning the northern termination of the Lepontine thermal dome in an area that did not suffer a previous HP/LT overprint. Hence, the entire field temperature gradient is expected to be solely related to the late-stage Barrow-type event. This is corroborated by the field thermal gradient shown in Fig. 3.7d, characterized by a continuous temperature decrease from some 560 °C at Pizzo Molare to 450 °C at Alp Tgom (sample 1) and finally to 360-375 °C at Garvera (sample 4), a high lateral field thermal gradient that can also be inferred from the close spacing of the isotherm contours in Fig. 3.6 which resembles the similarly high gradient recorded along Val Luzzzone and visualized in Fig. 3.7a.

Peak temperatures along the Misox Zone-Prättigau profile

The transition from subduction-related HP/LT metamorphism and associated subsequent greenschist facies overprint to collision-related Barrow-type metamorphism is also preserved along this profile (Fig. 3.7e), whereby the data from inside the frontal part of the Adula nappe complex (“internal Mesozoic”, Löw 1987) and from the adjacent northern Misox Zone (Aul unit), characterized by much higher peak-metamorphic temperatures, are also plotted. These units suffered an upper blueschist/eclogitic HP/LT event during which considerably higher temperatures were reached compared to the rest of the metasediments sampled during this study that only reached blueschist facies conditions (see presentation of the data for the Adula nappe complex below).

Due to the significantly lower density of investigated samples only a rough overview of this profile can be given. Peak-metamorphic temperatures range from 540-550 °C in the southern Misox Zone down to 130-140 °C in the north-eastern part of the Prättigau half-window (Fig. 3.6b). The highest temperatures of 540-550 °C measured S of the village of Mesocco can probably be attributed to the amphibolite facies Lepontine Barrow-type event (Fig. 3.7e). Towards the N the overall trend of decreasing

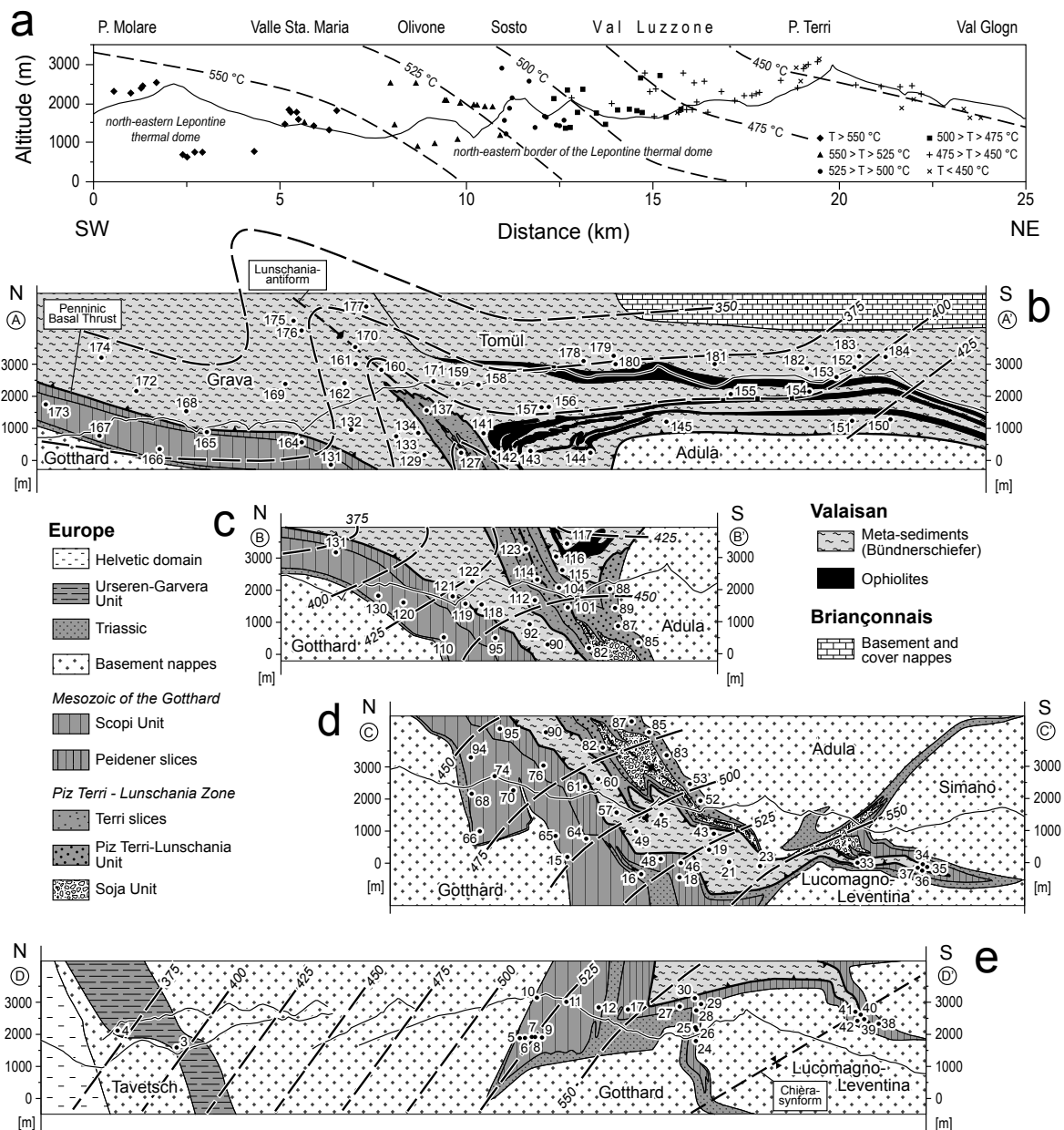


Fig. 3.8: Temperature-altitude cross-sections through the north-eastern rim of the Lepontine thermal dome and easterly adjacent areas. The trace of cross-section (a) is the same than for profile shown in Figure 3.7a (see inset in Fig. 3.7 for location), traces of these cross-sections (b), (c), (d) and (e) are indicated in Fig. 3.2; the across strike sections (Fig. 3.8b, c, d and e) show the main structural features (after Wiederkehr et al. 2008) for comparison. Peak-metamorphic temperatures inferred by the RSCM method are displayed in the form of isotherm contours (see text) derived from the samples listed in Table 3.1 using the calibrations given by Beyssac et al. (2002a). The slopes of the isotherms were estimated within the plane of the cross section after projecting the sample locations and associated peak-metamorphic into the cross-section plane. (a) Along-strike profile with samples horizontally projected from within a 14 km wide corridor and parallel to the constructed peak-metamorphic isolines shown in Figure 3.6. In case of the across strike profiles (see Wiederkehr et al. 2008 regarding structural details), width of the corridor from within which specimens were projected, and projection procedures are as follows: (b) 14 km wide corridor, projection towards east and west by using local azimuth and plunge of the Lunschania antiform (060/12) for the northern part and a plunge of 20° to the east for the southern part of the cross section (c) 12 km wide corridor, projection towards the east and west by using local azimuth and plunge of the Lunschania antiform (064/16); (d) corridor limited by 2.5 km to the E and some 6 km to the W of the profile trace, projection towards the east and west by using local azimuth and plunge of Chièra phase related fold axes (090/30); (e) 12 km wide corridor, projection east towards the east and west by using local azimuth and plunge of Chièra phase related fold axes (090/20).

temperatures is again not uniform. While a remarkable lateral field thermal gradient is found between Mesocco and Splügen, marked by a rapid decrease in temperatures from 540-550 °C down to 370-390 °C, the temperatures stay remarkably constant and vary between 350-375 °C (Fig. 3.7e) further to the north-east.

When closer focussing on the Misox zone the results indicate a more complex pattern: Samples 190 and 191 (Tab. 3.1), taken from the boundary region with the Adula nappe complex as well as samples 146-149 (Tab. 3.1) collected inside the northern Adula nappe complex, indicate locally higher temperatures in the range of 500-520 °C, not compiling with the overall trend of decreasing peak-metamorphic temperatures from S to N (“eclogitic HP/LT event” indicated in Figs. 3.7c & e). These anomalously high temperatures were obtained from Grt-Ctd micaschists found in the southern continuation of the Aul unit (Lower Uccello Zone; Gansser 1937; Steinmann 1994a) as well as from Ky-Grt-Ctd-Zo micaschists of the internal Mesozoic of the Adula nappe complex (see further explanations for the Adula below) that record metamorphic conditions established during a subduction-related upper blueschist/eclogitic event that affected the Adula nappe complex and adjacent Aul unit, as is discussed below.

Peak-metamorphic temperatures obtained for the northern Adula nappe complex

From the frontal part of the Adula nappe complex only four samples (Ky-Grt-Ctd-Zo micaschists of the so-called internal Mesozoic) were suitable for analysis (samples 146-149). The obtained peak-metamorphic temperatures all cluster around 500-520 °C. In respect to the surrounding metasediments, where maximum temperatures around 410-430 °C have been estimated, a jump in peak-metamorphic conditions in the order of some 100 °C must take place across the nappe boundary (Fig. 3.6). This jump in peak temperature clearly points towards a different metamorphic evolution of the Adula nappe complex in respect to the surrounding metasediments (except for the localities of samples 190 and 191 belonging to the Aul unit discussed above). These data were excluded for the contouring of the isothermatures depicted in Figure 3.6. Petrological investigations on eclogites, garnet peridotites and metapelites report temperature estimates related to high-pressure metamorphism of the northern Adula nappe that are consistent with our estimates: 470-540 °C (Löv 1987) and 450-550 °C (Heinrich 1986), respectively, but lower than the 640 °C postulated for this area by Dale and Holland (2003). Hence, the temperatures obtained from the northern part of the Adula nappe complex are associated with upper blueschist/eclogite facies characterized by considerably higher temperatures established during subduction-related HP/LT metamorphic conditions than the surrounding Fe-Mg carpholite bearing blueschist facies metasediments. The spatial and temporal relationships between this upper blueschist/eclogite facies event within the northern Adula nappe and the blueschist facies event and subsequent Barrow-type overprint recorded within the metasediments surrounding the Adula nappe, constituting the major part of our data set, are not yet clear. Structural arguments suggest a late-stage differential N-directed emplacement of the Adula nappe into the surrounding metasediments (Wiederkehr et al. 2008). Hence, we decided not to draw the isothermature contours across the frontal part of the Adula nappe complex in Figure 3.6.

Peak temperatures projected into a series of N-S-oriented tectonic cross sections

In order to better illustrate the three-dimensionality of the pattern of peak temperatures and the spatial relationships between isothermature contours and tectonic units, the inferred maximum temperatures were projected along strike into a series of N-S-oriented tectonic cross sections (Figs. 3.8b, c, d & e; see Wiederkehr et al. 2008 for a description of additional structural details revealed in these four cross sections). Using the measured axial plunge of the structures and assuming cylindricity of the

structures, the profiles are arranged such as to reveal the large-scale structure of the area. Note however, that, since the isotherm contours run across strike (see Fig. 3.6) they are discordant to these approximately cylindrical structures along strike and therefore should not be connected from one profile to the next perpendicular to strike. Hence, the contours are only valid for the individual profile for which they are drawn. It is also important to emphasize that the isotherm contours in Figs. 3.8b, c, d and e are by far less well constrained than is the case for the along-strike profile depicted in Fig. 3.8a discussed above. This is because Fig. 3.8a, given the higher density of data in the area, collects a much larger number of specimen locations.

Nevertheless, and in spite of considerable uncertainties regarding slope and position of the isotherm contours in case of Figs. 3.8b, c, d and e, the following salient features can be extracted from these cross sections with certainty: (1) The inclination of the isotherm contours flattens out in the southerly portions of Figs. 3.8c, d and e, while they steepen up in the northerly portions of the same cross sections. This reflects the fact that the Barrovian overprint, that determines the maximum temperatures in the northern part of these sections, also cuts across structures in a N-S direction, and not only across strike of these structures as is seen in map view (Fig. 3.6). (2) In Fig. 3.8b, which exhibits a more complex pattern, the isotherms are no more steeply dipping to the N at the northern end of the section while they become folded by the Lunschania antiform, which is not the case in the cross sections located further W (Figs. 3.8c, d & e). This supports the inferences already made based on Fig. 3.7b and c, namely that it is the older pre-Lunschania antiform LT event (blueschist facies metamorphism and/or subsequent greenschist facies overprint) that is recorded by the maximum temperatures in the eastern part of the working area, while the isotherm contours related to the Barrow-type late-stage metamorphic event cut across this antiform. This independently confirms inferences made by Wiederkehr et al. (2008) based on structural and other petrological criteria.

3.5. Discussion

3.5.1. Comparison of RSCM-derived maximum temperatures with temperatures inferred from other petrological data

In Figure 3.9 the RSCM-derived temperatures are compared with occurrences of index minerals, as well as with selected P-T-paths derived from mineral parageneses and thermodynamic modelling of equilibrium phase diagrams (Wiederkehr et al. 2008 and *in preparation*). Occurrences of Fe-Mg carpholite, a diagnostic mineral that is common in the metasediments of the Valaisan domain and parts of the metasediments derived from the distal European margin (Goffé & Oberhänsli 1992; Oberhänsli et al. 1995; Bousquet et al. 2002; Wiederkehr et al. 2008), document the HP/LT blueschist facies event in the eastern part of the working area. Going westwards from this LT area, relics of carpholite were found all the way up to the 500 °C isotherm contour, while pseudomorphs after carpholite were found even further and all the way to Pizzo Molare, i.e. up to >575 °C (Fig. 3.9). This clearly documents that formerly this western area was also part of a through-going belt characterized by blueschist facies metamorphism, stretching from the Engadine window all the way to the Western Alps (Bousquet et al. 2002, 2008). Other diagnostic minerals for this earlier subduction-related blueschist facies event are glaucophane (Gansser 1937; Nabholz 1945; Oberhänsli 1977, 1994) and jadeite (Santini 1992; Ring 1992). Within the low-grade Fe-Mg carpholite-bearing metasediments chloritoid is only rarely found inside Fe-Mg carpholite-bearing quartz-calcite parageneses, hence most chloritoid occurrences in the area formed

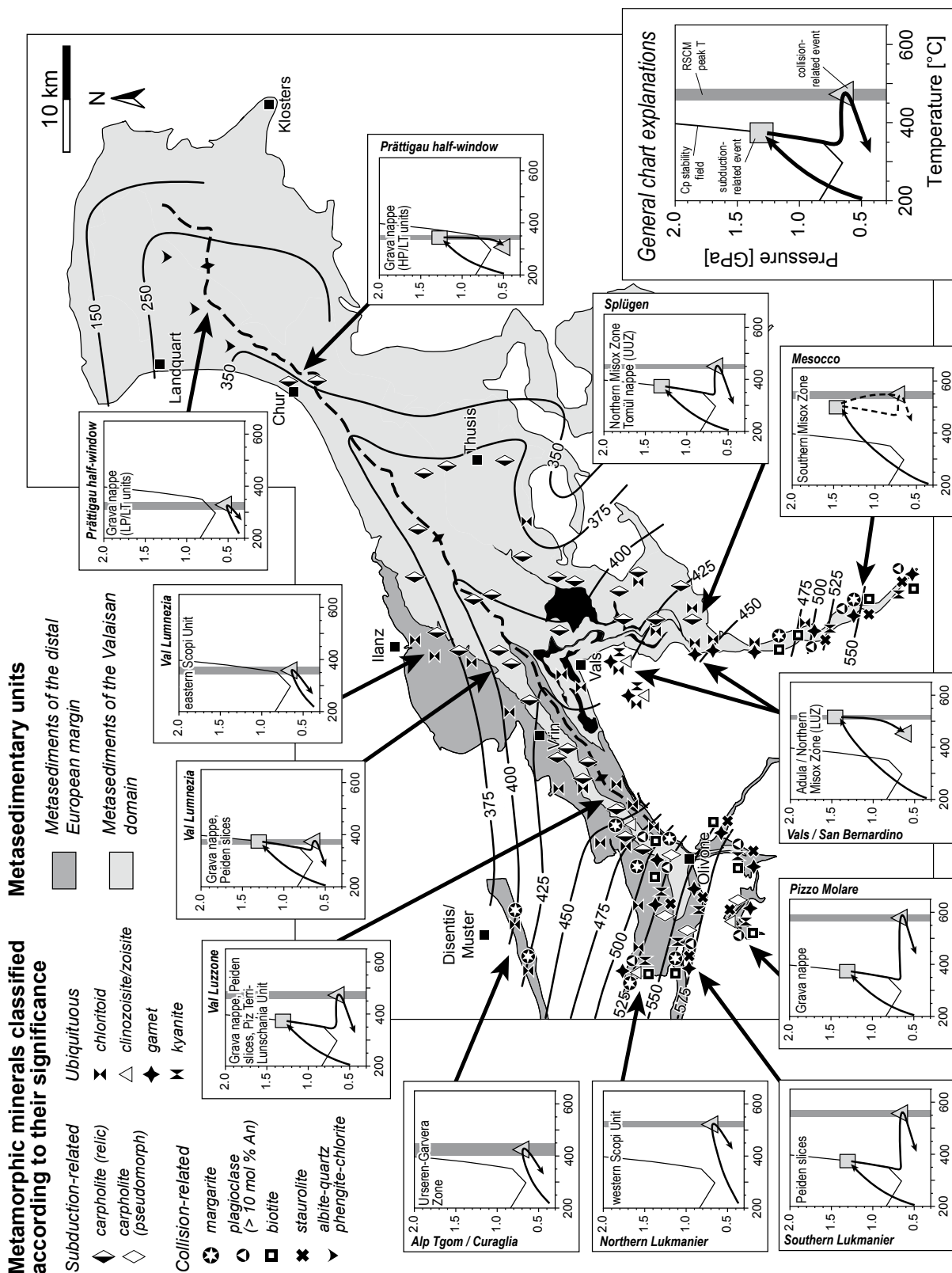


Fig. 3.9: Map providing a comparison between RSCM-derived temperatures (isotherm contours of Figure 3.6b and occurrences of index minerals, as well as selected P-T paths derived from mineral parageneses and thermodynamic modelling of equilibrium phase diagrams (Wiederkehr et al. 2008, *in preparation*) and literature data (Frey 1974; Frey et al. 1982; Teutsch 1982; Heinrich 1982, 1986; Löw 1987; Santini 1992; Ring 1992; Frey & Ferreiro Máhlmann 1999; Ferreiro Máhlmann et al. 2002 and references therein; Bousquet et al. 2002 and references therein). Inset: General chart explanations; LUZ = Lower Uccello Zone (corresponding to Aul unit; Steinmann 1994a); UUZ = Upper Uccello Zone (corresponding to Tomül nappe; Steinmann 1994a).

during the late-stage Barrow-type event. This is supported by the fact that chloritoid generally occurs as idiomorphic rosettes, bundles and prisms (Wiederkehr et al. 2008). Based on the mineral chemistry of the observed mineral assemblage, peak-metamorphic conditions of 1.2-1.4 GPa and 350-400 °C were estimated for the blueschist facies event that affected the metasediments of the Grava and Tomül nappes, as well as some of the metasediments derived from the distal European margin (Peiden slices and Piz Terri-Lunschania unit; Wiederkehr et al. 2008).

As shown by Bousquet et al. (2002) and Wiederkehr et al. (2008) for the blueschist facies areas not affected by the subsequent Barrow-type metamorphic event, isothermal or slightly cooling decompression of the Valaisan-derived Bündnerschiefer and the Europe-derived Peidener Schuppenzone did occur after the HP stage (see P-T-paths indicated in Fig. 3.9). This implies that a Barrow-type overprint possibly did not exist at all in easterly areas of Figure 3.9, or was only associated with temperatures lower than 425 °C, i.e. within temperature ranges previously reached during the blueschist event and/or subsequent greenschist facies overprint established during more or less isothermal decompression. Since folding leading to the Lunschania antiform took place after this decompression all isotherm contours at or below 425 °C are expected to appear folded by this antiform. This is actually the case (Figs. 3.7 & 3.8), demonstrating the high spatial resolution of the maximum temperature pattern that can be obtained with the RSCM method given a dense sampling network.

Increasing metamorphic grade from diagenesis to lower greenschist grade conditions prevailing in the eastern Prättigau half-window to greenschist facies conditions towards the W (i.e. Domleschg and Safiental) was described by previous work (e.g. Frey & Ferreiro Mählmann 1999; Ferreiro Mählmann et al. 2002; Petrova et al. 2002). This result is compatible with the temperature pattern derived by the RSCM method, particularly with that established when using the Rahl et al. (2005) method (Fig. 3.6b).

A similar increasing grade of metamorphism is also established in a N-S direction and across Europe-derived metasediments in the NW part of the working area (Fig. 3.9), an area that never experienced blueschist facies overprint. The predicted peak temperatures obtained by the RSCM method for the Urseren-Garvera Zone, ranging from 360 °C to 450 °C (Tab. 3.1), are in excellent agreement with chlorite-chloritoid and calcite-dolomite thermometers that yield 390-510 °C and 360-480 °C, respectively (Livi et al. 2002), and with temperature estimates based on chlorite-chloritoid and chlorite thermometry predicting 400 ± 50 °C (Rahn et al. 2002). The clear progressive metamorphic zoning to lower/middle amphibolite facies conditions around the Lukmanier and Pizzo Molare area in the S has been established early on (Chadwick 1968; Frey 1969, 1974, 1978; Thakur 1971; Fox 1978). Staurolite-kyanite-garnet-bearing micaschists indicate lower to middle amphibolite facies peak-metamorphic conditions at 0.5-0.8 GPa and 500-550 °C (Chadwick 1968; Engi et al. 1995; Todd & Engi 1997; Frey & Ferreiro Mählmann 1999). Recently published data along the metamorphic transect ranging from the Lukmanier area in the N to Pizzo Molare in the S predict 0.6-0.8 GPa at 530-575 °C for the Lukmanier area, 0.6 GPa at 550 °C in the northern Valle di Blenio and 0.7-0.85 GPa at 580-600 °C for Pizzo Molare (Janots et al. 2008). Hence, the predicted peak-metamorphic temperatures determined by the RSCM method are in good agreement with observed mineral assemblages in this part of the working area as well.

As discussed earlier, the frontal part of the Adula nappe complex suffered an upper blueschist/eclogitic overprint (Löw 1987; Heinrich 1986; Zulbati 2008), in contrast to the surrounding high-pressure terranes that suffered blueschist facies metamorphism associated with considerably lower temperatures as documented by the occurrences of Fe-Mg carpholite. The RSCM-derived temperatures are again in perfect agreement with the temperatures inferred for such an upper blueschist/eclogitic event.

Some isolated occurrences within the Misox Zone (i.e. outcrop “Neu Wahli”, possibly part of a mélange located in the Aul unit; Steinmann 1994a) containing glaucophane, garnet and omphacite (30-50% jadeite component; Oberhänsli 1977; Ring 1992; Santini 1992) also suffered upper blueschist/eclogite facies overprint.

The higher-grade Valaisan-derived metasediments found in the Lower Uccello Zone (Aul unit; Steinmann 1994a) of the Misox Zone (Fig. 3.9) are devoid of Fe-Mg carpholite, and chloritoid is commonly associated with garnet (Teutsch 1982), representing a characteristic assemblage for blueschist facies conditions in metasediments (e.g. Agard et al. 2001; Bucher & Bousquet 2007; Bousquet 2008). This indicates that relatively higher temperatures were associated with the blueschist facies event in this area. This is again in agreement with our temperature estimates that indicate southwards increasing temperatures in the Misox Zone. Staurolite first appears in the southernmost part of the Misox Zone, S of the 500°C isotherm contour, indicating that the southern part of the Misox Zone was affected by lower/middle amphibolite facies Barrovian overprint (Fig. 3.9; Wenk 1970; Thompson 1976; Teutsch 1982). Teutsch (1982) determined metamorphic conditions of 0.5-0.7 GPa and 500-550 °C near Mesocco, where we obtained 530-540 °C (samples 185 & 186, Tab. 3.1), which again demonstrates good agreement. Here in the S the temperatures established during late-stage collisional related Barrovian overprint, that led to the growth of staurolite may not differ significantly from those related to the earlier subduction-related high-pressure event that may well have reached eclogite grade in the southernmost Misox Zone. In any case, the temperatures related to the eclogite facies event continuously increase within the adjacent Adula nappe complex (i.e. Heinrich 1982, 1986), reflecting southward subduction of tectonic units during the formation of the Alpine orogenic belt. There, Nagel et al. (2002b) demonstrated that near-isothermal decompression lead to the growth of staurolite by paragonite breakdown. Hence, within the southernmost Misox Zone it may become meaningless to attribute the RSCM temperatures recorded to either the subduction-related HP event or the collision-related Barrovian overprint (indicated by stippled P-T paths in Fig. 3.9): Barrow-type overprint represents either isothermal decompression of an eclogitic stage as proposed by Nagel et al. (2002b) or a separate heating pulse as shown by Engi et al. (2001).

3.5.2. Relationships between isotherm contours and the polyphase thermal evolution of metasediments

Wiederkehr et al. (2008) showed that it is the first deformation event D1 (Safien phase), related to the formation of an accretionary wedge and subduction of the Valais Ocean including parts of the distal European margin, that is associated with blueschist facies metamorphism (350-400 °C, 1.2-1.4 GPa) as documented by Fe-Mg carpholite which is only preserved as hair-like fibres in shear fibre veins consisting of quartz and calcite. Substantial decompression to greenschist facies conditions was associated with D2 nappe stacking that led to thrusting of HP-rocks onto LP-units (Ferrera phase). Interestingly, the isotherm contours in the eastern part of the working area reflect the effect of the D3 (Domleschg phase) nappe-refolding phase, particularly that of the most prominent D3 structure, the Lunschania anti-form (Figs. 3.1 & 3.2; Voll 1976; Kupferschmid 1977; Steinmann 1994a; Weh and Froitzheim 2001)

The presented RSCM temperature data, combined with structural observations, show that progressive Barrovian overprint related to the Lepontine thermal dome in the south-western part of the study area clearly post-dates this D3 event (Wiederkehr et al. 2008), in that the isotherm contours crosscut the Lunschania structure at temperatures higher than those reached during the blueschist facies

event and/or subsequent greenschist facies overprint. The isotherm contours established for the western part of the study area rather spectacularly run across structures, both along strike and in N-S-profile view (Fig. 3.8), demonstrating that the RSCM method is a rather powerful tool for revealing the 3-D geometrical characteristics of the temperature field established during the late-stage collision-related metamorphic event. Note, however, that the original shape of the isotherm contours may have been modified by the last tectonic event (D4, Chièra phase), associated with back-folding and the formation of the Northern Steep Belt further to the W (Milnes 1974) that affected the south-western part of the study area.

Our study reveals a jump in maximum temperatures between the Adula nappe complex (internal Mesozoic) and the surrounding Valaisan-derived metasediments for the first time (Fig. 3.6). This is in contrast to earlier studies (e.g. Todd & Engi 1997) that all drew isotherm lines straight across the nappe boundary between Adula nappe complex and the easterly adjacent metasediments, assuming that such isotherm lines formed during the Barrowian event. The thermal discontinuity, together with the interpretation of these isotherms in the eastern part of the study area as being related to the HP-event and/or subsequent greenschist facies overprint, contradicts this view in case of the northern Adula nappe complex. However, as pointed out above, the isotherm contours may well cut across in the southernmost Misox Zone where, due to high temperatures already reached during the upper blueschist to eclogite facies conditions that were followed by isothermal decompression (Nagel 2008), may make a distinction between the temperatures reached during the two events meaningless.

3.5.3. Inferences regarding the graphitization process along a metamorphic gradient

The results of this investigation clearly show that the transformation of CM into graphite is a continuous and mainly temperature dependent process and that therefore the RSCM method is a reliable geothermometer for recording peak temperatures. Nevertheless, as was discussed earlier, some samples are characterized by large scattering of the estimated mean temperature. Others predict a peak-metamorphic temperature markedly different in respect to neighbouring samples for a number of reasons, depositional mixing of sedimentary detritus originating from different metamorphic sources (e.g. Diessel et al. 1978; Itaya 1981) possibly being the most important factor in case of the present study. Hence, dense sampling leading to a large data set is definitely needed.

3.6. Conclusions

Raman spectroscopy of carbonaceous material in metasediments at the margin of the Lepontine dome allows for a comparison between the Beyssac et al. (2002a) and Rahl et al. (2005) calibration by using a large dataset in the 150 to 600 °C temperature range. The two calibration methods essentially yield identical inferred temperatures above 330 °C, discrepancies being less than 30 °C; at lower temperatures only the Rahl et al. (2005) calibration does reliably reveal a field temperature gradient. Both methods are characterized by a large relative accuracy that allows to detect inter-sample variations in the order of ~10-15 °C, i.e. in the same order as found by Beyssac et al. (2004). The method can be successfully applied to specimens of low-grade metasediments that are devoid of indicative mineral assemblages (so-called Bündnerschiefer) that do not allow for a comparably accurate estimation of the metamorphic temperature based on conventional petrologic investigations.

The results of the three-dimensional mapping of isotherm contours show, after comparison with independent petrological and structural data (Wiederkehr et al. 2008), that the field temperature

gradients inferred from Raman spectroscopy of carbonaceous material faithfully reflect the present day distribution of peak-metamorphic temperatures that resulted from a superposition of distinct metamorphic events in three dimensions. It was found that (1) the RSCM-derived maximum temperatures favourably compare with temperatures inferred from other petrological data, (2) the derived temperatures reflect the maximum temperatures to which specimens were exposed to in areas that underwent a poly-phase thermal evolution, (3) the three-dimensional character of those parts of the isotherm contours that reflect the same metamorphic event reveal valuable relationships between deformation and metamorphism, and, (4) our data support the assumption, that the transformation of CM into graphite is a continuous and mainly temperature dependent process.

Within the north-eastern rim of the Lepontine dome the isotherm contours associated with the collision-related late-stage Barrow-type event clearly cut across nappe contacts and post-nappe stacking mega-folds, both along and across strike. Further to the NE the isotherm contours reflect temperatures reached during an earlier blueschist facies event and/or subsequent near-isothermal decompression and are folded around large-scale post-nappe stacking folds. A substantial “temperature jump” across the tectonic contact between the frontal Adula nappe complex and surrounding Valaisan-derived metasediments indicates that, in contrast to the postulates raised by earlier studies, equilibration of temperatures during the late-stage Lepontine event is found to be incomplete in this area.

Acknowledgements

Excellent preparation of numerous samples by W. Tschudin, as well as great support in the field by G. Derungs, both members of Basel University, is gratefully acknowledged. A. Riemann from Potsdam University is thanked for a supporting field trip as well as for the introduction and help in the Raman laboratory of Potsdam University. Substantial funding by the Swiss National Science Foundation (project NF-200020-113585 and precursor project NF-200020-103585) is gratefully acknowledged. S. Schmid acknowledges support by the Alexander von Humboldt Foundation during the last stages of the synthesis of the data presented.

Chapter 4

 $^{40}\text{Ar}/^{39}\text{Ar}$ dating of the subduction-collision transition in the Central Alps

This chapter is under review as: **Wiederkehr, M.**, Sudo, M., Bousquet, R., Berger, R. & Schmid, S.M. $^{40}\text{Ar}/^{39}\text{Ar}$ dating of the subduction-collision transition in the Central Alps. Submitted to *Tectonics*.

Abstract

The investigated HP/LT metasedimentary units of the Valaisan and adjacent European domains occupy a key position in the Alpine belt for understanding the transition from early subduction-related HP/LT event to collision-related MP/MT Barrovian metamorphism and the evolution of mountain belts in general. The timing of high-pressure metamorphism and subsequent retrogression was studied by dating several white mica generations, well characterized in terms of mineral chemistry, texture and associated mineral assemblages. Biotite was analyzed for constraining the timing of the subsequently following Barrow-type overprint.

Four distinct age populations of white mica (crystallization ages) record peak-pressure conditions and several stages of subsequent retrograde metamorphic evolution. Apparent white mica ages, exclusively found in isolated phengites, vary between 42-40 Ma; they record the timing of HP/LT metamorphism that is contemporaneous with D1 deformation (Safien phase). White mica intimately associated with chlorite, replacing carpholite, yield two different age groups, both interpreted as related to mica formation during breakdown of carpholite: a first age group (36-33 Ma) dates substantial decompression during D2 (Ferrera phase) nappe stacking, a second one dates subsequent greenschist facies overprint (32-29 Ma). Additionally, the white mica data also reveal a coherent apparent age cluster at ~ 25 Ma whose significance is yet not clear; a correlation with D3 deformation (Domleschg phase) is proposed.

Biotite isotopic analyses yield consistent apparent ages that cluster around 18-16 Ma and are slightly younger than published data on the age of the thermal peak of the second Barrow-type metamorphic event that occurred under quasi-static conditions and largely pre-dates D4 (Chièra phase) back-folding. The recorded isotopic data reveal a significant time gap in the order of some 20 Ma between subduction-related HP/LT metamorphism and collision-related MP/MT Barrovian overprint, supporting the notion of a polymetamorphic evolution associated with a bimodal P-T path.

4.1. Introduction

Understanding the metamorphic evolution of the earth's crust requires well-constrained time data. Such data are of particular importance regarding the geodynamics of subduction, followed by unroofing in a collisional scenario later on. Numerical models explore the effects of the thermal structure acquired during subduction on subsequent stages of the metamorphic history during collision and exhumation (e.g. Bousquet et al. 1997; Jamieson et al. 1998; Roselle et al. 2002; Goffé et al. 2003). In order to test such models by field studies we do not only need the constraints on the metamorphic evolution in P-T space that are widely available by now (e.g. Oberhänsli et al. 2004) but also more data on the evolution in time (e.g. Berger & Bousquet 2008). The Central Alps provide a unique example of an area, from which an unusually large and unique data set on the metamorphic evolution is available (e.g. Bousquet et al. 2008), but where the timing of the early blueschist facies stage of metamorphism is still very poorly constrained.

The Alps formed as a result of subduction- and subsequent collision-related processes due to plate convergence between Europe and Adria in Mesozoic times. The distal European continental margin and Tethyan oceanic lithosphere, including an intervening micro-continent (Briançonnais), were subducted and partially incorporated into an accretionary orogenic wedge sandwiched between the overlying Adria-derived nappes (Austroalpine) and the southward subducting underlying European plate (e.g. Trümpy 1960; Frisch 1979; Tricart 1984; Le Pichon et al. 1988; Schmid et al. 1996). Early-stage subduction-related processes took up most of the plate convergence and led to the formation of high-pressure belts that strike parallel to the orogen (e.g. Oberhänsli et al. 2004). It is now widely accepted that the Alpine orogenic belt incorporated three high-pressure belts, one being of Cretaceous age and only affecting the continental Austroalpine domain (e.g. Thöni 2006) while two Cenozoic belts are related to subduction processes within two branches of the Alpine Tethys, i.e. the southern Piedmont-Liguria and the northern Valaisan Ocean, respectively, separated by the Briançonnais micro-continent (e.g. Frisch 1979; Stampfli 1993; Oberhänsli 1994; Stampfli et al. 1998; Froitzheim et al. 2003).

Relics of the Piedmont-Liguria Ocean are characterized by a spectacular and well-known HP/LT metamorphic event (e.g. Bearth 1967; Chinner & Dixon 1973; Ernst & Dal Piaz 1978), for which numerous isotopic data are available by now, albeit their geodynamical interpretation is still difficult (see review by Berger & Bousquet 2008). This abundance of isotopic data contrasts with the scarcity of data from the northern and more external, at least partly oceanic, Valaisan units. Within Switzerland and the adjacent Italian-French Alps, the Valaisan mainly exposes voluminous low-grade Fe-Mg carpholite-bearing HP/LT metasediments (Goffé & Oberhänsli 1992; Oberhänsli 1994; Goffé & Bousquet 1997; Bousquet et al., 1998; 2002), associated with scarce and isolated fragments of mafic and ultramafic bodies. The timing of HP/LT metamorphism in this northern high-pressure belt is not only very poorly constrained but the few available ages grossly scatter (Berger & Bousquet 2008). The only isotopic data available for metasediments around the Petit St. Bernard area yield 34-27 Ma (Freeman et al. 1998; Cannic et al. 1999) but have to be considered with great caution due to the fact that the available studies were not aware of the presence of a HP/LT metamorphic event in the Valaisan domain. Ages reported for high-pressure metamorphism in the Antrona and Balma eclogites scatter between 46 and 39 Ma (Liati et al. 2005; Liati & Froitzheim 2006; Herwartz et al. 2008), but the attribution of these units to the Valaisan is controversial. Radiometric ages that claim to date the high-pressure event in the Eclogite Zone of the Tauern window, a unit that many authors (e.g. Schmid et al. 2004) associate with the subduction of the

Valaisan Ocean, are extremely controversial and vary between 31.5 Ma (e.g. Glodny et al. 2005) and \leq 45 Ma (e.g. Ratschbacher et al. 2004).

The area investigated by this study occupies a key location in the Central Alps, located at the north-eastern edge of the Lepontine dome (Fig. 4.1a). The area offers uninterrupted excellent exposure of metasedimentary units derived from the Valaisan and adjacent distal European domains within which subduction-related HP/LT metamorphism dominates in the north-east (Engadine window and Grisons area) while collision-related Barrow-type amphibolite facies metamorphism dominates in the south-west (Fig 4.1; see also Wiederkehr et al. 2008). This allows for collecting samples from a continuous along-strike section and for investigating the geodynamical relationships between these two contrasting tectono-metamorphic events. For the first time this study provides geochronological data regarding both stages of a polymetamorphic evolution and from within the same working area: HP/LT metamorphism including subsequent retrogression, followed by a second Barrow-type thermal metamorphic event. We analyzed samples that are well described in terms of their metamorphism (see Wiederkehr et al. 2008 and *submitted, b*; Bousquet et al. 1998) in order to date mineral growth and/or reactions by using $^{40}\text{Ar}/^{39}\text{Ar}$ techniques. We will present results of *in situ* $^{40}\text{Ar}/^{39}\text{Ar}$ dating of successive white mica generations reflecting the subduction-related metamorphism on the one hand, and dating of biotite grown during collision-related Barrovian overprint on the other hand. Additionally $^{40}\text{Ar}/^{39}\text{Ar}$ step-wise heating experiments on biotite grain separates were performed for comparison with *in situ* dating and complete the data set. These new data offer the opportunity to test and further quantify the geodynamic evolution proposed by Wiederkehr et al. (2008). Moreover, this work represents a case study that addresses the transition from subduction to collision in general and thereby provides important field and geochronological data for testing numerical models for the geodynamic evolution of orogenic belts (e.g. Bousquet et al. 1997; Jamieson et al. 1998; Roselle et al. 2002; Goffé et al. 2003).

4.2. Tectono-metamorphic background and sampling strategy

4.2.1. Geological setting

The studied area is located at the north-eastern edge of the Lepontine dome (Fig. 4.1a) that represents a dome both in a structural and thermal sense. Structurally, this dome consists of Europe-derived basement nappes (Sub-Penninic after Schmid et al. 2004; Fig. 4.1b) that represent the deepest exposures within the Central Alps (e.g. Froitzheim et al. 1996). These pre-Mesozoic basement nappes are tectonically overlain by Mesozoic-age metasedimentary units derived from both the distal European margin (Sub-Penninic cover nappes and slices) and the Valaisan oceanic domain (Lower Penninic), separated from each other by the Penninic Basal Thrust (Fig. 4.1b). In the easterly adjacent areas the Mesozoic metasediments of the Valaisan domain build up an up to 15 km thick pile of metasedimentary cover nappes (Hitz & Pfiffner 1997; see crustal-scale transect in Schmid et al. 1996, their Plate 1). Due to the general axial plunge of the whole nappe stack to the E, these Valaisan-derived metasediments are seen to be tectonically overlain by nappes derived from the Briançonnais, Piemont-Liguria Ocean, and Austroalpine domain, respectively, still further to the east (Fig. 4.1a). Within the Engadine window (Figs. 4.1a & c) the Valaisan Bündnerschiefer are again exposed within a local antiformal dome below the Austroalpine lid.

Lithologically the Valaisan-derived metasediments are a rather monotonous sequence that predominantly consists of calcschists with intercalations of limestones, shales, marls and sandy limestones,

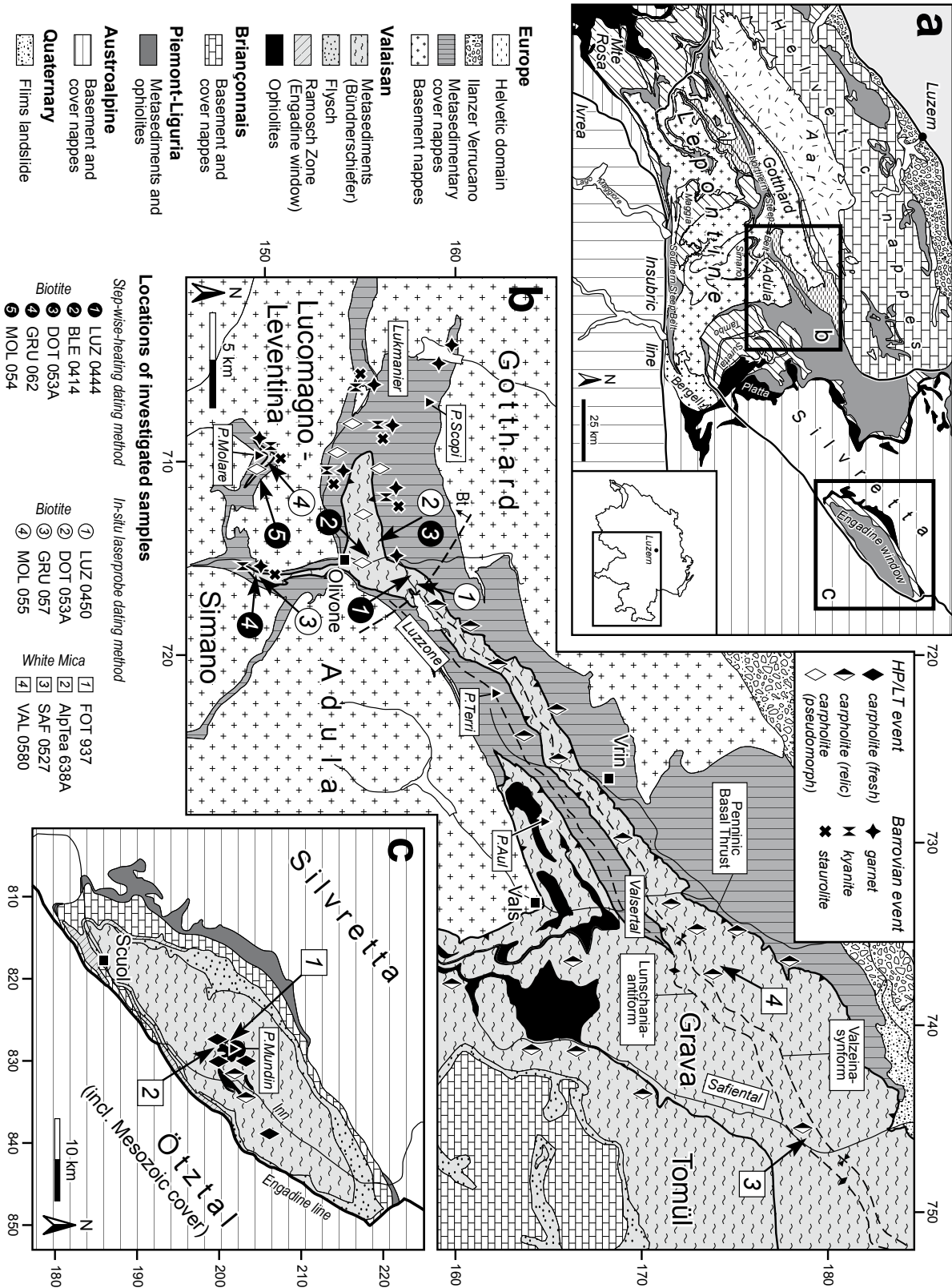


Fig. 4.1: Geological map of the investigated area and locations of the studied samples. (a) Tectonic map of the Central Alps after Schmid et al. (2004); the two black rectangles indicate the outlines of the more detailed map views shown in b & c. (b) Detailed map of the NE rim of the Lepontine dome and easterly adjacent areas also indicating the main geographical names mentioned in the text; biotite-in isograd and distribution of indicative minerals are based on Wiederkehr et al. (2008), and references therein. (c) Detailed map of the Engadine window; the distribution of HP/LT minerals is after Bousquet et al. (1998).

deposited in Cretaceous to Eocene times (Nänny 1948; Ziegler 1956; Steinmann 1994a; Steinmann & Stille 1999). In the west the Valaisan Bündnerschiefer are subdivided into Grava and Tomül nappes, based on stratigraphic criteria (Steinmann 1994a; Fig. 4.1b). The metasediments in the Engadine window are built up by the high-pressure Mundin unit, overlain by the low-pressure Arina unit (Bousquet et al. 1998; Fig. 4.1c). Scarce occurrences of mafic and ultramafic rocks are associated with these metasediments, mainly around Piz Aul and Piz Tomül in the W (Nabholz 1945; Fig. 4.1b) and around Piz Mundin of the Engadine window in the E (Fig. 4.1c). However, rather large bodies of serpentinized peridotite are found below the Grava unit (Aul unit, Nabholz 1945) and in the Engadine window. The latter are associated with ophicarbonates, serpentinite breccia, meta-gabbro and meta-basalt, forming the so-called Ramosch zone (Fig. 4.1c), interpreted as representing the transition between the continental Briançonnais and the oceanic Valaisan domain (Florineth & Froitzheim 1994; Froitzheim et al. 1996). These occurrences of mafic and ultra-mafic bodies clearly indicate that at least parts of the Valaisan-derived metasediments were deposited on oceanic crust (Steinmann 1994a; Steinmann & Stille 1999). In the Valaisan domain there is also clear evidence for subduction-related HP/LT metamorphism under blueschist facies conditions provided by the widespread occurrences of Fe-Mg carpholite in metasediments (Goffé & Oberhänsli 1992; Oberhänsli et al. 1995; Bousquet et al. 1998) as well as by rare findings of glaucophane in mafic rocks (Oberhänsli 1978; Bousquet et al. 1998). Metamorphic conditions of 1.2-1.4 GPa and 350-400 °C have been estimated (Bousquet et al. 2002). It has recently been shown that not only the Valaisan Bündnerschiefer but also parts of the metasedimentary units belonging to the European realm were affected by the same early HP/LT event, as documented by occurrences of Fe-Mg carpholite in both Peiden slices and Piz Terri-Lunschania unit (Wiederkehr et al. 2008 and *submitted, b*).

Only towards the SW were the metasediments of both the European and Valaisan realm affected by a Barrow-type thermal overprint; the temperatures progressively increase SW-wards, i.e. towards the centre of the Lepontine thermal dome. Such progressive Barrovian metamorphism is best documented within Europe-derived metasediments (Sub-Penninic cover nappes and slices) due the great chemical variability of these Triassic to lower/middle Jurassic sequences, consisting of meta-evaporites, metapelites, calcareous shales, carbonaceous calcschists and shales (Baumer et al. 1961; Probst 1980; Etter 1987; Steinmann 1994a; Berger et al. 2005). This chemical variability resulted in a corresponding variability of spectacular metamorphic assemblages that include hornblende, staurolite, kyanite, garnet, biotite, plagioclase chloritoid and zoisite/clinozoisite and which were the subject of pioneering studies on regional Barrow-type metamorphism (Chadwick 1968; Frey 1969; 1974; 1978; Niggli 1970; Wenk 1970; Fox 1975; Livi et al. 2002). Lower/middle amphibolite facies metamorphic conditions of 0.5-0.8 GPa and 500-550 °C have been estimated for such Barrow-type metamorphism in the north-eastern Lepontine dome (Engi et al. 1995; Todd & Engi 1997; Frey & Ferreiro Mählmann 1999).

4.2.2. Tectono-metamorphic evolution

Wiederkehr et al. (2008) showed that the metasedimentary units of the south-western part of the investigated area (i.e. in a transect between Val Luzzzone and Pizzo Molare; Fig 4.1b) are characterized by a bimodal P-T path; the early HP/LT event was followed by substantial “cold” decompression and was then overprinted by late-stage Barrovian amphibolite facies metamorphism (Fig. 4.2a; Bousquet et al. 2008; Wiederkehr et al. 2008). Such late-stage thermal overprint is totally missing in the easterly adjacent areas, i.e. east of Piz Terri and Engadine window (Figs. 4.1b & c). There, the metasediments

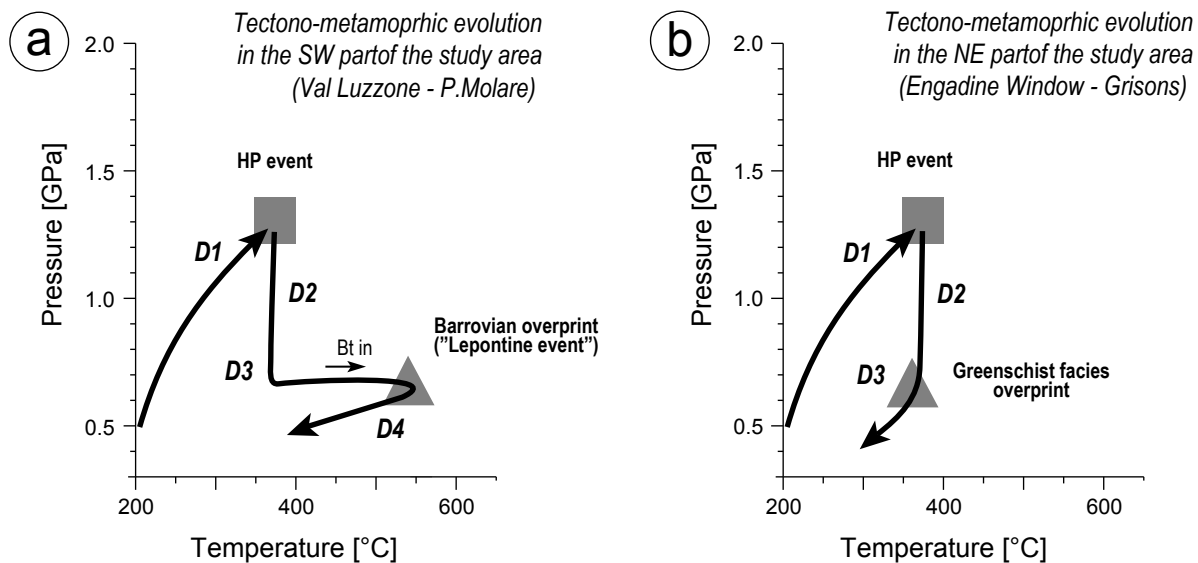


Fig. 4.2: Summary of the tectono-metamorphic evolution (see text for more information). (a) Bimodal P-T path typical for the south-western part of the study area (NE Lepontine dome) and associated deformation phases, established for the Valaisan- and Europe-derived metasediments. Note that biotite growth is related to Barrovian Lepontine metamorphism that represents a late-stage separate heating pulse and follows isothermal or slightly cooling decompression after the early HP/LT event. (b) Single P-T path typical for the north-eastern part of the study area, i.e. Valsertal, Safiental and Engadine window, respectively, characterized by an early HP/LT stage that was only followed by more or less isothermal decompression.

generally indicate greenschist facies conditions, established at more or less the same temperatures that prevailed during the earlier HP/LT event (Wiederkehr et al. *submitted, b*; Fig. 4.2b).

Detailed structural and petrological investigations revealed the following tectono-metamorphic evolution (Wiederkehr et al. 2008; Fig. 4.2): Blueschist facies metamorphism at 350-400 °C and 1.2-1.4 GPa was associated with a first deformation event D1 (Safien phase). This event is related to the formation of an accretionary wedge and subduction of the Valaisan Ocean and parts of the adjacent distal European margin. The HP/LT stage was followed by substantial isothermal or slightly cooling decompression to greenschist facies conditions, associated with D2 nappe stacking (Ferrera phase). This led to thrusting of HP-rocks onto LP-units. During D3 (Domleschg phase), representing a first nappe-refolding event, large-scale tight to isoclinal mega-folds with amplitudes up to some 10 km were formed, e.g. the Lunschania antiform that can be traced in map-view a long way (Fig. 4.1b). Clearly post-dating this D3 deformation, and under static conditions at least during the initial stages, the HP/LT rocks were overprinted by regional amphibolite facies metamorphism. Temperatures progressively increase towards the west, i.e. towards the north-eastern rim of the Lepontine thermal dome, from 475-500 °C in the Val Luzzone area to 570-590 °C at the Pizzo Molare and within a pressure interval of 0.6-0.7 GPa (Wiederkehr et al. *in preparation*; Fig. 4.2b). Finally, this Barrow-type metamorphism was severely overprinted by a last deformation phase D4 (Chièra phase), characterized by ductile nappe refolding and leading to the formation of the Chièra-synform and the Northern Steep Belt (Milnes 1974).

4.2.3. Sampling strategy

A total of 13 samples (Table 4.1), 12 deriving from Mesozoic metasediments (so-called "Bündnerschiefer" of the Valaisan domain) and one sample from metasediments of the distal European margin, were selected. These are well characterized with respect to the tectono-metamorphic evolution outlined above. In the north-eastern part of the study area, i.e. in the Valsertal and the Safiental as well as in the Engadine window (Figs. 4.1b & c) where pressure-dominated metamorphism is well preserved without

or with only a minor late stage thermal overprint (e.g. Bousquet et al. 2002), four samples that contain white mica associated with Fe-Mg carpholite were collected with the aim to unravel the early, pressure-dominated metamorphic stage. Towards the SW, where the HP/LT metasediments were progressively overprinted by Lepontine amphibolite facies metamorphism, nine samples containing biotite were collected (see Figs. 4.1b & c for locations). Note that biotite is exclusively found in these areas that experienced pervasive thermal overprint.

Table 4.1: Summary of investigated samples used for *in situ* UV laser probe (white mica and bioite) and CO₂ laser step-wise heating experiments (biotite). The sample locations are depicted in Figure 4.1. For each sample the precise location is given in Swiss map coordinates, and elevation in meter, tectonic unit and mineral assemblage present in the investigated samples are listed. Additionally estimated P-T conditions are indicated for each sample taken from the literature: ⁽¹⁾ Bousquet et al. (2002), ⁽²⁾ Wiederkehr et al. (*submitted, b*), ⁽³⁾ Wiederkehr et al. (*in preparation*).

Sample name	Swiss map coordinates		Elev. (m)	Tectonic Unit	Mineral assemblage	P-T conditions	
	X	Y				T (°C)	P (GPa)
Samples characterized by subduction-related HP/LT metamorphism							
<i>In situ laserprobe dating method</i>							
FOT 937	827°678	199°891	2550	Valaisan (Mundin)	Cp (fresh), WM, Chl, Qtz, Cc/Do	350-375 ⁽¹⁾	1.1-1.3 ⁽¹⁾
AlpTea 638A	829°031	198°676	2040	Valaisan (Mundin)	Cp (fresh), WM, Chl, Qtz, Cc/Do	350-375 ⁽¹⁾	1.1-1.3 ⁽¹⁾
SAF 0527	746°016	178°803	1300	Valaisan (Grava)	Cp (relic), WM, Chl, Qtz, Cc/Do	350-400 ^(1,2)	1.2-1.4 ^(1,2)
VAL 0580	736°871	174°310	1370	Valaisan (Grava)	Cp (relic), WM, Chl, Qtz, Cc/Do	350-400 ^(1,2)	1.2-1.4 ^(1,2)
Samples characterized by collision-related Barrow-type metamorphism							
<i>In situ laserprobe dating method</i>							
LUZ 0450	716°137	157°727	1410	Valaisan (Grava)	Bt, Plag, Zo/Czo, WM, Chl, Qtz, Cc/Do	475-525 ⁽³⁾	0.50-0.75 ⁽³⁾
DOT 053A	713°556	155°867	2100	Valaisan (Grava)	Bt, Plag, Zo/Czo, WM, Qtz, Cc/Do	510-560 ⁽³⁾	0.50-0.65 ⁽³⁾
GRU 057	715°621	148°504	700	Valaisan (Grava)	Bt, Plag, WM, Qtz, Cc/Do	560-590 ⁽³⁾	0.55-0.7 ⁽³⁾
MOL 055	709°715	149°780	2400	Valaisan (Grava)	Bt, Plag, WM, Qtz, Cc/Do	560-590 ⁽³⁾	0.6-0.8 ⁽³⁾
<i>Step-wise-heating dating method</i>							
LUZ 0444	716°017	157°831	1390	Valaisan (Grava)	Bt, Plag, Zo/Czo, WM, Chl, Qtz, Cc/Do	475-525 ⁽³⁾	0.50-0.75 ⁽³⁾
BLE 0514	715°112	155°757	1090	Valaisan (Grava)	Bt, Plag, Zo/Czo, WM, Chl, Qtz, Cc/Do	510-560 ⁽³⁾	0.50-0.65 ⁽³⁾
DOT 053A	713°556	155°867	2100	Valaisan (Grava)	Bt, Plag, Zo/Czo, WM, Qtz, Cc/Do	510-560 ⁽³⁾	0.50-0.65 ⁽³⁾
GRU 062	716°156	149°270	760	Valaisan (Grava)	Bt, Plag, WM, Qtz, Cc/Do	560-590 ⁽³⁾	0.55-0.7 ⁽³⁾
MOL 054	710°270	149°696	2270	Europe (Molare-Dangio)	St, Ky, Grt, Bt, Plag, WM, Qtz	560-590 ⁽³⁾	0.6-0.8 ⁽³⁾

4.3. Experimental procedure of ⁴⁰Ar/³⁹Ar dating

The ⁴⁰Ar/³⁹Ar dating was performed at the ⁴⁰Ar/³⁹Ar geochronology laboratory at Potsdam University. The procedure was as follows.

4.3.1. Sample preparation

For the *in situ* ⁴⁰Ar/³⁹Ar UV laser-probe dating technique (see e.g. Maluski & Monié 1988; Kelley et al. 1994) rock sections of ca. 1 mm thickness and 5 mm in diameter were drilled out from sample blocks that contain the analyzed polished surface whose opposite side was used for thin section preparation. Photographs of the polished surface and corresponding thin section provided an accurate reference frame for the analyzed sections. Additionally, we performed SEM investigations of the polished sections in order to firstly have an accurate pattern of the distribution of both K-bearing white mica and biotite, and secondly to have control over chemical zoning or alteration (e.g. chloritization of biotite). Both pieces of information were important for selecting the best suitable places for performing the Ar isotopic analyses. A total of eight thick sections were prepared for *in situ* ⁴⁰Ar/³⁹Ar UV laser ablation spot analysis, four sections containing white mica and four containing biotite.

For ⁴⁰Ar/³⁹Ar dating by the CO₂ laser step-wise heating technique five hand specimens of biotite bearing mica-schists were crushed and sieved. Highly enriched 250-315 µm fractions of biotite were

finally obtained by the “tapping or shaking paper method”, i.e. by spreading a small amount of sample powder on a clean sheet of paper and carefully tapping or shaking it by keeping the paper at an angle. Flat grains such as mica remain on the paper whilst round mineral grains roll off. About 25 mg of biotite concentrates were further purified by handpicking under the binocular microscope. Finally, pure biotite grain separates were washed in de-ionized water within a glass beaker in an ultrasonic bath and subsequently dried in an oven at some 80 to 100 °C.

4.3.2. Neutron activation by fast neutron

Neutron activation of polished sections and mineral separates was performed at Geesthacht Neutron Facility (GeNF), GKSS research centre, Germany. Both types of samples were wrapped in Al foil and subsequently loaded into a sample-container (35 mm in diameter and 43 mm in height) made of 99.999% pure Al. Finally, the sample container was wrapped in Cd foil with a thickness of 0.5 mm in order to cut off the unnecessary thermal neutron flux. Considering the smaller fast neutron flux of 1×10^{12} n/cm²/s compared to other research reactors, all samples were irradiated for 96 hours in order to induce reactions of $^{39}\text{K}(n,p)^{39}\text{Ar}$ in the samples. The $^{40}\text{Ar}/^{39}\text{Ar}$ ages were obtained as a relative age against a neutron flux (J value) monitoring mineral standard, i.e. Fish Canyon tuff sanidine, which was irradiated together with samples of unknown ages. The used sanidine was prepared at the Geological Survey of Japan and its age was determined as 27.5 Ma (Uto et al. 1997; Ishizuka 1998; Ishizuka et al. 2002). This age is consistent with that of 27.51 Ma obtained by Lanphere & Baadsgaard (2001). Additionally, crystals of K_2SO_4 and CaF_2 were also irradiated in order to correct the interference of Ar isotopes produced by reactions of K or Ca in the samples with neutron flux. After irradiation the samples were stored for one month at GeNF in order to cool down their activity. Finally, argon isotope analyses were performed at the $^{40}\text{Ar}/^{39}\text{Ar}$ geochronology laboratory at Potsdam University.

4.3.3. Ar isotopic analysis

The $^{40}\text{Ar}/^{39}\text{Ar}$ dating system consists of (1) a Micromass 5400 high sensitivity-low background sector-type noble gas mass spectrometer equipped with an electron multiplier for pulse counting system which effectively works for analysis of very small amounts of gas, (2) a New Wave Research DualWave laser ablation system comprising a 50 W CO_2 continuous laser (10.6 μm wavelength) and a 6 mJ UV pulsed laser (266 nm wavelength, frequency-quadrupled), and (3) an ultra-high vacuum metal purification line which includes Zr-Al SAES alloy getters and a cold trap. Each analysis involves 10 minutes for gas extraction and purification and 15 minutes for data acquisition by eight cycles of peak jumping from mass 40 to mass 36. System blanks were measured after every three unknown analyses. The isotopic ratios of the investigated samples were finally obtained after corrections of blank measurements, mass discrimination by analysis of standard-air Ar, interference of the Ar isotopes derived from Ca and K by the irradiation and the decay of the radiogenic Ar isotopes (^{37}Ar and ^{39}Ar) produced by the irradiation. The final calculation of ages and errors was conducted following Uto et al. (1997). The accuracy as well as the precision of the dating system was checked every irradiation by the independent analysis of other biotite K-Ar standards, HD-B1 biotite (K-Ar age, 24.21 ± 0.32 Ma; Hess & Lippolt 1994) and Sori93 biotite (K-Ar age, 92.6 ± 0.6 Ma; Sudo et al. 1998) that are loaded together each irradiation.

The *in situ* $^{40}\text{Ar}/^{39}\text{Ar}$ UV laser-probe experiments generally allow for analyses characterized by highly spatial resolution (e.g. Kelley et al. 1994). Hence, the high spatial resolution of the UV laser offers the best opportunity for successful *in situ* dating of tiny flakes of white mica found as inclusions

in quartz-calcite segregations together with preserved relics of Fe-Mg carpholite, indicative for HP/LT conditions presented in this study and documented by previous investigations (Agard et al. 2002). Generally the unknown section samples presented in this study were ablated by the UV pulse laser with the following conditions: a beam size of 35-75 μm for white mica and 50-150 μm for biotite, 2-4 minutes pulsing duration and a repetition rate of 10 Hz. Incision of the sample did not exceed 30 μm . However, the fine-grained occurrences of the investigated white mica (in the order of a few tens of microns), together with the relatively young ages, preclude the chance of accurate direct dating by *in situ* laser ablation. Although the size of the laser beam is adjustable to a minimum diameter to 5 μm , a spot size between 35-75 μm for white mica and 50-150 μm for biotite was selected in the presented study in order to generate a sufficient amount of gas which allows performing precise measurements. In the case of large biotite crystals reaching 2 mm in size, up to a maximum of 14 spots within one single biotite grain were measured. However, particularly in the case of the generally very small white mica grains (in the order of 10 μm in size), single grain ages in the strict sense could not be obtained. In such cases the *in situ* $^{40}\text{Ar}/^{39}\text{Ar}$ UV laser-probe data were collected from areas within a particular fabric domain enriched in mica. However, such areas cannot be considered as exclusively consisting of mica; particularly quartz and chlorite may also have been ablated during gas extraction. In order to enhance gas production of the tiny white mica samples during laser application the analyses were generally performed along profiles (“garlands”). Consequently, the obtained apparent ages from the white mica samples do not represent single grain ages at all, but rather ages determined by integrating over a certain domain that contains up to a few tens of crystals, depending on the size of the white mica grains.

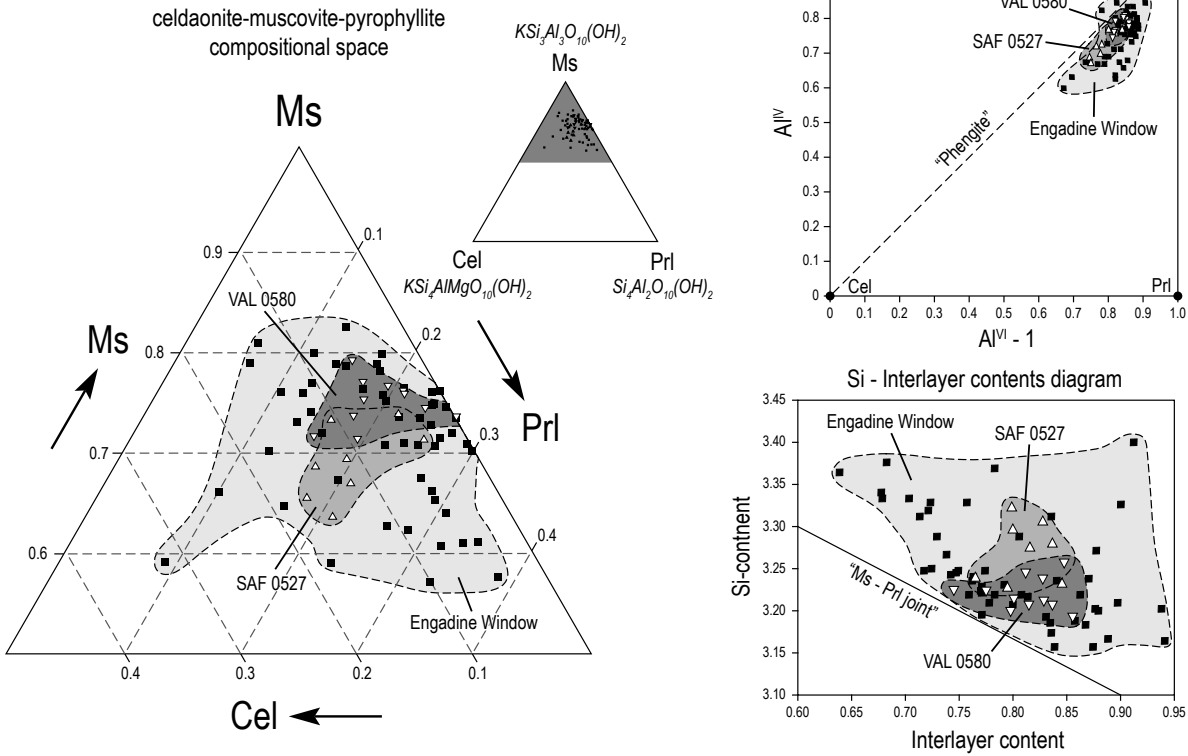
4.4. Sample description and mineral chemistry

The collected samples were studied in thin-section in order to analyze the microstructure as well as for separating texturally different phengite populations. Additionally, SEM pictures were taken for selecting the best-suited fabric domains for $^{40}\text{Ar}/^{39}\text{Ar}$ investigations and also for orientation during the *in situ* UV laser-probe experiments. Moreover, mineral compositions of studied micas were determined by wavelength-dispersive X-ray analysis (WDS) using a CAMECA SX-100 electron microprobe at the GeoForschungsZentrum (GFZ) Potsdam. The analytical conditions included an acceleration voltage of 15 kV, a beam current of 20 nA and beam diameters of 1-10 μm ; PAP corrections were applied. Natural and synthetic minerals were used as standards. Peak counting times were 10-20 s for major and 20-40 s for minor elements; backgrounds were counted for 5-20 s.

4.4.1. White mica

Relics of the HP/LT metamorphic stage are restricted to quartz-hosted fabric domains, generally found inside quartz-calcite segregations but never in the surrounding rock matrix. Therefore, all investigated white mica were picked as inclusions in quartz-calcite segregations and/or veins containing relics of Fe-Mg carpholite. This precludes the presence of detrital grains that are common in low-grade meta-sediments, and hence all dated white mica can be considered to be of metamorphic origin. However, white mica is stable during the entire metamorphic cycle, and hence several generations of white mica can be expected. White mica may be found (1) associated with Fe-Mg carpholite reflecting peak-pressure conditions or (2) together with chlorite as a part of the retrograde assemblage replacing carpholite, and (3) as a precursor for Fe-Mg carpholite (Agard et al. 2001; Wiederkehr et al. 2008). However, these different generations of white mica can be clearly distinguished by microstructural criteria.

a) *White mica composition*



b) *Biotite composition*

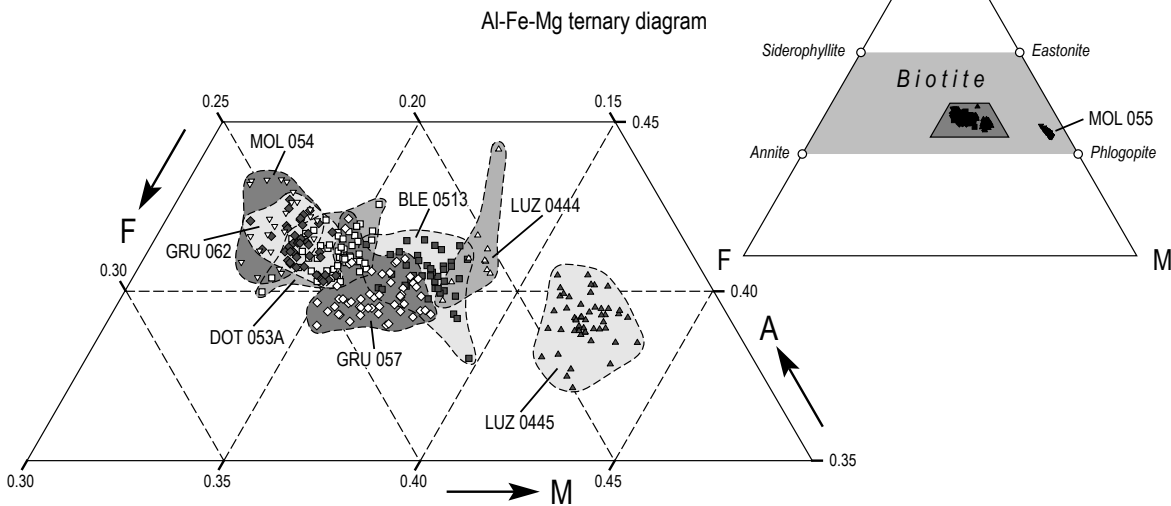


Fig. 4.3: Chemical composition of mica used for $^{40}Ar/^{39}Ar$ isotopic analysis. (a) White mica compositions determined by electron microprobe analysis, presented in celadonite-muscovite-pyrophyllite compositional space, in a phengite solid-solution graph, and in a Si-content vs. interlayer content diagram, respectively. (b) Al-Fe-Mg ternary diagram showing the chemical composition of the biotite samples.

The presence of multiple generations of white mica is also supported by electron microprobe investigations that show a significant variation of chemical composition inside this mineral group (Fig. 4.3a). In carpholite-bearing HP/LT metasediments the Si-content of phengite (Tschermak substitution) is highly pressure-sensitive (see Bousquet et al. 2008, and references therein). Maximum Si-contents for white mica associated with Fe-Mg carpholite vary between 3.30-3.40 Si p.f.u, whereas retrograde

phengite associated with chlorite replacing former carpholite cluster around 3.15-3.25 Si p.f.u (see Fig. 4.3a). The investigated phengites show a significantly lower interlayer content in the order of 0.90-0.65 p.f.u, generally attributed to the incorporation of a pyrophyllite component and resulting in vacancies in the interlayer (Vidal & Parra 2000; Bousquet et al. 2002; Parra et al. 2002a; Fig. 4.3a). Such incorporation of pyrophyllite leads to compositions of white mica that plot to the right of the celadonite to muscovite “perfect Tschermak substitution” as shown in the celadonite-pyrophyllite-muscovite triangle (Fig. 4.3a). Hence, as is typical for low-grade HP/LT metasedimentary rocks, the composition of white mica depends on both the pyrophyllite content and Tschermak substitutions, as is shown by large deviations from the ideal Tschermak substitution in the celadonite-muscovite-pyrophyllite compositional space (Bousquet et al. 2002; Parra et al. 2002a; Fig. 4.3a).

Fresh Fe-Mg carpholite is only found in the Engadine window (Bousquet et al. 1998 and 2002), such carpholite occurrences yielded the samples *AlpTea 638A* and *FOT 937* (see Tab. 4.1; Fig. 4.1c). Both samples contain large amounts of well-preserved carpholite trapped in quartz of syn-metamorphic quartz-calcite veins. Most of the white mica is associated with chlorite forming needle-shaped aggregates that partially or completely replace Fe-Mg carpholite crystals. Hence, white mica found inside such pseudomorphs after carpholite are unambiguously related to the retrograde evolution. But additionally, some rare white mica flakes were found to be closely associated with carpholite, precluding a retrograde formation because the surrounding quartz grain did not recrystallize into subgrains after trapping of carpholite and phengite. Hence, such isolated white mica can be related to HP/LT conditions and most likely represent a relic of peak-pressure white mica (see also Bousquet et al. 1998). The coexistence of retrograde phengite with relics of peak-pressure phengite is also documented by the significant chemical variations found in the Engadine window (Fig. 4.3a).

Further to the west, Fe-Mg carpholite is considerably less well preserved. In general it is partially or completely replaced by white mica and chlorite, and only some relics of carpholite could be found as quartz-hosted, hair-like fibres (Bousquet et al. 2002; Wiederkehr et al. 2008). Sample *SAF 0527* (Tab. 4.1; Fig. 4.1b) from the northern Safiental is similar to the samples from the Engadine window in that it shows the same textural features described above. However, a considerably stronger retrogression is observed in *SAF 0527*, as is documented by recrystallization of the surrounding quartz into subgrains; also tiny relics of carpholite and associated white mica are only found locally in older grains that escaped recrystallization. Again, needle-shaped aggregates of white mica and chlorite, interpreted as pseudomorphs after carpholite, are found to completely replace Fe-Mg carpholite. The chemical composition of the investigated phengites is significantly more homogeneous than in the Engadine window; Si-contents are between 3.20-3.35 p.f.u and an interlayer content of 0.75-0.85 p.f.u is determined (Fig. 4.3a).

Sample *VAL 0580*, collected in the eastern area of Valsertal (Tab. 4.1; Fig. 4.1b) is totally different from the above described investigated samples. It is characterized by large areas consisting of white mica and chlorite, oriented parallel to the main foliation surrounding several relic quartz grains within which tiny fibres of carpholite are still preserved. The chemical composition of the white mica is rather uniform, showing a maximum Si-content of 3.20-3.25 p.f.u and an interlayer content between 0.75-0.85 p.f.u (Fig. 4.3a). This rather uniform white mica composition points towards a pervasive retrogression and associated recrystallization of the earlier HP/LT stage.

In summary white mica may occur within at least the following three texturally distinguishable associations:

- (1) Completely isolated white mica flakes entrapped in quartz grains that also contain preserved relics of Fe-Mg carpholite, indicating that both white mica and carpholite formed under the same conditions, i.e. during HP/LT metamorphism.
- (2) White mica intimately associated with chlorite, forming needle-shaped aggregates entrapped in quartz grains, replacing Fe-Mg carpholite. Such mineral associations combined with their characteristic needle-shaped habit are interpreted to represent pseudomorphs after carpholite and are therefore related to the retrograde metamorphic evolution, i.e. they formed during decompression immediately after the peak-pressure stage.
- (3) White mica associated with chlorite, oriented parallel to the main foliation, forming large irregular shaped areas surrounding tiny quartz grains that may still contain some relics of Fe-Mg carpholite. This type of white mica was analyzed only in the case of sample *VAL 0580*.

4.4.2. Biotite

Biotite was only found in the south-west (southern Lukmanier and Pizzo Molare areas; Fig. 4.1b) where the Barrovian overprint reached lower/middle amphibolite facies conditions. A total of eight samples were selected for $^{40}\text{Ar}/^{39}\text{Ar}$ investigations, sample *DOT 043A* has been investigated using both step-wise-heating and *in situ* laser-probe dating (see Tab. 4.1 and Fig. 4.1b). Except for sample *MOL 055*, all investigated biotite samples are characterized by a rather uniform chemical composition clustering around intermediate XMg values slightly shifted towards phlogopite (Fig. 4.3b). Sample *LUZ 0445* is significantly shifted away from this cluster and shows a slightly higher Mg-content. Sample *MOL 055* is characterized by an Mg-content that almost represents phlogopite (Fig. 4.3b). Within a given sample the chemical composition of biotite was rather homogeneous, within core and rim of a given grain as well as between different grains. This low variation in chemical composition supports the interpretation that biotite formed as the result of a single metamorphic event, i.e. Barrow-type thermal overprint. This contrasts with the wide range of chemical composition in the investigated white micas that indicates the co-existence of several generations of white mica reflecting various stages established along the early metamorphic evolution, i.e. during the subduction-related HP/LT event and subsequent decompression, including greenschist facies overprint.

Biotite generally occurs as big flakes, up to a few mm in size, oriented parallel or across the main foliation. Particularly, the widespread occurrences of biotite that grew across the main foliation (so-called “Querbiotit”) document late-stage (post-D3) formation. Seven investigated biotite samples were collected from Valaisan-derived calcschists that are generally characterized by the mineral assemblage biotite - plagioclase - zoisite/clinozoisite - phengite - quartz - calcite/dolomite \pm chlorite \pm titanite. Only sample *MOL 054* from a staurolite - kyanite - garnet bearing micaschist, belonging to metasedimentary cover units of the distal European margin, shows a completely different mineralogical composition (Tab. 4.1 & Fig. 4.1b). Although all biotite samples were carefully selected and checked for freshness to avoid problems resulting from retrogression and alteration, chloritization of biotite is present in all investigated samples and includes chlorite lamellae within biotite (see also Allaz, 2008). To reduce the influence of chloritization as much as possible, the grain separates were purified with careful check by hand picking. Furthermore, the rock sections were investigated under the SEM prior to *in situ* $^{40}\text{Ar}/^{39}\text{Ar}$ laser-probe dating.

4.5. Results of the $^{40}\text{Ar}/^{39}\text{Ar}$ measurements

We first present the results of *in situ* laser-probe experiments on white mica and biotite, followed by the results of step-wise heating investigations on biotite. All recorded *in situ* ages are depicted on SEM images in Figures 4.4, 4.5 and 4.6, allowing for identification of the relationships between apparent ages and the location of the dated crystal domains in the microstructural context. All the results of the *in situ* laser-probe experiments and the step-wise heating experiments are listed in Tables 4.2, 4.3 and 4.4, respectively.

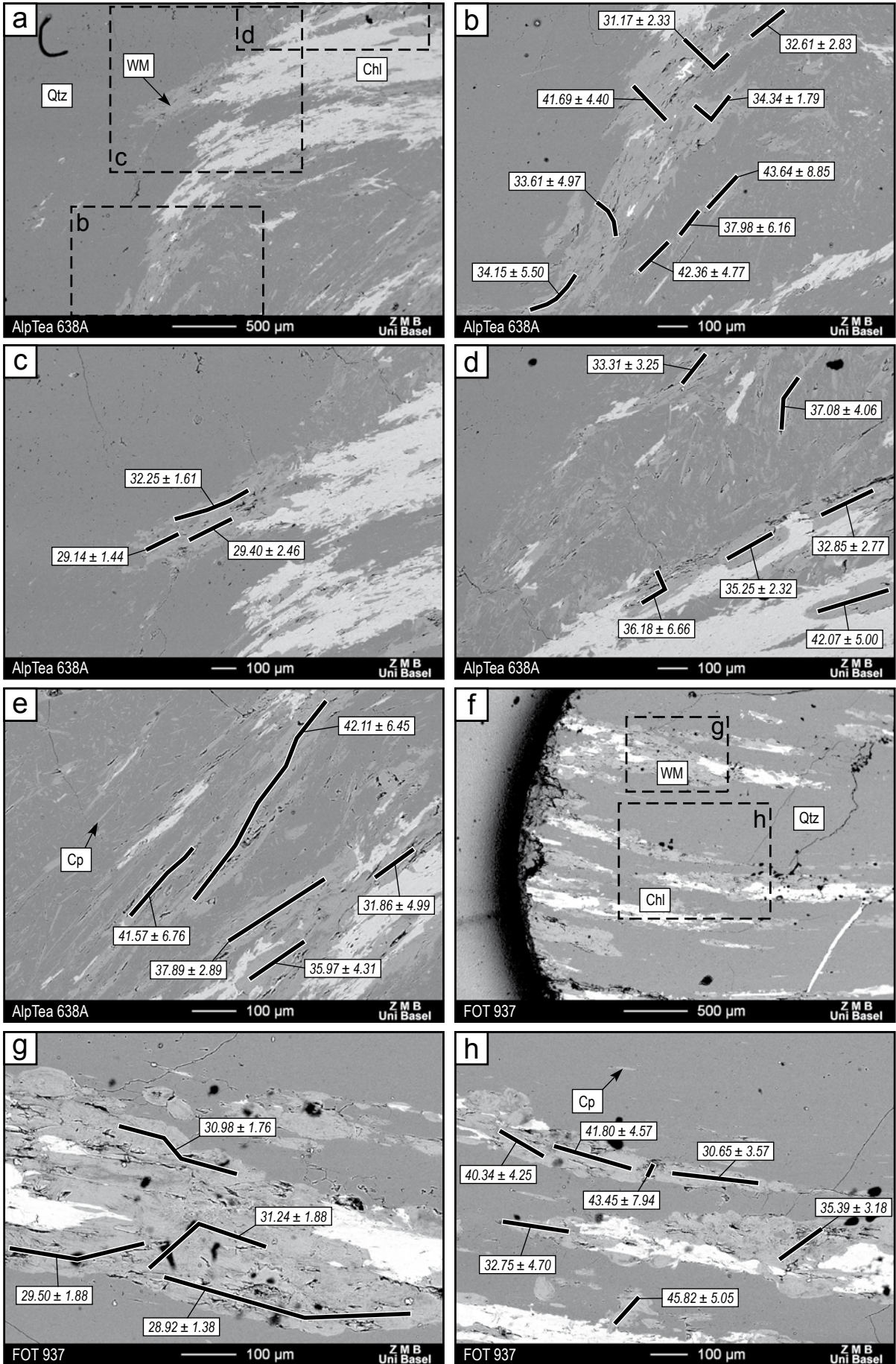
4.5.1. *In situ* $^{40}\text{Ar}/^{39}\text{Ar}$ UV laser-probe ages on white mica

Samples AlpTea 638A and FOT 937 (Engadine window)

Sample *AlpTea 638A* (Fig. 4.4a) contains a large, irregularly shaped aggregate consisting of white mica and chlorite, as well as numerous tiny and isolated carpholite needles and phengite flakes in the

Table 4.2: Full results of white mica $^{40}\text{Ar}/^{39}\text{Ar}$ *in situ* UV laser probe analysis. Uncertainties are given in 1σ , error on single ages does not include the uncertainty in the J value.

Run ID	$^{40}\text{Ar}/^{39}\text{Ar}$	$^{38}\text{Ar}/^{39}\text{Ar}$	$^{37}\text{Ar}/^{39}\text{Ar}$	$^{36}\text{Ar}/^{39}\text{Ar}$ ($\times 10^{-3}$)	$^{40}\text{Ar}^*$ (%)	$^{40}\text{Ar}^*/^{39}\text{Ar}_{\text{K}}$	Age (Ma) $\pm 1\sigma$
<i>Sample AlpTea 938A (J=0.001973)</i>							
U0800601	14.111 ± 0.157	0.015 ± 0.002	0.017 ± 0.033	19.256 ± 2.357	59.7	8.423 ± 0.710	29.7 ± 2.5
U0800605	32.281 ± 0.162	0.033 ± 0.001	0.016 ± 0.028	76.289 ± 1.694	30.2	9.739 ± 0.511	34.3 ± 1.8
U0800607	16.485 ± 0.163	0.017 ± 0.002	0.024 ± 0.037	24.517 ± 2.692	56.1	9.244 ± 0.810	32.6 ± 2.8
U0800608	68.080 ± 0.790	0.052 ± 0.004	0.082 ± 0.149	189.919 ± 6.376	17.6	11.970 ± 1.853	42.1 ± 6.4
U0800609	43.290 ± 1.096	0.032 ± 0.007	0.066 ± 0.054	106.550 ± 6.818	27.3	11.814 ± 1.944	41.6 ± 6.8
U0800610	20.840 ± 0.303	0.023 ± 0.003	0.033 ± 0.049	34.133 ± 2.679	51.6	10.758 ± 0.828	37.9 ± 2.9
U0800611	21.801 ± 0.208	0.027 ± 0.002	0.019 ± 0.017	39.945 ± 2.169	45.9	9.999 ± 0.662	35.2 ± 2.3
U0800612	32.100 ± 0.334	0.035 ± 0.005	0.033 ± 0.026	73.027 ± 3.892	32.8	10.525 ± 1.164	37.1 ± 4.1
U0800613	33.619 ± 0.359	0.033 ± 0.004	0.015 ± 0.058	81.810 ± 3.056	28.1	9.446 ± 0.928	33.3 ± 3.2
U0800614	12.117 ± 0.138	0.016 ± 0.002	0.013 ± 0.022	13.083 ± 1.340	68.1	8.252 ± 0.409	29.1 ± 1.4
U0800615	12.519 ± 0.114	0.017 ± 0.002	0.010 ± 0.021	11.437 ± 1.521	73.0	9.141 ± 0.460	32.2 ± 1.6
U0800616	26.911 ± 0.339	0.028 ± 0.004	0.040 ± 0.061	50.990 ± 4.273	44.0	11.848 ± 1.264	41.7 ± 4.4
U0800617	15.617 ± 0.177	0.022 ± 0.003	0.036 ± 0.052	20.616 ± 4.788	61.0	9.530 ± 1.421	33.6 ± 5.0
U0800618	18.063 ± 0.188	0.024 ± 0.004	0.040 ± 0.057	28.368 ± 5.315	53.6	9.685 ± 1.575	34.1 ± 5.5
U0800619	40.272 ± 0.737	0.038 ± 0.006	0.068 ± 0.089	94.320 ± 8.685	30.8	12.409 ± 2.547	43.6 ± 8.9
U0800620	19.137 ± 0.546	0.029 ± 0.006	0.050 ± 0.056	70.599 ± 6.025	34.1	10.782 ± 1.767	38.0 ± 6.2
U0800621	31.630 ± 0.384	0.022 ± 0.005	0.054 ± 0.078	24.008 ± 4.563	62.9	12.043 ± 1.370	42.4 ± 4.8
U0800622	15.692 ± 0.164	0.020 ± 0.002	0.025 ± 0.040	23.223 ± 2.218	56.3	8.832 ± 0.665	31.2 ± 2.3
U0800623	16.055 ± 0.244	0.020 ± 0.003	0.087 ± 0.075	19.824 ± 4.129	63.6	10.208 ± 1.234	36.0 ± 4.3
U0800624	16.647 ± 0.297	0.017 ± 0.005	0.036 ± 0.058	25.787 ± 4.780	54.3	9.031 ± 1.426	31.9 ± 5.0
U0800627	18.363 ± 0.176	0.028 ± 0.004	0.088 ± 0.076	21.714 ± 4.839	65.1	11.958 ± 1.437	42.1 ± 5.0
U0800628	15.336 ± 0.158	0.021 ± 0.003	0.097 ± 0.034	20.424 ± 2.647	60.7	9.314 ± 0.790	32.9 ± 2.8
U0800629	22.969 ± 0.343	0.033 ± 0.004	0.135 ± 0.070	43.048 ± 6.389	44.7	10.266 ± 1.908	36.2 ± 6.7
<i>Sample FOT 937 (J=0.001975)</i>							
U0800801	16.184 ± 0.090	0.024 ± 0.001	0.029 ± 0.036	27.097 ± 1.308	50.5	8.181 ± 0.392	28.9 ± 1.4
U0800802	15.167 ± 0.114	0.021 ± 0.002	0.002 ± 0.030	21.652 ± 1.674	57.8	8.769 ± 0.500	31.0 ± 1.8
U0800804	23.329 ± 0.155	0.027 ± 0.002	0.014 ± 0.038	50.705 ± 1.796	35.8	8.348 ± 0.535	29.5 ± 1.9
U0800805	19.363 ± 0.170	0.024 ± 0.003	0.025 ± 0.034	35.608 ± 1.779	45.7	8.844 ± 0.535	31.2 ± 1.9
U0800809	21.225 ± 0.368	0.025 ± 0.004	0.048 ± 0.084	31.689 ± 4.310	55.9	11.867 ± 1.312	41.8 ± 4.6
U0800810	18.752 ± 0.195	0.023 ± 0.002	0.016 ± 0.054	34.102 ± 3.407	46.3	8.677 ± 1.018	30.7 ± 3.6
U0800811	17.367 ± 0.353	0.028 ± 0.004	0.059 ± 0.046	27.408 ± 4.410	53.4	9.276 ± 1.344	32.8 ± 4.7
U0800814	19.031 ± 0.441	0.025 ± 0.003	0.032 ± 0.082	30.478 ± 2.810	52.7	10.029 ± 0.909	35.4 ± 3.2
U0800816	20.978 ± 0.553	0.014 ± 0.004	0.061 ± 0.081	32.280 ± 3.751	54.6	11.448 ± 1.218	40.3 ± 4.2
U0800817	21.529 ± 0.700	0.025 ± 0.004	0.069 ± 0.118	31.118 ± 7.397	57.3	12.343 ± 2.282	43.5 ± 7.9
U0800818	20.241 ± 0.666	0.025 ± 0.003	0.078 ± 0.145	24.457 ± 4.547	64.3	13.025 ± 1.453	45.8 ± 5.1
<i>Sample SAF 0527 (J=0.001970)</i>							
U0801102	60.570 ± 0.809	0.049 ± 0.003	0.041 ± 0.083	161.195 ± 3.709	21.4	12.943 ± 0.948	45.4 ± 3.3
U0801103	15.866 ± 0.113	0.019 ± 0.001	0.009 ± 0.021	21.764 ± 0.997	59.5	9.436 ± 0.304	33.2 ± 1.1
U0801104	20.927 ± 0.325	0.025 ± 0.003	0.040 ± 0.048	39.721 ± 3.601	43.9	9.195 ± 1.083	32.4 ± 3.8
U0801105	11.371 ± 0.139	0.020 ± 0.002	0.013 ± 0.020	9.046 ± 1.535	76.5	8.699 ± 0.468	30.7 ± 1.6
U0801106	29.132 ± 0.222	0.031 ± 0.002	0.004 ± 0.024	72.585 ± 1.759	26.4	7.684 ± 0.501	27.1 ± 1.8
U0801107	12.044 ± 0.076	0.018 ± 0.001	0.011 ± 0.015	11.161 ± 1.536	72.6	8.748 ± 0.459	30.8 ± 1.6
U0801108	22.386 ± 0.172	0.026 ± 0.002	0.055 ± 0.044	42.639 ± 2.801	43.7	9.794 ± 0.830	34.5 ± 2.9
U0801109	14.647 ± 0.102	0.016 ± 0.001	0.013 ± 0.012	16.143 ± 1.273	67.4	9.878 ± 0.383	34.8 ± 1.3
U0801110	11.712 ± 0.204	0.019 ± 0.001	0.004 ± 0.035	6.744 ± 1.520	83.0	9.720 ± 0.488	34.2 ± 1.7
U0801111	26.547 ± 0.326	0.026 ± 0.002	0.072 ± 0.049	49.810 ± 3.747	44.6	11.838 ± 1.136	41.6 ± 3.9
U0801112	19.664 ± 0.653	0.022 ± 0.006	0.010 ± 0.094	36.014 ± 8.196	45.9	9.023 ± 2.500	31.8 ± 8.7
<i>Sample VAL 0580 (J=0.001959)</i>							
U0801001	9.325 ± 0.085	0.019 ± 0.001	0.012 ± 0.016	6.254 ± 1.192	80.2	7.479 ± 0.361	26.4 ± 1.3
U0801002	8.875 ± 0.081	0.018 ± 0.001	0.004 ± 0.014	6.132 ± 0.882	79.6	7.063 ± 0.271	24.9 ± 1.0
U0801003	10.305 ± 0.084	0.018 ± 0.002	0.002 ± 0.026	9.462 ± 0.970	72.9	7.509 ± 0.296	26.5 ± 1.0
U0801004	10.541 ± 0.279	0.021 ± 0.002	0.011 ± 0.022	13.402 ± 1.395	62.4	6.582 ± 0.484	23.2 ± 1.7
U0801005	9.962 ± 0.113	0.019 ± 0.001	0.002 ± 0.035	8.775 ± 1.564	74.0	7.370 ± 0.474	26.0 ± 1.7
U0801006	8.963 ± 0.208	0.018 ± 0.001	0.012 ± 0.014	6.541 ± 0.682	78.5	7.032 ± 0.282	24.8 ± 1.0
U0801007	9.345 ± 0.183	0.016 ± 0.001	0.009 ± 0.014	7.150 ± 1.199	77.4	7.233 ± 0.394	25.5 ± 1.4
U0801008	10.417 ± 0.412	0.016 ± 0.003	0.039 ± 0.076	7.919 ± 4.411	77.6	8.082 ± 1.363	28.5 ± 4.8



immediate vicinity (Figs. 4.4b, d & e). The microstructure of sample *FOT 937* is dominated by numerous needle-shaped phengite-chlorite aggregates, replacing former Fe-Mg carpholite crystals (Figs. 4.4f, g & h) and interpreted as pseudomorphs after carpholite. The white mica in both samples yield ages that scatter between 45.82 ± 5.05 and 28.92 ± 1.38 Ma (Fig. 4.4, Tab. 4.2). Phengite that is closely associated with chlorite yields rather precise and consistent ages in the time interval 32.25 - 29.14 Ma in the case of sample *AlpTea 638A* (Fig. 4.4c), and between 31.24 - 28.92 Ma in the case of sample *FOT 937* (Fig. 4.4g). However, it was found that tiny phengite flakes, more or less isolated and entrapped in quartz, yield older ages between 43.64 ± 8.85 and 37.08 ± 4.06 Ma (Figs. 4.4b, d & e). Ages around 40 Ma or more were also recorded within a minor portion of domains that are well inside or close to phengite-chlorite aggregates (Figs. 4.4b & d), as well as inside chlorite-phengite associations that are interpreted to have replaced carpholite (Fig. 4.4h). An intermediate range of ages was found inside phengite-chlorite assemblages (Figs. 4.4b, d, e & h), scattering between 36.18 and 32.75 Ma, i.e. an age range bracketed by the pre-40 Ma ages and the well-defined age population around 30 Ma.

Sample SAF 0527 (Safiental)

The microstructure of sample *SAF 0527* is characterized by an irregularly shaped aggregate of white mica and chlorite fully entrapped in quartz. Phengite occurs as flower-like nuclei or as numerous tiny flakes (Figs. 4.5a & b). In some places white mica is intimately associated with chlorite. In the immediate vicinity numerous tiny quartz-hosted relics of carpholite needles also occur, being significantly less frequent and generally less preserved in comparison to the samples from the Engadine window. However, the recorded $^{40}\text{Ar}/^{39}\text{Ar}$ ages fall into exactly the same range as those from the Engadine window. They scatter between 45.42 ± 3.29 and 27.10 ± 1.76 Ma, most ages being found within the 35-31 Ma time interval (Fig. 4.5b, Tab. 4.2). No obvious trend between the obtained ages and their location in the microstructure is possible.

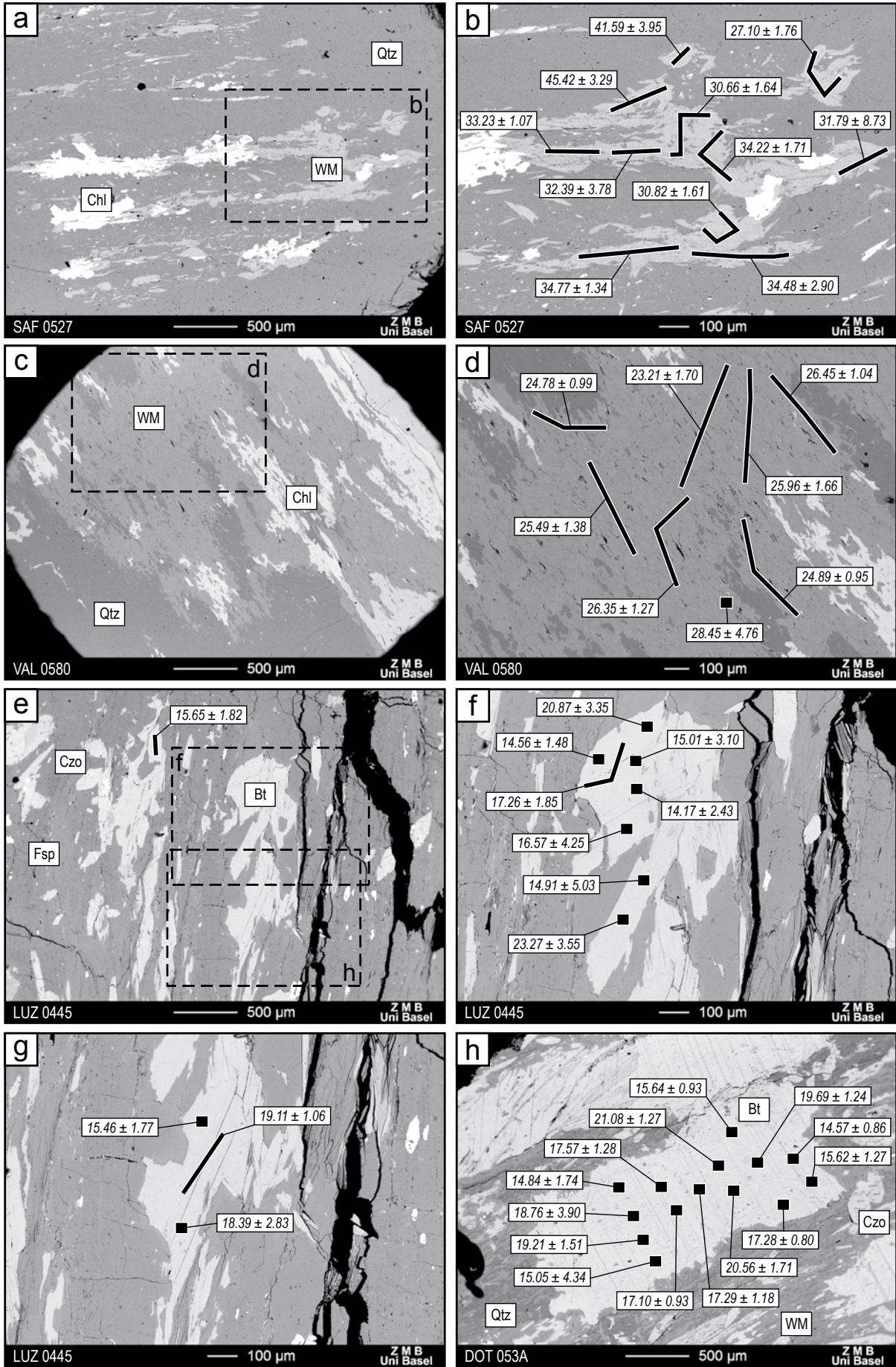
Sample VAL 0580 (Valsertal)

A completely different microstructure compared to the samples from the Engadine window and Safiental characterizes sample *VAL 0580* (Fig. 4.5c). White mica occurs as large aggregates oriented parallel to the main foliation and is intimately associated with chlorite; carpholite is only found as tiny quartz-hosted needles and restricted to relic quartz grains which are dispersedly distributed within the main foliation. The $^{40}\text{Ar}/^{39}\text{Ar}$ ages are well defined and consistently between 28.45 ± 4.76 and 23.21 ± 1.70 Ma (Fig. 4.5d, Tab. 4.2), the weighted average age yields 25.40 ± 0.45 Ma. Hence, significantly lower ages are found in sample *VAL 0580* compared to the other samples described before. Moreover, such uniform and consistent ages point towards the presence of one distinct generation of phengite (see later discussion).

4.5.2. *In situ* $^{40}\text{Ar}/^{39}\text{Ar}$ UV laser-probe ages of biotite

The results from four biotite-bearing samples investigated by the *in situ* $^{40}\text{Ar}/^{39}\text{Ar}$ UV laser-probe dating technique will be briefly presented in order of increasing temperatures related to Barrovian over-

Fig. 4.4: SEM back-scattered electron photomicrographs of carpholite-bearing synmetamorphic quartz-calcite segregations and location of the domains analyzed by laser ablation in white mica. Errors are 1σ and do not include the uncertainty in the J value. Mineral abbreviations used: Qtz = quartz, WM = white mica, Chl = chlorite, Cp = Fe-Mg carpholite. (a) Overview of the characteristic microstructure of sample *AlpTea 638A*; dashed lines denote outlines of Figs. b, c and d. (b) – (e) Indicate the locations of traces ablated during laser experiments as well as the obtained apparent ages on white mica in sample *AlpTea 638A*. (f) Overview of the microstructure of sample *FOT 937*; dashed lines denote outlines of Figs. (g) and (h) that indicate the locations of traces ablated during laser experiments as well as the obtained apparent ages on white mica in sample *FOT 937*.



print. The four samples occur between a location coinciding with the first biotite occurrence in Val Luzzone (*LUZ 0445*) and the maximum temperature area around Pizzo Molare (*MOL 055*; Fig. 4.1b, Tab. 4.1). All investigated biotite grains were very much larger compared to the analyzed white micas, which allows for numerous single spot analyses per grain. Hence, the measured biotite ages typically represent

Table 4.3: Full results of biotite $^{40}\text{Ar}/^{39}\text{Ar}$ *in situ* UV laser step-wise heating analysis. Uncertainties are given in 1σ , error on single ages does not include the uncertainty in the J value.

Run ID	$^{40}\text{Ar}/^{39}\text{Ar}$	$^{38}\text{Ar}/^{39}\text{Ar}$	$^{37}\text{Ar}/^{39}\text{Ar}$	$^{36}\text{Ar}/^{39}\text{Ar}$ ($\times 10^{-3}$)	$^{40}\text{Ar}^*$ (%)	$^{40}\text{Ar}^*/^{39}\text{Ar}_K$	Age (Ma) $\pm 1\sigma$
<i>Sample LUZ 0450 (J=0.001984)</i>							
U0800408	28.281 ± 0.357	0.028 ± 0.002	0.011 ± 0.016	81.890 ± 1.370	14.4	4.084 ± 0.417	14.6 ± 1.5
U0800409	45.208 ± 0.421	0.046 ± 0.004	0.163 ± 0.059	133.209 ± 3.265	13.0	5.866 ± 0.947	20.9 ± 3.4
U0800410	17.502 ± 0.212	0.026 ± 0.002	0.093 ± 0.041	45.023 ± 2.906	24.1	4.210 ± 0.874	15.0 ± 3.1
U0800411	19.259 ± 0.219	0.028 ± 0.001	0.004 ± 0.040	51.722 ± 2.270	20.6	3.976 ± 0.684	14.2 ± 2.4
U0800412	21.240 ± 0.307	0.025 ± 0.002	0.105 ± 0.054	56.186 ± 4.332	21.9	4.651 ± 1.274	16.6 ± 4.5
U0800414	32.043 ± 0.475	0.030 ± 0.002	0.003 ± 0.031	86.290 ± 3.335	20.4	6.544 ± 1.005	23.3 ± 3.6
U0800415	44.170 ± 0.501	0.040 ± 0.003	0.036 ± 0.074	135.338 ± 4.710	9.5	4.183 ± 1.417	14.9 ± 5.0
U0800417	37.025 ± 0.316	0.035 ± 0.001	0.009 ± 0.038	107.824 ± 2.636	13.9	5.164 ± 0.799	18.4 ± 2.8
U0800418	21.184 ± 0.153	0.025 ± 0.002	0.008 ± 0.028	57.010 ± 1.706	20.5	4.339 ± 0.498	15.5 ± 1.8
U0800419	17.210 ± 0.152	0.026 ± 0.002	0.008 ± 0.014	41.847 ± 1.737	28.2	4.845 ± 0.522	17.3 ± 1.9
U0800420	21.047 ± 0.157	0.028 ± 0.001	0.068 ± 0.017	53.091 ± 0.968	25.5	5.368 ± 0.300	19.1 ± 1.1
U0800422	105.072 ± 0.525	0.086 ± 0.002	0.004 ± 0.024	340.717 ± 2.181	4.2	4.391 ± 0.513	15.6 ± 1.8
<i>Sample DOT 053A (J=0.001987)</i>							
U0801401	26.260 ± 0.390	0.034 ± 0.003	0.041 ± 0.036	71.086 ± 3.815	20.0	5.259 ± 1.100	18.8 ± 3.9
U0801402	32.084 ± 0.302	0.041 ± 0.004	0.083 ± 0.045	94.347 ± 4.177	13.1	4.215 ± 1.222	15.0 ± 4.3
U0801403	14.514 ± 0.104	0.025 ± 0.002	0.014 ± 0.014	30.891 ± 1.411	37.1	5.388 ± 0.425	19.2 ± 1.5
U0801404	14.141 ± 0.502	0.027 ± 0.001	0.005 ± 0.005	33.789 ± 1.178	29.4	4.157 ± 0.490	14.8 ± 1.7
U0801405	17.886 ± 0.133	0.028 ± 0.001	0.000 ± 0.006	43.858 ± 1.192	27.5	4.926 ± 0.359	17.6 ± 1.3
U0801406	19.428 ± 0.129	0.030 ± 0.001	0.021 ± 0.006	49.533 ± 0.864	24.7	4.793 ± 0.262	17.1 ± 0.9
U0801407	18.740 ± 0.138	0.029 ± 0.001	0.006 ± 0.009	47.013 ± 1.102	25.9	4.848 ± 0.333	17.3 ± 1.2
U0801408	40.382 ± 0.201	0.043 ± 0.001	0.180 ± 0.021	117.210 ± 1.672	14.3	5.769 ± 0.481	20.6 ± 1.7
U0801409	35.122 ± 0.118	0.039 ± 0.001	0.055 ± 0.012	98.867 ± 1.227	16.8	5.914 ± 0.359	21.1 ± 1.3
U0801410	26.006 ± 0.099	0.036 ± 0.001	0.007 ± 0.007	69.320 ± 1.197	21.2	5.522 ± 0.350	19.7 ± 1.2
U0801411	13.663 ± 0.160	0.024 ± 0.001	0.049 ± 0.008	29.865 ± 0.674	35.5	4.844 ± 0.225	17.3 ± 0.8
U0801412	67.729 ± 0.229	0.061 ± 0.001	0.022 ± 0.005	214.399 ± 1.222	6.5	4.377 ± 0.357	15.6 ± 1.3
U0801413	18.711 ± 0.112	0.028 ± 0.001	0.013 ± 0.015	49.518 ± 0.780	21.8	4.080 ± 0.240	14.6 ± 0.9
U0801414	40.563 ± 0.191	0.045 ± 0.001	0.005 ± 0.008	122.446 ± 0.998	10.8	4.381 ± 0.261	15.6 ± 0.9
<i>Sample GRU 057 (J=0.001982)</i>							
U0800423	16.203 ± 0.189	0.025 ± 0.003	4.031 ± 0.112	46.681 ± 4.403	18.0	2.922 ± 1.314	10.4 ± 4.7
U0800501	19.220 ± 0.193	0.027 ± 0.004	0.807 ± 0.099	55.037 ± 5.047	15.9	3.059 ± 1.497	10.9 ± 5.3
U0800506	14.118 ± 0.104	0.027 ± 0.003	0.413 ± 0.048	31.101 ± 2.117	35.3	4.981 ± 0.629	17.7 ± 2.2
U0800509	59.368 ± 0.923	0.048 ± 0.004	0.512 ± 0.077	183.229 ± 5.137	8.9	5.290 ± 1.308	18.8 ± 4.6
U0800512	32.720 ± 0.358	0.033 ± 0.003	0.713 ± 0.079	95.548 ± 3.578	14.0	4.577 ± 1.051	16.3 ± 3.7
U0800514	36.416 ± 0.388	0.032 ± 0.002	0.302 ± 0.058	108.078 ± 2.784	12.4	4.518 ± 0.807	16.1 ± 2.9
U0800516	47.245 ± 0.540	0.052 ± 0.006	5.407 ± 0.153	146.988 ± 5.069	9.5	4.507 ± 1.449	16.0 ± 5.1
U0800518	21.730 ± 0.154	0.024 ± 0.003	1.974 ± 0.134	57.416 ± 3.090	23.1	5.019 ± 0.918	17.9 ± 3.3
U0800519	27.970 ± 0.297	0.029 ± 0.004	2.521 ± 0.162	80.772 ± 4.350	15.8	4.427 ± 1.297	15.8 ± 4.6
U0800520	26.896 ± 0.505	0.033 ± 0.006	5.691 ± 0.337	76.632 ± 6.459	18.4	4.987 ± 1.923	17.7 ± 6.8
U0800521	16.096 ± 0.271	0.022 ± 0.003	0.469 ± 0.076	43.933 ± 2.590	19.7	3.174 ± 0.776	11.3 ± 2.8
U0800522	27.070 ± 0.288	0.024 ± 0.002	1.497 ± 0.081	77.285 ± 4.495	16.3	4.426 ± 1.335	15.8 ± 4.7
U0800526	28.451 ± 0.543	0.041 ± 0.004	3.301 ± 0.123	79.388 ± 3.095	19.0	5.420 ± 0.854	19.3 ± 3.0
U0800527	22.738 ± 0.378	0.031 ± 0.006	3.287 ± 0.114	61.476 ± 3.441	21.9	4.997 ± 1.055	17.8 ± 3.7
U0800530	49.798 ± 0.662	0.045 ± 0.002	1.052 ± 0.054	151.435 ± 4.707	10.4	5.185 ± 1.274	18.4 ± 4.5
U0801111	67.431 ± 0.511	0.057 ± 0.004	2.689 ± 0.161	217.685 ± 6.163	5.1	3.449 ± 1.792	12.3 ± 6.4
U0801112	32.932 ± 0.330	0.038 ± 0.006	2.216 ± 0.242	98.579 ± 5.533	12.4	4.086 ± 1.654	14.6 ± 5.9
<i>Sample MOL 055 (J=0.001980)</i>							
U0801302	11.432 ± 0.214	0.026 ± 0.002	0.030 ± 0.058	19.178 ± 3.209	50.5	5.769 ± 0.958	20.5 ± 3.4
U0801303	25.711 ± 0.352	0.027 ± 0.003	0.038 ± 0.056	70.910 ± 3.824	18.5	4.762 ± 1.126	16.9 ± 4.0
U0801304	16.672 ± 0.249	0.026 ± 0.002	0.088 ± 0.040	38.893 ± 3.999	31.1	5.190 ± 1.197	18.4 ± 4.2
U0801305	16.077 ± 0.303	0.025 ± 0.003	0.247 ± 0.082	38.409 ± 5.093	29.6	4.759 ± 1.512	16.9 ± 5.4
U0801306	16.248 ± 0.367	0.027 ± 0.003	0.266 ± 0.090	33.941 ± 7.792	38.5	6.253 ± 2.317	22.2 ± 8.2
U0801307	22.191 ± 0.588	0.031 ± 0.006	0.057 ± 0.116	55.736 ± 8.440	25.8	5.729 ± 2.513	20.3 ± 8.9
U0801308	17.161 ± 0.432	0.031 ± 0.005	0.399 ± 0.097	41.457 ± 9.153	28.9	4.962 ± 2.723	17.6 ± 9.6
U0801309	21.317 ± 0.383	0.032 ± 0.004	0.069 ± 0.171	58.324 ± 5.714	19.2	4.091 ± 1.713	14.6 ± 6.1
U0801310	14.616 ± 0.329	0.017 ± 0.004	0.058 ± 0.186	33.662 ± 5.053	32.0	4.676 ± 1.507	16.6 ± 5.3
U0801311	10.646 ± 0.144	0.022 ± 0.002	0.168 ± 0.105	18.222 ± 3.140	49.6	5.283 ± 0.934	18.8 ± 3.3

Fig. 4.5: SEM back-scattered electron photomicrographs of investigated white mica- and biotite-bearing samples and location of the domains analyzed by laser ablation in white mica or biotite. Errors are 1σ and do not include the uncertainty in the J value. Mineral abbreviations used: Qtz = quartz, WM = white mica, Chl = chlorite, Bt = biotite, Czo = clinozoisite, Fsp = feldspar (plagioclase). (a) Overview of the microstructure of sample *SAF 0527*; dashed lines denote outlines of figure (b) that provides microstructural details of the same sample, indicates the location of the traces ablated during laser experiments and provides the apparent ages obtained on white mica. (c) General overview of the microstructure of sample *VAL 0580*; note the significantly different microstructure compared to the other mica samples, phengite and chlorite being oriented parallel to the main foliation. Dashed lines denote outlines of (d) providing microstructural details within sample *VAL 0580* and indicating the location of ablated points or traces and apparent ages obtained for white mica. (e) General overview of the microstructure of sample *LUZ 0445* within which biotite grains were investigated; dashed lines denote outlines of (f) and (g) that provide details of the microstructure of sample *LUZ 0445* and indicate the location of ablated points or traces and apparent ages obtained for biotite. (h) Biotite flake growing across the main foliation (“Querbiotit”) in sample *DOT 053A* and location of ablated points and apparent ages obtained for biotite.

single grain ages. Nevertheless, larger areas were occasionally ablated along profiles in order to enhance the amount of gas.

In sample *LUZ 0445* biotite grains or aggregates are found completely contained within large plagioclase porphyroblasts (Fig. 4.5e). Plagioclase also encloses numerous zoisite/clinozoisite grains and occasionally white mica. Typically, biotite, plagioclase and zoisite/clinozoisite are seen to have formed when temperatures increased during the late-stage Barrow-type thermal overprint (Wiederkehr et al. 2008). All recorded biotite ages scatter between 23.27 ± 3.55 and 14.17 ± 2.43 Ma (Figs. 4.5e, f & g;

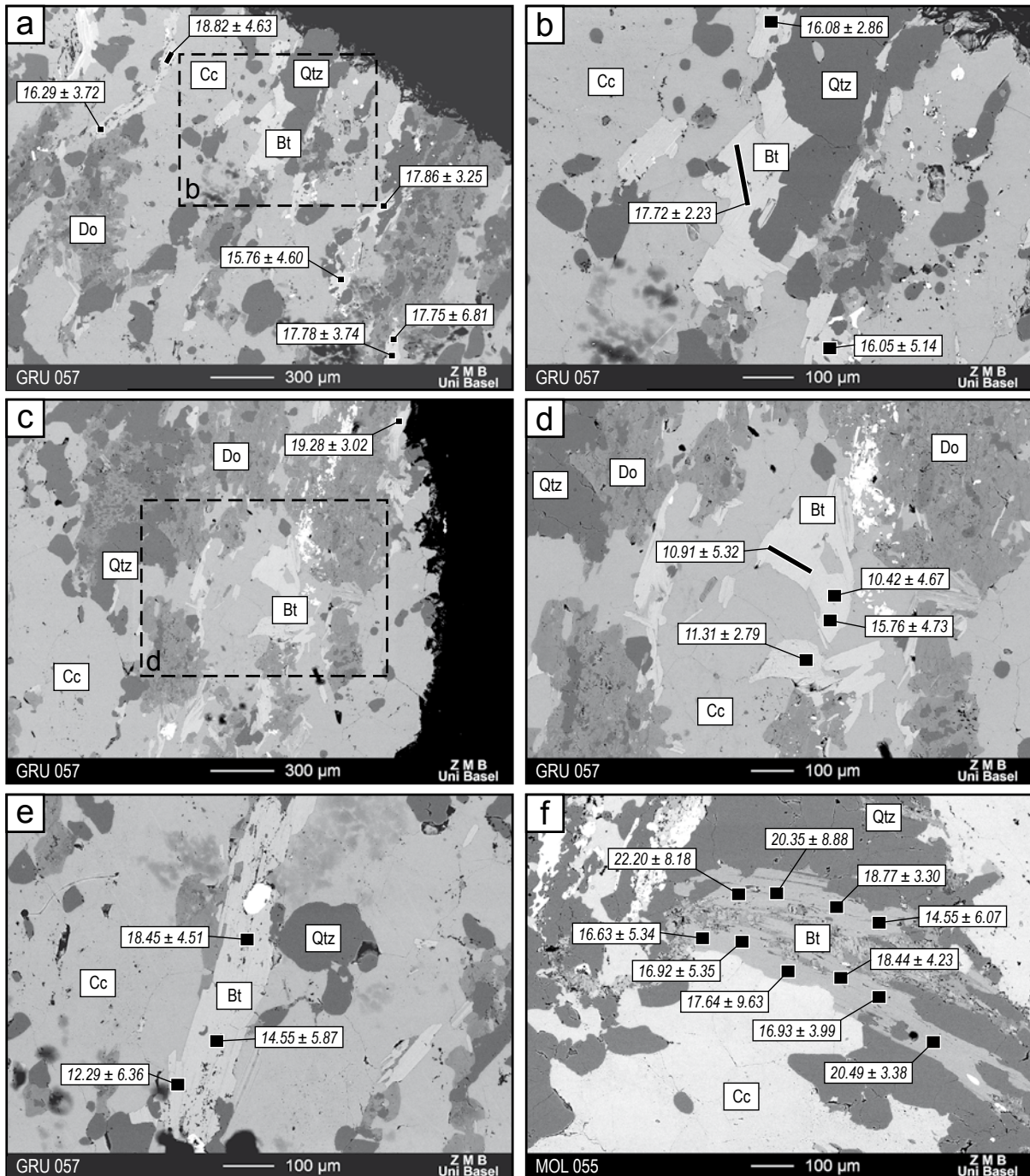


Fig. 4.6: SEM back-scattered electron photomicrographs of investigated biotite-bearing samples and location of the domains analyzed by laser ablation in biotite. Errors are 1σ and do not include the uncertainty in the J value. Mineral abbreviations used: Qtz = quartz, Bt = biotite, Cc = calcite, Do = dolomite. (a) – (e) Location of points and traces ablated and apparent ages obtained within sample *GRU 057*. The dashed rectangles denote the positions of the details shown in (b) and (d), respectively. (f) Biotite flake in sample *MOL 055* and locations of ablated points and apparent ages obtained for biotite.

Tab. 4.3). No obvious correlation between age and microstructural position could be detected (Figs. 4.5e, f & g). A weighted average age of 17.05 ± 0.59 Ma was calculated for this sample (see Fig. 4.7).

Within sample *DOT 053A* we investigated a ca. 2 mm long and 1 mm wide biotite grain that grew across the main foliation (typical “Querbiotit”; Fig. 4.5h). Given the large grain size the laser spot was opened up to a diameter of 150 μm . The obtained ages are bracket between 21.08 ± 1.27 and 14.57 ± 0.86 Ma (Tab. 4.3). Older ages are generally found in the core of the grain and cluster between 21-17 Ma; towards the rim the ages tend to be slightly younger and vary between 17-15 Ma (Fig. 4.5h). By including all age data a weighted average age of 17.17 ± 0.32 Ma is calculated (Fig. 4.7).

Sample *GRU 057* contains fine-grained biotite flakes that are oriented parallel to the only weakly developed main foliation and that are dispersedly distributed within a matrix mainly formed by calcite/dolomite with some minor amount of quartz (Figs. 4.6a & c). Due to the relatively small grain size (around 100 μm) it was possible to obtain more than one age per grain only in rare cases. Also, the extracted amount of gas was significantly lower, which results in larger uncertainties. In comparison to the other investigated samples the recorded ages of *GRU 057*, representing a population of single grain ages, show a larger scatter; most ages cluster in the 18-16 Ma time interval (Figs. 4.6a-e, Tab. 4.3), the weighted average age is 16.11 ± 0.92 Ma (Fig. 4.7c).

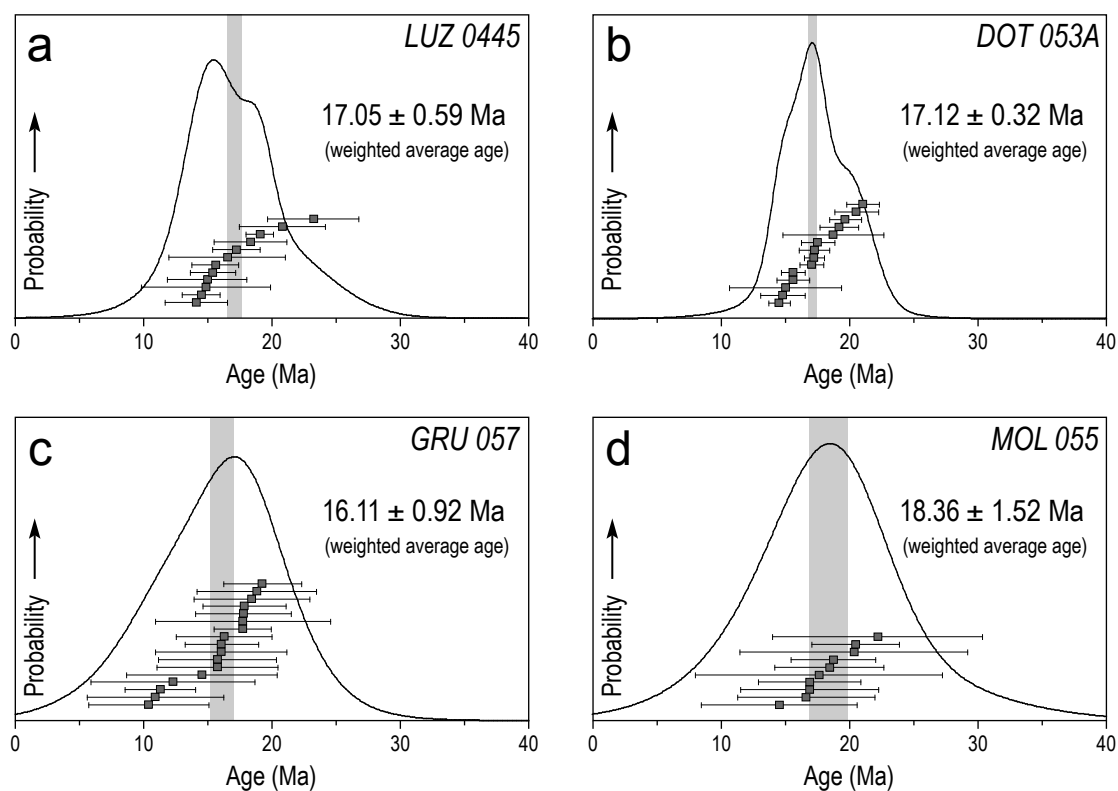


Fig. 4.7: Summary of apparent ages obtained on biotite by *in situ* laser-probe analyses and calculated cumulative probability curves. The resulting weighted average age is also denoted as grey bars; errors are 1σ and do not include the uncertainty in the J value. (a) Sample *LUZ 0445*. (b) Sample *DOT 053A*. (c) Sample *GRU 057*. (d) Sample *MOL 055*.

Within sample *MOL 055* a total of 10 ages was obtained from one single flake of biotite, approximately 0.75 mm long and 0.3 mm wide, embedded in a matrix consisting of quartz and calcite/dolomite (Fig. 4.6f). Since we used a small laser spot size, varying between 50-75 μm , only small amounts of gas were extracted which results in high uncertainties. The recorded ages between 22.20 ± 8.18 and 14.55

± 6.07 Ma (Tab. 4.3) yield a weighted average age of 18.36 ± 1.52 Ma (Fig. 4.7). This is only slightly older compared to the weighted average ages of the other three samples studied.

4.5.3. $^{40}\text{Ar}/^{39}\text{Ar}$ CO_2 laser step-wise heating of biotite

The $^{40}\text{Ar}/^{39}\text{Ar}$ age spectra for biotite separated from five samples show rather simple and well-developed plateaus that yield consistent ages between 17.27 and 15.48 Ma (Fig. 4.8, Tab. 4.4). Generally a significant plateau age is defined by (1) the occurrence of a series of adjacent steps that together

Table 4.4: Full results of $^{40}\text{Ar}/^{39}\text{Ar}$ CO_2 laser step-wise heating analysis of biotite. Uncertainties are given in 1σ , error on single ages does not include the uncertainty in the J value.

Step	Laser output	$^{40}\text{Ar}/^{39}\text{Ar}$	$^{38}\text{Ar}/^{39}\text{Ar}$	$^{37}\text{Ar}/^{39}\text{Ar}$	$^{36}\text{Ar}/^{39}\text{Ar}$ ($\times 10^{-3}$)	$^{40}\text{Ar}^*$ (%)	$^{39}\text{Ar}_K$ fr(%)	$^{40}\text{Ar}^*/^{39}\text{Ar}_K$	Age (Ma) $\pm 1\sigma$							
<i>Sample LUZ 0444 (J=0.001968)</i>																
1	1.2	17675.104 ±	909.449	12.0537 ±	0.6429	0.983 ±	1.475	60562.730 ±	3124.476	0.0	0.1	0.105 ±	71.473	0.4	±	253.7
2	1.4	3256.322 ±	54.969	2.1516 ±	0.0403	0.259 ±	0.139	11206.461 ±	190.564	-1.7	0.4	-55.168 ±	-8.161	-207.3	±	-32.5
3	1.6	403.998 ±	2.312	0.2765 ±	0.0049	0.017 ±	0.025	1375.101 ±	10.992	-0.6	1.7	-2.342 ±	-2.371	-8.3	±	-8.5
4	1.8	102.561 ±	0.321	0.0855 ±	0.0007	0.003 ±	0.004	341.074 ±	1.668	1.7	11.2	1.774 ±	0.477	6.3	±	1.7
5	2.0	26.702 ±	0.088	0.0327 ±	0.0003	0.001 ±	0.002	75.297 ±	0.358	16.7	25.7	4.451 ±	0.106	15.7	±	0.4
6	2.2	10.835 ±	0.025	0.0231 ±	0.0001	0.005 ±	0.001	20.072 ±	0.121	45.3	22.7	4.904 ±	0.039	17.3	±	0.2
7	2.4	9.190 ±	0.030	0.0221 ±	0.0001	0.011 ±	0.002	14.373 ±	0.075	53.8	10.8	4.944 ±	0.030	17.5	±	0.1
8	2.8	7.720 ±	0.022	0.0213 ±	0.0001	0.016 ±	0.009	9.212 ±	0.089	64.8	14.7	5.000 ±	0.031	17.7	±	0.1
9	3.2	6.764 ±	0.015	0.0216 ±	0.0002	0.024 ±	0.026	6.658 ±	0.069	71.0	9.2	4.799 ±	0.024	17.0	±	0.1
10	3.6	6.097 ±	0.041	0.0203 ±	0.0003	0.046 ±	0.007	4.614 ±	0.151	77.7	2.5	4.739 ±	0.057	16.7	±	0.2
11	4.0-4.4	6.752 ±	0.074	0.0214 ±	0.0011	0.361 ±	0.156	8.653 ±	0.463	62.8	0.6	4.241 ±	0.150	15.0	±	0.5
12	4.8-5.2	11.831 ±	0.345	0.0289 ±	0.0041	0.678 ±	1.138	32.440 ±	4.791	19.7	0.1	2.331 ±	1.445	8.3	±	5.1
13	6.0	10.793 ±	0.235	0.0317 ±	0.0023	1.049 ±	0.199	23.532 ±	2.013	36.8	0.2	3.974 ±	0.612	14.1	±	2.2
<i>Sample BLE 0513 (J=0.001976)</i>																
1	1.2	43727.734 ±	526.768	29.2058 ±	0.4093	1.500 ±	1.104	154713.189 ±	1866.944	0.0	0.0	0.270 ±	55.363	1.0	±	197.3
2	1.4	7165.997 ±	68.998	4.7195 ±	0.0635	0.270 ±	0.198	24835.872 ±	241.040	-2.4	0.3	-173.011 ±	-9.624	-754.7	±	-52.3
3	1.6	423.712 ±	2.601	0.2830 ±	0.0038	0.050 ±	0.037	1441.461 ±	9.752	-0.5	1.4	-2.234 ±	-1.263	-8.0	±	-4.5
4	1.8	97.399 ±	0.185	0.0760 ±	0.0006	0.039 ±	0.041	314.990 ±	0.949	4.4	6.5	4.325 ±	0.241	15.4	±	0.9
5	2.0	35.691 ±	0.063	0.0388 ±	0.0002	0.009 ±	0.001	109.182 ±	0.330	9.6	14.3	3.429 ±	0.097	12.2	±	0.3
6	2.2	20.221 ±	0.057	0.0290 ±	0.0002	0.010 ±	0.001	55.018 ±	0.200	19.6	13.3	3.964 ±	0.061	14.1	±	0.2
7	2.4	14.856 ±	0.048	0.0250 ±	0.0002	0.012 ±	0.002	35.784 ±	0.223	28.8	10.8	4.284 ±	0.070	15.2	±	0.3
8	2.6	11.009 ±	0.021	0.0230 ±	0.0002	0.011 ±	0.002	22.479 ±	0.097	39.7	11.8	4.367 ±	0.030	15.5	±	0.2
9	2.8	10.898 ±	0.031	0.0225 ±	0.0001	0.011 ±	0.002	22.248 ±	0.135	39.7	11.5	4.326 ±	0.045	15.4	±	0.1
10	3.0	12.526 ±	0.035	0.0239 ±	0.0002	0.012 ±	0.002	27.860 ±	0.163	34.3	10.8	4.295 ±	0.051	15.2	±	0.2
11	3.2	10.527 ±	0.041	0.0221 ±	0.0001	0.016 ±	0.002	20.211 ±	0.190	43.3	8.2	4.557 ±	0.061	16.2	±	0.2
12	3.4	8.751 ±	0.055	0.0223 ±	0.0004	0.027 ±	0.004	15.008 ±	0.265	49.4	4.9	4.320 ±	0.087	15.3	±	0.3
13	3.8	7.444 ±	0.056	0.0192 ±	0.0003	0.027 ±	0.005	10.363 ±	0.161	58.9	4.8	4.385 ±	0.064	15.6	±	0.2
14	4.2-5.0	7.399 ±	0.099	0.0190 ±	0.0009	0.115 ±	0.021	8.144 ±	0.543	67.7	1.1	5.008 ±	0.182	17.8	±	0.6
15	5.4	9.975 ±	0.202	0.0226 ±	0.0017	0.467 ±	0.346	13.651 ±	2.634	60.1	0.3	6.002 ±	0.796	21.3	±	2.8
<i>Sample DOT 053A (J=0.001963)</i>																
1	1.2	25033.052 ±	488.166	16.7006 ±	0.3593	0.774 ±	1.523	87645.099 ±	1706.561	0.0	0.1	0.207 ±	42.711	0.7	±	151.2
2	1.4	4280.595 ±	32.157	2.8717 ±	0.0291	0.252 ±	0.361	14889.006 ±	120.536	-2.8	0.3	-119.101 ±	-14.967	-480.4	±	-69.2
3	1.6	198.456 ±	0.860	0.1501 ±	0.0012	0.094 ±	0.013	677.009 ±	2.838	-0.8	3.1	-1.588 ±	-0.428	-5.6	±	-1.5
4	1.8	45.448 ±	0.122	0.0465 ±	0.0004	0.004 ±	0.007	141.421 ±	0.529	8.0	11.0	3.658 ±	0.154	12.9	±	0.5
5	2.0	23.383 ±	0.069	0.0334 ±	0.0003	0.045 ±	0.047	64.635 ±	0.324	18.3	13.6	4.289 ±	0.097	15.1	±	0.3
6	2.2	14.572 ±	0.041	0.0281 ±	0.0002	0.001 ±	0.004	34.111 ±	0.126	30.8	11.6	4.493 ±	0.040	15.8	±	0.2
7	2.4	10.752 ±	0.028	0.0256 ±	0.0004	0.019 ±	0.021	20.864 ±	0.183	42.7	11.9	4.589 ±	0.055	16.2	±	0.2
8	2.8	9.293 ±	0.025	0.0248 ±	0.0002	0.163 ±	0.023	15.476 ±	0.125	51.0	25.5	4.740 ±	0.041	16.7	±	0.2
9	3.2	7.763 ±	0.021	0.0231 ±	0.0001	0.056 ±	0.033	10.303 ±	0.116	60.9	17.7	4.726 ±	0.038	16.7	±	0.1
10	3.6	7.265 ±	0.028	0.0232 ±	0.0004	0.199 ±	0.054	9.138 ±	0.154	63.2	4.4	4.590 ±	0.051	16.2	±	0.2
11	4.0	7.145 ±	0.205	0.0274 ±	0.0022	1.160 ±	0.836	12.312 ±	2.917	51.1	0.2	3.655 ±	0.889	12.9	±	3.1
12	6.0	9.022 ±	0.217	0.0219 ±	0.0019	1.844 ±	0.788	16.061 ±	1.337	49.9	0.5	4.514 ±	0.440	15.9	±	1.5
<i>Sample GRU 062 (J=0.001959)</i>																
1	1.2	56609.150 ±	6045.036	37.7322 ±	4.0417	6.488 ±	7.078	193499.384 ±	20677.217	0.0	0.0	0.288 ±	233.779	1.0	±	825.8
2	1.4	10959.587 ±	235.825	7.2126 ±	0.1899	0.928 ±	1.488	37003.926 ±	810.389	0.2	0.2	25.063 ±	45.101	86.5	±	151.9
3	1.6	795.761 ±	2.112	0.5316 ±	0.0107	0.285 ±	0.282	2717.895 ±	10.679	-0.9	0.8	-7.343 ±	-2.617	-26.1	±	-9.4
4	1.8	132.505 ±	0.384	0.1002 ±	0.0017	0.010 ±	0.018	444.773 ±	1.722	0.8	4.9	1.076 ±	0.456	3.8	±	1.6
5	2.0	36.626 ±	0.110	0.0388 ±	0.0003	0.003 ±	0.006	107.980 ±	0.378	12.9	14.8	4.718 ±	0.108	16.6	±	0.4
6	2.2	20.435 ±	0.039	0.0277 ±	0.0002	0.012 ±	0.003	54.407 ±	0.182	21.3	18.9	4.359 ±	0.056	15.3	±	0.2
7	2.4	15.940 ±	0.047	0.0243 ±	0.0002	0.044 ±	0.022	39.138 ±	0.186	27.5	15.3	4.380 ±	0.058	15.4	±	0.2
8	2.6	12.626 ±	0.033	0.0222 ±	0.0003	0.035 ±	0.036	27.573 ±	0.256	35.5	8.5	4.482 ±	0.078	15.8	±	0.3
9	3.0	13.100 ±	0.031	0.0223 ±	0.0002	0.004 ±	0.005	29.230 ±	0.125	34.1	15.2	4.463 ±	0.038	15.7	±	0.1
10	3.4	14.086 ±	0.038	0.0230 ±	0.0002	0.031 ±	0.014	32.810 ±	0.150	31.2	12.5	4.394 ±	0.047	15.5	±	0.2
11	3.8	13.494 ±	0.042	0.0228 ±	0.0003	0.027 ±	0.031	30.561 ±	0.303	33.1	5.9	4.466 ±	0.089	15.7	±	0.3
12	4.4-5.0	12.684 ±	0.038	0.0220 ±	0.0004	0.167 ±	0.134	28.488 ±	0.448	33.8	2.6	4.288 ±	0.135	15.1	±	0.5
13	5.6-7.0	16.351 ±	0.264	0.0258 ±	0.0033	1.136 ±	0.797	31.134 ±	2.423	44.6	0.2	7.300 ±	0.728	25.6	±	2.5
<i>Sample MOL 054 (J=0.001954)</i>																
1	1.2	16964.056 ±	1316.759	11.1312 ±	0.8710	0.870 ±	0.699	58425.668 ±	4536.218	0.0	0.1	0.158 ±	34.703	0.6	±	122.3
2	1.4	1612.333 ±	7.062	1.0799 ±	0.0091	0.175 ±	0.126	5454.611 ±	24.724	0.0	0.6	0.517 ±	2.184	1.8	±	7.7
3	1.6	132.049 ±	0.254	0.1051 ±	0.0008	0.021 ±	0.009	441.656 ±	1.213	1.2	5.1	1.542 ±	0.266	5.4	±	0.9
4	1.8	32.272 ±	0.049	0.0390 ±	0.0002	0.007 ±	0.003	96.044 ±	0.330	12.1	16.5	3.891 ±	0.090	13.7	±	0.3
5	2.0	12.861 ±	0.019	0.0264 ±	0.0002	0.005 ±	0.009	28.535 ±	0.131	34.4	19.7	4.429 ±	0.040	15.5	±	0.2
6	2.2	9.633 ±	0.040	0.0234 ±	0.0002	0.008 ±	0.001	16.771 ±	0.151	48.6	13.8	4.678 ±	0.052	16.4	±	0.2
7	2.4	9.508 ±	0.046	0.0235 ±	0.0002	0.010 ±	0.001	16.520 ±	0.168	48.7	10.7	4.628 ±	0.057	16.2	±	0.2
8	2.8	11.545 ±	0.026	0.0260 ±	0.0003	0.006 ±	0.001	23.586 ±	0.087	39.6	17.6	4.576 ±	0.029	16.1	±	0.1
9	3.2	9.310 ±	0.046	0.0243 ±	0.0004	0.017 ±	0.016	16.146 ±	0.226	48.8	10.5	4.541 ±	0.073	15.9	±	0.3
10	3.6	8.568 ±	0.062	0.0253 ±	0.0005	0.027 ±	0.028	12.155 ±	0.308	58.1	3.0	4.980 ±	0.104	17.5	±	0.4
11	4.0-4.8	10.972 ±	0.088	0.0234 ±	0.0007	0.022 ±	0.028	17.978 ±	0.316	51.6	2.3	5.663 ±	0.112	19.9	±	0.4

comprise more than 50% of the total ^{39}Ar release, (2) the ages agree within 2σ error limits (excluding uncertainties in the J value) between each contiguous two fractions, and (3) one fraction consisting of the plateau comprise more than 3% of the total ^{39}Ar release (see McDougall & Harrison 1999, and references therein). The plateaus recorded in this study satisfy these conditions. The average grain size for all biotite separates was in the same range and varied between 250 and 315 μm . Usually, the first five or six low temperature steps, and in a less pronounced manner the last steps at high temperatures, are characterized by a disturbed pattern. Hence, the total gas ages, calculated by integrating over all steps, have no geological significance; they are between 3.04 and 0.6 Ma younger compared to the plateau ages (Fig. 4.8).

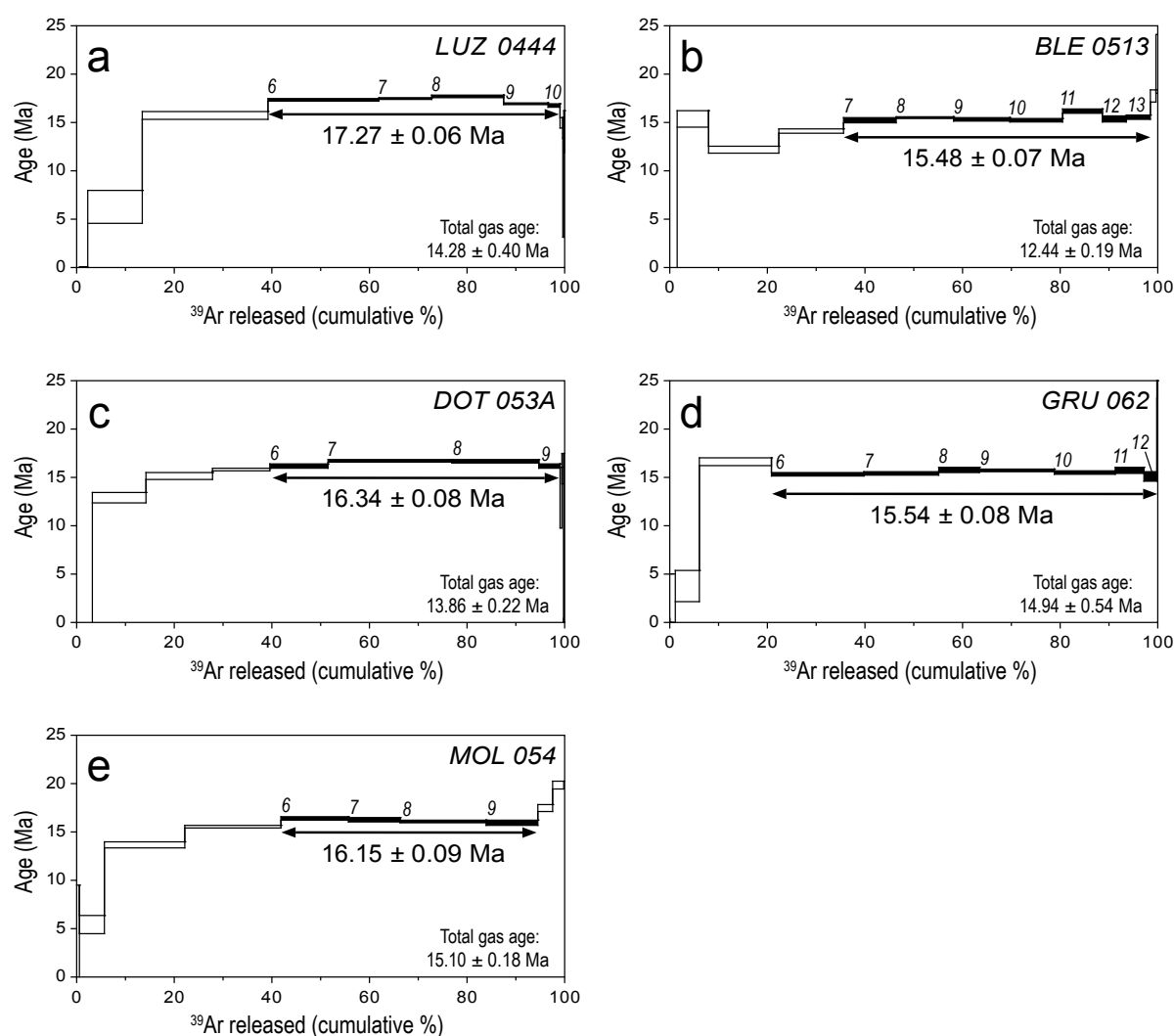


Fig. 4.8: Biotite $^{40}\text{Ar}/^{39}\text{Ar}$ age spectra obtained by CO_2 laser step-wise heating experiments. Total gas ages were determined by integrating over all steps. Steps attributed to the plateau are highlighted in black. Numbers refer to steps used for the calculation of the plateau ages listed in Table 4.4. Uncertainties are given in 1σ , error on plateau ages does not include the uncertainty in the J value. (a) Sample LUZ 0444. (b) Sample BLE 0513. (c) Sample DOT 053A. (d) Sample GRU 062. (e) Sample MOL 054.

4.6. Interpretations and discussion

4.6.1. Interpretation of individual age data

In general the presence of excess ^{40}Ar (extraneous or inherited argon) is due to the incorporation of additional ^{40}Ar by processes other than *in situ* decay during mineral growth and/or subsequent recrystallization, as well as by diffusion through grain boundaries. Several studies have shown that excess argon is commonly found in high-pressure and ultrahigh-pressure metamorphic rocks (e.g. Scaillet 1996; Sherlock & Kelley 2002; Di Vincenzo et al. 2006, and references therein). However, in our samples we find no indications for excess Ar. As shown later on, also the internal consistency of the data with microstructural data and structural field data, and additionally, the overlap with published results using independent methods (e.g. U-Th-Pb in allanite and monazite by Janots et al. 2009) confirm the absence of excess Ar problems in the case of our samples.

K/Ar (and Ar/Ar) data were often interpreted in the context of the “blocking temperature” (Jäger et al. 1967) or “closure temperature” (Dodson 1973) concept. The pioneering study of Purdy & Jäger (1976) proposed a “closure temperature” of 350 °C for the K-Ar isotopic system in muscovite. More modern studies increased this value up to some 550 °C or even more (Di Vincenzo et al. 2001; Philippot et al. 2001; Bucher 2003; Balogh & Dunkl 2005; Allaz 2008). On the other hand it has been shown that metamorphic reactions and/or deformation, commonly enhanced by the presence of a fluid, may induce isotopic resetting (e.g. Foland 1979; Chopin & Maluski 1980; Chopin & Monié 1984; Wijbrans & McDougall 1986; Villa 1998; Bucher 2003; Di Vincenzo et al. 2004; Gouzu et al. 2006; Glodny et al. 2008a, 2008b). In case of the phengites investigated by this study peak metamorphic temperatures of around ca. 350 °C are estimated for the occurrences in the Engadine window (Bousquet et al. 1998) and some 350-400 °C for those from Safiental and Valsertal (Bousquet et al. 2002; Wiederkehr et al. *submitted*, *b*). Hence, the peak metamorphic temperatures of all studied phengite are just at or below the range of suggested “closure temperatures”. Moreover, there is microstructural evidence for retrograde metamorphic reactions that are associated with recrystallization. In summary, we interpret the recorded apparent ages as formation/crystallization ages. We explain the observed scatter in age by the existence of mixed populations. This implies that even high-pressure relics can survive subsequent deformation and metamorphism, in accordance with recent observations (e.g. Agard et al. 2002; Bucher 2003; Villa 2006).

Biotite bearing samples reached significantly higher peak-metamorphic temperatures ranging from 475-525 °C near the “biotite-in isograd” in Val Luzzzone to 560-590 °C around Pizzo Molare inside the Lepontine dome (Fig. 4.1b; Wiederkehr et al. *in preparation*). Our weighted average ages determined by *in situ* investigations as well as the recorded plateau ages of biotite (18.36-15.48 Ma, Figs. 4.7 & 4.8) are slightly younger compared to the thermal peak at 18-19 Ma as presumably dated by U-Pb investigations on monazite (Janots et al. 2009). This small difference in age is best explained by retrograde chloritization of biotite, as is clearly evidenced by the omnipresence of retrograde chlorite. Hence, the individual apparent ages obtained for biotite are interpreted as formation ages that were rejuvenated by partial re-equilibration generally associated with major element and isotopic resetting. In summary, our isotopic data on biotite may be regarded as recrystallization ages that lay somewhere between biotite formation and subsequent retrogression (chloritization), the scatter in the individual ages being due to a variable intensity of chemical re-equilibration (Villa 2006; Allaz 2008).

4.6.2. Correlation between isotopic data and microstructural features

Recorded apparent ages often correlate with different white mica generations as evidenced by microstructural observations. In our case, the interpretation of apparent ages determined by the *in situ* laser-probe dating technique is unfortunately hampered by the large uncertainties in apparent age, often exceeding 10 % for 1σ errors. These large uncertainties are due to the low amount of gas ablated during the laser experiments, caused by the small diameter of the laser spot chosen in order to avoid contaminations by surrounding mineral grains, particularly quartz and chlorite. Overlap between apparent ages with associated uncertainties precludes the accurate discrimination between different generations based on statistical principles (Fig. 4.9).

Nevertheless, the resulting probability curve can be decomposed into three distinct peaks related to specific age populations in a qualitative way (Fig. 4.9). The main peak at 35-30 Ma is surrounded by a relatively broad shoulder towards older apparent ages, i.e. somewhere between 45-40 Ma, and a narrow and well-defined peak that produces a shoulder towards younger ages and located at around 25 Ma. A closer look at the main peak at 35-30 Ma reveals its weakly asymmetric shape with a shoulder towards younger ages. The latter feature possibly suggests that the 35-30 Ma population may consist of two sub-populations; a younger one being located at 30 Ma and an older one at around 35-33 Ma (indicated as grey bars in Fig. 4.9). Sample *VAL 0580* yields the youngest and best-defined apparent white mica ages, with a weighted average age of 25.40 ± 0.45 (depicted by grey bar in Fig. 4.9), an age that may indeed be responsible for the shoulder visible at around 25 Ma in the probability curve (Fig. 4.9). Such an interpretation is also consistent with the chemical and microstructural data presented above.

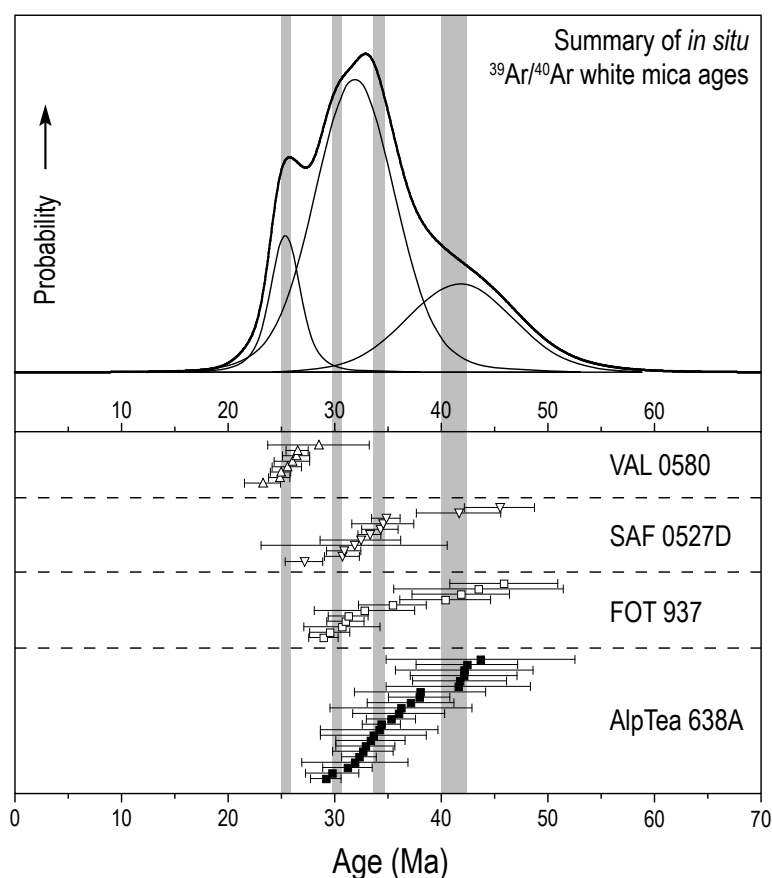


Fig. 4.9: Summary of apparent ages obtained on white mica by *in situ* laser-probe analyses and calculated cumulative probability curve. The complex shape of the cumulative probability curve reflects the presence of more than one white mica population as indicated by the decomposition of at least three distinct peaks related to different ages; the light-grey bar denotes the weighted average ages for the different populations (see text for discussion). Uncertainties are given in 1σ and do not include the uncertainty in the J value.

The isolated phengite flakes entrapped in quartz invariably yield the oldest individual apparent ages. These are in a range between 44 and 37 Ma (e.g. sample *AlpTea 638A*; Figs. 4.4b, d & e). Numerous fibres of Fe-Mg carpholite are found as inclusions within the same surrounding quartz grain, close to the isolated phengite. Since quartz did not recrystallize into subgrains, clearly the isolated phengite flakes and the relics of carpholite must have been entrapped within quartz under the same metamorphic conditions, i.e. at peak HP/LT conditions. Consequently, we interpret these oldest apparent ages obtained from isolated white mica as dating the peak-pressure. Similarly old ages in the range of 45-40 Ma are also found in needle-shaped aggregates (pseudomorphs after carpholite) that consist of white mica, which is intimately associated with chlorite (Figs. 4.4b, d, h & 4.5b). Note also that ages in the range of 45-40 Ma are only found in samples *AlpTea 638A*, *FOT 937* and *SAF 0527*, i.e. samples that are characterized by the occurrences of white mica showing a considerable celadonite-content as typical for high-pressure phengite (Fig. 4.3a; see also Bousquet et al. 1998). By considering all these ages as representing a single apparent age population a weighted average age of 41.23 ± 1.22 Ma can be calculated as displayed by the grey bar shown in Figure 4.9. The weighted average age clearly overlaps with the “oldest” decomposed peak representing the relatively broad shoulder towards older apparent ages of the resulting cumulative probability curve, i.e. between 45-40 Ma (Fig. 4.9).

Most of the individual apparent ages cluster in the time interval between 36 and 29 Ma as is also indicated by the peak of the cumulative probability curve (Fig. 4.9). However, such ages are exclusively found as needle-shaped aggregates that consist of phengite and chlorite, both together replace carpholite, embedded in quartz, i.e. within pseudomorphs after carpholite. Hence, the associated white mica is unambiguously related to the decay of carpholite, which is in turn induced by substantial decompression along the retrograde path. As mentioned above when discussing the decomposition of the cumulative probability curve shown in Figure 4.9, it is unclear if the range between 36 and 29 Ma represents a single event, or alternatively, a bimodal population. The slightly asymmetric shape of the maximum peak in the probability curve hints towards two distinctive age populations as indicated by the grey bars. Obviously white mica-chlorite aggregates replacing carpholite yield well-defined and accurate apparent ages between 32 and 29 Ma (Figs. 4.4c & 4.5g), clustering at the lower end of the 36-29 Ma age interval commonly recorded inside such pseudomorphs after carpholite.

In any case, the existence of substantially older ages, i.e. ages between 36-34 Ma points to either mixed ages of the older HP/LT event or yet another age population at around 36-34 Ma. Consequently, if the well-defined apparent ages clustering around 32-29 Ma are interpreted as a distinctive age population and all the other ages in the time interval between 36-33 Ma are assigned to a second, older one, the calculation of weighted average ages yields 34.16 ± 1.22 Ma for the older and 30.32 ± 0.49 Ma for the younger age population, as depicted by grey bars in Figure 4.9.

4.6.3. Conclusions regarding the age interpretation

Apparent ages in the 45-37 Ma range, with a weighted average age of 41.23 ± 1.22 Ma, are interpreted to represent the timing of peak-pressure conditions. This interpretation is supported by the fact that isolated phengites exclusively yield older ages compared to phengite-chlorite aggregates that replace carpholite; and by microstructural observations pointing to coeval trapping in quartz porphyroclasts of such isolated phengites and fibres of Fe-Mg carpholite under the same metamorphic conditions, i.e. under peak pressure conditions.

The retrograde path is basically pressure controlled, being characterized by isothermal or only slightly cooling decompression (Bousquet et al. 1998, 2002; Jolivet et al. 1998b; Wiederkehr et al. 2008). Because Fe-Mg carpholite and co-existing high-pressure phengite were destabilized to muscovite, chlorite and quartz (Fig. 4.10; Oberhänsli et al. 1995; Bousquet et al. 2002) the apparent ages recorded in white mica associated with chlorite, which are interpreted to represent pseudomorphs after carpholite, provide information on the timing of decompression. Apparent ages of this group cover a wide time interval ranging from 36-29 Ma, except for sample *VAL 0580* that will be discussed separately below. This time interval can possibly be subdivided into two distinct populations, an older one in the range of 36-34 Ma yielding an average age of 34.16 ± 1.22 Ma and a younger one between 32-29 Ma with a weighted average age of 30.32 ± 0.49 Ma (depicted by the grey bars in Fig. 4.9).

Sample *VAL 0580*, however, is characterized by significantly younger and well-defined apparent ages in the range of 28-23 Ma, with a weighted average age of 25.40 ± 0.45 Ma. In view of its distinctly different microstructure (Figs. 4.5c & d) it is most probable that partial recrystallization and/or exchange reactions along the retrograde metamorphic evolution did induce chemical re-equilibration and isotopic resetting in this particular sample (see discussion by Villa 1998). Such re-equilibration associated with isotopic resetting of white mica might possibly have been enhanced by D3 deformation. Hence we tentatively relate the weighted average age of 25.40 ± 0.45 Ma to D3 deformation (Domleschg phase), being aware that such an interpretation is highly speculative.

All the investigated biotite samples yield significantly lower apparent ages compared to ages obtained on white mica. Also, all investigated biotite domains give consistent ages that cluster in a range between 18-15.5 Ma. This is consistent with the fact that biotite is related to a single metamorphic event represented by Barrow-type overprint that only affects the south-western part of the study area and post-dates D3 deformation (Fig. 4.1b; Wiederkehr et al. 2008). The ages are also consistent with recently published $^{40}\text{Ar}/^{39}\text{Ar}$ ages of 18-16 Ma obtained by isotopic investigations on white mica and biotite for the Lucomagno and Pizzo Molare areas (Allaz 2008). The published monazite U-Pb ages of 19-18 Ma (Janots et al. 2009) are interpreted to reflect equilibrations close to the “garnet-in isograd”, i.e. very near the thermal peak of metamorphism. As also shown by Allaz (2008) the lower apparent ages obtained on biotite are most probably due to late re-equilibration, i.e. chloritization of biotite associated with isotopic resetting along the retrograde path.

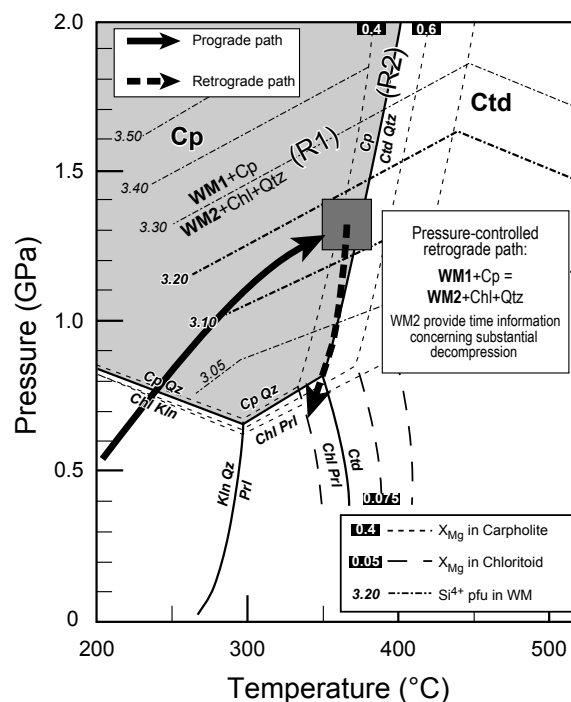


Fig. 4.10: P-T diagram for low-grade carpholite-bearing HP/LT metasediments showing the successive phengite generations formed during the P-T evolution. Phengite may either coexist together with Fe-Mg carpholite (generally characterized by higher Si contents, i.e. 3.3-3.4 Si p.f.u.) or, alternatively may be formed by the break-down of Fe-Mg carpholite due to substantial decompression (generally found in pseudomorphs after carpholite and characterized by lower Si contents, i.e. 3.2 Si p.f.u.). P-T diagram and calculated Si isopleths are taken after Bousquet et al. (2008); due to considerable inter-layer deficiency in the studied low-grade HP/LT metasediments the Si content p.f.u. representing the celadonite content was calculated following Bousquet et al. (2002).

4.6.4. Comparison with previously published isotopic and fission track data

White mica ages

The age of 41.23 ± 1.22 Ma that we interpret to date HP/LT metamorphism in the Valaisan domain north-east of the Lepontine dome appears reasonable when compared to the very few other available geochronological investigations of subduction-related metamorphism performed in units that belong to the Valaisan paleogeographical domain. For example, 46-39 Ma have been obtained within the western Lepontine (Antrona ophiolites; Liati et al. 2005). 45-40 Ma were postulated for the Tauern Eclogite Zone (Ratschbacher et al. 2004); albeit younger ages were postulated for the same high-pressure event in that same area based on an unconvincing interpretation of Rb-Sr white mica ages (Glodny et al. 2005). Our ages are somewhat older than the 40-35 Ma age range previously postulated for the Engadine window (Bertle 2004), but again considerably older than suggested by Rb-Sr and Ar-Ar white mica studies performed in metasediments exposed around Petit St. Bernard area that yielded ages around 34-27 Ma (Freeman et al. 1998; Cannic et al. 1999).

Geochronological investigations performed in the tectonically higher and more internal Briançonnais domain revealed 46 Ma for subduction-related HP/LT metamorphism in the Suretta nappe (Challandes et al. 2003). This older age is in agreement with the common assumption that the timing of high-pressure metamorphism propagates towards the foreland and hence progressively becomes younger towards more external units. Such a view is further supported by ages obtained within a younger 43-35 Ma time interval interpreted to date high-pressure metamorphism in the relatively more external Adula-nappe complex (Gebauer et al. 1992; Becker 1993; Gebauer 1996; Brouwer et al. 2005; Nagel 2008), a tectonic unit interpreted as representing the distal European margin.

The timing of the intrusion of the Bergell pluton at 32-30 Ma (von Blanckenburg 1992) still represents the hardest constraint for indirectly dating the tectono-metamorphic evolution of the Alps. This magmatic event post-dates a first nappe-refolding event (Niemet-Beverin phase; Schmid et al. 1990; Schreurs 1993) that followed the closure of the Valaisan Ocean and the subduction of the European continental margin (Adula nappe complex). The first part of the decompression path at around 36-33 Ma (with the corresponding weighted average age of 34.16 ± 1.22 Ma) as well as the high-pressure granulites of the Gruf complex (southern Adula, 33 Ma; Schmitz et al. *in press*) pre-dates the Bergell intrusion. This older exhumation is associated with pervasive recrystallization of white mica, related to the breakdown of Fe-Mg carpholite (Fig. 4.10) and the formation of the main foliation during D2 nappe stacking (Wiederkehr et al. 2008). It pre-dates D3 and overprints the syn-D1 HP/LT event. Hence, this main foliation was formed during the retrograde evolution while high-pressure relics, and associated isotopic ages, are only selectively preserved within the carpholite-bearing quartz-calcite veins. We conclude that it is very likely that the apparent ages determined by step-wise heating techniques of white mica separated from whole rock samples only provide information on the retrograde evolution during substantial decompression in the 36-34 Ma time interval. Also the ages obtained by Bertle (2004), recorded on white mica of the rock matrix close to carpholite-bearing quartz-calcite veins (40-35 Ma, giving a plateau age of 35.6 Ma), may fall into this same category of ages and reflect rather the timing of substantial decompression than peak-pressure conditions.

The younger post peak pressure event postulated for the 32-29 Ma age interval, with a weighted average age of 30.32 ± 0.49 Ma, would be more or less contemporaneous with the intrusion of the Bergell pluton (von Blanckenburg 1992). We interpret it to represent a separate greenschist facies overprint that occurred after a first stage of substantial decompression. Interestingly, *in situ* Th-Pb measurements

on allanite by SHRIMP from individual samples from the northern Lepontine (Piora and Lucomagno area) also yield ages between 32-29 Ma (Janots et al. 2009). Allanite generally appears at 400-450 °C and is therefore indicative for greenschist facies metamorphic conditions (e.g. Janots et al. 2006). All this indicates that the 32-29 Ma event probably reflects a significant stage of greenschist facies metamorphic overprint during the formation of the Alpine orogenic belt.

Biotite

We relate the biotite ages, clustering in the range between 18-15.5 Ma, to Barrovian metamorphism in the NE part of the Lepontine dome. There are numerous other isotopic data available for the northern Lepontine with K-Ar, Ar-Ar and Rb-Sr ages obtained from white mica and biotite ranging from 42 all the way to 14 Ma (see review given by Hunziker et al. 1992; Steck & Hunziker 1994, and references therein). Classical K-Ar and Ar-Ar ages obtained by pioneering isotopic investigations in the northern Lepontine yielded 25-16 Ma for white mica and 17-14 Ma for biotite (Armstrong et al. 1966; Purdy & Jäger 1976; Hunziker et al. 1986). These early pioneering isotopic investigations mainly focussed on basement units, which are generally characterized by a polyphase metamorphic evolution and where the interpretation of the obtained ages is hampered by inheritance from pre-Alpine metamorphic stages. To avoid such problems recent isotopic investigations were performed exclusively in Mesozoic metasediments that only suffered Alpine metamorphic overprint (Allaz 2008; Janots et al. 2009). For the north-eastern Lepontine dome, i.e. area around Val Piora-Lukmanier-Pizzo Molare, these recent Ar-Ar investigations revealed ages of 19-16 Ma for muscovite and 18-16 for biotite (Allaz, 2008). The obtained Ar-Ar ages were confirmed by *in situ* SHRIMP U-Pb dating of monazite yielding an age between 19-18 Ma for the same area, which is interpreted to reflect conditions near the thermal peak of metamorphism (Janots et al. 2009), in perfect agreement with our results. In summary, these recent investigations, combined with the results of this study, unambiguously demonstrate that Barrow-type amphibolite facies metamorphism in the northern Lepontine dome is surprisingly young, i.e. post 20 Ma.

Our biotite $^{40}\text{Ar}/^{39}\text{Ar}$ isotopic ages are also in agreement with fission track dating on apatite and zircon related to the latest stages of exhumation. In the northern Lepontine dome the zircon cooling central ages (at ca. 290 °C; Tagami & Shimada 1996) vary between 14-12.2 Ma while the apatite central ages (at 110-60 °C; Hurford 1990) are in the range of 9-5 Ma (Hurford 1986; Michalski & Soom 1990; Vernon et al. 2008). Within our study area (i.e. southern Gotthard massif near Lukmanier pass and frontal part of the Adula nappe complex around Olivone; Fig. 4.1b) recent investigations yielded zircon and apatite fission track central ages of 10-9 Ma and 7.5-6.5 Ma, respectively (Janots et al. 2009).

4.6.5. Implications regarding the tectono-metamorphic evolution

The new geochronological data presented in this study further constrain the timing of the subduction-collision transition in the Central Alps preserved within the Valaisan domain as summarized in Fig. 4.11. In the following we integrate the isotopic ages into the geodynamic model recently presented by Wiederkehr et al. (2008) and make an attempt to construct a complete P-T-d-t path for the high-pressure metasedimentary units NE of the Lepontine dome. The numbering and associated names of deformation events are those introduced by Wiederkehr et al. (2008).

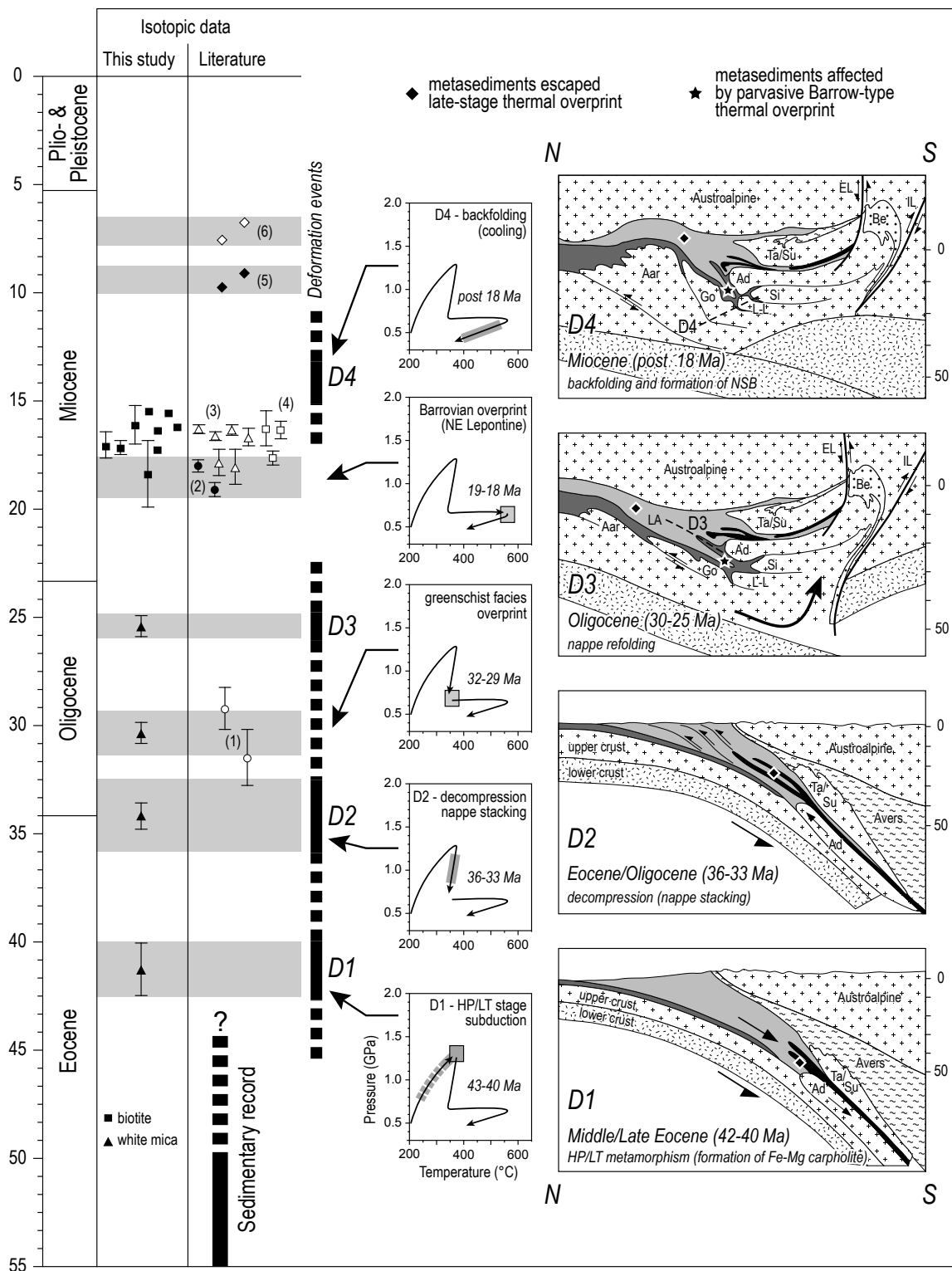


Fig. 4.11: Summary of age data, dating of P-T loops and tentative geodynamic evolution based on the interpretation of the isotopic data obtained for the study area. The sketches of the geodynamic stages are modified after Schmid et al. (1996). This summary is also based on a recent model proposed by Wiederkehr et al. (2008). Additional geochronological data from the study area were taken from ⁽¹⁾Th-Pb dating of allanite by Janots et al. (2009), ⁽²⁾U-Pb dating of monazite by Janots et al. (2009), ⁽³⁾⁴⁰Ar/³⁹Ar ages of white mica by Allaz (2008), ⁽⁴⁾⁴⁰Ar/³⁹Ar ages of biotite by Allaz et al. (2008), ⁽⁵⁾zircon fission track ages of Janots et al. (2009) and ⁽⁶⁾apatite fission track ages of Janots et al. (2009).

Eocene sediment-accretion and subduction (42-40 Ma; D1 Safien phase)

The huge pile of Valaisan Bündnerschiefer of the Grisons area, including the Engadine window, are generally interpreted to have formed an accretionary wedge during Cenozoic subduction of the Valaisan Ocean, followed by the subduction of the adjacent distal European margin beneath the Briançonnais micro-continent that was previously accreted to the Austroalpine upper plate. The age of the youngest sediments within this accretionary wedge ranges from 50 Ma (Valaisan domain; Steinmann 1994a) to some 40 Ma (more external Sardona unit; Lihou & Allen 1996). The high-pressure relics are restricted to syn-metamorphic quartz-calcite segregations formed during the first deformation event D1 (Safien phase) coeval with the HP/LT metamorphic event. Our isotopic ages on phengite, associated with Fe-Mg carpholite, revealed a weighted average age of 41.23 ± 1.22 Ma for this peak-pressure (350-400 °C and 1.2-1.4 GPa) D1 event (Fig. 4.11). The proposed time interval for high-pressure metamorphism is in accordance with the available stratigraphical constraints and the recognition of a Palaeocene-Eocene radiolaria species in carpholite-bearing metasediments in Safiental (Bousquet et al. 2002).

Nappe-stacking and decompression stage (36-33 Ma; D2 Ferrera phase)

Nappe-stacking in the Lepontine was associated with substantial decompression of the blueschist facies rocks (Fig. 4.11). The observation that carpholite is mainly destabilized by a mineral reaction producing white mica, chlorite and quartz points towards decompression under nearly isothermal or slightly cooling conditions (Fig. 4.10). All apparent ages in this 36-33 Ma time interval were recorded on white mica intimately associated with chlorite and interpreted to replace carpholite during decompression that is contemporaneous with D2 (Ferrera phase) nappe-stacking. The proposed 36-33 Ma age range supports the interpretation of Wiederkehr et al. (2008) that the D2 Ferrera nappe-stacking phase in the Valaisan post-dates earlier stages of nappe-stacking related to this same Ferrera phase as defined for the Briançonnais domain, where 46 Ma were reported for nappe-stacking (Challandes et al. 2003).

Greenschist facies event (32-29 Ma)

This event, recorded within a second population of phengites picked in chlorite-phengite associations replacing Fe-Mg carpholite and yielding well-defined apparent ages in the range of 32-29 Ma (weighted average age of 30.32 ± 0.49 Ma) coincides with an event recorded by Th-Pb dating of allanite that also dates greenschist facies conditions further west in the Lukmanier/Val Piora area (Janots et al. 2009). The geodynamical significance of this greenschist facies overprint associated with isotopic resetting is not clear at this stage. This event pre-dates the D3 deformation that we correlate with the so-called Domleschg phase, which hence post-dates the Bergell intrusion (Wiederkehr et al. 2008). Possibly, the accretion of the distal European margin to the orogenic wedge led to the relaxation of subduction-related down-folded isotherms by providing additional heat supply caused by high radiogenic heat production.

First nappe refolding event (~25 Ma; D3 Domleschg phase)

The D3 (Domleschg phase) nappe refolding event substantially modified the nappe-stack in the investigated area and produced tight to isoclinal mega-folds with amplitudes up to some 10 km, particularly the most prominent Lunschania antiform (Figs. 4.1b & 4.11). D3 deformation post-dates the ascent and emplacement of the Bergell pluton south of the working area (e.g. Schmid et al. 1996; Fig. 4.11) and overprints the previously established greenschist facies event, as is independently evidenced by isotherms related to this greenschist facies event that are folded around the Lunschania antiform (Wiederkehr et al. *submitted, b*). D3 deformation is associated with ongoing accretion of continental basement (e.g. Lucomagno-Leventina nappe and Gotthard-“massif”; Fig. 4.11). Based on the significantly young-

er apparent ages (weighted average age of 25.40 ± 0.45 Ma) found in the sample from Valsertal (sample *VAL 0580*), affected by pervasive D3 deformation and showing unambiguously different microtexture, we tentatively correlate these recorded apparent ages with the timing of D3 deformation, being aware that this is speculative.

Miocene Barrow-type thermal overprint (19-18 Ma)

Barrovian overprint of the south-western part of the study area represents a separate and younger heating event that initiated during a tectonically quiescent phase and that clearly post-dates D3 deformation. This is demonstrated by the isotherms related to this Barrovian metamorphism that are seen to crosscut the D3 Lunschania antiform (Wiederkehr et al. *submitted, b*). This event is recorded by the apparent ages of our biotite domains that cluster in the 18-15.5 Ma range; due to some retrograde chloritization of biotite we prefer the published monazite U-Pb ages of 19-18 Ma (Janots et al. 2009) for dating peak-temperatures during this event (Fig. 4.11).

Back-folding in the Northern Steep Belt (post-18 Ma; D4 Chièra phase)

Barrow-type amphibolite facies mineral assemblages have been severely deformed by a subsequent late-stage nappe refolding event that is associated with the formation of the Northern Steep Belt within the Penninic nappe-stack, and which is only very well developed west of our study area (Milnes 1974). There, a relatively tight synform, the Chièra synform, brings the nappe-stack into an overturned, steeply north-dipping position, while in our area (see profile in Fig. 4.11) such D4 backfolding is less severe. Since this D4 Chièra phase deformation outlasted Barrovian metamorphic overprint it must be very young (i.e. post-18 Ma), most probably contemporaneous with the N-directed thrusting in the Aar massif in the more external parts of the Alps and imbrications within the Subalpine molasse. Recently published isotopic data on a greenschist facies shear zone of the Aar Massif (External Crystalline Massif) report 21-17 Ma (Challandes et al. 2008) and may be correlated with this D4 deformation. The zircon fission track ages of 10-9 Ma, as well as apatite fission track ages of 7.5-6.5 Ma (Janots et al. 2009), indicate the final stages of the P-T path, i.e. the timing of cooling below some 200-330 °C for zircon, and 70-120 °C for apatite due to erosional unroofing that followed the thrusting of the external massifs.

4.7. Conclusions

The new age constraints obtained for the HP/LT metasedimentary units of the Valaisan and adjacent European domains provide valuable information regarding the timing of the transition from subduction-related peak high-pressure metamorphism to decompression and finally to a collision-related and second Barrow-type thermal overprint.

Phengites, texturally associated with Fe-Mg carpholite yield apparent ages of 42-40 Ma interpreted as dating HP/LT conditions at 350-400 °C and 1.2-1.4 GPa (D1, Safien phase). Age constraints belonging to the evolution during or immediately after decompression were revealed by white mica intimately associated with chlorite occurring in pseudomorphs after carpholite and yield two populations: an earlier one clusters at 36-33 Ma, a later one at 32-29 Ma, respectively. We relate the older retrograde stage to substantial decompression during which carpholite was destabilized by the reaction producing white mica, chlorite and quartz during D2 nappe stacking (Ferrera phase). The younger population is interpreted as related to greenschist facies metamorphism established at the end of decompression. Additionally, the white mica data also reveal a coherent apparent age cluster at ~ 25 Ma whose significance is yet not clear; a correlation with D3 deformation (Domleschg phase) is proposed. The still younger

apparent ages recorded by biotite, only occurring in the SW part of the study area and clearly related to collision-related amphibolite facies metamorphism of the north-eastern Lepontine dome, date a second and distinct pervasive Barrovian overprint and cluster around 18-16 Ma.

The presented isotopic ages support and further constrain the relative chronology of the tectono-metamorphic evolution presented by Wiederkehr et al. (2008 and *in preparation*) established on the basis of relationships between metamorphism and deformation. The consistency of the presented isotopic results presented in this study with such other and independent data indicates that an overall contamination by excess argon, as well as diffusional loss of $^{40}\text{Ar}^*$, can be ruled out, or is at least only of minor importance in the case of our study. Apparent ages deduced by the investigation of white mica are interpreted to represent formation and/or crystallization ages under temperature conditions that never exceeded 400 °C. The apparent ages of biotite, that yield slightly younger ages than the assumed thermal peak (19-18 Ma; Janots et al. 2009) probably represent re-crystallization ages that are affected by partial isotopic resetting during retrograde mineral reactions such as the chloritization of biotite which immediately followed peak temperature conditions (see also Allaz 2008).

The recorded isotopic data reveal a significant time gap in the order of some 20 Ma between the subduction-related HP/LT event (42-40 Ma) and the later collision-related MP/MT Barrovian overprint (19-18 Ma). This substantial time gap, together with the age constraints on white mica reflecting the retrograde metamorphic evolution of the HP/LT stage, support the notion of a polymetamorphic evolution associated with a bimodal P-T path (Wiederkehr et al. 2008). Amphibolite facies Barrow-type overprint of the NE Lepontine dome represents a clearly separated heating pulse that post-dates isothermal decompression after the early high-pressure stage. This considerable time interval is in accordance with the interpretation that it is the accretion of vast amounts of European continental crust (forming the present-day Lepontine dome) that provides high radiogenic heat production responsible for amphibolite facies metamorphism (e.g. Bousquet et al. 2008), being an entirely conductive and therefore rather slow process.

Acknowledgements

Excellent preparation of samples by W. Tschudin (Basel University) and Ch. Fischer (Potsdam University) is gratefully acknowledged. M. Timmerman from University of Potsdam is thanked for the help with sample selection and preparation as well as providing basic literature concerning $^{40}\text{Ar}/^{39}\text{Ar}$ dating techniques. O. Appelt and D. Rhede from the GeoForschungsZentrum Potsdam are thanked for their help with microprobe analyses. The introduction to the $^{40}\text{Ar}/^{39}\text{Ar}$ noble gas laboratory as well as the supporting field visit of A. Riemann (Potsdam University) is highly appreciated. J.-P. Hürzeler is thanked for the help with SEM investigations. Funding by the Swiss National Science Foundation (project NF-200020-113585 and precursor project NF-200020-103585) is gratefully acknowledged.

Chapter 5

Overprint of an earlier HP/LT metamorphic event by a later Barrow-type event: Metamorphic evolution and geodynamic implications

This chapter is in preparation for submission as: **Wiederkehr, M.**, Bousquet, R., Berger, A. & Schmid, S.M. Overprint of an earlier HP/LT metamorphic event by a later Barrow-type event: Metamorphic evolution and geodynamic implications.

Abstract

The determination of metamorphic events and their correlation to specific geodynamic stages, i.e. subduction- and/or collision-related, is crucial for the understanding of the geodynamic evolution of the Alpine orogenic belt. Thanks to continuous exposure over very large areas the investigation of metasediments allows for the observation of their structural and metamorphic evolution over a wide area along strike, providing a unique opportunity to decipher the geodynamic framework of the Alps. The sedimentary units of the Valaisan Ocean and parts of the sediments of the adjacent European margin located at the north-eastern border of Lepontine dome continuously expose a remarkable metamorphic gradient along strike, ranging from carpholite-bearing HP/LT conditions in the NE that become progressively overprinted by amphibolite facies Barrovian regional metamorphism towards the SW. This special situation represents a natural laboratory for investigating progressive Barrovian overprint of HP/LT metasediments and provides some hints for the understanding of the geodynamic evolution of orogenic belts in general, and the transition from subduction to collision in particular.

Detailed petrographic and structural investigations carried out in Valaisan- and European-derived Mesozoic metasedimentary units in the north-eastern border area of the Lepontine dome reveal a poly-metamorphic evolution that is characterized by a bimodal P-T path: (1) An Eocene-age (42-40 Ma) HP/LT metamorphic event (350-400 °C and 1.2-1.4 GPa) is documented by the widespread occurrences of Fe-Mg carpholite, (2) a first collision-related thermal event led to greenschist facies metamorphism (350-425 °C) during the Lower/Middle Oligocene (25 Ma), and (3) a second collision-related thermal event led to a substantially younger greenschist to amphibolite facies metamorphic event (450-590 °C and 0.5-0.8 GPa) of Middle Miocene-age (i.e. post 20 My), representing a Barrovian overprint of the north-eastern Lepontine caused by a clearly separate “isobaric” heating pulse.

5.1. Introduction

Detailed and well documented knowledge of the metamorphic evolution is essential for the reconstruction of the geodynamic evolution of the Alpine orogenic belt. Amphibolite facies Barrovian overprint of HP/LT rocks, interpreted to reflect the transition from subduction to collision (e.g. Wiederkehr et al. 2008) is of particular interest regarding the latest stages of orogeny. It was shown by earlier studies (e.g. Bousquet et al. 2008, and references therein) that metasediments in particular have a great potential for reconstructing the metamorphic evolution, due to their widespread and often continuous exposure that allows for correlating structural and metamorphic results over great distances. Particularly the low-grade metasediments (HP/LT and LP/LT rocks) are found widely distributed in the Alpine belt. Unfortunately, however, metamorphic data on low-grade metasediments are scarce or afflicted with large errors mainly due to the lack of characteristic mineral assemblages or due to great uncertainties or unknown thermodynamic data. These circumstances led to misinterpretations of metamorphic conditions. Consequently the geodynamic evolution of HP/LT metasedimentary belts in particular has been misunderstood. This can be illustrated by the identification of Fe-Mg carpholite in HP/LT metasedimentary rocks (Goffé et al. 1973) which modified the interpretation of the geodynamic evolution of several mountain belts (Goffé & Chopin 1986; Goffé et al. 1988, 1989; Goffé & Oberhänsli 1992; Goffé & Bousquet 1997; Theye et al. 1997; Bousquet et al. 1998; Oberhänsli et al. 2001; Rimmelé et al. 2003b; Wiederkehr et al. 2008). The recent review paper by Bousquet et al. (2008) summarises the presently available metamorphic data as well as new petrogenetic grids particularly for low-grade metapelites and clearly demonstrates the enormous potential of metasediments for deciphering the tectono-metamorphic evolution of mountain belts if the metamorphic mineralogy of metasediments is carefully considered and combined with structural and geochronological investigations. Surprisingly, combined metamorphic and structural data are still lacking in some key areas even though they are crucial for the understanding of the evolution of the Alps. One of these areas is located at the north-eastern border of the Lepontine dome, i.e. at the transition between collision-related Barrovian overprint and subduction-related HP/LT metamorphism.

This study presents for the first time petrologic data concerning amphibolite facies Barrow-type overprint of carpholite-bearing HP/LT metasediments from the Central Alps. The investigated area is located at the north-eastern border of the Lepontine structural and thermal dome and spans from Pizzo Molare in the south-west to Safiental and Hinterrhein in the north-east and east, respectively (Fig. 5.1). The relationships between the two contrasting types of metamorphic events in combination with the structural record have recently been unravelled and integrated in a model for the tectono-metamorphic evolution of the Valaisan and adjacent distal European margin (Wiederkehr et al. 2008). The P-T calculations presented in this study will complete the available tectono-metamorphic reconstruction. Furthermore the results of this investigation will be discussed in the frame of recently published findings based on the evolution of carbonaceous matter during metamorphic overprint (Wiederkehr et al. *submitted, b*) and new isotopic ages (Wiederkehr et al. *submitted, a*) in order to obtain valuable information regarding the geodynamic evolution of the Alps, i.e. the transition from subduction to collision within the Valaisan- and Europe-derived metasedimentary units in the Central Alps in particular and on collisional orogenic belts in general.

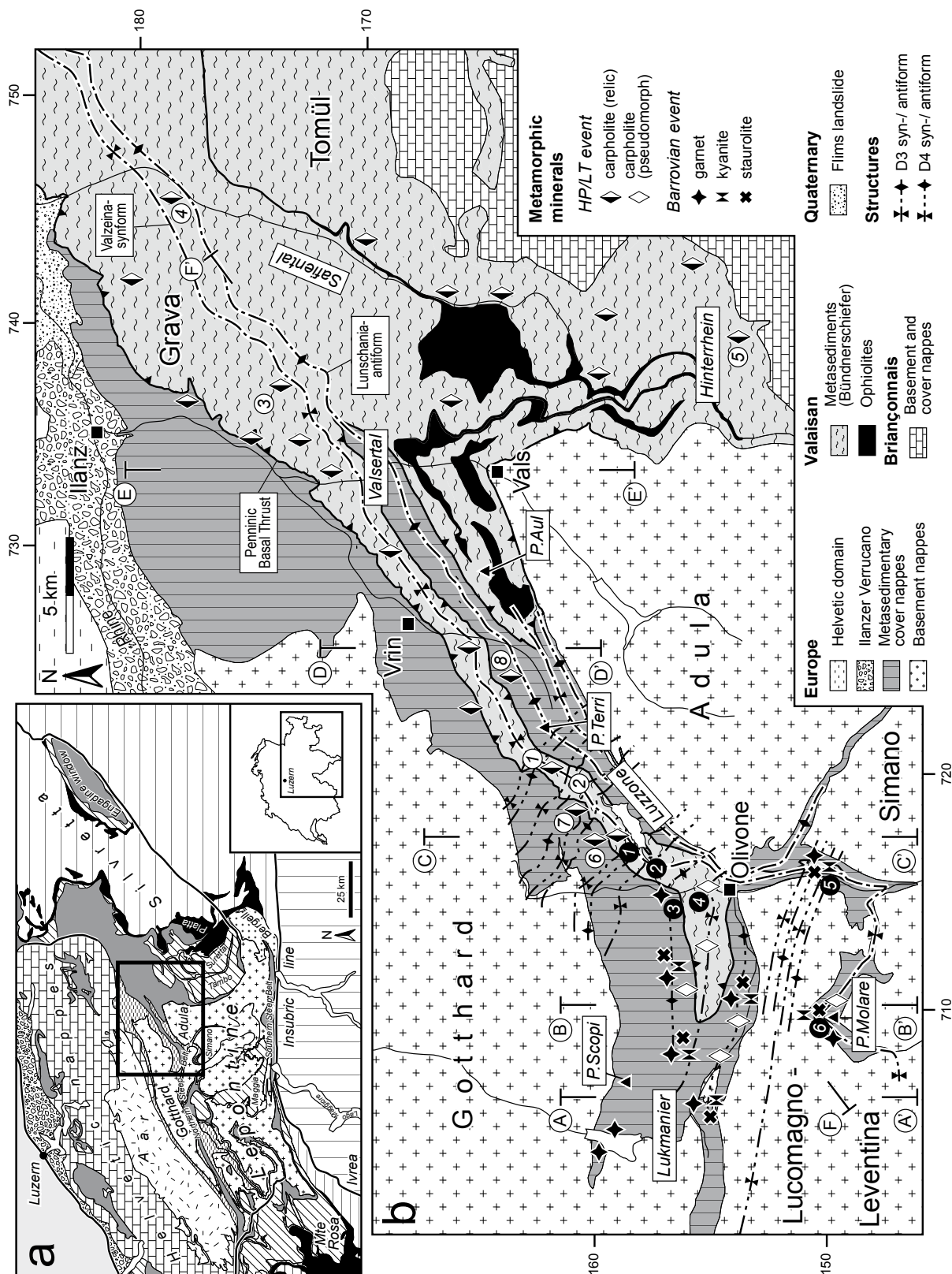


Fig. 5.1: Geological map of the investigated area and locations of the studied samples. (a) Tectonic map of the Central Alps after Schmid et al. (2004); the black rectangle delineates the outlines of the more detailed map view shown in b. (b) Detailed map of the NE rim of the Lepontine dome and easterly adjacent areas also indicating the main geographical names mentioned in the text; distribution of indicative minerals as well as traces of axial planes of major D3 and D4 are based on Wiederkehr et al. (2008) and references therein. Letters A-A', B-B', C-C', D-D', E-E' and F-F' mark the traces of cross-sections shown in Figures 5.7 and 5.10, respectively. Numbers show the locations of investigated samples listed in Table 5.1; samples characterized by subduction-related HP/LT are highlighted in white, samples characterized by collision-related Barrow-type overprint are highlighted in black.

5.2. Geological background

The Mesozoic-age metasedimentary units at the north-eastern rim of the Lepontine dome are characterized by a strong metamorphic gradient ranging from blueschist facies conditions in the NE to amphibolite facies Barrovian overprint in the SW. The Lepontine structural dome is formed by basement nappes that represent the former pre-Mesozoic substratum of the distal European margin (e.g. Schmid et al. 2004) and include, from bottom to top, Gotthard, Lucomagno-Leventina, Simano and Adula nappes (Fig. 5.1b). These basement nappes are overlain by Mesozoic-age sedimentary cover nappes and slices, in detail often complexly folded and wrapped around the frontal parts of the basement units (e.g. Thakur 1973; Milnes 1974; Probst 1980). Separated by the Penninic Basal Thrust these Mesozoic metasedimentary units can be subdivided into Sub-Penninic and Lower Penninic cover nappes and slices. These are derived from the distal European margin and the Valaisan Ocean, respectively (e.g. Probst 1980; Steinmann 1994a; Berger et al. 2005). The metasediments consist of shaly, sandy, calcareous, carbonaceous metapelites and calcschists and are generally referred to as “Bündnerschiefer” (see detailed description given in Baumer et al. 1961 and Berger et al. 2005). It has recently been shown that the Valaisan and adjacent parts of European margin exposed near the north-eastern Lepontine dome are characterized by a bimodal P-T path where Barrovian overprint represents a separate, late-stage heating event that followed isothermal decompression after the HP/LT stage (Wiederkehr et al. 2008).

5.3. Methods of investigations for P-T estimates

5.3.1. Mineral and whole rock chemistry

Mineral compositions were determined by wavelength-dispersive X-ray analysis (WDS) using a CAMECA SX-100 electron microprobe at the GeoForschungsZentrum (GFZ) Potsdam. The analytical conditions included an acceleration voltage of 15 kV, a beam current of 20 nA and beam diameters of 1-10 μm ; PAP corrections were applied. Natural and synthetic minerals were used as standards. Peak counting times were 10-20 s for major and 20-40 s for minor elements; backgrounds were counted for 5-20 s.

For obtaining bulk rock compositions of selected rock samples, wavelength-dispersive X-ray fluorescence analysis (WDXFRA) were performed on melted pellets by using a Bruker AXS SRS-3400. The pellets were manufactured from selected rock samples devoid of macroscopically detectable chemical in-homogeneities and/or weathering phenomena that were crashed and ground. WDXFRA was performed at the Mineralogical and Petrographical Institute at Basel University.

5.3.2. Methods used for P-T estimation

Stable mineral assemblages as well as mode and composition of solution phases have been computed for specific bulk rock compositions in the NaCaKFMASH(\pm C)-system by using the THERIAK-DOMINO software (De Capitani 1994; Biino & De Capitani 1995). This software calculates thermodynamic functions, equilibrium assemblages and rock-specific equilibrium assemblage diagrams (also referred to as pseudosections). The independent variables consist of a chosen combination of temperature, pressure and activity of a particular phase or compositional vectors. The equilibrium assemblage diagrams are based on the approach of a Gibbs free energy minimization and include highly non-ideal solution models for minerals with potential miscibility gaps (De Capitani & Brown 1987). In these equilibrium phase diagrams all phases are considered for each point in a given isochemical P-T space

assuming a complete thermodynamic equilibrium for the whole rock. Stability-fields for a particular assemblage are predicted. Hence, provided that attention focuses on assemblages, these equilibrium phase diagrams are very easy to interpret and they provide important information on mineral assemblage stability in a given isochemical P-T space.

It is problematic to use this “bulk rock equilibrium” method for natural rocks that exhibit a complex, two-stage metamorphic evolution, with an early HP/LT event followed by a clearly separate Barrovian heating pulse as is observed in case of the metasediments at the north-eastern Lepontine dome. The bulk rock chemistry may not be fully re-equilibrated, and relics of the earlier HP/LT metamorphic stage may still be present. This does not allow for an accurate P-T estimation. Hence, only samples devoid of relics from the earlier metamorphic evolution have been selected, based on the assumption that these rocks were fully re-equilibrated during the temperature peak of their evolution. Only in this case the “bulk rock equilibrium” method is used for constraining pressure and temperature of the separate, late-stage Barrovian overprint.

The updated JUN92.BS thermodynamic database of Berman (1988) has been used for all calculations concerning the late-stage amphibolite facies Barrovian overprint, after having been completed by the following thermodynamic data: Mg-chloritoid data of Vidal et al. (2001), Fe-chloritoid data of Vidal et al. (1994), staurolite data of Nagel (2002), alumino-celadonite data of Massonne & Szpurka (1997) and chlorite data of Hunziker (2003). Solid-solution models for phengite are from Keller et al. (2005c), for chlorite from Hunziker (2003), and for feldspar from Fuhrman & Lindsley (1988).

In the case of the early blueschist facies event, due to problems arising with the DOMINO-THERIAK software when calculating accurate P-T conditions for low-grade HP/LT metasediments that contain Fe-Mg carpholite, we applied the well established petrogenetic grid of Bousquet et al. (2002 & 2008) for estimating the metamorphic conditions. In contrast to equilibrium phase diagrams computed with DOMINO-THERIAK the petrogenetic grid method does not depend on a specific bulk rock composition and is merely based on “local equilibrium” which allows for estimating simultaneously P and T by using phases that are present in the studied thin section and checked for equilibrium using classical micro-textural criteria (Bousquet et al. 2002; Bousquet 2008, and references therein).

5.4. Metamorphic record of Valaisan and European margin derived meta-sedimentary units

Recent studies documented the two-stage metamorphic evolution in the working area; an early pressure-dominated event was subsequently overprinted by temperature-dominated Barrovian metamorphism (Bousquet et al. 2008; Wiederkehr et al. 2008 & *submitted, b*). Hence for an unambiguous interpretation of the metamorphic record, established within a rock sample at a given time along a P-T path, it is absolutely essential to understand whether the observed mineral assemblages formed during subduction-related HP/LT metamorphism or during collision-related MP/MT Barrow-type metamorphism. The recognition of occurrences and understanding of mineral assemblages indicative for specific metamorphic settings are of fundamental importance in order to decipher the tectono-metamorphic evolution of a given area.

In the following we summarise existing as well as new petrologic data and P-T estimates regarding both subduction- and collision-related metamorphism. This helps for understanding the significance of the detected spatial distribution of peak metamorphic conditions and provides a hint for unravelling

the geodynamic evolution of the investigated area. The samples investigated are listed in Table 5.1, the locations within the study area are shown in Figure 5.1b.

Table 5.1: Summary of samples used for P-T investigations. The numbers refer to sample locations depicted in Figure 5.1b. For each sample the precise location is given in Swiss map coordinates, elevation in meter, tectonic unit and mineral assemblage present in the investigated samples. Additionally peak-metamorphic temperatures T (°C) estimated by Raman spectroscopy of carbonaceous matter (RSCM) are indicated for each sample taken from Wiederkehr et al. (*submitted, b*).

#	Sample name	Swiss map coordinates		Elev. (m)	Tectonic Unit	Mineral assemblage	T (°C) (RSCM)
		X	Y				
Samples characterized by subduction-related HP/LT metamorphism							
1	LUZ 0432	720°938	162°275	2600	Valaisan (Grava)	Cp, Ctd, WM, Chl, Qtz, Cc/Do	440-460
2	LUZ 0416	719°235	160°052	2040	Valaisan (Grava)	Cp, WM, Chl, Qtz, Cc/Do	450-460
3	VAL 0580	736°871	174°310	1370	Valaisan (Grava)	Cp, WM, Chl, Qtz, Cc/Do	390-400
4	SAF 0527	746°016	178°803	1300	Valaisan (Grava)	Cp, WM, Chl, Qtz, Cc/Do	360-380
5	HINT 079	739°193	153°874	1670	Valaisan (Tomül)	Cp, Ctd, WM, Chl, Qtz, Cc/Do	430-450
6	LUZ 047	717°435	160°282	1850	Europe (Peiden slices, Forca)	Cp, Ctd, WM, Chl, Qtz, Cc/Do	460-490
7	LAR 061	718°531	160°727	1960	Europe (Peiden slices, Pianca)	Cp, WM, Chl, Qtz, Cc/Do	440-460
8	BLE 07.5	724°200	163°926	2050	Europe (Piz Terri-Lunschania)	Cp, WM, Chl, Qtz, Cc/Do	440-460
Samples characterized by collision-related Barrow-type metamorphism							
1	LUZ 055	716°865	158°363	1780	Valaisan (Grava)	Plag, Zo/Czo, WM, Chl, Qtz, Ttn/Rt	450-480
2	LUZ 0444	716°017	157°831	1390	Valaisan (Grava)	Bt, Plag, Zo/Czo, WM, Chl, Qtz, Cc/Do, Ttn/Rt	490-510
3	BLE 0410	715°029	156°841	1190	Europe (Peiden slices, Pianca)	Grt, Bt, Plag, Marg, WM, Chl, Qtz, Cc/Do	510-530
4	BLE 0510	715°112	155°757	1090	Valaisan (Grava)	Bt, Plag, WM, Zo/Czo, Qtz	530-550
5	GRU 053	714°990	149°545	630	Europe (Molare-Dangio)	St, Ky, Grt, Bt, Plag, WM, Qtz	560-590
6	MOL 051	710°270	149°696	2270	Europe (Molare-Dangio)	St, Ky, Grt, Bt, Plag, WM, Qtz	560-580

5.4.1. Significance of the observed mineral assemblages

Some minerals such as Fe-Mg carpholite, glaucophane, margarite and staurolite clearly indicate a specific metamorphic facies. But others such as kyanite, garnet, chloritoid and zoisite/clinozoisite are rather problematic due to the fact that they may have formed under different P-T conditions; they do not imply a specific metamorphic facies (see review given in Bousquet et al. 2008). Even for obtaining specific P-T conditions on the basis of unambiguous minerals a detailed and careful investigation of the observed associated mineral assemblage as well as a proper analysis of relationships between crystallization and discrete deformation phases needs to be performed. Given the fact that subduction-related HP/LT metamorphism is separated by at least two discrete deformation events from the following collision-related MP/MT Barrovian overprint (Wiederkehr et al. 2008) the two events can clearly be distinguished. Mineral assemblages reflecting these separate metamorphic events generally show unambiguous relationships between crystallization and deformation. The relics of the early HP/LT stage, such as widespread Fe-Mg carpholite, typically found in characteristic quartz-calcite segregations representing pseudomorphs after Fe-Mg carpholite have repeatedly been folded. Remnants of the late MP/MT Barrovian overprint, on the other hand, usually are part of a post-tectonic microstructure characterized by porphyroblasts that grow across the pre-existing main foliation (e.g. Wiederkehr et al. 2008). It is important to note that such rather simple relationships between deformation and crystallization as described by Wiederkehr et al. (2008) are strictly only valid for the metasedimentary units found near the north-eastern rim of the Lepontine dome. It has to be pointed out that Lepontine Barrow-type metamorphism is generally diachronous, becoming progressively younger from south to north (Köppel et al. 1981). Hence, different relations between deformation and crystallization are commonly observed (e.g. Berger et al. 2005).

In the following we briefly summarise the occurrences and distribution of remnants of both the subduction- and the collision-related metamorphism, as shown in Figure 5.2.

Remnants of subduction-related metamorphism

Fe-Mg carpholite represents a typical index mineral for HP/LT metamorphic conditions in meta-sediments (Goffé et al. 1973; Chopin & Schreyer 1983; Goffé & Chopin 1986; Theye et al. 1992; Vidal et al. 1992; Bousquet et al. 2008). In the investigated area occurrences of Fe-Mg carpholite are common for the Valaisan domain of the Grisons (Grava and Tomül nappes; Goffé & Oberhänsli 1992; Oberhänsli et al. 1995; Bousquet et al. 2002) as well as in its western continuation in the Val Luzzzone and at the Pizzo Molare well inside the Lepontine thermal dome (Wiederkehr et al. 2008; Fig. 5.2a). Recent investigations have shown that also parts of the tectonically underlying sediments of the distal European margin were affected by early blueschist facies metamorphism, as documented by occurrences of Fe-Mg carpholite in the Peiden slices (Wiederkehr et al. 2008) and the Piz Terri-Lunschania unit (Derungs 2008; Wiederkehr et al. *submitted, b*; Fig. 5.2a). In the investigated area Fe-Mg carpholite is exclusively found within quartz-calcite veins and/or segregations but never in the matrix of the rocks. These veins and/or segregations show a characteristic fibrous mesoscopic appearance along with a light green silvery colour resembling the typical Fe-Mg carpholite pseudomorphs described in the literature (e.g. Goffé & Chopin 1986; Fournier et al. 1991; Agard et al. 2001; Rimmelé et al. 2003b).

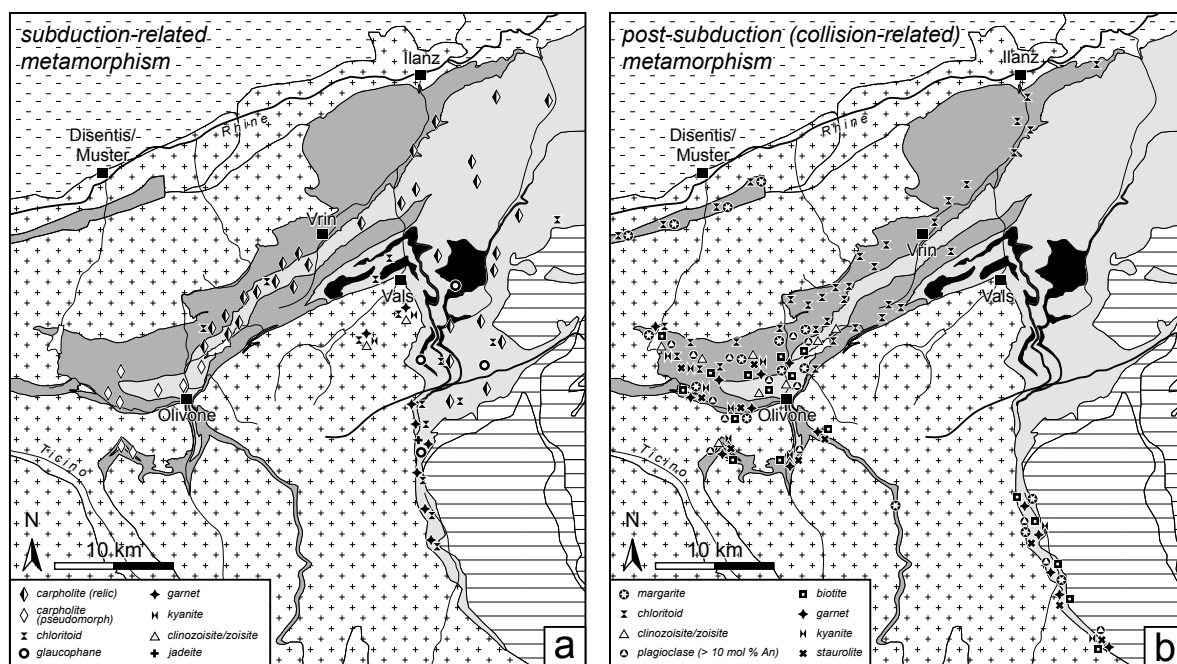


Fig. 5.2: Geological map showing the distribution of characteristic mineral assemblages indicative for specific metamorphic conditions reflecting geodynamic stages of the formation of the Alpine orogenic belt occurring in metasedimentary units northeast of the Lepontine dome (dark-grey: European-derived metasediments, light-grey: Valaisan derived metasediments). (a) Distribution of subduction-related HP/LT minerals. (b) Distribution of collision-related LP/LT and/or LP/HT minerals.

The interpretation of the significance of the occurrences of *chloritoid* for the metamorphic record is by far more delicate. Chloritoid is a common mineral phase in metamorphic assemblages found in the investigated area (Fig. 5.2), but this mineral may have formed during different geodynamic stages since it has a large stability field. In metasediments chloritoid may either have formed by the decay of Fe-Mg carpholite under blueschist facies conditions, or alternatively, by the breakdown of pyrophyllite during prograde greenschist facies metamorphism (see discussions in Rahn et al. 2002 and Oberhänsli et al. 2003). A distinction between high-pressure and low-pressure chloritoid can be done in low-grade metasediments (HP/LT, 350-400 °C) only by a careful microstructural analysis of the relationships be-

tween crystallization and deformation, or in higher-grade metasediments (HP/MT, 450-500°C), by the careful analysis of the entire mineral assemblage. In the case of the low-grade Fe-Mg carpholite-bearing metasediments found in both Valaisan (Grava and Tomül nappes) and European domains (Peiden slices) chloritoid can only rarely be found inside Fe-Mg carpholite-bearing quartz-calcite segregations/veins (Fig. 5.3a) or as fine prisms oriented parallel to the often strongly folded main foliation (e.g. around P. Beverin, Vals or Hinterrhein; Fig. 5.3b). In such cases the formation of chloritoid is interpreted as being related to HP/LT conditions.

In slightly higher grade metasediments devoid of Fe-Mg carpholite, such as found in the Misox Zone, *chloritoid* is mostly associated with *garnet* (Teutsch 1982; Fig. 5.2a). Both minerals have formed before the main deformation as evidenced by the fact that the main foliation bends around the porphyroblasts (Fig. 5.3f). The co-existence of garnet and chloritoid typically indicates (upper) blueschist facies conditions in metasediments (e.g. Agard et al. 2001; Wiederkehr 2004; Bucher & Bousquet 2007; Bousquet 2008; Bousquet et al. 2008). This assemblage formed at considerably higher temperatures during the high-pressure stage when compared to the carpholite bearing metasediments found further north.

The metasediments from the “internal Mesozoic” of the northern frontal part of the Adula nappe complex contain a co-existing and unambiguous assemblage of minerals formed by *chloritoid*, *garnet*, *kyanite* and *zoisite/clinozoisite* (e.g. Löw 1987; Fig. 5.2a). This mineral assemblage is indicative for upper blueschist to eclogite facies conditions in metasediments (Löw 1987; Bousquet et al. 2008).

Scarce remnants of the early pressure dominated subduction-related metamorphism can also be found in thin layers of mafic rocks that are spatially associated with the Mesozoic metasediments derived from the Valaisan Ocean. *Glaucophane* is a characteristic index mineral indicating HP/LT conditions for mafic rocks (e.g. Evans 1990) and has been identified near Tomülpass east of Vals (Oberhänsli 1977; Oberhänsli 1978), around Splügen (outcrop “Brennhoftobel”; Nabholz, 1945) as well as at the spectacular outcrop “Neu Wahli” north of the San Bernardinopass (Gansser 1937; Fig. 5.2a). In mafic rocks around Piz Aul west of Vals occurrences of some blue-greenish amphiboles have been reported, but these were not clearly identified as glaucophane (Kupferschmid 1977). Only one single outcrop in the northern Misox Zone (outcrop “Neu Wahli”) is known to preserve unambiguous Alpine-age eclogite facies relics within the Valaisan oceanic domain east of the Lepontine dome, as is documented by the co-existence of *glaucophane*, *garnet* and *omphacite* (30-50% jadeite component; Ring 1992; Santini 1992; Fig. 5.2a).

The available metamorphic data indicate a general increase of metamorphic conditions, both in terms of temperature and pressure, towards the south within the Valaisan domain; they range from Fe-Mg carpholite-bearing blueschist facies metasediments to glaucophane-bearing eclogite facies metabasites. A similar southward increase in P-T conditions has also been documented for the Adula nappe complex (Heinrich 1982; Heinrich 1986). This is generally interpreted to reflect southward subduction of tectonic units during the formation of the Alpine orogenic belt.

Remnants of collision-related metamorphism

The distribution of subduction- and collision-related index minerals is completely different (Wiederkehr et al. 2008) and obvious from inspection of Figure 5.2. While the subduction-related metamorphism forms a more or less orogen-parallel belt, collision-related Barrovian overprint represents a characteristic onion-shaped thermal dome whereby temperatures typically increase towards the southwest and clearly cross-cut both the pre-existing HP/LT metamorphic belt as well as all the major nappe contacts.

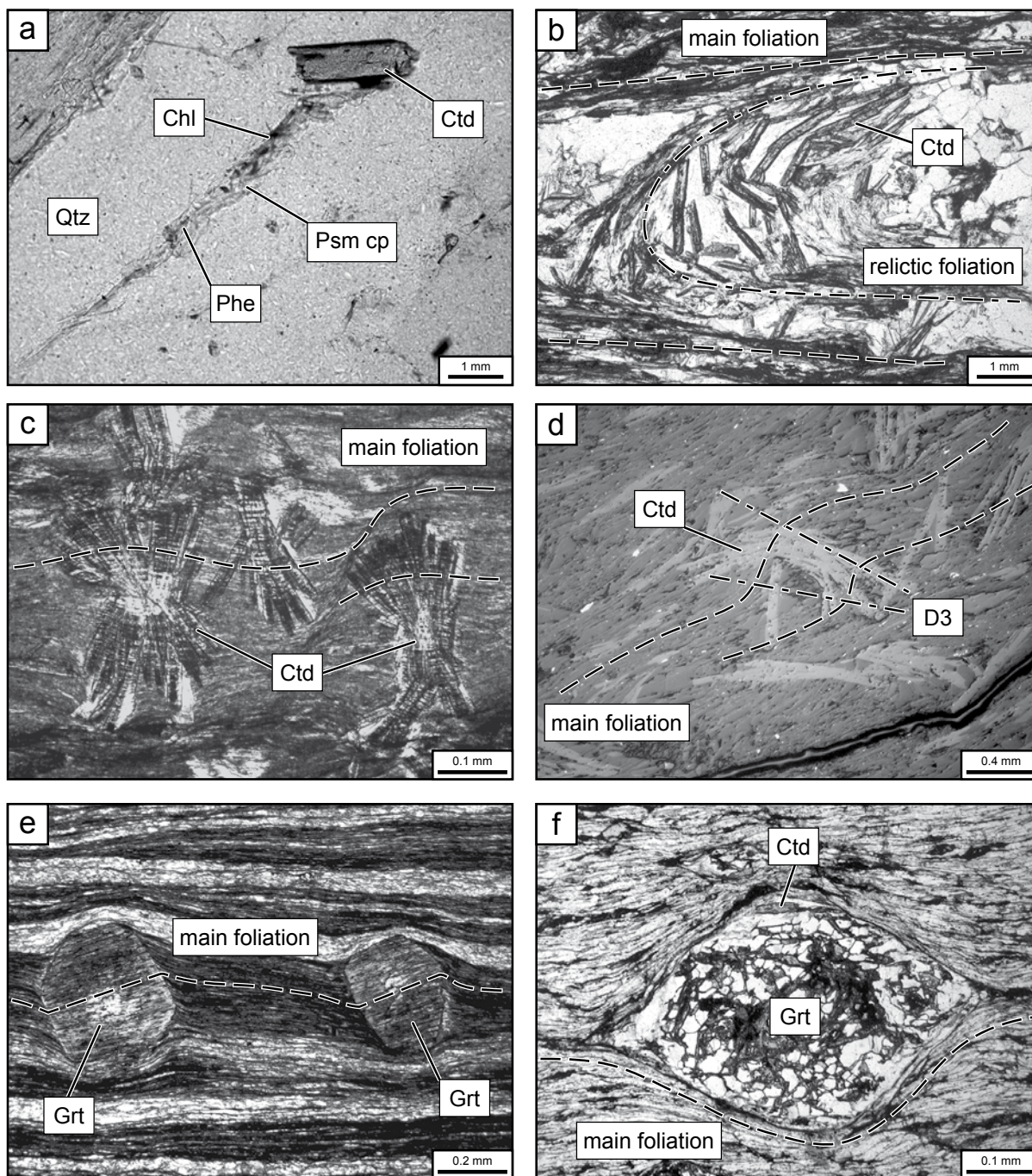


Fig. 5.3: Photomicrographs of thin sections showing different relationships between crystallization and deformation. (a) Prism of chloritoid inside a Fe-Mg carpholite-bearing quartz-calcite vein overgrowing a pseudomorph after carpholite consisting of phengite-chlorite-quartz. Sample from Valaisan-derived HP/LT metasediments, Grava nappe (LUZ 0432, 720°938/162°275, 2600 m). (b) Earlier foliation (S1) underlined by primes and needle-shaped chloritoid preserved in late stage (D2) fold hinges (microlithons) representing the main foliation. Sample from Valaisan-derived metasediments, Aul unit (VAL 0710, 731°370/163°971, 1960 m). (c) Bundles and rosettes of chloritoid clearly overgrowing the main foliation. Sample from Europe-derived HP/LT metasediments, Peiden slices/Forca unit (CAV 0517, 717°470/160°269, 1850 m). (d) Reflected light photomicrograph of a bundle of chloritoid growing over the main foliation and slightly bended by subsequent (D3) deformation. Sample from Europe-derived LP/LT metasediments, Scopi unit (VRI 072, 729°104/170°789, 1260 m). (e) Straight internal main foliation preserved inside of garnet. The deflection of the main foliation at the rim of the garnets is the effect of minor subsequent deformation (southern Misox Zone, MF 2042, 737°600/140450, 900 m). (f) Skeletal porphyroblast of garnet and prism of chloritoid are found together in a lense-shaped sigma-clast, the main foliation is strongly deflected around garnet and chloritoid. Sample from Valaisan-derived HP/LT metasediments, Northern Misox Zone/Aul unit (TP 34, 734°450/153°600, 1840 m). Samples MF 2042 and TP 34, shown in (e) and (f), respectively, were taken from the study of Petrova et al. (2002).

The clear progressive metamorphic zoning of this Barrow-type event ranges from greenschist facies conditions in the Urseren-Garvera Zone in the north to lower/middle amphibolite facies conditions around the Lukmanier and Pizzo Molare areas in the south. This metamorphic gradient has been observed and described in great detail in the past (Chadwick 1968; Frey 1969, 1974, 1978; Thakur 1971; Fox 1975) and represents a classical case for studying Barrow-type regional metamorphism. Recently this data set was completed by a detailed study on the progressive Barrow-type overprint of European- and Valaisan-derived metasediments (“Bündnerschiefer”) along a north-east south-west section ranging from Piz Terri in the east to Pizzo Molare in the west (Fig. 5.1b; Wiederkehr et al. 2008). All these studies clearly demonstrate that the sequential appearance of *margarite*, *chloritoid*, *zoisite/clinozoisite*, *plagioclase* (> 10 mol% An), *biotite*, *garnet*, *kyanite*, and *staurolite* corresponds to increasing temperatures related to Lepontine Barrow-type thermal overprint (Fig. 5.2b). Whereas the mineral assemblages corresponding to subduction-related HP/LT metamorphism typically show pre-kinematic microstructures in respect to the main foliation, mineral assemblages belonging to collision-related Barrow-type thermal overprint grew post-kinematically as clearly documented by porphyroblasts devoid of any shape preferred orientation overgrowing the main foliation (Fig. 5.3).

It is important to mention that *chloritoid* that most often formed at the expense of pyrophyllite under LP/LT conditions generally occurs as idiomorphic rosettes, bundles and prisms growing over the main foliation (Fig. 5.3c & d), while rare chloritoid porphyroblasts related to the breakdown of Fe-Mg carpholite are typically oriented parallel to the main foliation and are found well inside quartz-calcite veins/segregations still containing relics of Fe-Mg carpholite (Figs. 5.3a & b). Hence, the two different generations of chloritoid can unambiguously be distinguished based on careful microstructural observations (Wiederkehr et al. 2008). Occurrences of chloritoid are found a far distance to the east; obviously chloritoid shows a different zoning pattern compared to other index minerals by not being characterized by the rather concentric shape confining the Lepontine thermal dome such as seen for *margarite*, *biotite*, *kyanite* or *staurolite* (Fig. 5.2b; Niggli & Niggli 1965).

Contrasting with the well known metamorphic zoning in the north-eastern Lepontine dome (areas around Lukmanier, Pizzo Molare and Val Luzzzone; Fig. 5.1b) the metamorphic zoning and history are more problematic in the area of the Misox Zone. There it is generally accepted that the characteristic metamorphic conditions change from high-pressure conditions in the N to amphibolite facies Barrovian conditions in the S (Gansser 1937; Oberhänsli 1978; Teutsch 1982). Based on the first occurrences of *staurolite*, as well as on the anorthite content in *plagioclase*, amphibolite facies conditions are reached, going from N to S, at the level of Mesocco (Wenk 1970; Thompson 1976). The Barrovian overprint in the Misox Zone has been investigated by Teutsch (1982), but there the significance of the occurrences of particularly ambiguous minerals such as garnet and chloritoid is crucial but not easy to assess. According to the findings along a metamorphic profile around Lukmanier and Val Luzzzone the first occurrences of *biotite*, *margarite* and *plagioclase* (> 10 mol% An) in metasediments are characteristic for incipient Barrovian overprint (Frey 1978; Frey et al. 1982; Wiederkehr et al. 2008). In the case of the Misox Zone the first occurrences of these index minerals are found south of the area around San Bernardino, and they indicate the onset of increasing temperatures related to collision-related Barrovian overprint (Fig. 5.2b). Consequently, more northerly located occurrences of co-existing garnet and chloritoid are interpreted as having formed during the early subduction-related HP/LT metamorphic event rather than being related to the subsequent collision-related Barrovian overprint. Such an interpretation is supported by the obvious differences in the microstructural setting of garnet: Whereas in the north garnet is clearly seen

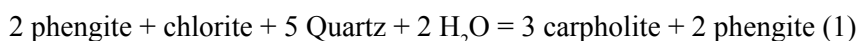
to have grown pre-kinematically, more southerly occurrences of garnet indicate post-kinematic growth whereby porphyroblasts overgrow a pre-existing main foliation (Figs. 5.3e & f).

5.4.2. P-T estimates along a profile with increasing Barrow-type metamorphic grade overprinted onto earlier HP/LT metamorphism

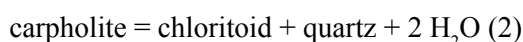
As shown by Wiederkehr et al. (2008) the relationships between an earlier HP/LT event and a subsequent MP/MT Barrovian overprint are by now well established along a metamorphic profile ranging from Pizzo Molare to Safiental. Hence, the area offers a natural laboratory for investigating progressive Barrovian overprint of former HP/LT metasediments. The detailed study of subsequent progressive Barrow-type overprint provides the possibility to unravel the late stage thermal evolution at the north-eastern rim of the Lepontine dome and to clarify the question whether this late-stage thermal overprint merely represents a single heating event during which only temperature is the changing parameter, hence representing an “isobaric heating event”, or alternatively, if the evolution is more complex and characterized by late-stage changes in pressure and temperature. In an attempt to answer this question insights for both the late-stage evolution as well as regarding speculations about the nature of Barrovian overprint can be achieved. Combined with the peak-metamorphic temperatures obtained by Raman spectroscopy of carbonaceous matter (RSCM; Wiederkehr et al. *submitted, b*) and the available isotopic dating (Wiederkehr et al. *submitted, a*) the additional new P-T data presented below will be used to unravel the tectono-metamorphic evolution in the investigated area, focussing on the transition from subduction to collision of the European margin and adjacent Valaisan Ocean.

Subduction-related HP/LT metamorphism

Within the investigated area peak-pressure conditions are documented by the widespread occurrences of the HP/LT mineral assemblage Fe-Mg carpholite – chlorite – phengite – quartz \pm chloritoid in metasediments derived from the Valaisan domain (Bousquet et al. 2002) and, as recently shown, also in metasediments derived from the distal European margin, i.e. in areas that are partly located well inside the amphibolite facies Lepontine thermal dome (Fig. 5.1b; Wiederkehr et al. 2008). Relics of this early pressure-dominated metamorphic stage can only be found in quartz-calcite segregations and never in the rock matrix (Wiederkehr et al. 2008). However, Fe-Mg carpholite is only preserved in the form of microscopic-scale, hair-like relics within such typically fibrous quartz-calcite segregations/veins that represent macroscopically visible pseudomorphs after large former Fe-Mg carpholite crystals. In thin section, fibrous quartz is full of inclusions of chlorite, phengite and paragonite. This assemblage often forms needle-shaped pseudomorphs after Fe-Mg-carpholite. Rarely chloritoid has also been found to be associated with such fibrous quartz-calcite veins. In order to estimate peak pressure and temperature conditions using the well established petrogenetic grid for carpholite-bearing, low-grade metapelites provided by Bousquet et al. (2002 & 2008) and shown in Figure 5.4, the chemical compositions of co-existing HP/LT minerals such as Fe-Mg carpholite, phengite, chlorite, and if present, also chloritoid were determined by electron microprobe (EMP) analysis and listed in Table 5.2. The pressure conditions for carpholite-bearing rocks are defined by the location of the equilibrium (Fig. 5.4):



while the stability field of Fe-Mg carpholite towards higher temperature is limited by the equilibrium:



A total of eight samples have been investigated belonging to both Valaisan and distal European margin and collected along a cross-section between Val Luzzzone in the south-west, already well affected

Table 5.2: Representative mineral analysis of subduction-related HP/LT assemblages found as inclusions in quartz-calcite veins representing pseudomorphs after carpholite of Valaisan (Grava and Tomül nappes) and European (Peidener slices and Piz Terri-Lunschiana unit) metasedimentary units given in weight-%. The structural formulae were calculated for carpholite using 5 cations for Si and 3 cations for Al, Fe, Mn and Mg following Goffé & Oberhänsli (1992), for chlorite using 14 oxygens, for white mica using 11 oxygens and for chloritoid using 12 oxygens following Chopin et al. (1992). The sums of analyses have been corrected for fluorine content; the values given under “Total corr.” take into account that fluorine occupies an oxygen site. The following abbreviations have been used: Cp = Fe-Mg carpholite, Ctd = chloritoid, Chl = chlorite, Phe = phengite, Pg = paragonite.

Unit	Valaisan domain						Valaisan domain						distal European margin					
	Sample	Cp	Ctd	Chl	Phe	Pg	Sample	Cp	Chl	Phe	Cp	Chl	Phe	Sample	Cp	Chl	Phe	
Valaisan domain	Minerals	Cp	Ctd	Chl	Phe	Pg	Cp	Chl	Phe	Cp	Chl	Phe	Cp	Chl	Phe	Cp	Chl	Phe
	<i>Minerals</i>	<i>Cp</i>	<i>Ctd</i>	<i>Chl</i>	<i>Phe</i>	<i>Pg</i>	<i>Cp</i>	<i>Chl</i>	<i>Phe</i>	<i>Cp</i>	<i>Chl</i>	<i>Phe</i>	<i>Cp</i>	<i>Chl</i>	<i>Phe</i>	<i>Cp</i>	<i>Chl</i>	<i>Phe</i>
	SiO ₂	37.40	24.46	25.58	49.46	48.43	37.63	25.30	48.60	37.96	25.77	49.67	37.18	25.97	49.53	37.28	25.73	48.18
	TO ₂	0.19	0.04	0.06	0.20	0.04	0.25	0.06	0.17	0.14	0.17	0.14	0.14	0.17	0.14	0.17	0.14	0.17
	Al ₂ O ₃	31.11	39.36	22.91	33.52	40.30	31.31	22.40	34.08	32.43	21.06	33.10	31.57	21.64	31.62	31.74	21.41	35.77
	FeO	11.44	25.42	27.57	1.34	0.20	12.64	26.51	1.24	1.02	23.07	1.07	11.51	22.70	1.43	12.83	25.66	1.29
	MnO	0.25	0.02	0.00	0.00	0.01	0.30	0.05	0.00	1.02	0.08	0.01	0.24	0.10	0.01	0.08	0.02	0.01
	MgO	6.32	1.85	12.73	1.39	0.12	5.68	13.39	1.20	6.02	13.61	1.63	5.66	13.25	2.24	5.02	10.32	0.92
	CaO	0.00	0.00	0.00	0.00	0.07	0.02	0.01	0.00	0.02	0.00	0.00	0.02	0.00	0.00	0.00	0.01	0.01
	Na ₂ O	0.00	0.00	0.04	0.67	7.26	0.00	0.00	0.76	0.02	0.03	0.64	0.05	0.02	0.35	0.02	0.01	0.01
	K ₂ O	0.04	0.00	0.02	8.82	1.11	0.03	0.01	9.12	0.04	0.02	9.17	0.04	0.02	9.36	0.04	0.00	8.49
	F	0.65	0.00	0.00	0.00	0.00	0.77	0.00	0.00	0.59	0.00	0.00	0.40	0.00	0.00	0.04	0.00	0.00
	Total	87.43	91.15	88.48	95.39	97.54	88.64	87.72	95.16	88.63	83.68	95.44	86.83	83.68	95.68	86.83	83.21	95.67
	Total corr.	87.17	91.16	88.49	95.40	97.54	88.32	87.73	95.17	88.39	83.68	95.43	86.67	83.70	95.69	86.67	83.22	95.66
	Si	2.00	2.05	2.67	3.24	3.02	2.00	2.67	3.20	2.00	2.81	3.25	2.00	2.82	3.31	2.00	2.85	3.14
	Ti	0.01	0.00	0.00	0.01	0.00	0.01	0.00	0.01	0.01	0.00	0.01	0.01	0.01	0.01	0.01	0.00	0.01
	Al	1.96	3.90	2.84	2.59	2.96	1.96	2.79	2.64	2.01	2.70	2.56	2.00	2.77	2.44	2.00	2.77	2.75
Fe ³⁺	0.04	0.05	0.05	-	-	0.04	-	-	0.00	-	-	0.00	-	-	0.00	-	-	
Fe ²⁺	0.47	1.74	2.41	0.07	0.01	0.52	2.34	0.07	0.49	2.10	0.06	0.52	2.06	0.08	0.01	0.01	0.00	
Mn	0.01	0.00	0.00	0.00	0.00	0.01	0.00	0.00	0.01	0.01	0.00	0.01	0.01	0.00	0.01	0.01	0.00	
Mg	0.50	0.23	1.99	0.14	0.01	0.45	2.11	0.12	0.47	2.21	0.16	0.45	2.14	0.22	0.45	2.14	0.22	
Ca	0.00	0.00	0.00	0.00	0.00	0.00	0.00	0.00	0.00	0.00	0.00	0.00	0.00	0.00	0.00	0.00	0.00	
Na	0.00	0.00	0.01	0.08	0.88	0.00	0.00	0.10	0.00	0.01	0.08	0.01	0.00	0.04	0.01	0.00	0.04	
K	0.00	0.00	0.00	0.74	0.09	0.00	0.00	0.77	0.00	0.00	0.77	0.00	0.00	0.78	0.00	0.00	0.78	
F	0.11	0.00	0.00	0.00	0.00	0.13	0.00	0.00	0.10	0.00	0.00	0.07	0.00	0.00	0.07	0.00	0.00	
XMg	0.51	0.12	0.45	0.00	0.00	0.46	0.47	0.00	0.48	0.51	0.00	0.46	0.51	0.00	0.46	0.51	0.00	
Unit	Valaisan domain						Valaisan domain						distal European margin					
Sample	HINT 079 (Tomül)						LIZ 047 (Peiden slices, Forca slice)						LAR 061 (Peiden slices, Planca slice)					
Minerals	<i>Cp</i> <i>Ctd</i> <i>Chl</i> <i>Phe</i>						<i>Cp</i> <i>Chl</i> <i>Phe</i>						<i>Cp</i> <i>Chl</i> <i>Phe</i>					
<i>Minerals</i>	<i>Cp08453</i> <i>Ctd08427</i> <i>Chl08457</i> <i>Phe08438</i>						<i>Cp0849</i> <i>Chl08207</i> <i>Phe08224</i>						<i>Cp08952</i> <i>Chl08962</i> <i>Phe08960</i>					
SiO ₂	37.50	24.55	26.58	49.48	48.43	37.85	25.32	47.18	38.00	38.00	38.00	47.20	37.28	25.73	48.18	37.28	25.73	48.18
TO ₂	0.38	0.00	0.06	0.19	0.00	0.00	0.00	0.13	0.00	0.00	0.00	0.13	0.00	0.00	0.00	0.00	0.00	
Al ₂ O ₃	31.96	40.29	21.74	30.89	32.41	38.80	22.73	35.94	22.55	26.21	30.81	36.34	31.74	21.41	31.74	21.41	35.77	
FeO	11.44	21.32	22.64	1.80	10.92	12.55	26.21	0.81	11.90	13.90	0.49	12.83	12.83	1.29	12.83	10.32	0.92	
MnO	0.94	0.66	0.17	0.02	0.06	0.27	0.07	0.00	0.03	0.08	0.01	0.08	0.08	0.02	0.08	0.02	0.01	
MgO	5.30	2.09	13.79	2.28	6.27	2.83	12.97	0.85	6.49	12.62	0.62	5.02	10.32	0.92	5.02	10.32	0.92	
CaO	0.00	0.01	0.00	0.00	0.01	0.00	0.01	0.00	0.00	0.03	0.02	0.00	0.00	0.01	0.00	0.01	0.01	
Na ₂ O	0.01	0.02	0.03	0.50	0.01	0.00	0.00	0.84	0.04	0.03	0.92	0.02	0.01	0.01	0.02	0.01	0.01	
K ₂ O	0.01	0.00	0.00	9.07	0.02	0.01	0.01	8.75	0.00	0.02	8.59	0.00	0.00	8.49	0.00	0.00	8.49	
F	0.32	0.00	0.00	0.00	0.49	0.00	0.00	0.00	0.00	0.00	0.00	0.04	0.00	0.00	0.04	0.00	0.00	
Total	85.00	85.00	85.00	94.27	88.03	89.78	87.72	94.50	87.28	86.08	94.19	87.28	83.21	95.67	87.28	83.21	95.67	
Total corr.	87.73	88.94	85.01	94.23	87.83	89.78	86.33	94.50	86.09	86.09	94.19	86.26	83.22	95.66	86.26	83.22	95.66	
Si	2.00	2.09	2.83	3.30	2.00	2.13	2.61	3.12	2.00	2.57	3.12	2.00	2.85	3.14	2.00	2.85	3.14	
Ti	0.02	0.00	0.00	0.01	0.00	0.00	0.00	0.01	0.00	0.00	0.00	0.00	0.01	0.00	0.01	0.00	0.01	
Al	2.01	4.04	2.73	2.43	2.02	3.85	2.88	2.80	1.86	2.90	2.83	2.01	2.80	2.75	2.01	2.80	2.75	
Fe ³⁺	0.00	0.00	-	-	0.00	0.02	-	-	0.00	0.14	-	0.00	-	-	0.00	-	-	
Fe ²⁺	0.51	1.77	2.02	0.10	0.52	1.56	2.36	0.04	0.47	2.46	0.03	0.58	2.38	0.07	0.58	2.38	0.07	
Mn	0.04	0.05	0.02	0.00	0.00	0.02	0.01	0.00	0.00	0.01	0.00	0.00	0.00	0.00	0.00	0.00	0.00	
Mg	0.42	0.27	2.19	0.23	0.49	0.35	2.08	0.08	0.51	2.04	0.06	0.40	1.71	0.09	0.40	1.71	0.09	
Ca	0.00	0.00	0.00	0.00	0.00	0.00	0.00	0.11	0.00	0.00	0.12	0.00	0.00	0.10	0.00	0.00	0.10	
Na	0.00	0.00	0.00	0.06	0.00	0.00	0.00	0.74	0.00	0.00	0.72	0.00	0.00	0.71	0.00	0.00	0.71	
K	0.00	0.00	0.00	0.77	0.08	0.00	0.00	0.00	0.00	0.00	0.77	0.00	0.00	0.78	0.00	0.00	0.78	
F	0.05	0.00	0.00	0.00	0.08	0.00	0.00	0.00	0.00	0.00	0.00	0.00	0.00	0.00	0.00	0.00	0.00	
XMg	0.43	0.13	0.52	0.00	0.49	0.48	0.47	0.00	0.52	0.45	0.00	0.46	0.51	0.00	0.46	0.51	0.00	

by subsequent Barrovian thermal overprint, and Safiental/Hinterrhein in the east, where no substantial re-heating is observed (samples are listed in Table 5.1, locations are given in Figure 5.1b). These eight samples were selected in order to cover all the Fe-Mg carpholite-bearing tectonic units belonging to the Valaisan domain (Grava and Tomül nappes) as well as the realm of the distal European margin (Peiden slices and Piz Terri-Lunschania unit).

The chemical composition of Fe-Mg carpholite $[(\text{Mg},\text{Fe},\text{Mn})\text{Al}_2\text{Si}_2\text{O}_6(\text{OH},\text{F})_4]$ is rather constant, X_{Mg} $[\text{Mg}/(\text{Mg}+\text{Fe}+\text{Mn})]$ only varying between 0.4-0.5 (Tab. 5.2). Only the relics of Fe-Mg carpholite belonging to the Piz Terri-Lunschania unit show significantly lower values of X_{Mg} , ranging between 0.3-0.4. In general the composition of carpholite is within the same range already found in earlier studies for the Valaisan domain over the entire Grisons area (Goffé & Oberhänsli 1992; Oberhänsli et al. 1995; Bousquet et al. 2002; Oberhänsli et al. 2003). The Si^{4+} content of white mica occurrences found within carpholite-bearing quartz-calcite segregations ranges from 3.31 in the Valaisan Bündnerschiefer to 3.14 p.f.u in the Sub-Penninic Peiden slices of the distal European margin (Tab. 5.2). Only in a few cases was also chloritoid found to be associated with quartz-calcite segregations that contain relics of Fe-Mg carpholite; in such cases chloritoid is typically found either inside the Fe-Mg carpholite-bearing quartz-calcite segregations (Fig. 5.3a) or aligned parallel to the main foliation in close contact to such quartz-calcite segregations. Such high-pressure related chloritoid forms small prisms, the X_{Mg} -values vary between 0.12 in the Valaisan Bündnerschiefer and 0.20 in the Europe-derived metasediments (Tab. 5.2) and is interpreted to have formed during prograde metamorphism by a mineral reaction at the expense of Fe-Mg carpholite, as shown by Vidal et al. (1992). Hence, such chloritoid formed during the high-pressure stage rather than during a subsequent greenschist facies overprint (see discussion given by Oberhänsli et al. 2003).

From the above-described equilibria (1) and (2), determined by the mineral chemistry of the observed assemblages, peak metamorphic conditions of 1.2-1.4 GPa and 350-400 °C are estimated for both the metasediments derived from the Valaisan Ocean (Grava and Tomül nappes) as well as those derived from the distal European margin (Peiden slices and Piz Terri-Lunschania unit) as shown in Figure 5.4. These peak-pressure metamorphic conditions are similar to those found further to the east in the Grisons area (e.g. Bousquet et al. 2002).

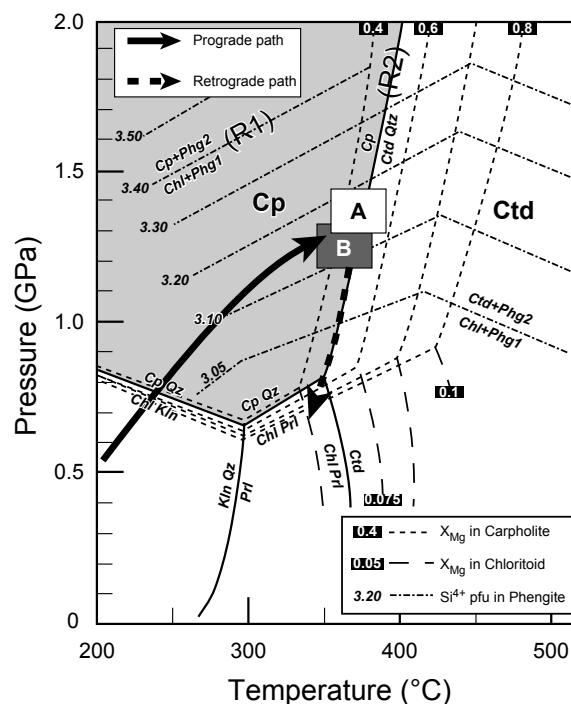


Fig. 5.4: Estimated P-T conditions for peak-pressure conditions of metasedimentary units derived from the Valaisan (Grava and Tomül nappes; A) and European margin (Peiden slices and Piz Terri-Lunschania unit; B). P-T conditions have been estimated for HP/LT assemblages consisting of Fe-Mg carpholite – phengite – chlorite – quartz \pm chloritoid, only preserved in quartz-calcite veins, using the chemistry of the different minerals listed in Table 5.2 according to reactions R1 & R2 (see explanations in the text). The celadonite component of phengite (reflecting the Si content p.f.u.) has been estimated following the decomposition of white micas given in Bousquet et al. (2002). The petrogenetic grid for HP/LT metapelites have been adopted from Bousquet et al. (2008).

Collision-related Barrovian overprint

As recently shown by Wiederkehr et al. (2008) the HP/LT rocks were progressively overprinted by a Barrow-type thermal event characterized by increasing temperatures towards the south-west. This offers the unique opportunity to investigate progressively increasing conditions related to Barrow-type amphibolite facies metamorphism overprinting HP/LT rocks.

In order to study the P-T conditions along a gradient with increasing Barrow-type overprint six samples have been selected. They range from greenschist facies in the Val Luzzzone to lower/middle amphibolite conditions at the Pizzo Molare (samples are listed in Table 5.1 and shown in Figure 5.1b). The investigated metasedimentary samples derive from both Valaisan and European domain and are generally well equilibrated during this second, late-stage Barrovian overprint as is evidenced by the lack of relics related to the earlier HP/LT event. Equilibrium phase diagrams (also referred to as pseudo-sections) have been computed for the NaCaKFMASH(\pm C)-system using the THERIAK-DOMINO software (De Capitani 1994; Biino & De Capitani 1995) to visualise stable assemblages as well as mode and composition of solution phases for specific bulk rock compositions. The bulk rock compositions of the six investigated samples used for P-T modelling by the THERIAK-DOMINO software are given in Table 5.3. In the following we briefly present the studied samples between Val Luzzzone and Pizzo Molare in order of increasing temperatures. Thereby a short description of the observed mineral assemblage as well as the microstructure will be given. Phase equilibrium diagrams for each sample are shown in Figure 5.5, presenting P-T conditions for the observed peak-metamorphic assemblage. Additionally, the corresponding peak-metamorphic temperatures recently estimated by the RSCM method (see Wiederkehr et al. *submitted, b*) are also displayed for a more accurate determination of the peak-metamorphic conditions. Corresponding representative EMP analyses are listed in Table 5.4.

Table 5.3: Representative bulk rock geochemical data of analyzed Valaisan and European metasedimentary units given in weight-%.

Sample	Valaisan			distal European margin		
	LUZ 055	LUZ 0444	BLE 0510	BLE 0410	GRU 053	MOL 051
SiO ₂	52.54	51.38	46.71	59.60	56.61	47.62
TiO ₂	1.33	0.98	1.75	0.88	1.15	1.5
Al ₂ O ₃	27.03	22.43	27.06	15.97	23.60	28.35
Fe ₂ O ₃	4.44	4.68	6.36	10.10	7.18	10.79
MnO	0.01	0.04	0.02	0.19	0.09	0.1
MgO	1.96	3.10	3.89	1.72	2.99	4.70
CaO	5.76	13.08	7.98	7.96	1.76	1.93
Na ₂ O	4.81	2.16	1.85	0.66	1.64	1.81
K ₂ O	1.79	2.32	4.34	1.29	5.53	3.78
Total	99.67	100.17	99.96	98.37	100.55	100.58

LUZ 055: This sample belongs to the metasedimentary units of the Valaisan domain and was collected close to quartz-calcite segregations/veins that contain still preserved relics of Fe-Mg carpholite that formed during the early HP/LT metamorphic stage. The observed assemblage consists of plagioclase, zoisite/clinozoisite, white mica, chlorite and quartz as well as minor amounts of both titanite and rutile. Both white mica and chlorite form the main foliation, whereas plagioclase, zoisite/clinozoisite and titanite clearly overgrow this main foliation. Plagioclase forms large porphyroblasts up to 1.5 cm in size and is the dominant phase. It overgrows all other phases, as is documented by inclusions of white mica, chlorite, zoisite/clinozoisite and titanite/rutile. Zoisite/clinozoisite is found as fine-grained needle-shaped or platy crystals oriented parallel or across the main foliation. Due to late-stage deformation the

main foliation is gently crenulated and also affects zoisite/clinozoisite and plagioclase that grew at a late stage. This late deformation was induced by the formation of the Northern Steep Belt (Chièra phase) and it clearly postdates the onset of Barrovian overprint (Wiederkehr et al. 2008).

Figure 5.5a shows the equilibrium phase diagram calculated in the NaCaKFMASH system for the bulk rock composition of this sample as given in Table 5.3. The observed peak metamorphic assemblage has a very large stability field ranging from 0.3-0.95 GPa and 300-525 °C that does not allow for an accurate P-T estimation. However, the combination of peak-metamorphic temperatures obtained by the RSCM method with the pressures calculated from Si-isopleths in white mica allows for a further restriction of the pressure and temperature range during peak-metamorphic conditions and yields 0.6-0.8 GPa and 450-500 °C.

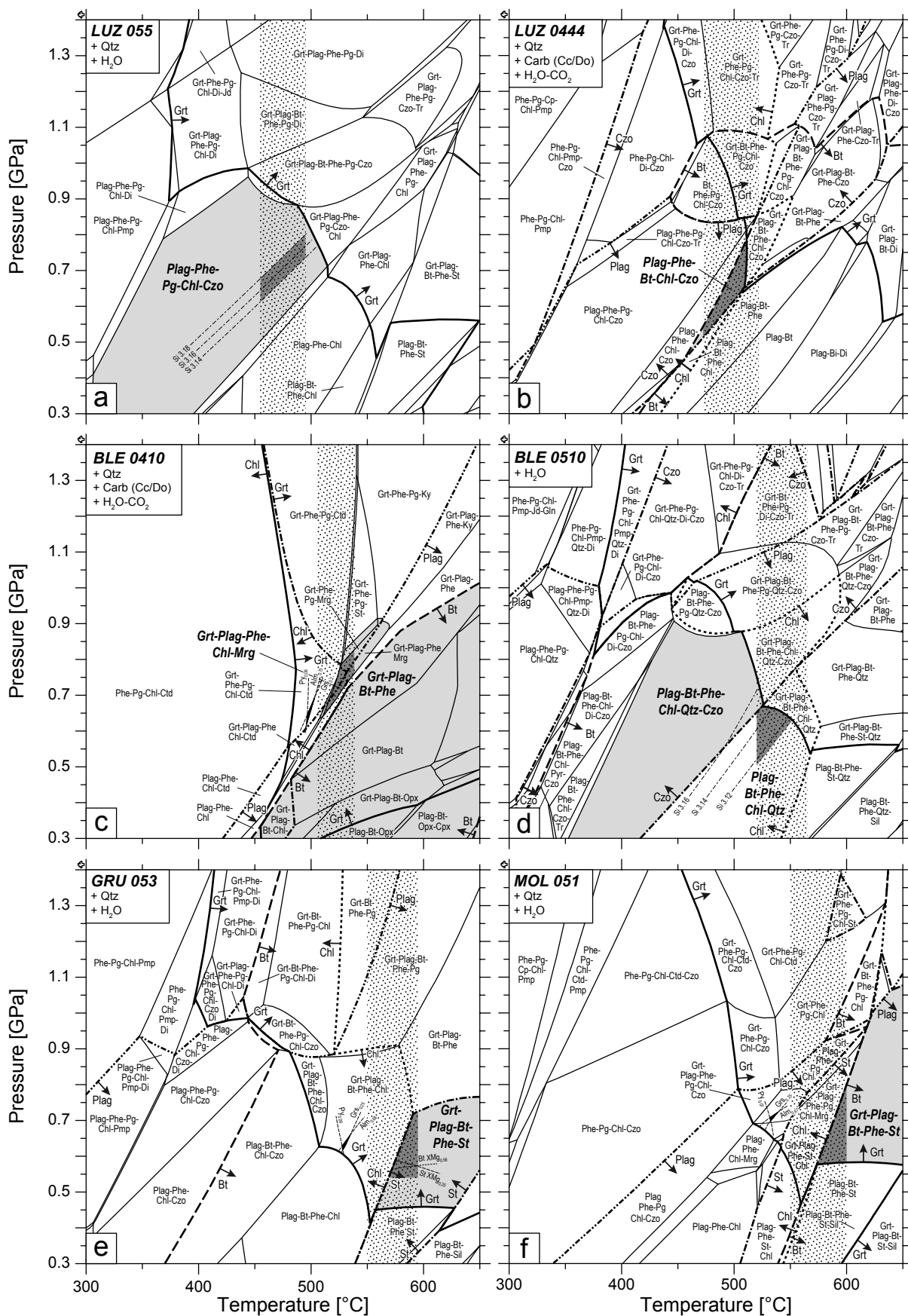
LUZ 0444: This sample also belongs to the Valaisan but is slightly higher in metamorphic grade as documented by the appearance of biotite. The mineral assemblage consists of biotite, plagioclase, zoisite/clinozoisite, white mica, chlorite, quartz, calcite/dolomite and some minor amounts of titanite/rutile. As also found in the previous sample large porphyroblasts of plagioclase and prisms of zoisite/clinozoisite overgrow a pre-existing main foliation, whereas white mica forms the main foliation. Zoisite/clinozoisite is obviously much more frequent in this sample and forms spectacular rosettes up to 5 cm in diameter (Wiederkehr et al. 2008). Chlorite is only visible as small flakes oriented parallel to the main foliation or surrounds some opaque phases; it is obviously less frequent than in the previous sample. Biotite is found as flakes oriented both parallel as well as across the main foliation. The first appearance of well developed biotite that unambiguously overgrew the pre-existing main foliation (referred to as “Querbiotit”) along this profile clearly indicates the late-stage formation of biotite.

Figure 5.5b shows the equilibrium phase diagram calculated in the NaCaKFMASHC system for the bulk rock composition given in Table 5.3. Due to non-negligible amounts of calcite/dolomite and the obvious involvement of carbonates during the formation of plagioclase the H₂O activity has been reduced by adding some CO₂ to the fluid. The equilibrium diagram predicts a relatively narrow stability field of 0.45-0.8 GPa and 450-525 °C, i.e. over a wider range of pressures but better defined in temperature. The temperature interval is constrained by the disappearance of biotite towards lower temperatures and by the disappearance of zoisite/clinozoisite towards higher temperatures. Towards higher pressures and higher temperatures the appearance of garnet delimits the calculated stability field. The RSCM peak temperatures independently predict 490-520 °C which perfectly overlaps with the computed stability field. This also allows for an additional restriction of the peak-metamorphic conditions to 0.5-0.8 GPa and 475-525 °C.

BLE 0410: In contrast to the two samples presented above, sample BLE 0410 originates from metasedimentary units derived from the European margin and belonging to the Peiden slices (i.e. Pianca slice, southern slice). The most obvious difference in respect to the samples described above is the presence of large porphyroblasts of garnet, up to 1 cm in diameter. The observed mineral assemblage consists of garnet, biotite, margarite, plagioclase, white mica, chlorite, quartz and minor amounts of calcite/dolo-

Fig. 5.5: Equilibrium phase diagrams computed with DOMINO for specific bulk rock compositions of various metasediments including both Valaisan and European domains listed in Table 5.3. Corresponding representative EMP analyses of constituents of observed mineral assemblages representing peak conditions established during Barrovian overprint are given in Table 5.4. Dark grey shaded areas indicate peak P-T conditions reached during Barrovian overprint. The observed mineral assemblage is highlighted in light-grey, the dotted bars represent peak-metamorphic temperatures estimated by the RSCM method given by Wiederkehr et al. (*submitted, b*). Figures (a)-(f) showing calculated equilibrium phase diagrams in order of increasing temperatures established during late-stage Barrow-type thermal overprint (see also text for further explanations).

mite. Garnet and plagioclase unambiguously overgrow a pre-existing main foliation, whereas flakes of biotite are seen to have grown either within or across the main foliation (“Querbiotit”). Fibres of margarite are oriented parallel to the main foliation. Interestingly, the large porphyroblasts of garnet show



practically no chemical zonation (Tab. 5.4), they have an almandine rich composition which is typical for Barrow-type regional metamorphism ($\text{Alm}_{0.71}\text{Prp}_{0.06}\text{Grs}_{0.21}\text{Sps}_{0.02}$).

Figure 5.5c shows the resulting equilibrium phase diagram calculated for the NaCaKFMASHC system, corresponding to the bulk rock composition given in Table 5.3. The activity of H_2O was reduced by adding some CO_2 to the fluid composition. This was mainly done for obtaining margarite as a stable phase in the computed equilibrium phase diagram, which was not possible when assuming a pure H_2O fluid. The presence of minor amounts of calcite/dolomite supports the addition of some CO_2 to the fluid. No stability field that includes all observed phases could be computed in the equilibrium phase diagram. Biotite and margarite were never predicted to co-exist within a stable assemblage at the given bulk rock chemical composition. Consequently, biotite is inferred not to be part of the peak-metamorphic assemblage. It was probably produced by incremental isothermal decompression to pressures slightly below those of the margarite stability field (Fig. 5.5c). Hence, the observed “peak-metamorphic assemblage” rather consists of two “sub-assemblages” and does not represent a single equilibrium assemblage. The equilibrium phase diagram predicts a relatively narrow stability field for margarite. Further restrictions towards higher pressure are given by the disappearance of plagioclase as well as the appearance of staurolite. Hence, peak-metamorphic conditions are estimated at 0.65-0.8 GPa and 500-540 °C (Fig. 5.5c). Additional information, especially regarding the prograde path, can be deduced by the intersection of the computed isopleths of the garnet cores reflecting the P-T conditions established during the initiation of the garnet growth. The intersection of garnet isopleths is considerably shifted away from the “garnet-in” line, indicating 0.6-0.7 GPa around 500 °C for the initial stages of garnet growth (Fig. 5.5c). As mentioned above, biotite appears to have formed along the retrograde path after a slight decompression from the peak-metamorphic stage. Peak-metamorphic temperatures around 525 °C obtained by the RSCM method confirm the estimates based on the computation of the equilibrium phase diagram and are in agreement with a retrograde formation of biotite.

BLE 0510: This sample belongs to the Valaisan derived metasediments. The appearance is very similar to that of sample LUZ 0444. The mineral assemblage again consists of biotite, plagioclase, white mica, chlorite and quartz although the metamorphic conditions related to Barrow-type overprint are considerably higher. It is noteworthy to mention that zoisite/clinozoisite is mostly found in the form of inclusions in biotite and plagioclase and only rarely in the rock matrix where it shows considerable resorption. As described in the above samples porphyroblasts related to Barrovian overprint such as plagioclase, biotite and zoisite/clinozoisite show no shape preferred orientation and clearly overgrow a pre-existing main foliation. Particularly biotite, referred to as “Querbiotit”, forms spectacular flakes up to 0.5 cm in size and grows across the main foliation.

The equilibrium phase diagram calculated in the NaCaKFMASH system for the bulk rock composition given in Table 5.3 is shown in Figure 5.5d. The predicted stability field of the observed peak-metamorphic assemblage is very large and ranges between 0.3-0.9 GPa and 350-525 °C, respectively. The temperature interval is constrained by the disappearance of zoisite/clinozoisite towards higher temperatures and by the disappearance of biotite towards lower temperatures. The appearance of garnet delimits the stability field towards higher pressures. Obviously, the peak-metamorphic temperatures obtained by the RSCM method does not overlap with the predicted stability field of the observed assemblage and is considerably shifted towards higher temperatures in the 530-540 °C range, i.e. beyond the “zoisite/clinozoisite-out line” (Fig. 5.5d). However, as mentioned above, zoisite/clinozoisite is mainly found as inclusions in biotite and plagioclase and only to a minor extent in the rock matrix where it is resorbed.

This supports the slightly higher temperatures predicted by the RSCM method and the establishment of peak-metamorphic conditions that originally lay beyond the “zoisite/clinozoisite-out line”. The combination of calculated isopleths for the Si-content in white mica as well as peak-metamorphic temperatures obtained by the RSCM method allow for a further restriction of peak-metamorphic conditions of 0.5-0.65 GPa and 510-550 °C for late-stage Barrow-type thermal overprint (Fig. 5.5d).

GRU 053 & MOL 051: These two samples are Al-rich metapelites from Europe-derived metasediments that tectonically directly underlie the Valaisan Bündnerschiefer, i.e. they are from the same tectonic position as the so-called Peiden slices. The observed mineral assemblage consists of staurolite, kyanite, garnet, biotite, plagioclase, white mica and quartz, an assemblage that is characteristic for metapelites from the north-eastern Lepontine thermal dome (southern Lukmanier and Pizzo Molare areas; Fig. 5.1b) indicating peak-metamorphic conditions of lower/middle amphibolite facies conditions. Garnet generally shows an almandine-rich composition with a typical prograde zoning characterized by a spessartine component that decreases from core to rim and a pyrope content increasing from core to rim. The zoning regarding the grossular and almandine component is weak, however (Tab. 5.4). Such “normal/prograde zoning” is generally interpreted to result from primary growth during increasing temperatures (e.g. Spear et al. 1991; Spear & Markussen 1997; Tinkham & Ghent 2005). As above described for the other samples all porphyroblasts related to Barrovian overprint, such as staurolite, kyanite, garnet, biotite and plagioclase, show no shape preferred orientation and clearly overgrow a pre-existing main foliation.

The equilibrium phase diagrams calculated in the NaCaKFMASH system for the bulk rock compositions given in Table 5.3 are shown in Figures 5.5e and f. Although kyanite is unambiguously present in both samples no stability field could be computed for co-existing staurolite and kyanite. The reason for the absence of kyanite in the calculated stability fields is not known, but most probably related to problems in the thermodynamic database. Ignoring the absence of kyanite a stability field ranging from 0.45-0.75 GPa and 550-650 °C is predicted for sample GRU 053, while 0.5-1.1 GPa and 575-650 °C are computed for sample MOL 051 (Figs. 5.5e & f). In both samples the appearance of chlorite delimits the stability field towards lower temperatures while the pressure is constrained by the disappearance of garnet towards lower pressures. The disappearances of staurolite in sample GRU 053 and that of biotite in sample MOL 051 constrains the upper bound of the pressure interval. Calculations of isopleths for X_{Mg} in staurolite and X_{Mg} in co-existing biotite for sample GRU 053, as well as the peak-metamorphic temperatures in the range of 550-590 °C determined by the RSCM method allow for a further restriction of the equilibrium stability field, and predicting peak-metamorphic conditions for Barrovian overprint of 0.55-0.8 GPa and 560-600 °C (Figs. 5.5e & f). Additional information regarding the prograde path, i.e. the initial stages of garnet growth are deduced from the intersection of the computed isopleths from the garnet cores revealing P-T conditions around 0.6-0.65 GPa at 520-535 °C, as well as 0.7-0.75 GPa and 525-540 °C for GRU 053 and MOL 051, respectively. (Figs. 5.5e & f).

5.4.3. Transition from subduction- to collision-related metamorphism

In the previous chapter we presented new P-T estimates for both the early HP/LT metamorphic event documented by the mineral assemblage consisting of Fe-Mg carpholite, chloritoid, white mica and chlorite as well as subsequent gradual Barrow-type overprint increasing from north-east to south-west. Figure 5.6 summarizes all these peak-metamorphic estimates and clearly shows the two contrasting types of metamorphic events present in the investigated area: subduction-related HP/LT metamorphism

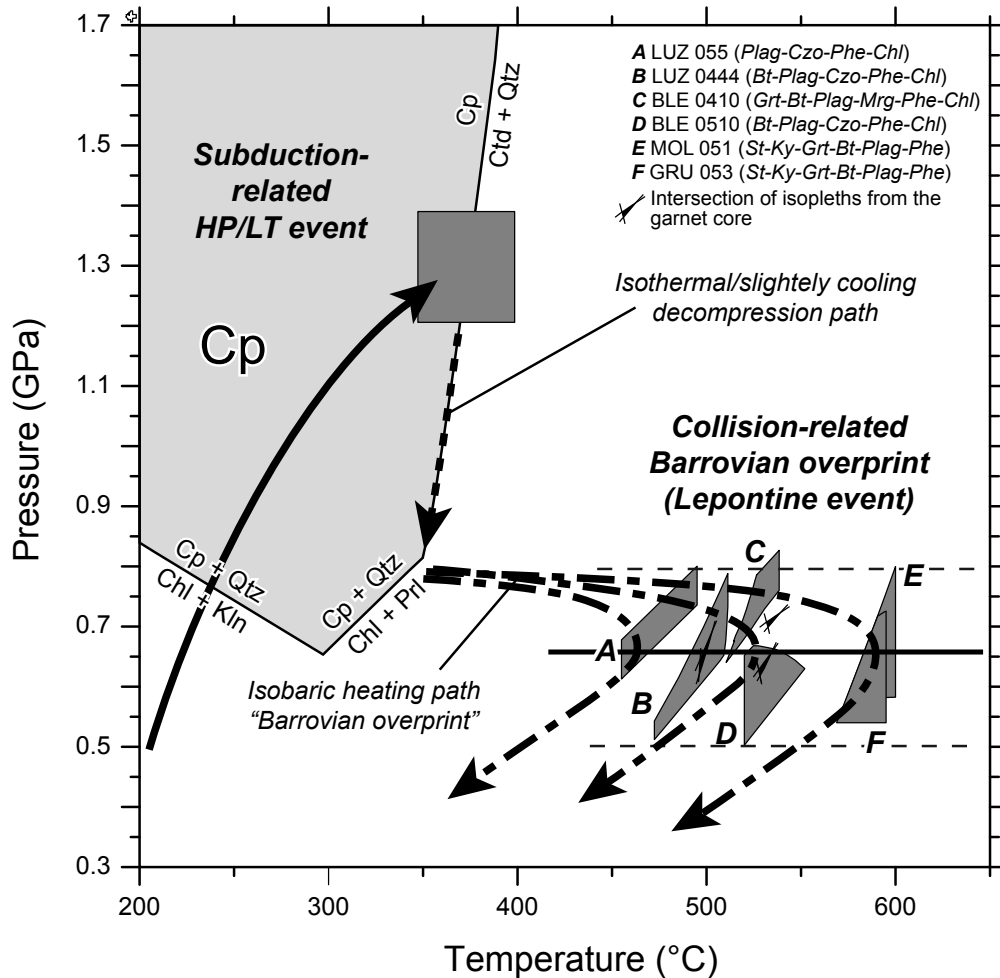


Fig. 5.6: Summary of P-T estimates for all studied samples including both metamorphic events: early subduction-related HP/LT event documented by the occurrences of assemblages containing Fe-Mg carpholite followed by a collision-related Barrovian overprint (generally referred to as Lepontine metamorphism) gradually increasing towards the south-west (as indicated by the succession A-F). Peak-pressure conditions were taken from Figure 5.4. Fields A-F represent the overlap between the stability fields computed with DOMINO and the peak-metamorphic temperature range estimated by the RSCM method presented in Figure 5.5. Additionally three intersections of isopleths (almandine, grossular and pyrope) from cores of garnet porphyroblasts are also shown and indicate P-T conditions established during the initial stages of garnet growth.

at 1.2-1.4 GPa and 350-400 °C and collision-related Barrovian overprint at 0.6-0.75 GPa with gradually increasing temperatures towards the south-west that range from 450-480 °C in the Val Luzzzone up to 570-590 °C at Pizzo Molare. Wiederkehr et al. (2008) demonstrated that Barrow-type overprint unambiguously represents a late, discrete heating pulse separated by at least two deformation events including already substantial decompression from the early HP/LT event. The new P-T data presented in this study address the progressive, gradual Barrovian overprint of the HP/LT rocks and clearly show that the Barrow-type overprint is dominated by increasing temperatures from north-east towards south-west, while pressures remain rather constant and are at around 0.6-0.75 GPa (Fig. 5.6). Hence, Barrovian thermal overprint at the north-eastern Lepontine dome represents a late-stage, more or less "isobaric" metamorphic event.

5.5. Deformation history and discussion of the regional variability regarding orientation and intensity of studied structures

In the investigated area four ductile deformation phases (D1 – D4) are separated from each other and clearly documented by overprinting patterns visible on a macroscopic to microscopic scale. A detailed description of the distinct deformation events and its associated structures as well as a correlation with adjacent tectonic units is given in Wiederkehr et al. (2008). Hence, the different deformation events and corresponding structures will only briefly be presented here and the following attention will focus on the discussion of their regional variability.

5.5.1. Variability of the overall architecture of the study area

As depicted in Figure 5.7 the overall architecture of the study area is characterized by complex and polyphase folding of metasediments in the frontal parts of Europe-derived basement nappes (i.e. from bottom to top Gotthard, Leventina-Lucomagno, Simano and Adula; Thakur 1973; Milnes 1974; Voll 1976; Kupferschmid 1977; Probst 1980; Etter 1987; Wiederkehr et al. 2008). The present day geometry is largely dominated by the interaction of D3 and D4 deformation events (corresponding to Domleschg and Chièra phase, respectively), both representing late-stage nappe-refolding events that induced strong modifications of the already established nappe-stack (e.g. Schmid et al. 1996; Wiederkehr et al. 2008). D3 deformation is characterized by large-scale tight to isoclinal folding reaching amplitudes of some 10 km, the most prominent one being represented by the Lunschania antiform (Voll 1976; Probst 1980). However, also the corresponding Valzeina and Alpettas synforms as well as the Darlun antiform are attributed to the D3 event (Fig. 5.7; Derungs 2008; Wiederkehr et al. 2008). Towards the south-west all D3 syn- and antiforms were progressively overprinted by subsequent D4 deformation, characterized by rather open, staircase-like syn- and antiforms related to back-folding, best expressed by the large-scale, tight Chièra synform producing the Northern Steep Belt (Milnes 1976). However, this Northern Steep Belt is only well developed in the westernmost portions of the study area (Fig. 5.7e) and in the westerly adjacent areas of the northern Lepontine dome. Towards the east, i.e. Val Luzzzone and the area around Vrin east of Piz Terri (Fig. 5.1b) the Northern Steep Belt and associated D4 deformations progressively fade out as is expressed by a gradual and drastic reduction of D4 strain intensity (Fig. 5.7). While the overall structure in the SW, i.e. around the Lukmanier and Pizzo Molare areas, is dominated by a steeply N-dipping main foliation and tight D4 folds, the Chièra and Dötra synforms being the most prominent ones (Figs. 5.7d & e; Etter 1987), the main foliation gradually rotates through the vertical and finally steeply dips towards the S in the Val Luzzzone further east (Fig. 5.7c). Only moderately S-dipping foliations are typical for the more easterly adjacent areas (Figs. 5.7a & b). Associated with the overall change in orientation of the main foliation is a gradual decrease in the intensity of D4 folding as such, relatively tight folds in the SW change to rather open folds towards the NE (Figs. 5.7b & c). Around the easternmost area of Vrin D4 deformation is completely absent (Fig. 5.7a).

5.5.2. Variability of structural elements corresponding to distinct deformation events

All measured structural elements related to distinct deformation events are plotted in Figure 5.8. Due to the strong changes in the overall architecture the study area was subdivided into six domains, i.e. the areas around Molare, Lukmanier, Luzzzone, Vrin, Vals/Safien S, and Vals/Safien N, respectively (see map in the lower right of Fig. 5.8 for extensions of the different domains). In the following we briefly

present the overall trends of the different structural elements and in particular we highlight the variability of the measured structural elements.

The orientation of the main foliation changes dramatically due to the presence of polyphase deformation events. Whereas in the westernmost part of the study area, i.e. around Lukmanier the main foliation generally deeply dips towards the N (Northern Steep Belt), a general south-dip is found in the

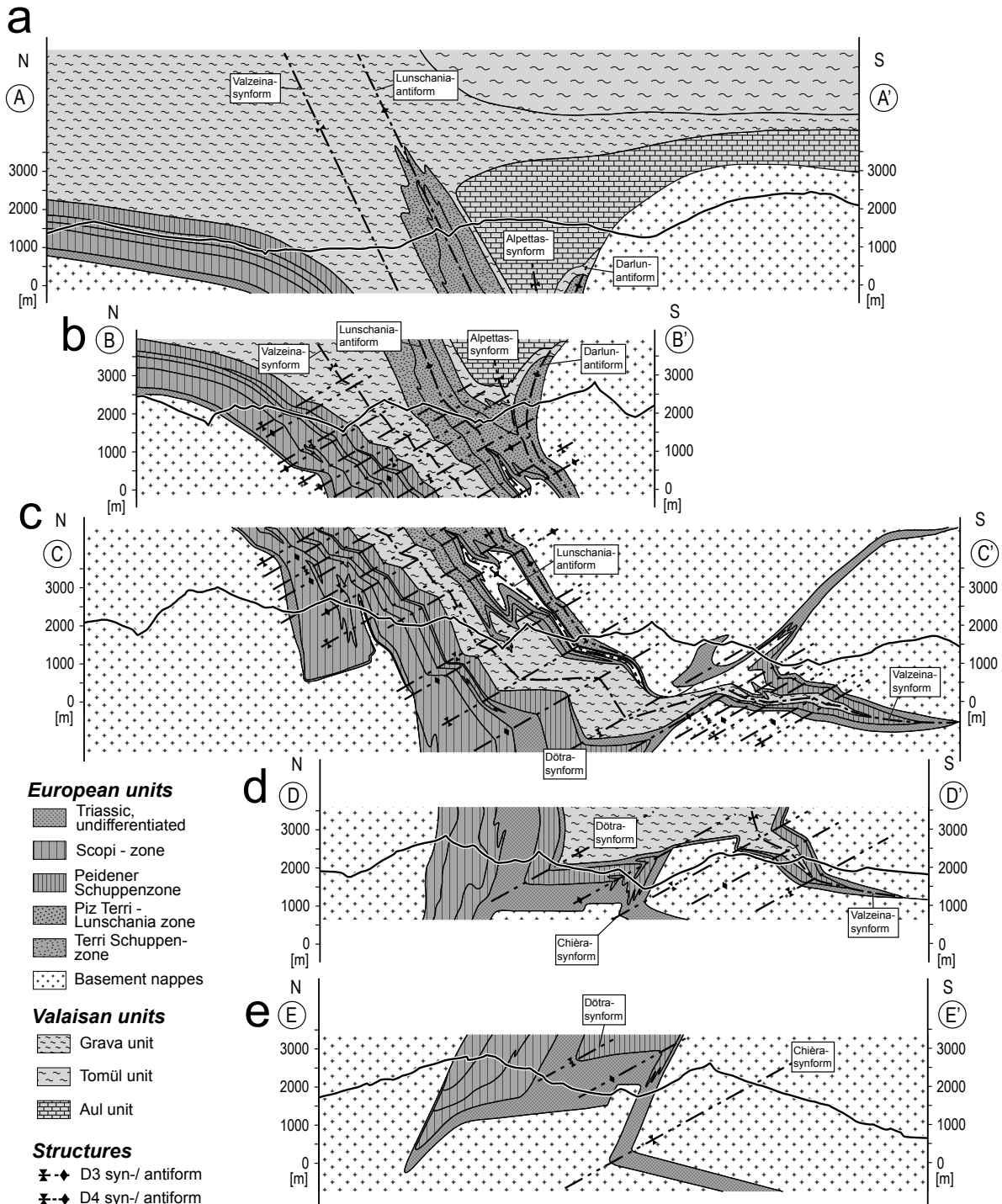


Fig. 5.7: Across-strike cross-sections through the north-eastern rim of the Lepontine structural dome and easterly adjacent areas. Traces of cross-sections (a) - (e) are indicated in Fig. 5.1b. The cross-sections were constructed by projection towards east and west by using (a) local azimuth and plunge of the Lunschania antiform (060/12) for the northern part and a plunge of 20° to the east for the southern part of the cross section; (b) local azimuth and plunge of the Lunschania antiform (064/16); (c) local azimuth and plunge of Chièra phase related fold axes (090/30); (d) local azimuth and plunge of Chièra phase related folds axes (090/15) for the northern part and (110/12) for the southern part of the cross-section; (e) local azimuth and plunge of Chièra phase related folds axes (090/20).

northern parts of Valsertal and Safiental, respectively (Fig. 5.8). In the intermediate domains the poles to the main foliation are distributed along great circles, indicating subsequent folding caused by D3 and D4. Whereas the calculated great circles and corresponding poles reflect a D4 fold axis around Molare and Luzzzone (Molare = 113/13, Luzzzone = 081/28), overprint by D3 is inferred for the easterly adjacent areas Vrin and Vals/Safien S, based on the already mentioned fact that D4 deformation fades out towards

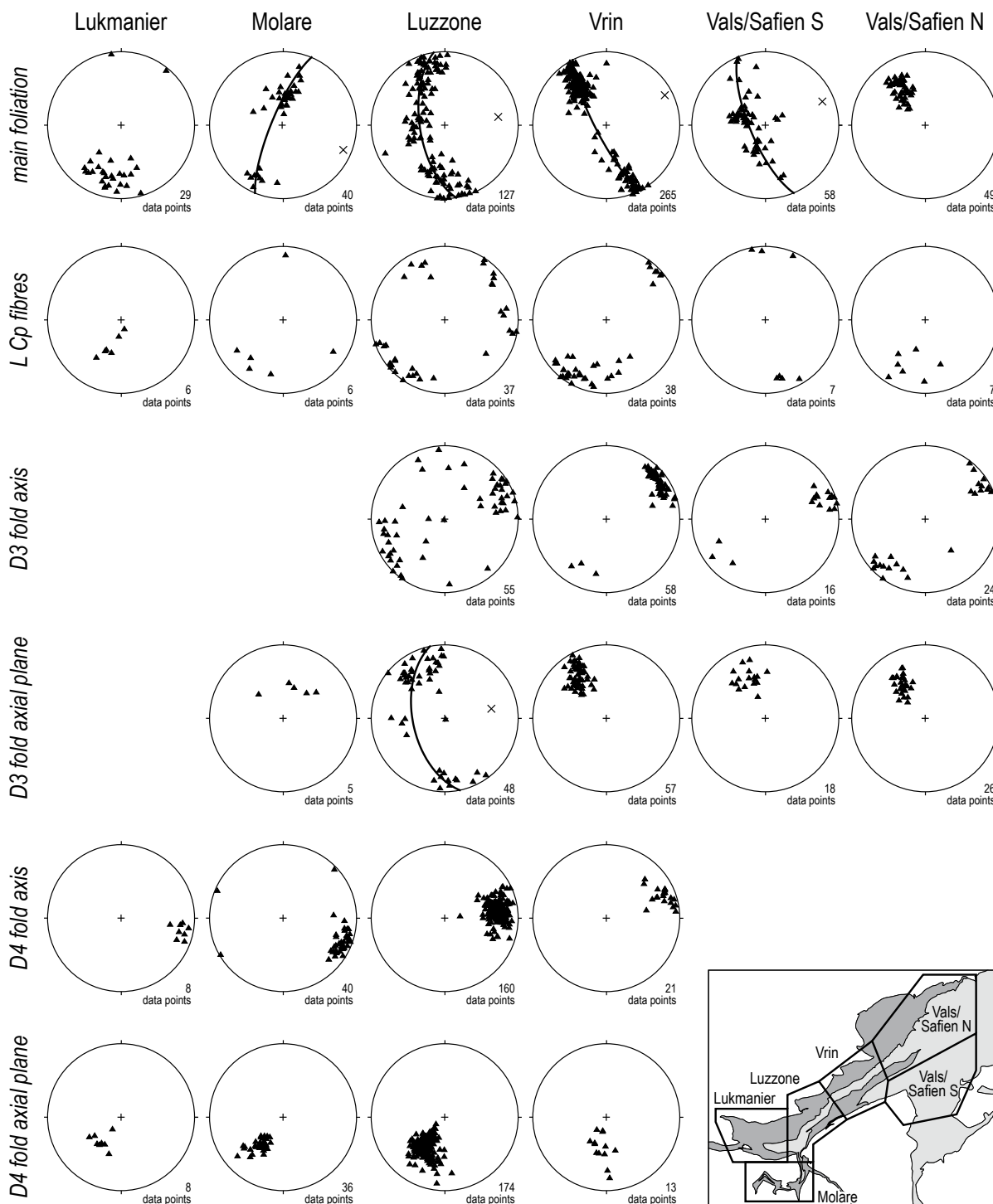


Fig. 5.8: Structural data from the study area grouped into six domains. The location of the different domains is given in the map on the lower right. Note that all planar structural elements are plotted as poles. The following poles of great circles have been calculated for main foliation: 113/13 (Molare), 081/28 (Luzzzone), 063/12 (Vrin), 067/17 (Vals/Safien S); for D2 fold axial plane: 078/36 (Luzzzone). L Cp fibres: lineation formed by fibrous quartz representing pseudomorphs after Fe-Mg carpholite.

the E and also based on the similarities between constructed and measured D3 fold axes (Vrin = 063/12, Vals/Safien S = 067/17; Fig. 5.8).

Structural elements corresponding to D3 deformation are generally characterized by NE – SW trending fold axes and rather steep to the SE dipping fold axial planes (Fig. 5.8). D3 fold axes commonly dip at low angles to the NE or, particularly in the areas of Luzzzone and Vals/Safien N, are rather flat lying and dipping towards NE and SW, respectively. Mainly in the Luzzzone area the D3 fold axes show a large variability in orientation, due to pervasive overprint by subsequent D4 folding; a NE – SW trend can be guessed at nevertheless. The effect of D4 deformation is also visible by a look at the orientation of D3 fold axial planes that show completely different geometries in the areas around Luzzzone and Molare, respectively. Particularly in the Luzzzone area a clear interference between D3 and D4 folding is deduced by the great circle distribution of poles corresponding to D3 fold axial planes (calculated pole of the constructed great circle = 078/36, similar to the orientation of D4 fold axis).

Fold axes and fold axial planes formed during D4 show rather consistent orientations in the different domains (Fig. 5.8). Whereas the fold axial planes remain constant over the entire study area, dipping moderately towards N – NE, the D4 fold axes are characterized by considerable rotation from an ESE trend at Lukmanier/Molare to an E or ENE trend towards Luzzzone and Vrin (Fig. 5.8). Additionally, a significant change of dip is observed going from SW to NE: While D4 fold axes around Lukmanier/Molare in the SW and near Vrin in the NE are characterized by a moderate dip they significantly steepen in some portions of the Val Luzzzone (Fig. 5.8).

As shown by Wiederkehr et al. (2008) and mentioned above relics of the early HP/LT event are restricted to carpholite-bearing quartz-calcite veins/segregations. These veins are generally characterized by a fibrous appearance representing macroscopically visible pseudomorphs after Fe-Mg carpholite fibres and have been interpreted as shear fibre veins (Weh & Froitzheim 2001). These fibres are interpreted to represent a lineation formed by fibrous growth of Fe-Mg carpholite during the formation of these veins at HP/LT conditions by D1. The orientation of these fibres is characterized by a large variability but a general NE – SW to NW – SE strike can be inferred (Fig. 5.8; L Cp fibres). However, it is difficult to attribute a specific geodynamic significance to this syn-D1 lineation due to the fact that the carpholite fibres merely represent the opening of the veins/segregations than a real transport direction reflecting tectonic movements. Also, the orientation of this D1 lineation is no more the original one due to intense overprinting and reorientation by later deformations.

5.5.3. Relationships between deformation and metamorphism

The relationships between deformation and metamorphism were recently highlighted by detailed structural and petrological investigations (Wiederkehr et al. 2008) and by the assessment of isotherm contours obtained by Raman spectroscopy of carbonaceous matter (RSCM method) in three domains (Wiederkehr et al. *submitted, b*). Both these studies showed that (1) subduction-related HP/LT metamorphism and collision-related Barrovian overprint are clearly separated by two deformation events, and (2) that amphibolite facies overprint post-dates D3 deformation as expressed by mineral isograds and isotherm contours cross-cutting the D3 Lunschania antiform. In the following we discuss the relationships between the variability of the structural elements and the inclination of the isotherm contours obtained by the RSCM method.

The study of Wiederkehr et al. (2008) clearly showed that the mineralogy of the metasediments exposed along the Val Luzzzone dramatically changes and is characterized by the progressive appearance

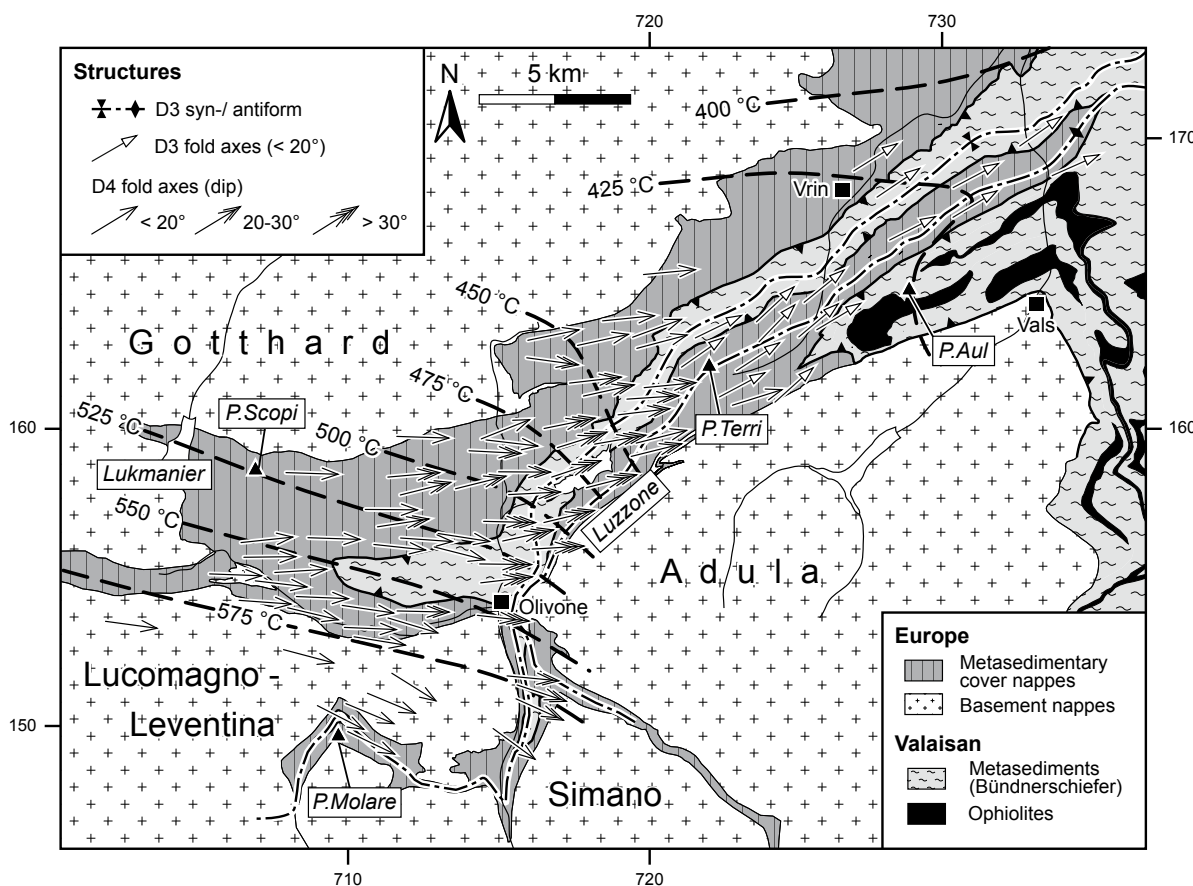


Fig. 5.9: Geological map of the north-eastern border of the Lepontine dome showing the relationships between isotherm contours determined by the RSCM method (see Wiederkehr et al. *submitted, b*) following the calibration given by Rahl et al. (2005) and overall trend of azimuth and plunge of D3 and D4 fold axes.

of newly grown minerals related to Barrovian overprint such as zoisite/clinozoisite, plagioclase, biotite and garnet. Another recent study presented peak-metamorphic temperatures determined by the RSCM method and demonstrated that the Val Luzzone is characterized by a strong thermal gradient, documented by the narrow spacing of the constructed isotherm contours (Wiederkehr et al. *submitted, b*). Hence, both studies showed that the NE border of the Lepontine thermal dome is located in the Val Luzzone. Figure 5.9 shows the relationships between constructed isotherm contours determined by the calculation of peak-metamorphic temperatures following the calibration given by Rahl et al. (2005) and the fold axes of D4 and D3, respectively. Towards the north-east D4 deformation gradually fades out and further east the geometry of the nappe-stack is dominated by D3 structural elements, as well as by isotherm contours that are folded around the Lunschania antiform. Considering the measured structural elements presented in Figure 5.8 it is noteworthy that the D4 fold axes, representing the overall inclination of the entire nappe stack in the SW part of the study area, are characterized by a rather moderate plunge around Lukmanier and Pizzo Molare as well as around Piz Terri, whereas in the intermediate part (i.e. Val Luzzone) the D4 fold axes are significantly steeper. Interestingly, this steepening of the D4 fold axes coincides with the area where the isotherm contours are more closely spaced (Fig. 5.9). As shown by Wiederkehr et al. (*submitted, b*) and also visualized in Figure 5.10 these closely spaced isotherm contours are directly coupled with steeply inclined contours in along strike profile view. Consequently, the location of the steep isotherm contours coincides with the steepening of D4 fold axes (Fig. 5.10).

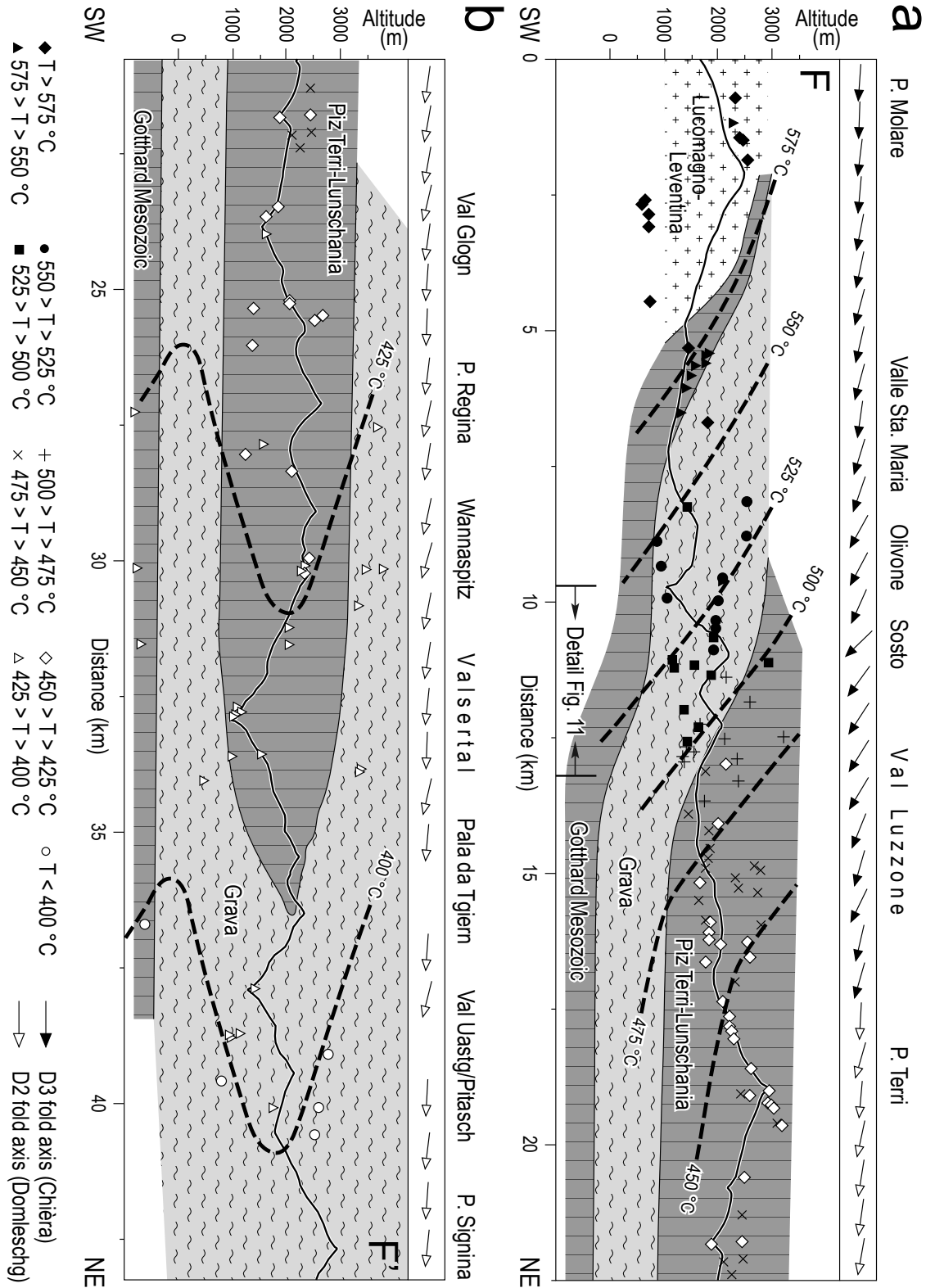


Fig. 5.10: Along-strike profile with samples projected from within a 14 km wide corridor parallel to D3 Lunschania antiform axial trace (050/10). Trace of the cross-section is given in Fig. 5.1b. The slopes of the isotherm contours were estimated within the plane of the cross section after projecting the sample locations and associated peak-metamorphic temperature into the cross-section plane. The geological information has tentatively constructed by the intersection of across-strike profiles shown in Figure 5.7 and by considering the general trend of major structural elements such as D3 and D4 fold axes as well as plunge of the main foliation. Samples were projected horizontally and parallel to the constructed peak-metamorphic isotherm contours given by Wiederkehr et al. (submitted, b) based on the RSCM temperatures estimated following the calibration given by Rahl et al. (2005) in the case of isotherms cross cutting through the Lunschania antiform; and in the case of folded isotherms the samples were projected by taking into account the plunge of the main foliation. (a) south-western part of cross-section, (b) north-eastern part of the cross-section.

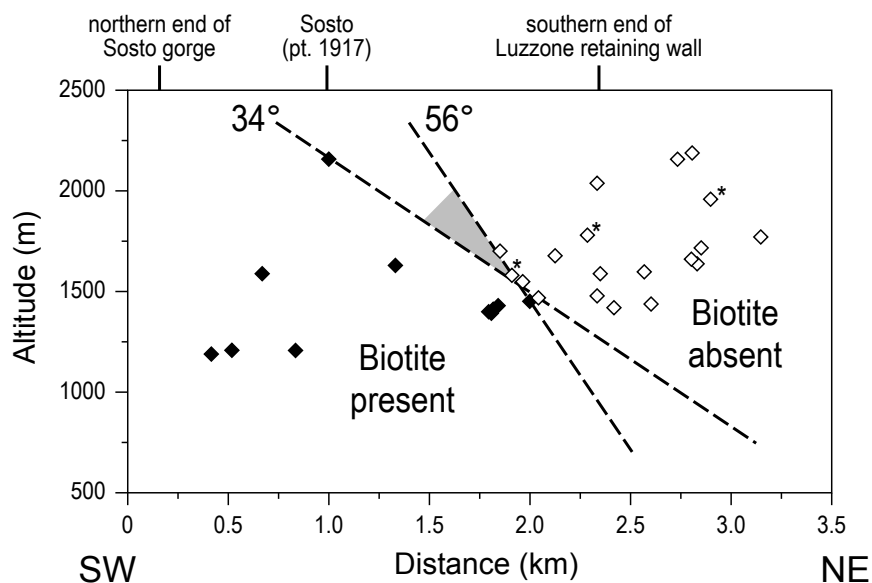


Fig. 5.11: Altitude vs. distance diagram showing the occurrences of biotite in the Val Luzzzone, see Figure 5.10 for exact location of the profile. The samples were projected horizontally from within a 4 km wide corridor and perpendicular to the trace of axial plane of D3 Lunschania antiform. From the distribution of biotite a plunge of 34-56° for the “biotite-in isograde” is inferred. Samples marked with an asterisk are taken from Frey (1967).

From the altitude vs. distance diagram shown in Figure 5.10a an inclination of some 40° towards the NE is inferred for the isotherm contours related to Barrovian overprint. This is slightly steeper than for the plunge of the D4 tectonic structures observed along a SW – NE cross-section. The inclination of the contours has been validated by considering the “biotite-in isograde” cross-cutting the Lunschania antiform in the Val Luzzzone; the occurrences of biotite were projected into the trace of cross-section presented in Figure 5.10 and an inclination for the “biotite-in isograde” in the range of 34-56° can be deduced, in good agreement with the estimates based on the RSCM method (Fig. 5.11). Towards the NE the overall geometry of the metasedimentary units is characterized by rather flat lying D3 fold axes gently dipping towards the NE, as well as by isotherm contours folded by the Lunschania antiform as tentatively delineated in Figure 5.10b.

The following conclusions regarding the relationships between structures and constructed isotherm contours reflecting peak-metamorphic temperatures can be made (see also Figs. 5.9 & 5.10):

- 1) The strongest thermal gradient represented by the narrowly spaced arrangement of steeply inclined isotherm contours is found in the Val Luzzzone and coincides with the significant steepening of D4 fold axes.
- 2) The constructed isotherm contours cross-cutting the D3 Lunschania antiform are related to late-stage Barrovian overprint and are more or less oriented parallel to the traces of the fold axial planes of D4 (compare Figs. 5.1b & 5.9).
- 3) The Val Luzzzone is characterized by narrowly spaced and steeply dipping isotherm contours at the north-eastern border of the Lepontine thermal dome. A maximum dip of 34-56° towards the NE is inferred by considering peak-metamorphic temperatures (Fig. 5.10) as well as by the occurrences of first biotite (“biotite-in isograde”; Fig. 5.11); this dip is slightly steeper compared to the overall plunge towards the E of the entire nappe-stack as evidenced by the D4 fold axes.
- 4) The inclination of the isotherm contours is strongly coupled with the overall trend of the plunge of the D4 fold axes; it is rather flat lying around Pizzo Molare and Piz Terri and considerably steeper in Val Luzzzone.

- 5) Towards the north-east D4 deformation continuously fades out and D3 fold axes become the dominant structural elements further east. This structural change coincides with the transition in the attitude of the constructed isotherm contours. In general the isotherm contours cut through the D3 Lunschania antiform in the presence of D4 deformation, i.e. west of Piz Terri. Towards the E and in the absence of D4 structures, however, the contours are seen to be folded by the Lunschania antiform.

5.6. Interpretation and geodynamic implications

5.6.1. Timing constraints and metamorphic evolution of the study area

The new P-T data and structural observations combined with recent investigations in the same area (see Wiederkehr et al. 2008; *submitted, a*; *submitted, b*) allow for reconstructing a complete P-T-t-d path that provides essential constraints regarding the geodynamic evolution of the Valaisan and adjacent European paleogeographical domains. Based on the investigations of carbonaceous matter at least three temporally distinct thermal events have been recorded and can be related to specific geodynamic stages by linking the peak-metamorphic temperatures with the observed mineral assemblages indicative for characteristic P-T conditions (Wiederkehr et al. *submitted, b*).

Relics of the early subduction-related high-pressure metamorphic event have been found in the northern, frontal part of the Adula nappe complex as well as in some portions of the Misox Zone showing peak-temperatures based on the RSCM method in the range of 500-520 °C, in perfect agreement with P-T estimates for the peak-pressure conditions in both northern Adula nappe complex (1.2-1.5 GPa at 470-540 °C, Löw 1987; and 1.1-1.3 GPa at 450-550 °C, Heinrich 1986) as well as the northern Misox Zone (1.0-1.1 GPa at 590-630 °C, Santini 1992; and >1.2 GPa at 460-560 °C, Ring 1992). The interpretation in terms of an “old” thermal structure is supported by the fact that the observed isotherms run parallel to the present day nappe and other tectonic contacts (see discussion in Wiederkehr et al. *submitted, b*). In other words, significant jumps in the RSCM temperatures are found along tectonic contacts. For example, between the northern Adula nappe complex and the surrounding metasediments a “jump” of almost 100 °C is observed. To a minor amount a jump is also observed in the northern Misox Zone where a gap of some 80 °C is found between the Fe-Mg carpholite-bearing Tomül nappe and the upper blueschist/eclogite facies Aul unit. Consequently, the thermal structure pre-dates nappe-emplacement and therefore a connection to the early, pre nappe-stacking high-pressure event is proposed.

The exact timing of peak-pressure metamorphism of both Valaisan as well as adjacent European margin is not well constrained. Some data exist for the Adula nappe complex and indicate an Eocene-age for high-pressure metamorphism based on garnet Sm/Nd isochrons at 42 and 38 Ma (Becker 1993), as well as on zircon SHRIMP data that yield ages in the range of 43 to 35 Ma (Gebauer 1996). For carpholite-bearing metasediments of the Valaisan domain an age of 42-40 Ma for peak-pressure conditions and 36-33 Ma for the following substantial decompression was recorded by $^{40}\text{Ar}/^{39}\text{Ar}$ investigations on white mica associated with Fe-Mg carpholite (Wiederkehr et al. *submitted, a*).

In the eastern part of the study area the observed thermal structure in the temperature interval between 350-425 °C is seen to be affected by D3 deformation, i.e. the constructed isotherms are seen to be folded by the D3 Lunschania antiform (Wiederkehr et al. *submitted, b*). Furthermore the constructed isotherms can be continuously followed across tectonic contacts, i.e. from the high-pressure units such as the Grava nappe and Peiden slices to the low-pressure Scopi unit. This observation clearly indicates

that the establishment of the observed thermal structure post-dates nappe-stacking but pre-dates deformation associated with the formation of the D3 Lunschania antiform. According to Froitzheim et al. (1994) and Schmid et al. (1996) an age between 30 and 25 Ma was inferred for D3 deformation (Domleschg phase) and recently evidenced by $^{40}\text{Ar}/^{39}\text{Ar}$ dating of white mica yielding 25 Ma (Wiederkehr et al. *submitted, a*).

The significance of the thermal event corresponding to the observed temperature distribution pattern is best explained by a greenschist facies overprint. Although the observed peak-metamorphic temperatures are in the same range than the earlier HP/LT event, i.e. 350-400 °C we emphasize a correlation with post high-pressure greenschist facies overprint mainly based by the fact, that the constructed isotherms can be followed continuously across tectonic contacts separating HP- from LP-units. Most probably the formation of post-tectonic chloritoid, typically seen as rosettes that are found to be widespread in the study area far away towards the east in both high-pressure (Peiden slices) as well as low-pressure units (Scopi unit), is related to this metamorphic event. This interpretation is based on the observation, that rosettes of chloritoid became deformed by D3 deformation (Domleschg phase; Fig. 5.3d) indicating that the formation of chloritoid pre-dates D3 Domleschg phase deformation. Probably this interpretation can also explain the rather different distribution of chloritoid in respect to other index minerals such as staurolite, kyanite, biotite, garnet, plagioclase and zoisite/clinozoisite (Fig. 5.2b; Niggli & Niggli 1965; Wiederkehr et al. 2008). Whereas the distribution of staurolite and kyanite agrees well with the concentric shape of the Lepontine dome in the structural and thermal sense, chloritoid can be found far away towards the east around the area of Chur (Niggli & Niggli 1965). The different shape of the mineral isograds indicates that the formation of these index minerals was most probably related to several thermal events that took place at different times. This interpretation is consistent with the observations of Rahn et al. (2002) that suggest an Early Oligocene-age for the formation of chloritoid near Curaglia in the Urseren-Garvera Zone, based on micro-structural observations. The existence of an earlier greenschist facies overprint in respect to Lepontine Barrovian overprint has recently improved by isotopic investigations on allanite occurring in the northern Lepontine (Janots et al. 2009). The formation of allanite is seen to correlate with the appearance of chloritoid and is commonly thought to retain its isotopic signature, and consequently record the age of prograde metamorphism at greenschist facies conditions (Janots et al. 2008). *In situ* SHRIMP Th-Pb dating of allanite yields 31.5-29.2 Ma, which is interpreted to represent the onset of greenschist facies metamorphism at around 430-450 °C (Janots et al. 2009). Furthermore, recently presented $^{40}\text{Ar}/^{39}\text{Ar}$ data of white mica sampled in the Valaisan domain (Engadine window and Safiental) yield ages between 32-29 Ma (Wiederkehr et al. *submitted, a*), i.e. ages that are exactly in the same range as those found by allanite dating. In summary, we interpret the observed thermal structure in the range of 350-425 °C characterized by isotherms folded by the Lunschania antiform and observed in the north-east of the study area to be related to a post nappe-stacking, greenschist facies overprint that was most probably established around some 30 Ma ago, as is indicated by the isotopic ages. This conclusion directly implies more or less isothermal decompression of the HP/LT stage during the 36-33 Ma time interval, as documented by the occurrences of Fe-Mg carpholite pointing to peak-pressure conditions of 1.2-1.3 GPa at 350-400 °C also proposed by earlier studies (Bousquet et al. 2002; Wiederkehr et al. 2008).

Towards the south-west all constructed isotherms clearly cut through the D3 Lunschania antiform, hence indicating that the recorded thermal structure in the range between 450-570/590 °C is younger in respect to D3 deformation (Figs. 5.9 & 5.10). The characteristic onion-shaped distribution of isotherms

typically indicating increasing temperatures towards the south and south-west is related to the so-called Lepontine thermal dome, representing a classical area of Barrovian-type amphibolite facies overprint (e.g. Frey & Ferreiro Mählmann, 1999). Associated with Barrovian thermal overprint is the gradual occurrence of a sequence of porphyroblasts related to progressively increasing temperatures, as documented by the succession in appearance of zoisite/clinozoisite, plagioclase, biotite, garnet, kyanite and staurolite in the order of increasing metamorphic conditions, i.e. peak-metamorphic temperatures (Chadwick 1968; Frey 1969; Fox 1975; Wiederkehr et al. 2008). Recently, Wiederkehr et al. (2008) showed that the initial growth of porphyroblasts related to Barrovian overprint in the beginning stages was entirely static in the north-eastern Lepontine and clearly post-dated D3 deformation. This thermal overprint was sustained until the beginning stages of the last tectonic event (D4, Chièra phase) related to the formation of the Northern Steep Belt. As revealed by our P-T investigations this late stage thermal overprint is mainly controlled by temperature and only minor changes in pressure were found. This observation suggests a more or less “isobaric” thermal overprint, which is in perfect agreement with its late-stage timing in respect to the formation of the Alpine orogenic belt at the time when the present-day architecture of the orogen was almost completed. As shown by recent isotopic studies in the northern Lepontine dome an age of post 20 Ma was inferred for this event (Allaz 2008; Janots et al. 2009; Wiederkehr et al. *submitted, a*). Ages based on monazite dating using *in situ* SHRIMP U-Pb dating yield 19-18 Ma for Barrovian metamorphism in the northern Lepontine dome. This age is interpreted to date the formation of monazite by the breakdown of allanite supposed to be around 560-580 °C, i.e. near the thermal peak of amphibolite facies metamorphism (Janots et al. 2009). Ages in the same range were also obtained by $^{40}\text{Ar}/^{39}\text{Ar}$ dating on both white mica and biotite, yielding ages in the range of 19.0-18.5 Ma for white mica and slightly younger (> 1 Ma) ages for biotite (Allaz 2008; Wiederkehr et al. *submitted, a*). This substantially younger amphibolite facies Barrovian overprint represents a second, collision-related thermal event only observed in the south-western part of the study area.

5.6.2. Implications for the exhumation of HP/LT units

The results presented in this study, combined with findings recently presented by Wiederkehr et al. (2008; *submitted, a*; *submitted, b*), allow for a qualitative discussion concerning the exhumation mechanism of carpholite-bearing blueschist facies metasedimentary units. There are numerous models for the mechanisms responsible for exhumation. These include corner flow, extension or buoyancy forces and many others (see discussion by Platt 1993; Froitzheim et al. 2003). For the investigated area there are two main basic conditions that need to be fulfilled by any model regarding the exhumation mechanism:

1. As revealed by Wiederkehr et al. (2008) substantial decompression took place during the early stages of the formation of the Alpine belt, i.e. during D2 deformation that is associated with nappe stacking and dated at 36-33 Ma (Wiederkehr et al. *submitted, a*). Hence, exhumation was active at an early stage of the formation of the Alpine belt, i.e. during ongoing compression and subduction that includes nappe-stacking associated with thrusting of high-pressure units onto low-pressure units.
2. The overall spatial relationships between the former paleogeographic domains need to be conserved during the exhumation stage, since in general more internal units were thrust onto relatively more-external ones.

These two conditions are satisfied by models that postulate ascent by extrusion within and parallel to a subduction channel by active, forced extrusion (Michard et al. 1993; Burov et al. 2001; Gerya et al.

2002), promoted by slab extraction (Froitzheim et al. 2003) and/or buoyant ascent (Wheeler 1991), but not by models that invoke extension such as those suggested by Ballèvre et al. (1990) and Rolland et al. (2000) for the Western Alps, and by Jolivet et al. (1998b) for the Engadine window. A syn nappe-stacking exhumation process has also been favoured by Bucher et al. (2003 & 2004) for a similar scenario described in the Western Alps (e.g. Le Bayon et al. 2006; Bousquet 2008).

5.7. Conclusions

The metamorphic evolution of the metasedimentary units at the north-eastern rim of the Lepontine dome experienced a polyphase metamorphic evolution characterized by (1) an early, subduction-related HP/LT event at 1.2-1.4 GPa at 350-400 °C documented by the appearance of Fe-Mg carpholite in both Valaisan (Grava and Tomül nappes) and European (Peiden slices and Piz Terri-Lunschania unit) domains. (2) Towards the south-west the blueschist facies metasediments were gradually affected by progressive, collision-related Barrow-type thermal overprint related to amphibolite facies metamorphism of the Lepontine thermal dome starting at 450-500 °C in the Val Luzzzone and reaching 560-600 °C in the northern Valle di Blenio and around Pizzo Molare at more or less constant pressure interval of 0.6-0.75 GPa. Consequently, Barrovian overprint in the north-eastern Lepontine represents a rather “isobaric” thermal event as suggested by a late-stage metamorphic event. This thermal overprint represents a clearly separated heating pulse following isothermal decompression of the earlier HP/LT stage. The two contrasting types of metamorphic events, i.e. subduction-related high-pressure metamorphism and collision-related amphibolite facies overprint are separated by an intermediate greenschist facies stage.

From the new petrologic data presented in this study, combined with recently presented results of investigations by Raman spectroscopy of carbonaceous matter as well as by $^{40}\text{Ar}/^{39}\text{Ar}$ dating we suggest a succession of three distinct metamorphic events:

- 1) *Subduction-related metamorphism* is evidenced by the occurrences of Fe-Mg carpholite in both European (Peiden slices and Piz Terri-Lunschania unit) and Valaisan metasedimentary units (Grava and Tomül nappes) and indicates blueschist facies conditions at 350-400 °C and 1.2-1.4 GPa established at 42-40 Ma. Considerably higher tempered peak-pressure conditions (500-525 °C) are preserved in the internal Mesozoic of the northern, frontal part of the Adula nappe complex as well as in parts of the Misox Zone (Aul unit) reaching upper blueschist to eclogite facies conditions. Substantial decompression of the Valaisan domain was contemporaneous with D2 nappe stacking at 36-33 Ma and was mostly achieved by active extrusion within and parallel to a subduction channel.
- 2) *Early-stage collision-related greenschist facies overprint* preserved only in the eastern part of the investigated area affecting both high-pressure (Peiden slices, Grava and Tomül nappes) as well as low-pressure units (Scopi unit) and is characterized by peak-metamorphic temperatures in the range of 350-425 °C, almost in the same temperature interval as the earlier HP/LT event documented by the existence of Fe-Mg carpholite. Consequently, a more or less isothermal decompression is suggested for the high-pressure units. The thermal structure established during this early greenschist facies overprint is pervasively overprinted by D3 phase deformation, i.e. isotherms are folded by the Lunschania antiform. Recent isotopic investigations based on Th-Pb dating of allanite and $^{40}\text{Ar}/^{39}\text{Ar}$ dating of white mica infer an Oligocene-age around 32-29 Ma for this early-stage collision-related metamorphic overprint.

- 3) *Late-stage collision-related amphibolite facies Barrovian overprint* represents the youngest thermal event only appearing in the south-western part of the study area and is characterized by progressive increasing temperatures starting from 450 °C near Piz Terri up to 570-590 °C around Pizzo Molare as well as south of Mesocco. The concentric, onion-shaped isotherm pattern belongs to the so-called amphibolite facies Lepontine thermal dome and clearly post-dates D3 deformation as shown by isotherms cross-cutting the Lunschania antiform. P-T estimates suggest that a more or less isobaric thermal overprint occurred during a late stage of the Alpine evolution, i.e. substantially after nappe-stacking and -emplacement. Isotopic studies on monazite (U-Pb dating) as well as on white mica and biotite ($^{40}\text{Ar}/^{39}\text{Ar}$ dating) indicate a substantially younger age, i.e. 19-18 Ma for Barrovian overprint in the north-eastern Lepontine dome, compared to both the previous pressure-dominated metamorphism and the up to now unknown early greenschist facies overprint.

This study unambiguously demonstrates the importance of metasediments for the reconstruction of the metamorphic evolution of mountain belts. Furthermore, we showed that particularly low-grade (HP/LT, LP/LT) metasediments, typically devoid of indicative mineral assemblages, were often misinterpreted and provide crucial information concerning the geodynamic evolution of the Alpine orogenic belt when applying a combination of detailed structural, petrologic and geochronological investigations.

Acknowledgements

Excellent preparation of numerous samples by W. Tschudin, as well as great support in the field by G. Derungs, both members of Basel University, is gratefully acknowledged. O. Appelt and D. Rhede from the GeoForschungsZentrum Potsdam are thanked for their help with microprobe analyses. Substantial funding by the Swiss National Science Foundation (project NF-200020-113585 and precursor project NF-200020-103585) is gratefully acknowledged.

Chapter 6

Metamorphism of metasediments at the scale of an orogen: A key to the Tertiary geodynamic evolution of the Alps

This chapter is published as: Bousquet, R., Oberhänsli, R., Goffé, B., **Wiederkehr, M.**, Koller, F., Schmid, S.M., Schuster, R., Engi, M., Berger, A. & Martinotti, G. (2008): Metamorphism of metasediments in the scale of an orogen: A key to the Tertiary geodynamic evolution of the Alps. In: Siegesmund, S. et al. (Eds.): Tectonic Aspects of the Alpine-Dinaride-Carpathian system. Geological Society Special Publications 298, 393-411.

Abstract

Major discoveries in metamorphic petrology, as well as other geological disciplines, have been made in the Alps. The regional distribution of Late Cretaceous – Tertiary metamorphic conditions, documented in post-Hercynian metasediments across the entire Alpine belt from Corsica – Tuscany in the west to Vienna in the east, is presented in this paper. In view of the uneven distribution of information, we concentrate on type and grade of metamorphism; and we elected to distinguish between metamorphic paths where either pressure and temperature peaked simultaneously, or where the maximum temperature was reached at lower pressures, after a significant temperature increase on the decompression path.

The results show which types of process caused the main metamorphic imprint: a subduction process in the Western Alps, a collision process in the Central Alps, and complex metamorphic structures in the Eastern Alps, owing to a complex geodynamic and metamorphic history involving the succession of the two types of processes. The Western Alps clearly show a relatively simple picture, with an internal (high-pressure dominated) part thrust over an external greenschist to low-grade domain, although both metamorphic domains are structurally very complex. Such a metamorphic pattern is generally produced by subduction followed by exhumation along a cool decompression path. In contrast, the Central Alps document conditions typical of subduction (and partial accretion), followed by an intensely evolved collision process, often resulting in a heating event during the decompression path of the early-subducted units. Subduction-related relics and (collisional/decompressional) heating phenomena in different tectonic edifices characterize the Tertiary evolution of the Eastern Alps. The Tuscan and Corsica terrains show two different kinds of evolution, with Corsica resembling the Western Alps, whereas the metamorphic history in the Tuscan domain is complex owing to the late evolution of the Apennines. This study confirms that careful analysis of the metamorphic evolution of metasediments at the scale of an entire orogen may change the geodynamic interpretation of mountain belts.

6.1. Introduction

After more than a century of investigations, the Alps still represent an outstanding natural laboratory for the study of geodynamic processes linked to the evolution of mountain belts in general. The integration of regional geology and metamorphic evolution provides highly needed constraints for increasingly complex quantitative models (e.g. Escher & Beaumont 1996; Henry et al. 1997; Pfiffner et al. 2000).

Major discoveries in metamorphic petrology, as well as other geological disciplines, have been and are still made in the Alps. For example, eclogites were described for the first time in the Eastern Alps (Koralpe, Saualpe massifs) by Haüy (1822). More recently, the discovery of coesite in the Dora Maira unit (Chopin 1984, 1987) proved that continental crust went into subduction, contrary to a still widely held opinion, and returned from great depths. Many others, occasionally less spectacular yet important, petrological discoveries, were also made in the Alps. For instance, studies of metapelites in the Alps starting at the beginning of the 1970s, revealed a specific mineralogy reflecting high-pressure conditions. The most emblematic minerals found in such rocks are ferro- and magnesiocarpholites (Goffé et al. 1973). Besides such discoveries, many holistic attempts have been made to assess the dynamics of this orogen. Niggli & Niggli (1965) applied Barrow's concept to the central Alps and presented a mineral distribution map with mineral isograds reflecting a Lepontine high-temperature event. Zwart (1973) and Zwart et al. (1978) compiled mineral distributions at the scale of the orogen, using the facies concept and available age data in the Alps and elsewhere.

Based on such mineralogical work, Ernst (1971) was able to use the plate tectonic concept for proposing a first modern model for the evolution of the Alps. Such ideas developed further on the basis of work such as that of Dal Piaz et al. (1972), Dal Piaz (1974a, b) and Hunziker (1974), just to name a few. Frey (1969), as well as Trommsdorff (1966), started to investigate metamorphism in isochemical systems provided by shales and siliceous carbonates, respectively. This allowed for quantitatively constraining the Cenozoic temperature evolution in the central Alps. Frey et al. (1999) compiled all available information on the peak temperature distribution, and used the occurrences of eclogites to display the dynamics of the Alpine evolution. Previous works of this kind led to the compilation of a new map showing the metamorphic structure of the Alps (Oberhänsli et al. 2004). This new map was also based on: (1) new tectonic concepts and maps (Schmid et al. 2004); (2) a wealth of new radiogenic age data (for references see e.g. Handy & Oberhänsli 2004, and Berger & Bousquet 2008); and (3) an extension of the facies concept based on mafic to metapelitic rock compositions.

In the Alps, many areas are devoid of index minerals classically observed in mafic and quartzofeldspathic rock systems, allowing a direct comparison to be made. Petrological investigation on metasediments greatly helps to constrain geodynamic evolution of such areas (see Bousquet 2008). One tool to understand such problems better at the orogen scale are maps (Niggli & Niggli 1965; Niggli 1970; Frey et al. 1999; Oberhänsli et al. 2004). This study combines these different sources of information: presenting metamorphism in maps and combining this with metamorphic evolution data. This provides insights into the geodynamics of metasediments inside the orogen. The metamorphism of metasediments can be subdivided into general geodynamic groups: (1) pressure-dominated metamorphism; (2) temperature-dominated metamorphism at intermediate pressures (Barrovian metamorphism), which is often referenced in the literature as HT metamorphism; and (3) contact metamorphic aureoles which are temperature-dominated metamorphism at low pressures. The latter type will be excluded from this contribution because it is only of minor importance in the Alps.



Fig. 6.1: Structural units of the Alps involved and metamorphosed during the late Cretaceous – Tertiary orogeny from Vienna (Austria) to Corsica and Tuscany. The distribution of metasediments, ophiolites and basement rocks is not homogeneous over the whole alpine edifice. In the west, in Tuscany, Corsica and Western Alps, the belt is mainly built of post Hercynian metasediments from oceanic (mainly Piemont-Liguria) or continental (Briançonnais cover and European platform) origin. Several ophiolitic complexes are associated with oceanic sediments (Zermatt, Lanzo, Viso, Voltri). Scarce fragment of basement rocks occur as structural domes (Monte Rosa, Gran Paradiso, Ambin, Dora Maira, Tenda) in the internal parts or are located at the external border of the belt (Mont Blanc, Belledonne, Pelvoux, Argentera). From the Simplon line in the Central Alps to the Eastern Alps mainly basement rocks have been imbricated into the orogenic pile (Leptontine dome, Tauern Window) except for the Engadine window. Upper Austroalpine units are not detailed on the map. Map modified after Froitzheim et al. (1996) and Schmid et al. (2004) with additional data from Bigi et al. (1990) and Koller & Höck (1987).

This paper reviews existing data and presents ongoing work in an attempt to integrate metamorphic studies and Late Cretaceous–Tertiary geodynamic concepts in the Alps. We will illustrate how mineral data obtained from metasediments may constrain the geodynamic evolution of mountain belts in general.

6.2. Metamorphic mineralogy of metasediments

In contrast to mafic complexes or meta-igneous rocks, metasediments commonly crop out continuously over very large areas in many mountain belts, such as the Alps (Fig. 6.1). Since these metasediments cover large areas, this allows to simultaneously observe their structural and metamorphic evolution, and thus to decipher the geodynamic frame. However, since Barrow (1893, 1912) and Eskola (1929), the definition of metamorphic facies, as well as petrographic work on metamorphic rocks, was mainly focused on mafic systems (Evans 1990; Frey et al. 1991; Carswell 1990).

Detailed studies on pelitic systems (Yardley 1989; Koons & Thompson 1985; Spear 1993; McDade & Harley 2001) are only available for medium- to high-temperature metamorphic conditions. Metamorphic studies addressing low-temperature conditions extended methods taken from studies on diagenesis or anchimetamorphism, such as illite crystallinity, vitrinite reflectance or clay mineralogy (Frey & Robinson 1999) which lack good possibilities of pressure and temperature calibration. Spectacular improvements on the knowledge of mountain belt evolution based on the study of metasediments could only be made starting with the discovery of coesite in metasediments (Chopin 1984) and other work on ultra high-pressure rock systems (UHP) in general (Coleman & Wang 1995; Chopin & Sobolev 1995; Massonne & O'Brien 2003).

6.2.1. Petrogenetic grids

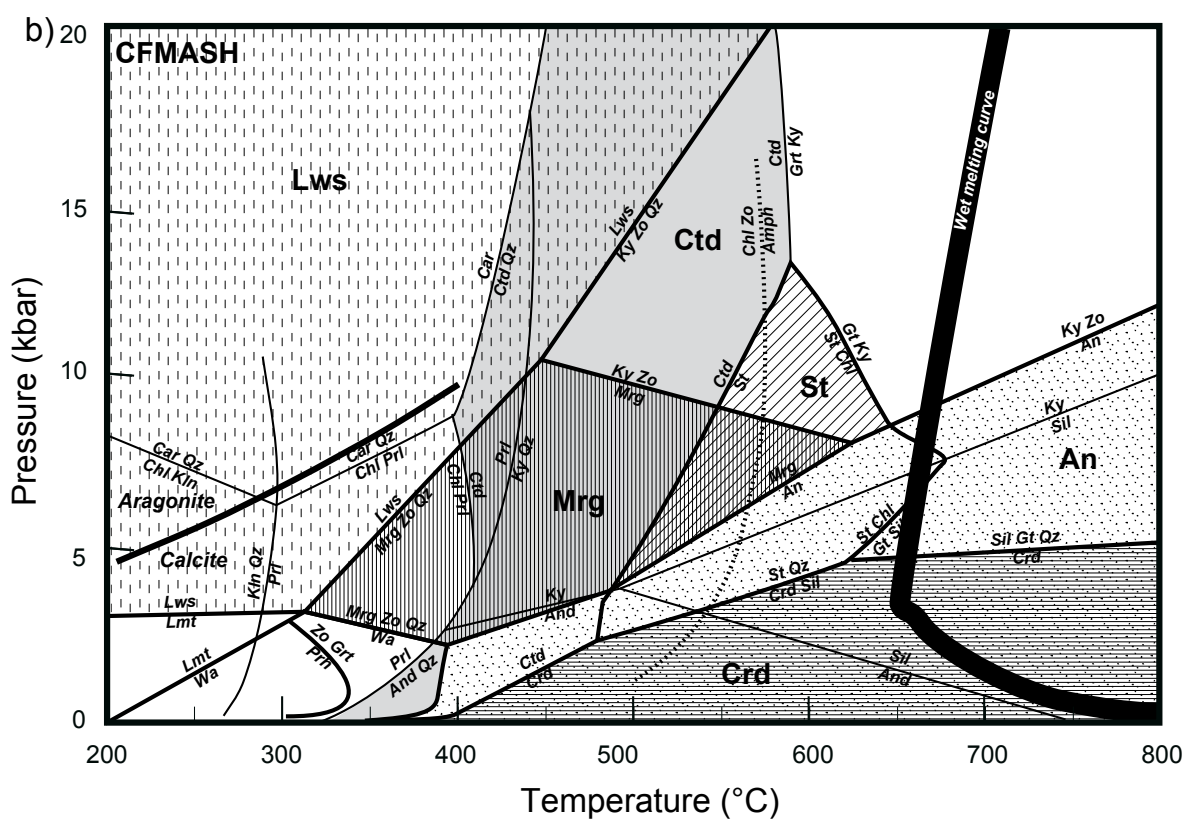
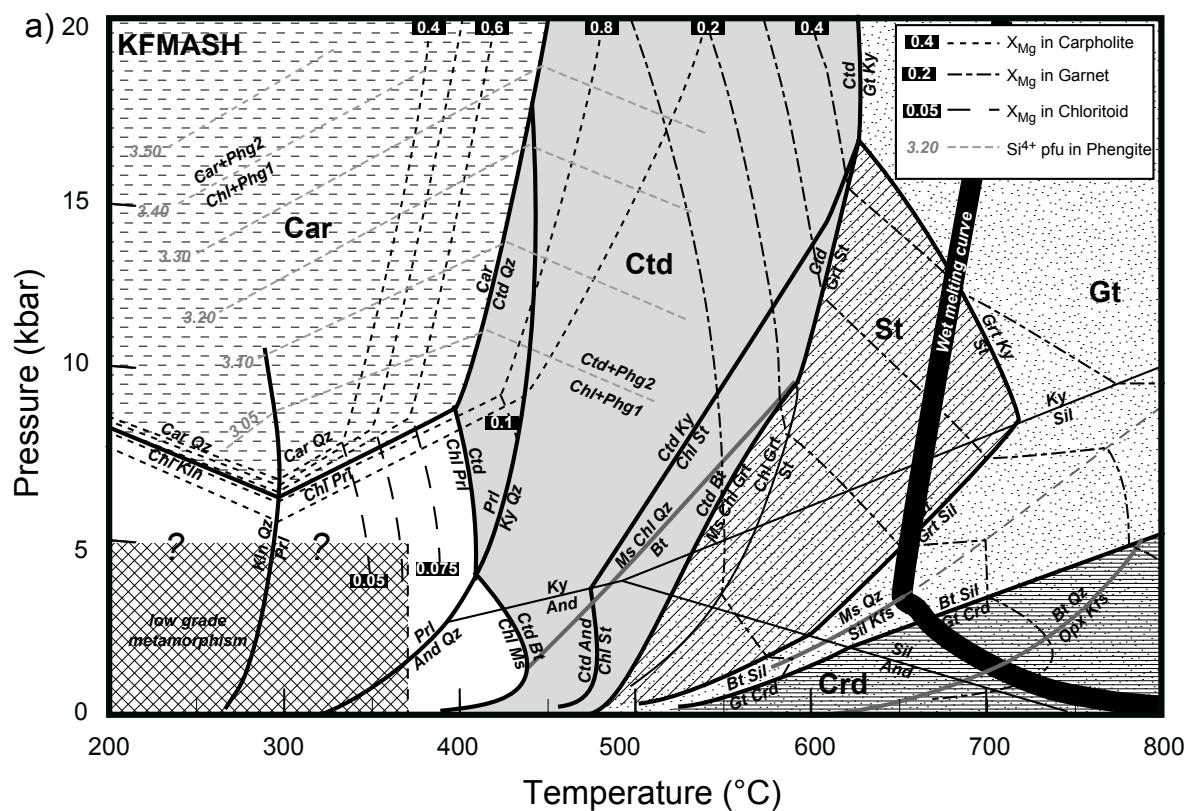
Classical index minerals, such as pumpellyite, glaucophane or jadeite, observed in mafic and quartzofeldspathic rock systems, are unfortunately rarely observed in Alpine metasediments. Nevertheless, metasediments have highly variable chemical and mineralogical compositions that represent an important geothermobarometric potential. Figure 6.2 shows petrogenetic grids for the KFMASH and CFMASH subsystems that integrate field observations, experimental data and thermodynamic modelling using an internally consistent database. This new kind of compilation covers a large P–T space, extending from low- to high-pressure (0–2 GPa) as well as from low- to high-temperature (200–800°C).

Mineral assemblage containing ferro-magnesiochloritoid with phengite, chlorite and quartz is one of the most emblematic mineral assemblages of metasediments in the KFMASH system (De Ro-

Fig. 6.2: Petrogenetic grids for metapelites for a temperature range from 200 to 800°C. (a) in the KFMASH (K_2O -FeO-MgO- Al_2O_3 - SiO_2 - H_2O) system, the grid is strongly temperature-controlled. The appearance of assemblages, from (Fe, Mg)-carpholite assemblage at HP or from chlorite-pyrophyllite assemblage delimits the low-temperature domain from the middle temperature one at around 400°C. The exact temperature limit depends on rock and mineral chemistry. At higher temperature conditions, the breakdown of chloritoid into garnet or staurolite indicates the transition towards high-temperature domains between 500 and 600°C depending on pressure conditions as well as on rock and mineral chemistry. (b) In the CFMASH (CaO-FeO-MgO- Al_2O_3 - SiO_2 - H_2O) system, the temperature control is less important. While under LT conditions, lawsonite is the main stable mineral, sometimes coexisting with (Fe, Mg)-carpholite, at middle and HT conditions, margarite and staurolite stability fields are pressure-dependent. We note a large cordierite-stability field in the CFMASH system.

Diagrams drawn from field experience and theoretical studies after Spear and Cheney (1989), Spear & Wang (1991), Vidal et al. (1992), Oberhänsli et al. (1995), Bousquet et al. (2002), Proyer (2003), Wei et al. (2004), Wei & Powell (2004), Wei & Holland (2003), Chatterjee (1976), Frey (1972), Zeh (2001), Pattison et al. (2002), McDade & Harley (2001), Kohn & Spear (1993), Hébert & Ballèvre (1993) as well as own calculation using the Theriak-Domino software (De Capitani & Brown 1987, De Capitani (1994) using Berman database (1988) completed by recent thermodynamic data: Mg-chloritoid data of B. Patrick (listed in Goffé & Bousquet 1997), Fe-chloritoid data of Vidal et al. (1994), chlorite data of Vidal et al. (2001), and aluminoceladonite data from Massonne & Szpurka (1997). Mineral abbreviations are from Bucher & Frey (2002) except for (Fe, Mg)-carpholite (Car).

ever 1951; Goffé et al. 1973; Chopin & Schreyer 1983; Goffé & Chopin 1986; Rimmelé et al. 2003b). It is encountered in various rock types, such as aluminium-rich metapelites, quartzites, marbles and albite-free pelitic schists in which it is abundant, often in veins. Textural and mineralogical observations in these rocks reveal that at low-temperatures the main equilibrium reactions of ferro- and magnesio-



carpholite involve quartz, kaolinite, pyrophyllite, kyanite, chlorite, chloritoid and phengite (Fig. 6.2a). At high-temperatures, large P–T fields are dominated by an assemblage containing staurolite, biotite and garnet (Spear & Cheney 1989). Fe–Mg variations in mineral composition, as a function of P and T (Goffé 1982; Spear & Selverstone 1983; Vidal et al. 1992; Theye et al. 1992), as well as Si isopleths in phengite (Massone & Schreyer 1987; Oberhänsli et al. 1995; Massone & Szpurka 1997; Bousquet et al. 2002) allow for relatively precise P–T estimates (Vidal et al. 2001; Parra et al. 2002a, b; Rimmelé et al. 2005) for some metapelitic compositions.

In the CFMASH system, for comparison, there is less resolution at low-temperature conditions. In carbonaceous systems, the stability field of the index mineral lawsonite covers the whole low-grade space, including the stability field of carpholite and the aragonite–calcite transition. While the staurolite field is substantially smaller in the CFMASH system, as compared to the KFMASH system, margarite and zoisite are characteristic of medium P and T conditions.

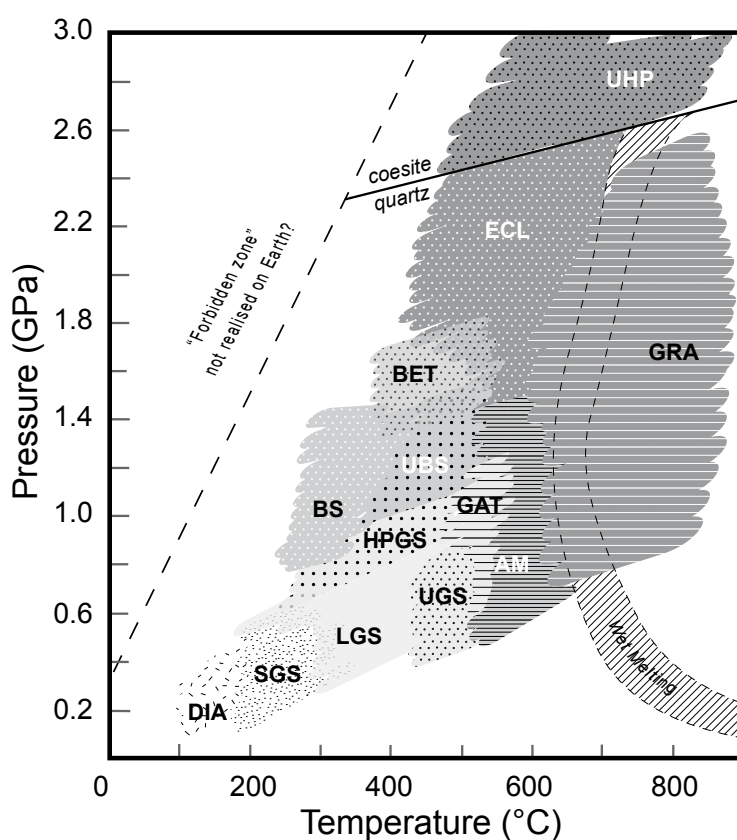
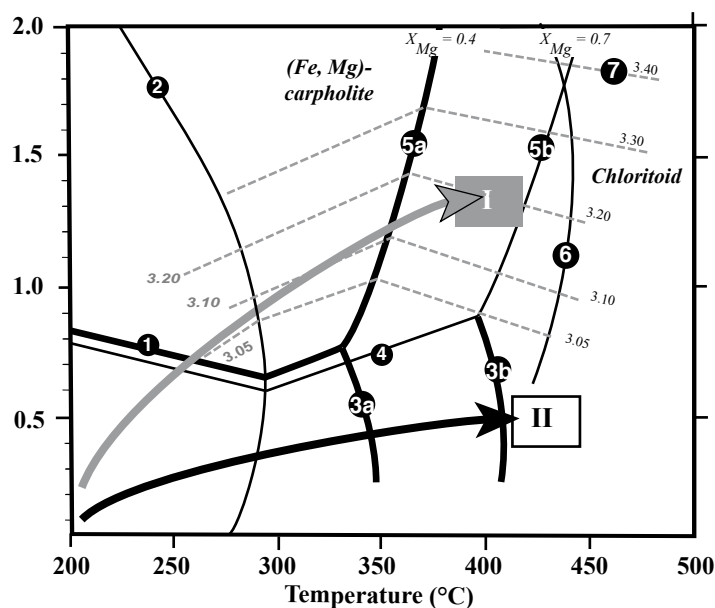


Fig. 6.3: Metamorphic facies diagram for metapelites and metabasites (modified after Oberhänsli et al. 2004). This diagram has been used for Figures 6.6 and 6.7. For abbreviations see Table 6.2. This diagram is in good agreement with previous published facies diagram (e.g. Yardley 1989; Spear 1993; Bousquet et al. 1997).

Oberhänsli et al. (2004) proposed a new type of metamorphic facies grid that better integrated field observations into models of the geodynamic. This facies grid also took into account the importance of metasediments, which is less clear in traditional grids. The proposed grid also involved more subdivisions, which are based on the understanding of the metasediments. Based on these compilations, a revised version of this tool is presented in Figure 6.3, and it will be used in this paper.

6.2.2. Ambiguity of some mineral assemblages in the Alps

While some parageneses unambiguously grow only within a certain geodynamic context (Table 6.1), other mineral assemblages commonly occur over a large field of P–T conditions and may evolve in diverse geodynamic contexts. Examples of unambiguous mineral assemblages containing lawsonite and carpholite only form under low-temperature/high-pressure conditions, typical for subduction processes; mineral assemblages containing staurolite and andalusite are typical high-temperature phases occurring during collision processes (i.e. Barrovian-type metamorphism).



1: Chl + 4Kln	=	Qz + 5Car + 2W
2: 2Qz + Kln	=	Prl + W
3a: 4Prl + Chl	=	5Ctd + 14Qz + 3W ($^{Chl}X_{Mg}=0.4$)
3b: 4Prl + Chl	=	5Ctd + 14Qz + 3W ($^{Chl}X_{Mg}=0.7$)
4: 5Car + 9Qz	=	4Prl + Chl + 2W
5a: Car	=	Qz + Ctd + W ($^{Car}X_{Mg}=0.4$)
5b: Car	=	Qz + Ctd + W ($^{Car}X_{Mg}=0.7$)
6: Prl	=	Ky + 3Qz + W
7: 2Ms + Chl + 2Qz	=	3Ctd + 2ACel + W

Fig. 6.4: Ambiguity of chloritoid-quartz as index assemblage. Depending on the P–T path, chloritoid-quartz can be formed either by breakdown of (Fe, Mg)-carpholite at HP conditions (reaction 5) or by breakdown of pyrophyllite at LP conditions (reaction 3). Chloritoid-quartz assemblage alone cannot be used as index for pressure conditions. Its significance depends on the mineral reaction and on the associated minerals.

On the other hand, recurrent minerals such as chloritoid, zoisite, kyanite and garnet may form at different P–T conditions. This hampers their use for an interpretation of the geodynamic setting. Chloritoid – phengite assemblage, for example, can be produced in different geodynamic settings. Moreover, it may occur in tectonic units in close spacial juxtaposition although these units formed in different geodynamic scenarios (Oberhänsli et al. 2003). Figure 6.4 clearly illustrates that two P–T paths may lead to different mineral reactions that produce chloritoid–phengite–chlorite mineral assemblages. The P–T path along a cold geotherm leads to the formation of chloritoid–phengite–chlorite as a result of the breakdown of Fe–Mg carpholite (Chopin & Schreyer 1983) while under higher geothermal gradients this assemblage can also form by the breakdown of pyrophyllite (Frey & Wieland 1975).

The high-pressure aluminosilicate polymorph, kyanite, is particularly difficult to interpret as an indicator of geodynamic processes. It may occur in UHP associations such as the Dora Maira unit, as well

Table 6.1: Mineralogical description of the metamorphic facies presented in the Figure 6.3 for basic rocks as well as for meta-pelitic rocks.

Facies Name	Abb.	Basic rocks	Metapelites
diagenesis / sub anchizone	DIA	zeolite	illite-kaolinite
sub greenschist	SGS	laumontite-prehnite - pumpellyite	illite
lower greenschist	LGS	albite-chlorite	pyrophyllite-chlorite ± chloritoid
upper greenschist	UGS	Actinolite-epidote-chlorite	biotite-chlorite-kyanite ± chloritoid
high-pressure greenschist	HPGS	albite-lawsonite-chlorite±crossite	lawsonite-chlorite ± chloritoid ± kyanite
greenschist-amphibolite transition	GAT	albite-epidote-amphibole	biotite-garnet-chloritoid or phengite-chloritoid-kyanite
amphibolite	AM	plagioclase-hornblende-garnet	biotite-garnet-staurolite-phengite=kyanite
blueschist	BS	glaucofane-lawsonite	carpholite-phengite±pyrophyllite
upper blueschist	UBS	glaucofane-epidote-garnet	chloritoid-phengite ± garnet
blueschist-eclogite transition	BET	glaucofane-zoisite-garnet±clinopyroxene	garnet-Mg-rich chloritoid-phengite
eclogite	ECL	garnet-omphacite-zoisite-quartz ± amphibole ± phengite	garnet-Mg-rich chloritoid-kyanite or garnet-lawsonite
ultrahigh-pressure	UHP	garnet-omphacite-kyanite ± phengite	coesite or Mg-rich chloritoid-talc-phengite
granulite	GRA	plagioclase-clinopyroxene (augite) - orthopyroxene (hyperstene) ± garnet ± olivine ± spinel	clinopyroxene (diopside) - orthopyroxene (enstatite) - K-feldspath ± garnet ± cordierite ± sapphirine

as in temperature-dominated areas such as the Leontine dome. It indicates a subduction-type low geothermal gradient in the first, but a high collision-related geotherm in the latter case.

6.2.3. Ambiguity of some metamorphic facies

Assignment of a metamorphic rock to a metamorphic facies is based on its mineralogy. In the best case, a rock might undergo a simple metamorphic evolution in a distinct geodynamic setting, leading to a peak metamorphic paragenesis (simultaneous P and T peaks) possibly followed by later retrogression (Fig. 6.5a). However, a metamorphic pressure peak related to one geodynamical scenario may also have been overprinted by a thermal peak that resulted from a second and different geodynamic scenario (Fig. 6.5b). Hence, in such a case the metamorphic facies is ambiguous in that it is difficult to distinguish between continuous and discontinuous evolutions. It is only the exact shape of the P–T path, details that are often difficult to constrain, which is specific for a complex geodynamic evolution. For example, the significance of the amphibolite facies mineralogy is ambiguous. It may either represent a single path that entirely formed in a collision setting; or alternatively, it may merely represent an exhumation stage that formed during ongoing subduction and before final collision (Fig. 6.5a). In the case of dual peak paths, details regarding amphibolite facies overprint are crucial for better understanding exhumation processes in general and details of the transition from subduction to collision in particular.

6.3. The metamorphic data in a geodynamic context

The above-described importance of metasediments and the presented tool of a facies grid with its characteristic mineral assemblages can be well used in the Alps. The Alps are well suited for such a compilation because they are a relatively small and well-investigated orogen (e.g. Frey et al. 1974, 1980; Goffé & Chopin 1986; Roure et al. 1990; Dal Piaz 2001; Oberhänsli et al. 2004; Schmid et al. 2004). The Alps are developed by subduction of two different oceans followed by col-

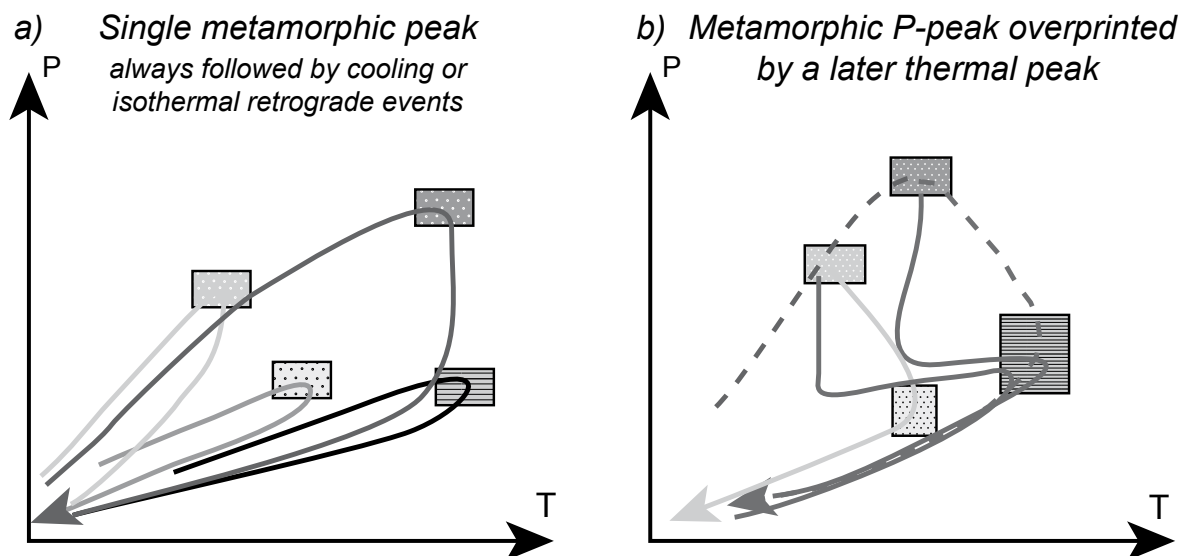


Fig. 6.5: Ambiguity of some metamorphic facies. (a) a rock undergoes a simple metamorphic evolution in a distinct geodynamical setting, leading to only one peak metamorphic paragenesis (simultaneous P and T peaks) followed by later retrogression. (b) In some cases certain metamorphic P-T paths show distinct pressure and temperature peaks. The pressure-peak can be related to one geodynamical scenario and it may have been overprinted by a thermal peak that resulted from a second and different geodynamical scenario.

lision between two main continents (Adria and Europe). The relics of the oceans (Piemont–Liguria, Valaisan) and the separating microcontinent (Briançonnais) are still existing and are now sandwiched between Adria and Europe. The palaeogeographic (tectonic) overview of the present-day situation is principally inspired from Schmid et al. (2004) and Bigi et al. (1990), and can so be combined with metamorphic information of the different units. This approach will be presented below.

6.4. Subduction-related minerals and their distribution

All the way from the Adriatic margin preserved in the lower Austroalpine nappes to Europe-derived nappes, the tectonic units (i.e. Piemont–Liguria, Briançonnais, Valais) contain metasediments that recorded the Late Cretaceous–Cenozoic subduction history. The minerals indicating subduction-related processes are listed in Table 6.2 and their distribution is shown in Figure 6.6.

We recognize the HP–LT imprint on the European continental margin (Tauern window, Adula nappe and surrounding covers), on all the metasediments derived from the partly oceanic Valaisan domain, as well as on the Piemont–Ligurian realm (Rechnitz window, Matrei zone, Avers, Zermatt–Saas zone, Entrelor, Cottian Alps, Voltri group, Tuscany and Corsica). The situation is more complex for the

Table 6.2: Main metamorphic minerals or mineral assemblages found in metasediments in the Alps, classified according to their meaning.

HP-LT “minerals”	Low-grade/ greenschists “minerals”	HT “minerals”	“Ambiguous” minerals
Fe,Mg-Carpholite <i>Car</i>	Margarite (Mgr)	Andalusite (And)	Chloritoid (Ctd)
Lawsonite <i>Lws</i>	Pyrophyllite (Prl)	Sillimanite (Sil)	Kyanite (Ky)
Aragonite <i>Arg</i>	Kaolinite (Kln)-Quartz	Cordierite (Crd)	Garnet (Gt)
Coesite <i>Cs</i>	Riebeckite (Rbk)	Staurolite (St)	Clinozoisite / Zoisite (c/Zo)
Talc <i>Tlc</i>	Glauconite (Glt)	Wollastonite (Wo)	Cookeite (Cook)
Glaucofanane <i>Gln</i>	Stilpnomelane (Stl)	Diopside (Di) <i>in marble</i>	Sudoite (Sud)
Jadeite <i>Jd</i>	Albite-quartz-phengite-chlorite	Tremolite (Tr) <i>in marble</i>	
	quartz-phengite-chlorite		

units derived from the Briançonnais terrane. Going from internal to external, they indicate eclogite and UHP conditions in the ‘internal massifs’ (Monte Rosa, Gran Paradiso, Dora Maira), blueschist conditions (Suretta cover, Mont Fort, Ruitor, Vanoise, Acceglio, Ligurian Alps, Tenda), and subduction-related greenschist and low-grade conditions (Tasna, Schams, Zone Houillère). Based on structural arguments, some authors dispose of this complexity by changing the palaeogeographic attribution of the ‘internal massifs’ (Froitzheim 2001; Pleuger et al. 2005). We are agreeing with the fact that the geodynamic evolution is complex and that the ‘internal massifs’ are part of the Briançonnais (see e.g. Polino et al. 1990; Borghi et al. 1996; Froitzheim et al. 1996; Dal Piaz 1999).

In the following, we will present four examples (Cottian Alps, Ruitor, Entrelor and Valais Ocean) that document and demonstrate the use of metamorphic studies on metasediments for unravelling different P-T evolutions during the early subduction-related history of the Alps.

Continuous P increase within sediments from one single palaeogeographic unit (Cottian Alps).

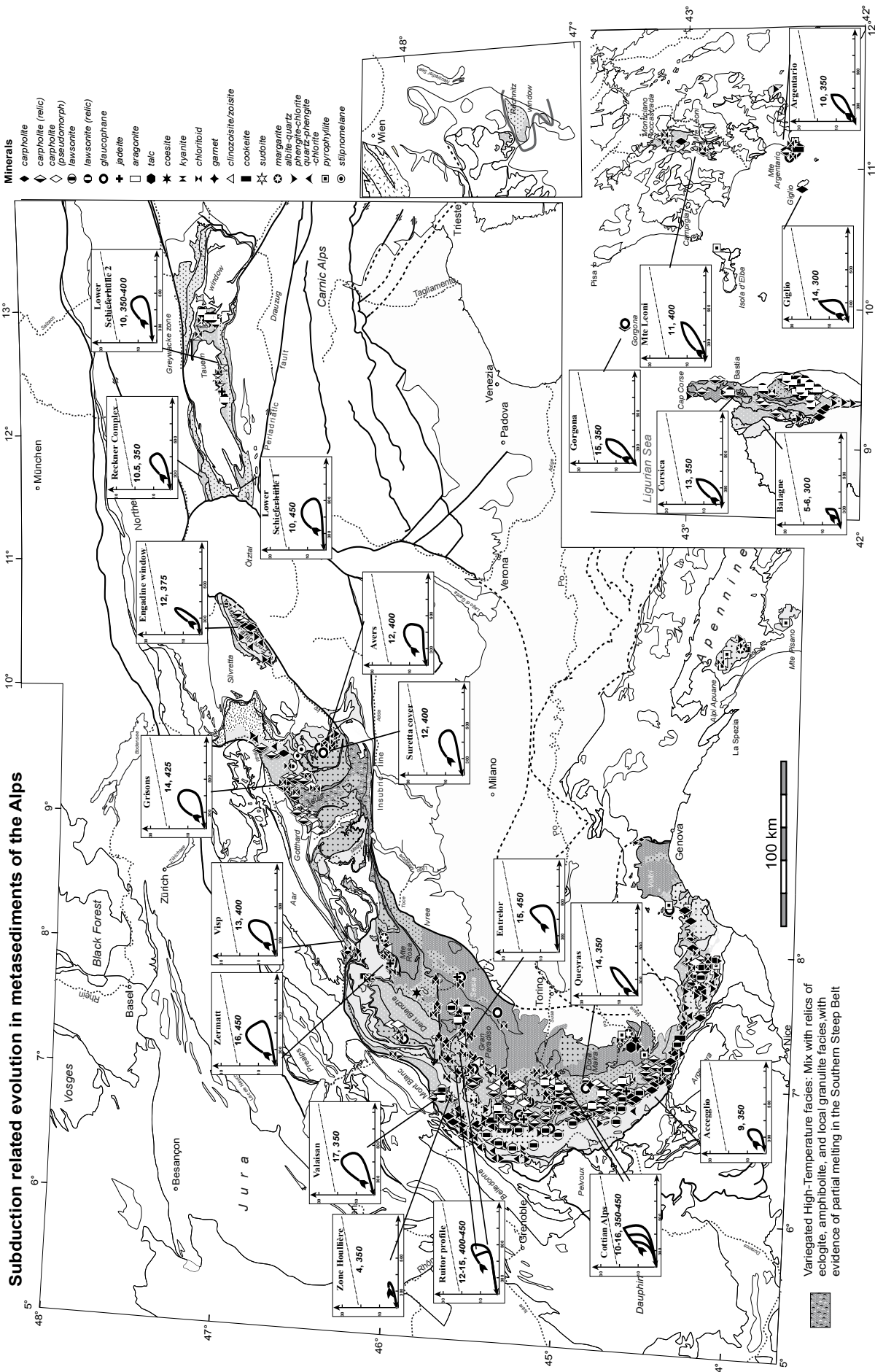
The Schistes Lustrés complex in the Cottian Alps is formed by intensely folded Upper Jurassic (Malm; De Wever & Caby 1981) to Upper Cretaceous calcschists deposited in the oceanic Piemont–Liguria trough (Coniacian–Santonian; Lemoine & Tricart 1986; Deville et al. 1992), with a few mantle slivers (mainly serpentinites) representing the floor of this Alpine realm largely devoid of mafic oceanic crust (Lagabrielle & Lemoine 1997). The study of metamorphic sediments shows that carpholite-bearing assemblages are present in the western part (Goffé & Chopin 1986; Agard et al. 2001) while chloritoid-bearing assemblages as well as garnet-lawsonite-glaucophane assemblages in marbles (Ballèvre & Lagabrielle 1994) occur in the eastern part. On the basis of metapelite mineralogy, P–T estimates at maximum pressure increase from west to east across the study area from c. 1.2–1.3 GPa at 300–350°C (Agard et al. 2001) to 1.4–1.5 GPa at 450–500°C (Ballèvre & Lagabrielle 1994; Agard et al. 2000).

Bimodal evolution within a single paleogeographic unit (Ruitor area).

The metamorphic evolution of the basement units derived from the Briançonnais micro-continent was always a matter of debate (Desmons et al. 1999; Monié 1990). In the south-western Alps, a HP imprint is well documented by occurrences of Fe-Mg carpholite (Goffé 1977, 1984; Goffé et al. 1973, 2004; Goffé & Chopin 1986), and aragonite (Gillet & Goffé 1988) in metasediments and by occurrences of lawsonite and jadeite in metabasites (Lefèvre & Michard 1965; Schwartz et al. 2000). In the north-western Alps in contrast, only the uppermost unit of the Briançonnais domain (the Mont Fort nappe) displays blue-schist facies conditions (Schaer 1959; Bearth 1963).

In the Zone Houillère and in its Permo-Triassic cover as well as in the Briançonnais basement, metamorphic mineral assemblages are mainly composed of white micas with varying chemical composition, chloritoid and garnet. This same assemblage may occur within different lithologies (meta-arkose, meta-pelite, meta-sandstone). The increase in metamorphic grade from greenschist facies conditions in the north-west (Zone Houillère) to the transition between blueschist and eclogite facies conditions in the south-east (Internal Briançonnais) is well documented (Bucher & Bousquet 2007). A major discontinuity in metamorphic grade, as documented by a pressure gap of ca. 0.7 GPa, is located at a tectonic contact within the Briançonnais terrane, namely that between the Zone Houillère and Ruitor unit (Caby et al. 1978; Bucher 2003).

Fig. 6.6: Mineral distribution (and some associated P-T paths) of subduction-related processes in post-Hercynian metasediments of the Alps. We note a wide distribution of HP events over the entire alpine edifice. See references in Appendix.



Rock associations displaying different metamorphic peak conditions (Entrelor area).

Two types of metamorphic rocks (blueschist and eclogites) have been described in this area, which is part of the Piemont–Liguria units of the Western Alps (Dal Piaz 1999). Recently, the rock assemblage in the Entrelor area has been interpreted as a metamorphic mix, consisting of eclogitic rocks that were embedded into a blueschist facies matrix consisting of metapelites and greenstones (Bousquet 2008). The two kinds of HP metamorphic rocks reveal different peak metamorphic conditions (1.2 GPa at 450°C vs. 2.3 GPa at 550°C); it is their contemporaneous exhumation within a subduction channel which juxtaposed them at a shallower crustal level. This evolution illustrates that subduction processes cannot be considered as a single-pass process; instead, return flow of a considerable portion of crustal and upper mantle material must be accounted for (Gerya & Stockhert 2002), and the exhumation of the different rock types cannot be considered independently from each other (Engi et al. 2001). The rocks of the Entrelor area can be viewed as an exhumed part of a frozen subduction channel consisting of a mix of metamorphic rocks that have different metamorphic evolutions, and which were accreted at great depths.

Geometry of the subduction (units derived from the Valais ocean).

In the Eastern and Central Alps, blueschist-facies rocks derived from the Valais ocean are exposed structurally below the Austroalpine nappes over an area of 300 x 20 km² (from the Tauern window to the Grisons area) and have a thickness of around 10 km. This large volume of blueschist-facies rocks is in contrast with that of the eclogite-facies rocks of the Western Alps that only form a small 2 to 5 km thick slice. The difference in volume and metamorphic conditions from east to west is probably due to a change in style and geometry of subduction.

In the Eastern and Central Alps, the blueschist metasediments formed within a wide accretionary wedge with a thickness of 40–50 km which underlies the orogenic lid formed by the Austroalpine nappes and they were exhumed before the final collision between the European and Apulian continents (see discussion in Bousquet et al. 2002). Subduction occurred at a high angle to the strike of the orogen. In the Western Alps, where only a narrow accretionary wedge formed (Ceriani & Schmid 2004), producing low-grade metamorphic conditions (Ceriani et al. 2003), subduction occurred in a sinistrally transpressive environment, i.e. at a small angle to strike of the orogen (Schmid & Kissling 2000, Ceriani et al. 2001). The blueschist and eclogite facies metasediments of the Versoyen area (Petit St. Bernard and Versoyen units, Goffé & Bousquet 1997) were also subducted and extruded along a N–S direction, i.e. at a small angle to the orogen (Fügenschuh et al. 1999). Moreover, the Western Alps were never overlain by an orogenic lid formed by the Cretaceous-age Austroalpine nappe stack, but at best by rather thin basement silvers attributed to the Margna–Sesia fragment (Schmid et al. 2004).

Despite the fact that metamorphism related to Latest Cretaceous to Cenozoic subduction is scattered all over the Alps, information on these processes is unevenly distributed. Areas with wide occurrences of metasediments (Fig. 6.1) allow for the best insight into the early geodynamic evolution of the Alps. In the Western Alps, all stages of a subduction process in P–T frame (from UHP to greenschist conditions), as well as its evolution in time (from the latest Cretaceous to the Oligocene, i.e. between 70 and 33 Ma), are recorded. Contrarily in the Eastern Alps and in the Tauern window (we exclude the Cretaceous-age high-pressure metamorphism from this discussion since it was related to a different orogeny; Froitzheim et al. 1996) the metamorphic record of the metasediments is limited, and the HP rocks only exhibit Eocene ages (45–35 Ma).

6.5. Minerals related to collision processes and their distribution

Collision-related minerals apparently do not occur over the whole Alpine edifice. Minerals produced during collision are mainly indicative for temperature-dominated metamorphic conditions (Barrovian-type metamorphism). They occur in the External zones, as well as in the Central Alps (Lepontine dome) and in the Tauern window of the Eastern Alps (Fig. 6.7).

In the External zones, the metamorphic evolution reaches maximum lower greenschist conditions, metamorphism resulting from collisional deformation as nappe emplacement, thrusting and folding (Frey & Ferreiro Mählmann 1999; Burkhard & Goy-Eggenberger 2001; Ferreiro Mählmann 2001). Burial processes both control metamorphic conditions in the External zones and limit it to low grade. The area of the Lepontine dome and the Tauern window, however, experienced higher metamorphic conditions, at least amphibolite facies.

Three examples will elucidate geodynamic processes that led to high-temperature metamorphic overprinting of metasediments in more internal zones.

Continental underplating (Tauern window).

In the post-Variscan metasediments of the Tauern window, a high-temperature event is mainly indicated by the occurrence of Fe/Ca-rich garnet (Droop 1981; Selverstone 1985). Only a few occurrences of staurolite have been reported, indicating maximum amphibolite facies conditions. The mineral distribution pattern indicates two dome-like structures with concentric temperature gradients. This pattern resulted from the underthrusting of Europe-derived continental basement (Kurz et al. 1999) and its accretion to the overlying Austroalpine basement complex (Apulian Plate). This geodynamic scenario led to simple and continuous P–T paths (Fig. 6.6) that indicate decompressional heating from HP conditions into amphibolite facies conditions.

In the Schieferhülle, the earlier HP-stage (blueschist facies conditions, Selverstone & Spear 1985) at 36 Ma was overprinted by HT conditions (amphibolite facies conditions) at around 30–27 Ma ago (Christensen et al. 1994; Zimmermann et al. 1994).

Continental wedging (Lepontine dome).

High-temperature metamorphic conditions in the Central Alps (the Lepontine area) were based on the study of metasediments in the early works on Alpine geology (e.g. Schmidt & Preiswerk 1908; Preiswerk 1918). Since these pioneering descriptions, several workers have dealt with metasediments from the Lepontine in order to understand progressive metamorphic evolution in isochemical systems (siliceous carbonates system: Trommsdorff 1966; pelitic and marly compositions: Frey 1969). The Lepontine area is characterized by extensive amphibolite facies conditions, reaching migmatization and/or granulite facies conditions. The thermal overprint (Fig. 6.6) progressively decreases from UHT-conditions in the south to greenschist facies conditions outwards (Streckeisen et al. 1974; Engi et al. 1995; Todd & Engi 1997). The northern margin of the amphibolite grade Lepontine dome is defined by the appearance of staurolite in pelitic systems. However, to the south it is truncated by the Insubric line, along which granulites and migmatites are juxtaposed to rocks of the Southern Alps that did not experience substantial Alpine metamorphism.

Thin Mesozoic metasedimentary bands separate large volumes of basement rocks belonging to various nappes stacked below the Austroalpine nappes and in front of the Southern Alps (Apulian Plate). The accretion of vast amounts of crustal material derived from the European margin (Adula, Simano,



Fig. 6.7: Mineral distribution (and some associated P-T paths) of collision-related processes in post-Hercynian metasediments of the Alps. Two types of metamorphism can be distinguished. The lower one up to greenschist facies conditions has a large distribution all over the Alpine belt and occurs in the external part. The second type is characterized by an important thermal event from greenschist to granulite conditions. It occurs only in three specific areas (Tauern, Lepontine dome and Tuscany). In these areas, the thermal event can overprint an earlier HP event. See references in Appendix.

Leventina) and the Briançonnais terrane (i.e. Maggia nappe) allowed for high radiogenic heat production (Verdoya et al. 2001; Roselle & Engi 2002) producing HT assemblages.

The P-T paths deduced from the high-grade metasediments often, but not always (see Nagel et al. 2002; Keller et al. 2005a for more simple P-T paths), show bimodal trends (Fig. 6.6): a HP event is followed by a phase of heating (Engi et al. 2001; Berger et al. 2005; Brouwer et al. 2005; Wiederkehr et al. 2007). Shortly after the HP event, which probably occurred at around 45 Ma (51–47 Ma, Bucher 2003; 42.6 Ma, Lapen et al. 2007; see discussion in Berger & Bousquet 2008), HT metamorphic conditions prevailed over a long period of time until 30 Ma ago in the south and 15 Ma in the north, respectively (Hunziker et al. 1992).

Post-orogenic heating (Tuscany).

In western Tuscany, Quaternary magmatism is witnessed by volcanic as well as intrusive rocks. This magmatism is associated with crustal thinning and high heat flow values (Scrocca et al. 2003). Consequently, metasediments not only exhibit HP mineral assemblages, but also minerals such as andalusite, staurolite, chloritoid, epidote that document the high-temperature evolution. A bimodal P-T path has been reconstructed from Giglio, indicating both an HP and HT event. (Rossetti et al. 1999).

The inferred palaeotemperature distribution pattern resembles an asymmetric thermal high defined by the appearance of kyanite, similar to the present geothermal pattern of the Tuscan crust (Francheselli et al. 1986), as indicated by a series of geothermal anomalies passing through the northern Apennines (Della Vedoya et al. 2001). The age of the HT event (from 15 to 8 Ma, Kligfield et al. 1986; Brunet et al. 2000; Molli et al. 2000a, b) clearly post-dated the HP stage (31–26.7 Ma, Brunet et al. 2000) in Tuscany.

Summary

Remnants of the high-temperature event are unevenly distributed throughout the Alps. They are localized in the Tauern window, the Lepontine dome, and in Tuscany. In contrast, large areas lack such an HT overprint: the entire Western Alps and the Engadine window located between the Lepontine dome and Tauern window. Both the Lepontine and the Tauern domes are made up of continent-derived granitoid upper crustal metamorphic sequences (Lammerer & Weger 1998; Neubauer et al. 1999; Schmid et al. 1996), while the Engadine window (Bousquet et al. 2002) and the southwestern Alps (Agard et al. 2002; Lardeaux et al. 2006) are mainly built up of oceanic-metasedimentary sequences.

Hence we conclude that the high-temperature event in the Eastern and Central Alps is due to large local accumulations of crustal material during continental collision, while in Tuscany it records a post-orogenic event, associated with thinning of the lithosphere (Rossetti et al. 1999).

6.6. Metamorphic structure of the Alps

Sediments occur throughout mountain belts such as the Alps and represent a large variety of palaeo-environments and chemical compositions. Moreover, several of these compositions are very sensitive to temperature and pressure variations. Thus, they have a high potential for registering the different stages of their geodynamic evolution. Mineral distributions in metasediments, combined with previous works on metabasites, allow for deciphering the complexity of the Late Cretaceous–Tertiary alpine history (Figs 6.8 & 6.9).

Map representation (Fig. 6.8) allows the clear separation of different areas in the Alps. Corsica and the Western Alps as well as the far Eastern Alps (Rechnitz window) have recorded only the subduc-

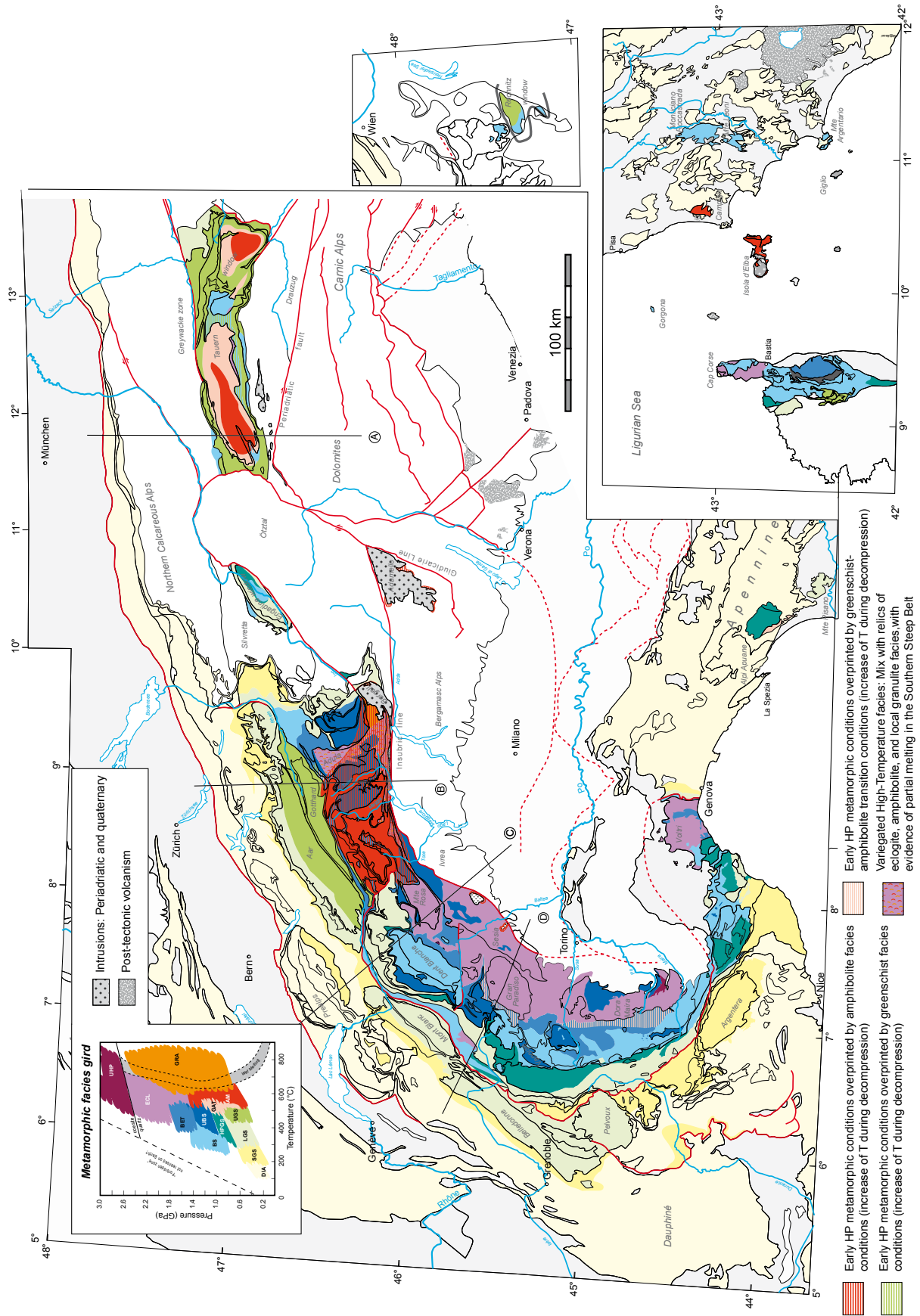


Fig. 6.8: Metamorphic facies distribution (and related magmatism and volcanism) in the Alps from Vienna (Austria) to Corsica and Tuscany. On the map, the different stages of the geodynamic evolution are indicated. This map, largely modified from Oberhänsli et al. (2004) is a synthesis of Figure 6.6 and 6.7. Traces of profiles presented on the Figure 6.9 are indicated.

tion-related evolution, characterized by HP metamorphism. The Central Alps and the Eastern Alps (Tauern window) are displaying a more complex history. In these areas, the HP phase is overprinted by higher temperature conditions.

Alpine eclogite facies remnants in the central Lepontine area appear to be restricted to a metamorphic mix (Berger et al. 2007). They are isolated occurrences in a belt that includes relics of variegated high-grade metamorphism, from granulite facies to eclogite to amphibolite facies. This structure is interpreted as representing remnants of a tectonic accretion channel (Engi et al. 2001), which had developed along the convergent plate boundary during Alpine subduction.

From the metamorphic map (Fig. 6.8) and using four major geological transects (Schmid et al. 2004), we propose metamorphic transects across the Alps down to 15–20 km depth (Fig. 6.9). In the eastern transect (Fig. 6.9a, along the TRANSALP profile), the main alpine metamorphic features show the thermal overprint. Only scarce relics of the HP history are preserved. In the Central Alps (Fig. 6.9b, NFP 20 east profile), HP and HT metamorphic rocks coexist. The thermal overprinting of different subduction patterns can be observed: eclogites of the Adula complex, rocks undergone into blueschist conditions (European margin, i.e. north of Adula, Simano; Valais; Briançonnais, i.e. Tambo, Suretta) as well as rocks that have not been subducted (Maggia nappe for the Briançonnais) have been thermally overprinted by the Late Tertiary event. A wedge-type structure built against the Insubric line can be clearly distinguished on the Central Alps profile. In the northwestern Alps (Fig. 6.9c, NFP 20 west profile), while the subduction-related metamorphism is widespread, the thermal overprinting is limited to the European platform (sediments, i.e. Helvetic nappes or Dauphiné; basement rocks, e.g. Mt. Rosa, Antrona). In the Western Alps (Fig. 6.9d, ECORS-CROP profile), subduction-related metamorphism is the main

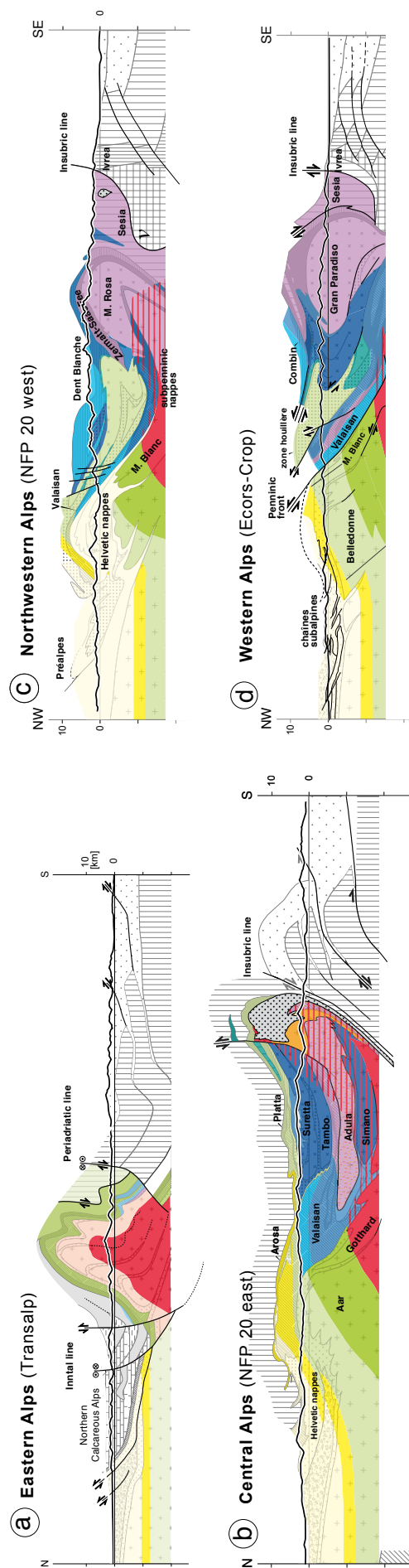


Fig. 6.9: Metamorphic structure of the Alps. We report metamorphic data along four geological transects of Schmid et al. (2004) down to 15–20 km depth. Below this depth, the past metamorphic history should be overprinted by the present thermal regime. (a) Eastern transect along the TRANSALP seismic profile. (b) Central Alps transect (along the NFP 20 east seismic profile). (c) Northwestern Alps transect along the NFP 20 west seismic profile. (d) Western Alps transect, along the ECORS_CROP seismic profile.

record. The thermal overprint appears west of the Penninic front and it is limited to the European platform (Belledonne, Pelvoux, Dauphiné). The most internal units are completely lacking an HT event. It can only be assumed for the deepest units (at around 20 km depth). Two subduction zones, indicated by HP metamorphic conditions, can be clearly evidenced. One (in the east) is formed by the Piemont–Liguria rocks, the Gran Paradiso massif and the most internal part of the Briançonnais. The second subduction zone is formed only by the Valais rocks and is rooted at depth. Both zones are separated from each other by the external Briançonnais (Zone Houillère) which lacks evidence for HP metamorphism. The arrangement of the nappe pile in the Western Alps clearly shows a subduction-type structure in which most of the tectonic units dip southwestward.

6.7. Discussion

Evidence for HP metamorphism recording prolonged subduction processes during at least over 37 Ma (from 70 Ma in Sesia to 33 Ma in Valaisan, see Bousquet et al. 2002, and Berger & Bousquet 2008, for timing constraints). The evidence for these long-lasting processes is also widespread over the entire orogen, from the Rechnitz window in the east to Corsica and Tuscany in the southwest. All palaeogeographic units, of continental and oceanic origin, were involved in these subduction processes. The nappes derived from the Penninic–Austroalpine transition zone (Margna–Sesia fragment), the Piemont–Ligurian Ocean, the Briançonnais terrane, the Valais Ocean and the European margin all were successively subducted under the Apulian Plate (Berger & Bousquet 2008).

In contrast, high-temperature metamorphism is a relative short-lived process, lasting for some 15 Ma (30 to 15 Ma). The evidence for such HT metamorphism is also localized in specific regions. It is limited to areas where considerable amounts of continental crust were accumulated into accreted nappe stacks. High-temperature conditions (more than 650 °C, up to 800 °C; granulites and migmatites) were reached in the Lepontine dome where a huge amount of continental crust allowed for high radiogenic heat production. In the Tauern, a less important amount of imbricated continental crust led to amphibolite facies conditions (up to 600°C). In the Engadine window (Hitz 1995, 1996), as well as in the western Alps, the relative scarcity of continental crust involved in the orogenic wedge does not allow for such a high heat production and associated high-temperature overprint.

The transition between the western Alps, lacking such an HT overprint, and the Lepontine dome can be observed in the Monte Rosa area. There, only the lower parts exposed in deep valleys (Domodossola) show an amphibolite facies overprint (650 °C, Keller et al. 2005b).

Thermal overprint is primarily related to the amount of crust involved in the subduction and collision processes (Bousquet et al. 1997; Goffé et al. 2003) rather than to processes of shear or viscous heating (Burg & Gerya 2005). The latter mechanism, which suppose high deformation rate, will not allow for the preservation of HP–LT assemblages within high-grade rocks, as is found for example in the southern Adula complex (Nagel et al. 2002).

The relation between the volume of continental crust imbricated and intensity of high-temperature orogenic metamorphism can be generalized over the entire Alpine edifice, except for Tuscany where the late (< 8 Ma) thermal overprint is clearly related to lithospheric thinning.

6.8. Conclusions

Based on metamorphic studies in metasediments, we evidence substantial differences in the metamorphic and hence the geodynamical evolution along strike of the Alpine orogen.

The Western Alps did not reach the mature stage of a head-on colliding belt as is indicated by a continuous metamorphic evolution, representing all the subduction-related processes ranging from lower greenschist to UHP conditions. All the metamorphic rocks behind the Pennine frontal thrust were already exhumed to upper crustal level during ongoing oceanic and continental subduction and before collision with the Dauphinois domain from around 32 Ma onwards (Fügenschuh & Schmid 2003; Leloup et al. 2005). Hence, the Western Alps represent a frozen-in subduction zone. Since then, only exhumation by erosional processes affected the inner parts of the orogen.

The rest of the Alpine orogen later underwent a more important collision process due to the ongoing head-on geometry of subduction and collision. It therefore often but not always shows a bimodal metamorphic evolution with two distinct P and T peaks. The intensity of the thermal overprint relates to the amount of crustal material incorporated to the orogenic wedge.

Acknowledgments

This article benefits from discussions with many colleagues. All cannot be cited, but RB wants to specially thank M. Ballèvre, B. Fügenschuh, S. Bucher, R. Caby, R. Polino, D. Marquer, G. Gosso, M.-I. Spalla, V. Höck, O. Vanderhaeghe, S. Duchêne, R. Ferreiro Mählmann, J.-M. Lardeaux and P. Rossi. We are indebted to N. Froitzheim for his corrections and comments. He helped us to clarify and improve the manuscript. Despite the cutting tone of his review, we thank K. Stüwe: some of his comments were useful. Without the encouragement, the editorial work and the patience of S. Siegesmund, this paper would not have existed.

Appendix

List of the references used to build the maps on Figures 6.5–6.7. Eastern Alps: Bousquet (this study), Bousquet et al. (1998), Dachs (1986, 1990), Droop (1981, 1985), Franz (1983), Höck (1974, 1980), Leimser & Purtscheller (1980), Matile & Widmer (1993), Miller et al. (2007), Selverstone et al. 1984.

Central Alps: Bousquet (this study), Bousquet et al. (2002), Droop & Bucher-Nurminen (1984), Frey (1969, 1978), Frey & Niggli (1972), Frey & Wiedeland (1975), Frey et al. (1973, 1974, 1980), Frey & Ferreiro Mählmann (1999), Goffé & Oberhänsli (1992), Irouschek (1983), Oberhänsli et al. (1995, 2003), Niggli & Niggli (1965), Staub (1926), Trommsdorff (1966), Wiederkehr et al. (2007).

Western Alps: Agard et al. (2000, 2001), Ballèvre (1988), Ballèvre & Lagabrielle (1994), Bousquet (2007), Bousquet et al. (2004), Bucher & Bousquet (2007), Caron & Saliot (1969), Caron (1974), Ceriani et al. (2003), Chopin (1981, 1984), Chopin et al. (2003), Cigolini (1995), Desmons et al. (1999), Gillet & Goffé (1988), Goffé (unpub.), Goffé et al. (1973), Goffé (1977, 1982, 1984), Goffé & Chopin (1986), Goffé & Velde (1984), Goffé & Bousquet (1997), Goffé et al. (2004), Henry (1990), Jullien & Goffé (1993), Le Bayon et al. (2006), Leikine et al. (1983), Martinotti (unpub.), Saliot (1979), Venturini (1995).

Corsica and Tuscany: Caron & Péquignot (1986), Caron (1994), Daniel & Jolivet (1995), Daniel et al. (1996), Franceschelli et al. (1986, 1989), Franceschelli & Memmi (1999), Giorgetti et al. (1997), Goffé (unpub.), Goffé (1982), Jolivet et al. (1998a), Leoni et al. (1996), Molli et al. (2006), Rossetti et al. (1999, 2001), Theye et al. (1997), Tribuzio & Giacomini (2002).

Chapter 7

Summary and conclusions

Here the various conclusions and discussions extracted from the individual chapters are summed up and synthesized. In a first step the structural, petrological and geochronological data will be presented chronologically and integrated into the tectono-metamorphic evolution, as derived from the structural analysis. In a second step the resulting conclusions will be extrapolated to the scale of the entire orogen, discussing the geodynamic evolution of the Central Alps as well as orogenic belts in general.

7.1. Tectono-metamorphic evolution (P-T-d-t path)

The combined metamorphic, structural and geochronological study of metasediments at the north-eastern border of the Lepontine thermal dome revealed a bimodal P-T path for the Valaisan and parts of the adjacent European domains. The following “pressure-temperature-deformation-time path” has been inferred by this study:

Sediment accretion and subduction-related HP/LT metamorphism (42-40 Ma, D1 Safien phase)

The Valaisan Bündnerschiefer (mainly Grava and Tomül nappes) that presently build up a several kilometres thick accretionary wedge of metasediments formed during Cenozoic subduction of the Valais Ocean and the adjacent distal European margin beneath the Briançonnais micro-continent. Deeper parts of this sedimentary accretionary wedge experienced pressure-dominated metamorphism under blueschist facies conditions, including parts of the sedimentary cover of the adjacent distal European margin (Peidener slices and Piz Terri-Lunschania unit), detached from their crystalline basement and incorporated into the HP/LT part of the accretionary wedge.

Relics of the early subduction-related blueschist facies metamorphic event represented by the mineral assemblage Fe-Mg carpholite – phengite – chlorite ± chloritoid are widespread in the study area and only preserved within syn-metamorphic quartz-calcite veins/segregations but never in the rock matrix. These veins represent oblique fibrous veins that opened in a transtensive manner by re-precipitation from hydrous solutions, which led to the growth of the fibrous carpholite, quartz and calcite during the formation of these veins/segregations. Since no major folding structures formed during D1 and since the surrounding rock matrix is occasionally found virtually undeformed (as indicated by the presence of undeformed crinoids close to occurrences of carpholite), a semi-ductile behaviour during D1, largely characterized by solution and re-precipitation processes, is inferred. From the above mentioned mineral assemblage peak-pressure conditions for syn-D1 blueschist facies metamorphism of 350-400 °C and 1.2-1.4 GPa has been estimated.

Since the HP/LT mineral assemblage carpholite – chlorite – phengite ± chloritoid is found in metasediments of both Valaisan (Grava and Tomül nappes) and European units (Peidener slices and Piz Terri-Lunschania unit), the tectonic contact between the most distal European margin and the Valais Ocean, the Penninic Basal Thrust, must have already formed during D1. Although the more external European units (e.g. Scopi unit) may also have been affected by D1, these units lack carpholite-bearing veins.

The timing of the first deformation phase D1 (Safien phase), correlated with peak-pressure conditions, was addressed by isotopic investigations using $^{40}\text{Ar}/^{39}\text{Ar}$ *in situ* dating technique. White mica tex-

turally associated with Fe-Mg carpholite yield apparent $^{40}\text{Ar}/^{39}\text{Ar}$ ages of 42-40 Ma interpreted as dating peak-pressure conditions (350-400 °C and 1.2-1.4 GPa).

Substantial decompression during nappe-stacking (36-33 Ma; D2 Ferrera phase)

Nappe-stacking was associated with substantial decompression of the blueschist-facies rocks during which internal (i.e. Valaisan) units were thrust onto external (i.e. Europe) as well as high-pressure units (i.e. Valaisan, Peiden slices and Piz Terri-Lunschania unit) were emplaced over low-pressure ones (i.e. Scopi unit). This overall nappe-stack architecture suggests that ascent and extrusion of HP units did occur within and parallel to a subduction channel by active/forced extrusion and/or buoyant ascent.

Nappe-stacking and associated D2 deformation clearly post-date D1, since the carpholite-bearing quartz-calcite veins are isoclinally folded and overprinted by the S2 penetrative main and axial planar schistosity. This D2 schistosity completely transposes bedding, and possibly, relics of an earlier D1 schistosity that may have existed in pelitic lithologies.

The presence of relics of Fe-Mg carpholite combined with the observation that carpholite is mainly destabilized by the pressure sensitive mineral reaction producing white mica, chlorite and quartz points towards decompression under nearly isothermal or slightly cooling conditions. By $^{40}\text{Ar}/^{39}\text{Ar}$ *in situ* dating of white mica intimately associated with chlorite, both together replacing former Fe-Mg carpholite, yield apparent ages in the range of 36-33 Ma. This is interpreted to date the timing of substantial decompression and nappe-stacking.

Early-stage collision-related greenschist facies overprint (32-29 Ma)

The results obtained by different investigations (including petrologic investigations, Raman spectroscopy of carbonaceous matter, and $^{40}\text{Ar}/^{39}\text{Ar}$ dating) combined with the structural record independently revealed the existence of a greenschist facies metamorphic event clearly post-dating D2 nappe-stacking but pre-dating D3 first-stage nappe-refolding. The following results/observations points towards such a metamorphic overprint:

- (1) Detailed investigations regarding the distribution of characteristic minerals revealed that occurrences of chloritoid forming bundles and rosettes overgrowing the pre-existing main foliation can be found in both HP and LP units far beyond towards the east and therefore shows an obviously different zoning pattern, which is not characterized by the rather concentric shape confining the Lepontine thermal dome, as seen for the distribution of i.e. margarite, biotite, kyanite and staurolite (Niggli & Niggli 1965). Furthermore, it was found that porphyroblasts of chloritoid were deformed by subsequent D3 deformation. Both the eastward excursion of chloritoid occurrences as well as the relationships between deformation and crystallization favour an early-stage formation of chloritoid, clearly separated from the well-known “Lepontine” amphibolite facies Barrovian overprint.
- (2) The thermal structure of the study area was recorded by Raman spectroscopy of carbonaceous matter. In the north-eastern part of the study area the constructed isotherm contours can be continuously followed across tectonic contacts separating HP and LP units. Furthermore, these isotherm contours are spectacularly folded around the large-scale Lunschania antiform representing a major D3 nappe-refolding structure. Both observations favour the timing of the establishment of the thermal structure after D2 nappe-stacking but prior D3 nappe-refolding.
- (3) Isotopic investigations presented by this study yield well-defined apparent $^{40}\text{Ar}/^{39}\text{Ar}$ ages of 32-29 Ma obtained on white mica associated with chlorite. These results point towards a resetting of the

$^{40}\text{Ar}/^{39}\text{Ar}$ isotopic system most probably induced by recrystallization and/or metamorphic reaction possibly enhanced by the presence of a fluid. The results presented by this investigation are supported by additional isotopic studies performed in the south-western part of the study area (Lukmanier/Piora), where Th-Pb ages of allanite yield exactly the same ages (Janots et al. 2009) and therefore provide strong evidence that the recorded ages represent a specific metamorphic stage. In summary, all results independently revealed the existence of a greenschist facies event that clearly post-dates D2 nappe-stacking and pre-dates D3 nappe re-folding.

The geodynamical significance of this greenschist facies overprint is not clear at this stage. Possibly, the accretion of distal European margin to the orogenic wedge led to the relaxation of subduction-related down-folded isotherms by providing additional heat supply caused by high radiogenic heat production.

First nappe refolding event (~25 Ma; D3 Domleschg phase)

This D3 nappe folding event substantially modified the nappe stack in the working area. It post-dates an earlier nappe re-folding phase established only within structurally higher Valaisan and Briançonnais units east of the working area (Niemet-Beverin phase). D3 deformation produces tight megafolds such as the Lunschania antiform, as well as folds observable at the mesoscopic and microscopic scale. A second strong axial planar cleavage S3 is associated with D3 folding. However, the distinction between S2 and S3 can only be made in D3 fold hinges where S3 represents a spaced cleavage, while S3 completely transposes S2 in F3 fold limbs.

D3 deformation post-dates the ascent and emplacement of the Bergell pluton south of the working area and overprints the previously established greenschist facies event, as is independently evidenced by isotherm contours related to this greenschist facies event that are folded around the Lunschania antiform. Note that D3 deformation is associated with ongoing accretion of continental basement units (e.g. Lucomagno-Leventina nappe and Gotthard-“massif”) and is interpreted as contemporaneous with back-thrusting along the Insubric mylonite belt (formation of the Southern Steep Belt).

Based on the significantly younger apparent $^{40}\text{Ar}/^{39}\text{Ar}$ ages (weighted average age of 25.40 ± 0.45 Ma) found in one sample from Valsertal, affected by pervasive D3 deformation and showing unambiguously different micro-texture, we tentatively correlate these recorded apparent age with the timing of D3 deformation, being aware that this is speculative.

Note that the following metamorphic and tectonic events only affected the western part of the working area, i.e. in an area east of Piz Terri.

Barrovian thermal overprint (19-18 Ma)

Barrovian overprint of the south-western part of the study area represents a separate and younger heating event that initiated during a tectonically quiescent phase and that clearly post-dates D3 deformation. This is demonstrated by the isotherms related to this Barrovian metamorphism that are seen to crosscut the D3 Lunschania antiform as well as associated porphyroblasts (such as plagioclase, biotite, garnet, kyanite, staurolite) showing a clear post-tectonic microstructure. Petrologic investigations yield 450 °C at the north-eastern border of the Lepontine dome (Luzzone) up to 570-590 °C around Pizzo Molare at 0.5-0.8 GPa. Hence amphibolite facies Barrovian overprint represents a more or less “isobaric” late-stage thermal overprint that was sustained until the beginning stages of the last tectonic (D4) event.

The timing of this late-stage thermal event is recorded by the apparent $^{40}\text{Ar}/^{39}\text{Ar}$ ages of investigated biotite clustering in the 18-15.5 Ma range; due to some retrograde chloritization of biotite we prefer the published monazite U-Pb ages of 19-18 Ma (Janots et al. 2009) for dating peak-temperatures during this event.

Back-folding in the Northern Steep Belt and subsequent cooling (post-18 Ma; D4 Chièra phase)

Barrow-type amphibolite facies mineral assemblages have been severely deformed by a subsequent late-stage nappe refolding event that is associated with the formation of the Northern Steep Belt within the Penninic nappe-stack and which is only very well developed west of our study area. There, a relatively tight synform, the Chièra synform, brings the nappe-stack into an overturned, steeply north-dipping position, while in our area such D4 back-folding is less severe.

D4 deformation is only observed in the SW part of the investigated area, strain intensity rapidly decreasing towards the NE. D4 deformation sets in east of Piz Terri while intensive folding affects the area around Pizzo Molare and between the southern Lukmanier area and Olivone. Typically, D4 folds have an undulating and wavy appearance, producing a staircase-like set of syn- and antiforms on the macroscopic scale, striking E-W to ESE-WNW.

Since this D4 Chièra phase deformation outlasted Barrovian metamorphic overprint it must be very young (i.e. post-18 Ma), most probably contemporaneous with the N-directed thrusting in the Aar massif in the more external parts of the Alps and imbrications within the Subalpine molasse.

The zircon fission track ages of 10-9 Ma, as well as apatite fission track ages of 7.5-6.5 Ma, indicate the final stages of the P-T path, i.e. the timing of the cooling below some 200-330 °C for zircon, and 70-120 °C for apatite (Janots et al. 2009) due to erosional unroofing that followed the thrusting of the external massifs.

7.2. Implications regarding the geodynamic evolution of the Alps

Based on the field data presented in this study we regard radiogenic heat production by accretion of continental crust during the collisional and post-collisional stages of Alpine orogeny, associated with rising isotherms, to be mainly responsible for Barrovian metamorphism that represents a separate late-stage heating event at the north-eastern rim of the Lepontine dome. We propose that the Lepontine and Tauern thermal and structural domes both largely resulted from the local accretion of massive volumes of Sub-Penninic basement nappes derived from the distal European margin. This well explains the substantial Barrow-type thermal gradient observed at the north-eastern rim of the Lepontine dome, cutting across former nappe contacts almost perpendicular to strike. We infer that the observable crosscutting isotherms are most likely related to a late stage of purely conductive heat transfer. We emphasize, however, that in the southern parts of the Lepontine dome (Southern Steep Belt) other heat sources such as heat advection by rising eclogitic bodies and melts are probably also very important.

The metamorphic evolution of the investigated metasediments provides important information for the understanding of the formation of the Central Alps as well as the transition from subduction to collision orogenic belts in general. The three distinct metamorphic events reflect geodynamic stages and associated thermal regimes. Therefore the metamorphic record preserved in the studied metasediments is directly related to the evolution of isotherms in the Alpine orogenic wedge. These three events are as follows:

- (1) The low-temperature regime is associated with an early subduction and sediment accretion stage (42-40 Ma, HP/LT metamorphism) and led to the formation of mineral assemblages that are typical for subduction processes and related down-folding of the isotherms. During ongoing subduction, deeper parts of the orogenic wedge were thrust onto lower pressure units, a process that is accompanied with nearly isothermal or cooling decompression (36-33 Ma).
- (2) The final collision between Europe and Adria led to excessive thickening of the orogenic wedge by the accretion of distal European margin, effectively “clogging” the subduction system. Thereby the subduction of rather cold material to great depths ceased and the negative temperature anomaly typical for subduction zones started to recover. Furthermore, the accretion of distal European margin to the orogenic wedge led to the relaxation of subduction-related down-folded isotherms by providing additional heat supply caused by high radiogenic heat production. It is most likely that the recorded early-stage greenschist facies overprint (32-29 Ma) is caused by the relaxation of isotherms, and therefore this metamorphic event marks the timing during which an early collision-related thermal regime was established.
- (3) Due to massive accretion of continental crustal material after collision, the rock composition within the orogenic wedge changes dramatically: large amounts of upper-crustal European granitoid rocks were accumulated within the wedge (Sub-Penninic nappe-stack). This accumulation of vast amounts of heat-producing crustal material is responsible for increasing temperatures by the up-bending of isotherms inducing the late-stage amphibolite-facies Barrovian overprint observed in the working area (19-18 Ma). Note that these rising isotherms, in the absence of mass transport, elegantly explain the Barrow-type amphibolite facies overprint of HP/LT units that already experienced substantial decompression before, as is the case in our study area.

The recorded isotopic data reveal a significant time gap in the order of some 20 Ma between the subduction-related HP/LT event (42-40 Ma) and the later collision-related MP/MT Barrovian overprint (19-18 Ma). This considerable time interval is in accordance with the interpretation that it is the accretion of vast amounts of European continental crust (forming the present-day Lepontine dome) that provides high radiogenic heat production responsible for amphibolite facies metamorphism, being an entirely conductive and therefore rather slow process.

The new data from the north-eastern rim of the Lepontine dome provide strong evidence for the former existence of a contiguous HP/LT belt, representing a second northern suture zone associated with the closure of the Valais Ocean. Moreover, absolute timing constraints indicate that both HP/LT metamorphism and Barrow-type overprint were diachronous at the scale of the Alpine orogen; hence all indicators of metamorphic zonation such as index mineral zone boundaries must be strongly diachronous.

This study unambiguously demonstrates the importance of metasediments for the reconstruction of the metamorphic evolution of mountain belts. Furthermore, we showed that especially low-grade (HP/LT, LP/LT) metasediments that typically are devoid of indicative mineral assemblages and that therefore often were misinterpreted do provide a lot of information on the geodynamic evolution of the Alpine orogenic belt provided that a combination of detailed structural, petrologic and geochronological investigations is applied.

Bibliography

- Abbott, R.N. (1992): A petrogenetic grid for medium and high grade metabasites. *American Mineralogist* 67, 865-876.
- Agard, P., Goffé, B., Touret, J.L.R. & Vidal, O. (2000): Retrograde fluid evolution in blueschist-facies metapelites (Schistes lustrés unit, Western Alps). *Contributions to Mineralogy and Petrology* 140, 296-315.
- Agard, P., Jolivet, L. & Goffé, B. (2001): Tectonometamorphic evolution of the Schistes Lustrés complex: implications for the exhumation of HP and UHP rocks in the Western Alps. *Bulletin de la Société Géologique de France* 172, 617-636.
- Agard, P., Monié, P., Jolivet, L. & Goffé, B. (2002): Exhumation of the Schistes Lustrés complex: in situ laser probe $^{40}\text{Ar}/^{39}\text{Ar}$ constraints and implications for the Western Alps. *Journal of Metamorphic Geology* 20, 599-618.
- Allaz, J. (2008): Metamorphic evolution in the northern Central Alps: Linking ^{39}Ar - ^{40}Ar dating with thermobarometry. Unpub. PhD thesis, Universität Bern. 208 pp.
- Allaz, J., Janots, E., Engi, M., Berger, A. & Villa, I.M. (2007): Understanding Tertiary metamorphic ages in the northern Central Alps. *Geophysical Research Abstracts* 9, EGU2007-A-07684.
- Armstrong, R.L., Jäger, E. & Eberhardt, P. (1966): A comparison of K-Ar and Rb-Sr ages on Alpine biotites. *Earth and Planetary Science Letters* 1, 13-19.
- Ballèvre, M. (1988): Collision continentale et chemins P-T: l'unité pennique du Grand Paradis, Alpes Occidentales. Centre Armoricaïn d'études structurales des socles, Rennes.
- Ballèvre, M. & Lagabriele, Y. (1994): Garnet in Blueschist-facies marbles from the Queyras unit (Western Alps) - its occurrence and its significance. *Schweizerische Mineralogische und Petrographische Mitteilungen* 74, 203-212.
- Ballèvre, M., Lagabriele, Y. & Merle, O. (1990): Tertiary ductile normal faulting as a consequence of lithospheric stacking in the Western Alps. *Mémoires de la Société Géologique Suisse* 1, 227-236.
- Balogh, K. & Dunkl, I. (2005): Argon and fission track dating of Alpine metamorphism and basement exhumation in the Sopron Mts. (Eastern Alps, Hungary): thermochronology or mineral growth? *Mineralogy and Petrology* 83, 191-218.
- Barrow, G. (1893): On an intrusion of muscovitibiotite gneiss in the south-eastern Highlands of Scotland, and its accompanying metamorphism. *The Quarterly Journal of the Geological Society* 49, 330-358.
- Barrow, G. (1912): On the geology of the lower Deeside and the souther Highland border. *Proceedings of the Geologists' Association* 23, 268-284.
- Baudin, T., Marquer, D. & Persoz F. (1993): Basement-cover relationships in the Tambo nappe (Central Alps, Switzerland) – geometry, structure and kinematics. *Journal of Structural Geology* 15, 543-553.
- Baumer, A. (1964): Geologie der gotthardmassivisch-penninischen Grenzregion im oberen Bleniotal. Geologie der Blenio-Kraftwerke. Beiträge zur Geologie der Schweiz, Geotechnische Serie 39, 105 pp.
- Baumer, A., Frey, J.D., Jung, W. & Uhr, A. (1961): Die Sedimentbedeckung des Gotthard-Massivs zwischen oberen Bleniotal und Lugnez (Vorläufige Mitteilung). *Eclogae geologicae Helvetiae* 54, 478-491.
- Bearth, P. (1963): Contribution à la subdivision tectonique et stratigraphique du cristallin de la nappe du Grand Saint-Bernard dans le Valais (Suisse). In: Durand Delga, M. (Ed): *Livre à la mémoire du Professeur Fallot. Mémoire de la Société géologique de France*, Paris, 407-418.
- Bearth, P. (1967): Die Ophiolithe der Zone von Zermatt-Saas Fee. Beiträge zur Geologischen Karte der Schweiz - NF 132, 130 pp.
- Becker, H. (1993): Garnet peridotite and eclogite Sm-Nd mineral ages from the Lepontine dome (Swiss Alps) - New evidence for Eocene high-pressure metamorphism in the Central Alps. *Geology* 21, 599-602.

- Berger, A. & Bousquet, R. (2008): Subduction related metamorphism in the Alps: Review of isotopic ages based on petrology and their geodynamic consequences. In: Siegesmund, S. et al. (Eds.): Tectonic Aspects of the Alpine-Dinaride-Carpathian system. Geological Society Special Publications 298, 117-144.
- Berger, A., Rosenberg, C. & Schmid, S.M. (1996): Ascent, emplacement and exhumation of the Bergell pluton within the Southern Steep Belt of the Central Alps. Schweizerische Mineralogische und Petrographische Mitteilungen 76, 357-382.
- Berger, A., Mercolli, I. & Engi, M. (2005): The central Lepontine Alps: Notes accompanying the tectonic and petrographic map sheet Sopra Ceneri (1:100,000). Schweizerische Mineralogische und Petrographische Mitteilungen 85, 109-146.
- Berger, A., Burri T., Alt-Epping, P. & Engi, M. (2007): Tectonically controlled fluid flow and water-assisted melting in the middle crust: An example from the Central Alps. Lithos 102, 598-615.
- Berman, R.G. (1988): Internally-consistent thermodynamic data for minerals in the system Na₂O-K₂O-CaO-MgO-FeO-Fe₂O₃-Al₂O₃-SiO₂-TiO₂-H₂O-CO₂. Journal of Petrology 29, 445-522.
- Bertle, R.J. (2004): Zur Geologie des Piz Mundin-Gebietes (Engadiner Fenster, Österreich-Schweiz): Stratigraphie, Geochronologie, Strukturen. Unpub. PhD thesis, Universität Wien. 578 pp.
- Beysac, O., Goffé, B., Chopin, C. & Rouzaud, J.N. (2002a): Raman spectra of carbonaceous material in metasediments: a new geothermometer. Journal of Metamorphic Geology 20, 859-871.
- Beysac, O., Rouzaud, J.N., Goffé, B., Brunet, F. & Chopin, C. (2002b): Graphitization in a high-pressure, low-temperature metamorphic gradient: a Raman microspectroscopy and HRTEM study. Contributions to Mineralogy and Petrology 143, 19-31.
- Beysac, O., Brunet, F., Petitet, J.P., Goffé, B. & Rouzaud, J.N. (2003a): Experimental study of the microtextural and structural transformations of carbonaceous materials under pressure and temperature. European Journal of Mineralogy 15, 937-951.
- Beysac, O., Goffé, B., Petitet, J.P., Froigneux, E., Moreau, M. & Rouzaud, J.N. (2003b): On the characterization of disordered and heterogeneous carbonaceous materials by Raman spectroscopy. Spectrochimica Acta Part A - Molecular and Biomolecular Spectroscopy 59, 2267-2276.
- Beysac, O., Bollinger, L., Avouac, J.P. & Goffé, B. (2004): Thermal metamorphism in the lesser Himalaya of Nepal determined from Raman spectroscopy of carbonaceous material. Earth and Planetary Science Letters 225, 233-241.
- Beysac, O., Simoes, M., Avouac, J.P., Farley, K.A., Chen, Y.G., Chan, Y.C. & Goffé, B. (2007): Late Cenozoic metamorphic evolution and exhumation of Taiwan. Tectonics 26, TC6001, doi:10.1029/2006tc002064.
- Bigi, G., Castellarin, A., Coli, M., Dal Piaz, G.V., Sartori, R., Scandone, P. & Vai, G.B. (1990): Structural model of Italy. In: Progetto Geodinamica, SELCA, Firenze.
- Biino, G.G. & De Capitani, C. (1995): Equilibrium assemblage calculations: a new approach to metamorphic petrology. In: B. Lombardo (Ed.): Studies on metamorphic rocks and minerals of the western Alps. A Volume in Memory of Ugo Pognante. Bolletino Museo Regionale di Scienze Naturali, Torino 13, 11-53.
- Bollinger, L., Avouac, J.P., Beysac, O., Catlos, E.J., Harrison, T.M., Grove, M., Goffé, B. & Sapkota, S. (2004): Thermal structure and exhumation history of the Lesser Himalaya in central Nepal. Tectonics 23, TC5015, doi:10.1029/2003TC001564.
- Bonijoly, M., Oberlin, M. & Oberlin, A. (1982): A possible mechanism for natural graphite formation. International Journal of Coal Geology 1, 238-312.
- Borghi, A., Compagnoni, R. & Sandrone, R. (1996): Composite P-T paths in the internal Penninic massifs of the western Alps: Petrological constraints to their thermo-mechanical evolution. Eclogae geologicae Helvetiae 89, 345-367.
- Bossard, L. (1925): Der Bau der Tessiner Kulmination. Eclogae geologicae Helvetiae 19, 504-521.
- Bossard, L. (1929): Zur Petrographie unterpenninischer Decken im Gebiet der Tessiner Kulmination. Schweizerische Mineralogische und Petrographische Mitteilungen 9, 47-106.
- Bousquet, R. (2008): Metamorphic heterogeneities within a single HP unit: Overprint effect or metamorphic mix? Lithos 103, 46-69.

- Bousquet, R., Goffé, B., Henry, P., Le Pichon, X. & Chopin, C. (1997): Kinematic, thermal and petrological model of the Central Alps: Lepontine metamorphism in the upper crust and eclogitisation of the lower crust. *Tectonophysics* 273, 105-127.
- Bousquet, R., Oberhänsli, R., Goffé, B., Jolivet, L. & Vidal, O. (1998): High-pressure-low-temperature metamorphism and deformation in the Bündnerschiefer of the Engadine window: implications for the regional evolution of the eastern Central Alps. *Journal of Metamorphic Geology* 16, 657-674.
- Bousquet, R., Goffé, B., Vidal, O., Oberhänsli, R. & Patriat, M. (2002): The tectono-metamorphic history of the Valaisan domain from the Western to the Central Alps: New constraints on the evolution of the Alps. *Geological Society of America Bulletin* 114, 207-225.
- Bousquet, R., Engi, M., Gosso, G., Oberhänsli, R., Berger, A., Spalla, M.I., Zucali, M. & Goffé, B. (2004): Transition from the Western to the Central Alps. In: Oberhänsli, R. (Ed): Explanatory note to the map "Metamorphic structure of the Alps". *Mitteilungen der Österreichischen Mineralogischen Gesellschaft* 149, 145-156.
- Bousquet, R., Oberhänsli, R., Goffé, B., Wiederkehr, M., Koller, F., Schmid, S.M., Schuster, R., Engi, M., Berger, A. & Martinotti, G. (2008): Metamorphism of metasediments in the scale of an orogen: A key to the Tertiary geodynamic evolution of the Alps. In: Siegesmund, S. et al. (Eds.): *Tectonic Aspects of the Alpine-Dinaride-Carpathian system*. Geological Society Special Publications 298, 393-411.
- Brouwer, F.M. & Engi, M. (2005): Staurolite and other aluminous phases in Alpine eclogite from the Central Swiss Alps: Analysis of domain evolution. *Canadian Mineralogist* 43, 105-128.
- Brouwer, F.M., Burri, T., Engi, M. & Berger, A. (2005): Eclogite relics in the Central Alps: PT-evolution, Lu-Hf ages and implications for formation of tectonic mélange zones. *Schweizerische Mineralogische und Petrographische Mitteilungen* 85, 147-174.
- Brown, T.H., Berman, R.G. & Perkins, E.H. (1988): GEO-CALC – Software package for calculation and display of pressure-temperature-composition phase diagrams using IBM or compatible personal computer. *Computer and Geosciences* 14, 279-289.
- Brunet, C., Monié, P., Jolivet, L. & Cadet, J.-P. (2000): Migration of compression and extension in the Tyrrhenian Sea, insights from $^{40}\text{Ar}/^{39}\text{Ar}$ ages on micas along a transect from Corsica to Tuscany. *Tectonophysics* 321, 127-155.
- Bucher, K. & Frey, M. (2002): *Petrogenesis of metamorphic rocks*. 7th edition, Springer, Berlin, 341 pp.
- Bucher, S. (2003): The Briançonnais units along the ECORS-CROP transect (Italian-French Alps): structures, metamorphism and geochronology, Unpub. PhD thesis, Universität Basel, 169 pp.
- Bucher, S. & Bousquet, R. (2007): Metamorphic evolution of the Briançonnais units along the ECORS-CROP profile (Western Alps): New data on metasedimentary rocks. *Swiss Journal of Geosciences* 100, 227-242.
- Bucher, S., Schmid, S.M., Bousquet, R. & Fügenschuh, B. (2003): Late-stage deformation in a collisional orogen (Western Alps): nappe refolding, back-thrusting or normal faulting? *Terra Nova* 15, 109-117.
- Bucher S., Ulardic, C., Bousquet R., Ceriani, S., Fügenschuh B. & Schmid, S.M. (2004): Tectonic evolution of the Briançonnais units along a transect (ECORS-CROP) through the Italian-French Western Alps. *Eclogae geologicae Helvetiae* 97, 321-345.
- Burckhardt, C.E. (1942): Geologie und Petrographie des Basodino-Gebietes (nordwestliches Tessin). *Schweizerische Mineralogische und Petrographische Mitteilungen* 22, 99-188.
- Burg, J.P. & Gerya, T.V. (2005): The role of viscous heating in Barrovian metamorphism of collisional orogens: thermomechanical models and application to the Lepontine Dome in the Central Alps. *Journal of Metamorphic Geology* 23, 75-95.
- Burkhard, M. (1988): L'Helvétique de la bordure occidentale du massif de l'Aar (évolution tectonique et métamorphique). *Eclogae geologicae Helvetiae* 81, 63-114.
- Burkhard, M. & Goy-Eggenberger, D. (2001): Near vertical iso-illite-crystallinity surfaces cross-cut the recumbent fold structure of the Morcles nappe, Swiss Alps. *Clay Minerals* 36, 159-170.
- Burov, E., Jolivet, L., Le Pourhiet, L. & Poliakov, A. (2001): A thermomechanical model of exhumation of high pressure (HP) and ultra-high pressure (UHP) metamorphic rocks in Alpine-type collision belts. *Tectonophysics* 342, 113-136.

- Burri, T., Berger, A. & Engi, M. (2005): Tertiary migmatites in the Central Alps: Regional distribution, field relations, conditions of formation, and tectonic implications. *Schweizerische Mineralogische und Petrographische Mitteilungen* 85, 215-232.
- Buseck, P.R. & Bo-Jun, H. (1985): Conversion of carbonaceous material to graphite during metamorphism. *Geochimica et Cosmochimica Acta* 49, 2003-2016.
- Bustin, R.M., Ross, J.V. & Moffat, I. (1986): Vitrinite anisotropy under differential stress and high confining pressure and temperature: preliminary observations. *International Journal of Coal Geology* 6, 343-351.
- Bustin, R.M., Ross, J.V. & Rouzaud, J.N. (1995): Mechanisms of graphite formation from kerogen: experimental evidence. *International Journal of Coal Geology* 28, 1-36.
- Caby, R. (1996): Low-angle extrusion of high-pressure rocks and the balance between outward and inward displacements of Middle Penninic units in the western Alps. *Eclogae geologicae Helvetiae* 89, 229-267.
- Caby, R., Kienast, J.-R. & Saliot, P. (1978): Structure, métamorphisme et modèle d'évolution tectonique des Alpes Occidentales. *Revue de Géographie physique et de Géologie dynamique* XX, 307-322.
- Cannic, S., Mugnier, J.-L. & Lardeaux, J.-M. (1999): Neogene extension in the western Alps. In: Gosso G. et al. (Eds): 3rd workshop on Alpine geological studies. *Memorie di Scienze Geologiche* 51, 33-45.
- Caron, J.-M. (1974): Rapports entre diverses 'générations' de lawsonite et les déformations dans les Schistes lustrés des Alpes cottiennes septentrionales (France et Italie). *Bulletin de la Société Géologique de France* 16, 255-268.
- Caron, J.-M. (1994): Metamorphism and deformation in Alpine Corsica. *Schweizerische Mineralogische und Petrographische Mitteilungen* 74, 105-114.
- Casasopra, S. (1939): Studio petrografico dello gneiss granitico Leventina. *Schweizerische Mineralogische und Petrographische Mitteilungen* 19, 449-709.
- Caron, J.-M. & Saliot, P. (1969): Nouveaux gisements de lawsonite et de jadeite dans les alpes franco-italiennes. *Comptes Rendus de l'Académie des Sciences Paris* 268, 3153-3156.
- Caron, J.-M. & Pequignot, G. (1986): The transition between blueschists and lawsonite-bearing eclogites based on observations from Corsican metabasalts. *Lithos* 19, 205-218.
- Carswell, D.A. (1990): *Eclogite facies rocks*. Blackie Academic and Professional, London.
- Ceriani, S., Fügenschuh, B. & Schmid, S.M. (2001): Multi-stage thrusting at the "Penninic Front" in the Western Alps between Mont Blanc and Pelvoux massifs. *International Journal of Earth Sciences* 90, 685-702.
- Ceriani, S., Fügenschuh, B., Potel, S. & Schmid, S.M. (2003): Tectono-metamorphic evolution of the Frontal Penninic units of the Western Alps: correlation between low-grade metamorphism and tectonic phases. *Schweizerische Mineralogische und Petrographische Mitteilungen* 83, 111-131.
- Ceriani, S. & Schmid, S.M. (2004): From N-S collision to WNW-directed post-collisional thrusting and folding: Structural study of the Frontal Penninic Units in Savoie (Western Alps, France). *Eclogae geologicae Helvetiae* 97, 347-369.
- Chadwick, B. (1968): Deformation and Metamorphism in the Lukmanier Region, Central Switzerland. *Geological Society of America Bulletin* 79, 1123-1150.
- Challandes, N., Marquer, D & Villa, I.M. (2003): Dating the evolution of C-S microstructures: a combined ⁴⁰Ar/³⁹Ar step heating and UV laserprobe analysis of the Alpine Roffina shear zone. *Chemical Geology* 197, 3-19.
- Challandes, N., Marquer, D. & Villa, I.M. (2008): P-T-t modelling, fluid circulation, and ³⁹Ar-⁴⁰Ar and Rb-Sr mica ages in the Aar Massif shear zones (Swiss Alps). *Swiss Journal of Geosciences* 101, 269-288.
- Chamberlain, C.P. & Sonder, L.J. (1990): Heat-producing elements and the thermal and baric patterns of metamorphic belts. *Science* 250, 763-769.
- Chatterjee, N.D. (1976): Margarite stability and compatibility relations in the system CaO-Al₂O₃-SiO₂-H₂O as a pressure-temperature indicator. *American Mineralogist* 61, 699-709.

- Chinner, G.A. & Dixon, J.E. (1973): Some high-pressure parageneses of Allalin Gabbro, Valais, Switzerland. *Journal of Petrology* 14, 185-202.
- Chopin, C. (1981): Talc-phengite: a widespread assemblage in high-grade pelitic blueschists of the Western Alps. *Journal of Petrology* 22, 628-650.
- Chopin, C. (1984): Coesite and pure pyrope in high grade blueschists of the western alps: a first records and some consequences. *Contributions to Mineralogy and Petrology* 86, 107-118.
- Chopin, C. (1987). Very-high-pressure metamorphism in the Western Alps: implications for subduction of continental crust. *Philosophical Transactions of the Royal Society of London* 321, 183-195.
- Chopin, C. & Maluski, H. (1980): ^{40}Ar - ^{39}Ar dating of high-pressure metamorphic micas from the Gran Paradiso area (Western Alps) - evidence against the blocking temperature concept. *Contributions to Mineralogy and Petrology* 74, 109-122.
- Chopin, C. & Schreyer, W. (1983). Magnesiochloritoid and magnesiochloritoid: two index minerals of pelitic blueschists and their preliminary phase relations in the system $\text{MgO-Al}_2\text{O}_3\text{-SiO}_2\text{-H}_2\text{O}$. *American Journal of Science* 283, 72-96.
- Chopin, C. & Monié, P. (1984): A unique magnesiochloritoid-bearing, high-pressure assemblage from the Monte-Rosa, Western Alps - petrologic and ^{40}Ar - ^{39}Ar radiometric study. *Contributions to Mineralogy and Petrology* 87, 388-398.
- Chopin, C. & Sobolev, N.V. (1995): Principal mineralogic indicators of UHP in crustal rocks. In: Coleman, R.G. & Wang, X. (Eds): *Ultrahigh pressure metamorphism*. Cambridge University Press, 96-131.
- Chopin, C., Seidel, E., Theye, T., Ferraris, G., Ivaldi, G., & Catti, M. (1992): Magnesiochloritoid, and the Fe-Mg series in the chloritoid group. *European Journal of Mineralogy* 4, 67-76.
- Chopin, C., Goffé, B., Ungaretti, L. & Oberti, R. (2003): Magnesiochloritoid and zincostaurilitoid: mineral description with a petrogenetic and crystal-chemical update. *European Journal of Mineralogy* 15, 167-176.
- Christensen, J.N., Selverstone, J., Rosenfeld, J.L. & DePaolo, D.J. (1994): Correlation by Rb-Sr geochronology of garnet growth histories from different structural levels within the Tauern Window, Eastern Alps. *Contributions to Mineralogy and Petrology* 118, 1-12.
- Cigolini, C. (1995): Geology of the Internal Zone of the Grand Saint Bernard Nappe: a metamorphic Late Paleozoic volcano-sedimentary sequence in South-Western Aosta Valley (Western Alps). In: Lombardo, B. (Ed.): *Studies on metamorphic rocks and minerals of the western Alps. A Volume in Memory of Ugo Pognante*. Bolletino Museo Regionale di Scienze Naturali, Torino, 13, 293-328.
- Coleman, R.G. & Wang, X. (1995): *Ultrahigh pressure metamorphism*. Cambridge University Press, Cambridge.
- Dachs, E. (1986): High-pressure mineral assemblages and their breakdown-products in metasediments South of the Grossvenediger, Tauern Window, Austria. *Schweizerische Mineralogische und Petrographische Mitteilungen* 66, 145-162.
- Dachs, E. (1990): Geothermobarometry in metasediments of the southern Grossvenediger area (Tauern Window, Austria). *Journal of Metamorphic Geology* 8, 217-230.
- Dal Piaz, G.V. (1974): Le métamorphisme alpin de haute pression-basse température dans l'évolution structurale du bassin ophiolitique alpino-appenninique. 1ère partie. *Bolletino della Società Geologica Italiana* 93, 437-468.
- Dal Piaz, G.V. (1974): Le métamorphisme alpin de haute pression-basse température dans l'évolution structurale du bassin ophiolitique alpino-appenninique. 2ème partie. *Schweizerische Mineralogische und Petrographische Mitteilungen* 54, 399-424.
- Dal Piaz, G.V. (1999): The Austroalpine-Piedmont nappe stack and the puzzle of Alpine Tethys. In: Gosso, G. et al. (Eds): *3rd Workshop on Alpine Geological Studies*. Memorie di Scienze Geologiche, Padova, 155-176.
- Dal Piaz, G.V. (2001): History of tectonic interpretations of the Alps. *Journal of Geodynamics* 32, 99-114.
- Dal Piaz, G.V., Hunziker, J.C. & Martinotti, G. (1972): La Zona Sesia - Lanzo e l'evoluzione tettonico-metamorfica delle Alpi Nordoccidentali interne. *Memorie della Società Geologica Italiana* 11, 433-460.

- Dale, J. & Holland, T.J.B. (2003): Geothermobarometry, P-T paths and metamorphic field gradients of high-pressure rocks from the Adula Nappe, Central Alps. *Journal of Metamorphic Geology* 21, 813-830.
- Daniel, J.-M. & Jolivet, L. (1995): Detachment faults and pluton emplacement - Elba Island (Tyrrhenian sea). *Bulletin de la Société Géologique de France* 166, 341-354.
- Daniel, J.-M., Jolivet, L., Goffé, B. & Poinssot, C. (1996): Crustal-scale strain partitioning: footwall deformation below the Alpine Oligo-Miocene detachment of Corsica. *Journal of Structural Geology* 18, 41-59.
- De Capitani, C. (1994): Gleichgewichts-Phasendiagramme: Theorie und Software. Beihefte zum *European Journal of Mineralogy*, 72. Jahrestagung der Deutschen Mineralogischen Gesellschaft 6.
- De Capitani, C. & Brown, T.H. (1987): The computation of chemical equilibrium in complex systems containing non-ideal solutions. *Geochimica et Cosmochimica Acta* 51, 2639-2652.
- De Roever, W.P. (1951): Ferrocapholite, the hitherto unknown ferrous iron analogue of capholite proper. *American Mineralogist* 36, 736-745.
- Derungs, G. (2008): Structural and metamorphic evolution of metasediments at the contact between Valaisan Oceanic domain and adjacent distal European margin. Unpub. Master thesis, Universität Basel.
- De Wever, P. & Caby, R. (1981): Datation de la base des schistes lustrés postophiolitiques par des radiolaires (Oxfordien- Kimmeridgien moyen) dans les Alpes Cottiennes (Saint Véran, France). *Comptes Rendus de L'Académie des Sciences* 292, 467-472.
- Della Vedoya, B., Bellani, S.G.P. & Squarci, P. (2001). Deep temperatures and surface heat flow distribution. In: Vai, G.B. & Martini, P. (Eds): *Anatomy of an orogen: the Apennines and adjacent Mediterranean basins*. Kluwer Academic Publishers, Dordrecht, Netherlands, 65-76.
- Desmons, J., Aprahamian, J., Compagnoni, R., Cortesogno, L. & Frey, M. (1999): Alpine Metamorphism of the Western Alps: I. Middle to high T/P metamorphism. *Schweizerische Mineralogische und Petrographische Mitteilungen* 79, 89-110.
- Deville, E., Fudral, S., Lagabrielle, Y., Marthaler, M. & Sartori, M. (1992): From oceanic closure to continental collision: A synthesis of the «Schistes lustrés» metamorphic complex of the Western Alps. *Bulletin of the Geological Society of America* 104, 127-139.
- Di Vincenzo, G., Ghiribelli, B., Giorgetti, G. & Palmeri, R. (2001): Evidence of a close link between petrology and isotope records: constraints from SEM, EMP, TEM and in situ ^{40}Ar - ^{39}Ar laser analyses on multiple generations of white micas (Lanterman Range, Antarctica). *Earth and Planetary Science Letters* 192, 389-405.
- Di Vincenzo, G., Carosi, R. & Palmeri, R. (2004): The relationship between tectono-metamorphic evolution and argon isotope records in white mica: Constraints from in situ ^{40}Ar - ^{39}Ar laser analysis of the Variscan basement of Sardinia. *Journal of Petrology* 45, 1013-1043.
- Di Vincenzo, G., Tonarini, S., Lombardo, B., Castelli, D. & Ottolini, L. (2006): Comparison of ^{40}Ar - ^{39}Ar and Rb-Sr data on phengites from the UHP Brossasco-Isasca unit (Dora Maira Massif, Italy): Implications for dating white mica. *Journal of Petrology* 47, 1439-1465.
- Diessel, C.F.K., Brothers, R.N. & Black, P.M. (1978): Coalification and graphitization in high-pressure schists in New Caledonia. *Contributions to Mineralogy and Petrology* 68, 63-78.
- Dodson, M.H. (1973): Closure temperature in cooling geochronological and petrological systems. *Contributions to Mineralogy and Petrology* 40, 259-274.
- Droop, G.T.R. (1981): Alpine metamorphism of pelitic schists in the southeast Tauern Window, Austria. *Schweizerische Mineralogische und Petrographische Mitteilungen* 61, 237-273.
- Droop, G.T.R. (1985): Alpine metamorphism in the south-east Tauern Window, Austria: 1. P-T variations in space and time. *Journal of Metamorphic Geology* 3, 371-402.
- Droop, G.T.R. & Bucher-Nurminen, K. (1984): Reaction textures and metamorphic evolution of sapphirine-bearing granulites from Gruf Complex, Italian Central Alps. *Journal of Petrology* 25, 766-803.
- Egli, W. (1966): Geologisch-petrographische Untersuchungen an der NW-Aduladecke und in der Sojaschuppe (Bleniotal, Kanton Tessin). Unpub. PhD Thesis, ETH Zürich, 160 pp.
- Engi, M., Todd, C.S. & Schmatz, D.R. (1995): Tertiary metamorphic conditions in the eastern Lepontine Alps. *Schweizerische Mineralogische und Petrographische Mitteilungen* 75, 347-369.

- Engi, M., Berger, A. & Roselle, G.T. (2001): Role of the tectonic accretion channel in collisional orogeny. *Geology* 29, 1143-1146.
- Engi, M., Bousquet, R. & Berger, A. (2004): Metamorphic structure of the Central Alps. In: Oberhänsli, R. (Ed): Explanatory notes to the map "Metamorphic structure of the Alps". *Mitteilungen der Österreichischen Mineralogischen Gesellschaft* 149, 157-173.
- Ernst, W.G. (1971): Metamorphic zonation on presumably subducted lithospheric plates from Japan, California and the Alps. *Contributions to Mineralogy and Petrology* 34, 43-59.
- Ernst, W.G. & Dal Piaz, G.V. (1978): Mineral parageneses of eclogitic rocks and related mafic schists of the Piemonte ophiolite nappe, Breuil-St. Jacques area, Italian Western Alps. *American Mineralogist* 63, 621-640.
- Escher, A. & Beaumont, C. (1997): Formation, burial and exhumation of basement nappes at crustal scale: a geometric model based on the Western Swiss-Italian Alps. *Journal of Structural Geology* 19, 955-974.
- Eskola, P. (1929): Om mineral facies. *Geologiska Föreningens i Stockholm Förhandlingar* 51, 157-172.
- Etter, U. (1987): Stratigraphische und strukturgeologische Untersuchungen im gotthardmassivischen Mesozoikum zwischen dem Lukmanierpass und der Gegend von Ilanz. Unpub. PhD Thesis, Universität Bern, 162 pp.
- Evans, B.W. (1990): Phase relation of epidote blueschists. *Lithos* 25, 3-23.
- Ferreiro-Mählmann, R. (2001): Correlation of very low grade data to calibrate a thermal maturity model in a nappe tectonic setting, a case study from the Alps. *Tectonophysics* 334, 1-33.
- Ferreiro Mählmann, R., Petrova, T.V., Pironon, J., Stern, W.B., Ghanbaja, J., Dubessy, J. & Frey, M. (2002): Transmission electron microscopy study of carbonaceous material in a metamorphic profile from diagenesis to amphibolite facies (Bündnerschiefer, Eastern Switzerland). *Schweizerische Mineralogische und Petrographische Mitteilungen* 82, 253-272.
- Florineth, D. & Froitzheim, N. (1994): Transition from continental to oceanic basement in the Tasna nappe (Engadine window, Graubünden, Switzerland): Evidence for Early Cretaceous opening of the Valaisan Ocean. *Schweizerische Mineralogische und Petrographische Mitteilungen* 74, 437-448.
- Foland, K.A. (1979): Limited mobility of argon in a metamorphic terrain. *Geochimica et Cosmochimica Acta* 43, 793-801.
- Fournier, M., Jolivet, L., Goffé, B. & Dubois, R. (1991): Alpine Corsica metamorphic core complex. *Tectonics* 10, 1173-1186.
- Fox, J.S. (1975): Three-dimensional isograds from the Lukmanier-Pass, Switzerland, and their tectonic significance. *Geological Magazine* 112, 547-564.
- Franceschelli, M. & Memmi, I. (1999): Zoning of chloritoid from kyanite-facies metapsammites, Alpi Apuane, Italy. *Mineralogical Magazine* 63, 105-110.
- Franceschelli, M., Leoni, L., Memmi, I. & Puxeddu, M. (1986): Regional distribution of Al-silicates and metamorphic zonation in the low-grade Verrucano metasediments from the Northern Apennines, Italy. *Journal of Metamorphic Geology* 4, 309-321.
- Franceschelli, M., Mellini, M., Memmi, I. & Ricci, C.A. (1989): Sudoite, a rock-forming mineral in Verrucano of the Northern Apennines (Italy) and the sudoite-chloritoid-pyrophyllite assemblage in prograde metamorphism. *Contributions to Mineralogy and Petrology* 101, 274-279.
- Frank, E. (1983): Alpine metamorphism of calcareous rocks along a cross-section in the Central Alps: occurrence and breakdown of muscovite, margarite and paragonite. *Schweizerische Mineralogische und Petrographische Mitteilungen* 63, 37-93.
- Franz, G. & Spear, F.S. (1983): High pressure metamorphism of siliceous dolomites from the central Tauern Window, Austria. *American Journal of Science* 283A, 396-413.
- Freeman, S.R., Butler, R.W.H., Cliff, R.A., Inger, S. & Barnicoat, T.A.C. (1998): Deformation migration in an orogen-scale shear zone array: An example from the basal Briançonnais thrust, internal Franco-Italian Alps. *Geological Magazine* 135, 349-367.
- French, B.M. (1964): Graphitization of organic material in a progressively metamorphosed Precambrian iron formation. *Science* 146, 917-918.

- Frey, J.D. (1967): Geologie des Greinagebietes (Val Camadra - Valle Cavalasca - Val di Larciolo - Passo della Greina). Beiträge zur Geologischen Karte der Schweiz - NF 137, 112 pp.
- Frey, M. (1969): Die Metamorphose des Keupers vom Tafeljura bis zum Lukmanier-Gebiet. Beiträge zur Geologischen Karte der Schweiz NF 137, 160 pp.
- Frey, M. (1974): Alpine metamorphism of pelitic and marly rocks of the Central Alps. Schweizerische Mineralogische und Petrographische Mitteilungen 54, 489-506.
- Frey, M. (1978): Progressive low-grade metamorphism of a black shale formation, Central Swiss Alps, with special reference to Pyrophyllite and Margarite bearing assemblages. *Journal of Petrology* 19, 95-135.
- Frey, M. & Niggli, E. (1972): Margarite, an important rock-forming mineral in regionally metamorphosed low-grade rocks. *Naturwissenschaften* 59, 214-225.
- Frey, M. & Wieland, B. (1975): Chloritoid in autochthon-paraautochthonen Sedimenten des Aarmassivs. Schweizerische Mineralogische und Petrographische Mitteilungen, 55, 407-418.
- Frey, M. & Ferreiro Mählmann, R. (1999): Alpine metamorphism of the Central Alps. Schweizerische Mineralogische und Petrographische Mitteilungen 79, 135-154.
- Frey, M., Hunziker, J.C., Roggwiler, P. & Schindler, C. (1973): Progressive niedriggradige Metamorphose glaukonitführender Horizonte in den helvetischen Alpen der Ostschweiz. *Contributions to Mineralogy and Petrology* 39, 185-218.
- Frey, M., Hunziker, J.C., Frank, W., Boquet, J., Dal Piaz, G.V., Jäger, E. & Nigli, E. (1974): Alpine metamorphic of the Alps a review. Schweizerische Mineralogische und Petrographische Mitteilungen 54, 247-291.
- Frey, M., Bucher, K., Frank, E. & Mullis, J. (1980): Alpine metamorphism along the geotraverse Basel-Chiasso - a review. *Eclogae geologicae Helvetiae* 73, 527-546.
- Frey, M., Bucher, K., Frank, E. & Schwander, H. (1982): Margarite in the Central Alps. Schweizerische Mineralogische und Petrographische Mitteilungen 62, 21-45.
- Frey, M., De Capitani, C. & Liou, J.G. (1991): A new petrogenetic grid for low-grade metabasites. *Journal of Metamorphic Geology* 9, 497-509.
- Frey, M., Desmons, J. & Neubauer, F. (1999): Metamorphic map of the Alps. 1:500'000. Schweizerische Mineralogische und Petrographische Mitteilungen 79.
- Frisch, W. (1979): Tectonic progradation and plate tectonic evolution of the Alps. *Tectonophysics* 60, 121-139.
- Froitzheim, N. (2001): Origin of the Monte Rosa nappe in the Pennine Alps—A new working hypothesis. *Bulletin of the Geological Society of America* 113, 604-614.
- Froitzheim, N., Schmid, S.M. & Conti, P. (1994): Repeated change from crustal shortening to orogen-parallel extension in the Austroalpine units of Graubünden. *Eclogae geologicae Helvetiae* 87, 559-621.
- Froitzheim, N., Schmid, S.M. & Frey, M. (1996): Mesozoic paleogeography and the timing of eclogite-facies metamorphism in the Alps: A working hypothesis. *Eclogae geologicae Helvetiae* 89, 81-110.
- Froitzheim, N., Pleuger, J., Roller, S. & Nagel, T. (2003): Exhumation of high- and ultrahigh-pressure metamorphic rocks by slab extraction. *Geology* 31, 925-928.
- Fügenschuh, B. & Schmid, S.M. (2003): Late stages of deformation and exhumation of an orogen constrained by fission-track: A case study in the Western Alps. *Bulletin of the Geological Society of America* 115, 1425-1440.
- Fügenschuh, B., Loprieno, A., Ceriani, S. & Schmid, S.M. (1999): Structural analysis of the Subbriançonnais and Valais units in the area of Moutiers (Savoy, Western Alps): paleogeographical and tectonic consequences. *International Journal of Earth Sciences* 88, 201-218.
- Fuhrman, M.L. & Lindsley, D.H. (1988): Ternary-feldspar modeling and thermometry. *American Mineralogist* 73, 201-215.
- Gansser, A. (1937): Der Nordrand der Tambodecke. Schweizerische Mineralogische und Petrographische Mitteilungen 17, 291-523.

- Gebauer, D. (1996): A P-T-t path for a high-pressure ultramafic rock-association and their felsic country-rocks based on SHRIMP-dating of magmatic and metamorphic zircon domains. Example: Alpe Arami (Central Swiss Alps). In: Hart, A. & Basu, S.R. (Eds.): Reading the isotope code. American Geophysical Union, Washington D.C., 307-328.
- Gebauer, D., Grünenfelder, M., Tilton, G., Trommsdorff, V. & Schmid, S.M. (1992): The geodynamic evolution of garnet-peridotites, garnet-pyroxenites and eclogites of Alpe Arami and Cima di Gagnone (Central Alps) from Early Proterozoic to Oligocene. *Schweizerische Mineralogische und Petrographische Mitteilungen* 72, 107-111.
- Gerya, T.V. & Stöckhert, B. (2002). Exhumation rates of high pressure metamorphic rocks in subduction channels: The effect of Rheology. *Geophysical Research Letters* 29, GL1261. doi: 10.1029/2001gl014307
- Gerya, T.V., Stöckhert, B. & Perchuk, A.L. (2002): Exhumation of high-pressure metamorphic rocks in a subduction channel: A numerical simulation. *Tectonics* 21, TC1056. doi: 10.1029/2002tc001406.
- Gillet, P. & Goffé, B. (1988): On the significance of aragonite occurrence in the Western Alps. *Contributions to Mineralogy and Petrology* 99, 70-81.
- Giorgetti, G., Memmi, I. & Nieto, F. (1997): Microstructures of intergrown phyllosilicate grains from Verrucano metasediments (northern Apennines, Italy). *Contributions to Mineralogy and Petrology* 128, 127-138.
- Glodny, J., Ring, U., Kühn, A., Gleissner, P. & Franz, G. (2005): Crystallization and very rapid exhumation of the youngest Alpine eclogites (Tauern Window, Eastern Alps) from Rb/Sr mineral assemblage analysis. *Contributions to Mineralogy and Petrology* 149, 699-712.
- Glodny, J., Kühn, A. & Austrheim, H. (2008a): Diffusion versus recrystallization processes in Rb-Sr geochronology: isotopic relics in eclogite facies rocks, Western Gneiss region, Norway. *Geochimica et Cosmochimica Acta* 72, 506-525.
- Glodny, J., Kühn, A. & Austrheim, H. (2008b): Geochronology of fluid-induced eclogite and amphibolite facies metamorphic reactions in a subduction-collision system, Bergen Arcs, Norway. *Contributions to Mineralogy and Petrology* 156, 27-48.
- Goffé, B. (1977): Succession de subfacies métamorphiques en Vanoise méridionale (Savoie). *Contributions to Mineralogy and Petrology* 62, 23-41.
- Goffé, B. (1982): Définition du faciès à Fe,Mg-carpholite-chloritoïde, un marqueur du métamorphisme de HP-BT dans les métasédiments alumineux. Unpub. PhD thesis Université P. et M. Curie, Paris.
- Goffé, B. (1984): Le faciès à carpholite-chloritoïde dans la couverture Briançonnaise des Alpes Lignes: un témoin de l'histoire tectono-métamorphique régionale. *Memorie della Società Geologica Italiana* 28, 461-479.
- Goffé, B. & Velde, B. (1984): Contrasted metamorphic evolution in thrust cover units of the Briançonnais zone (French Alps): a model for the conservation of HP-BT metamorphic mineral assemblages. *Earth and Planetary Science Letters*, 68, 351-360.
- Goffé, B. & Chopin, C. (1986): High-pressure metamorphism in the Western Alps: zoneography of metapelites, chronology and consequences. *Schweizerische Mineralogische und Petrographische Mitteilungen* 66, 41-52.
- Goffé, B. & Oberhänsli, R. (1992): Ferro- and magnesiocarpholite in the «Bündnerschiefer» of the eastern Central Alps (Grisons and Engadine Window). *European Journal of Mineralogy* 4, 835-838.
- Goffé, B. & Bousquet, R. (1997): Ferrocarpholite, chloritoïde et lawsonite dans les métapelites des unités du Versoyen et du Petit St Bernard (zone valaisanne, Alpes occidentales). *Schweizerische Mineralogische und Petrographische Mitteilungen* 77, 137-147.
- Goffé, B., Goffé-Urbano, G. & Saliot, P. (1973): Sur la présence d'une variété magnésienne de la ferrocarpholite en Vanoise (Alpes françaises): sa signification probable dans le métamorphisme alpin. *Comptes Rendus de l'Académie des Sciences Paris* 277, 1965-1968.
- Goffé, B., Michard, A., Kienast, J.R. & Le Mer, O. (1988): A case study of obduction-related high-pressure low-temperature metamorphism in the upper crustal nappes, Arabian continental margin, Oman: P-T paths and kinematic interpretation. *Tectonophysics* 151, 363-386.

- Goffé, B., Michard, A., Garcia-Dueñas, V., Gonzalez-Lodeiro, F., Monié, P., Campos, J., Galindo-Zaldivar, J., Jabaloy, A., Martinez-Martinez, J.M. & Simancas, J.F. (1989): First evidence of high-pressure, low-temperature metamorphism in the Alpujarride nappes, Betic Cordilleras (SE Spain). *European Journal of Mineralogy* 1, 139-142.
- Goffé, B., Bousquet, R., Henry, P. & Le Pichon, X. (2003): Effect of the chemical composition of the crust on the metamorphic evolution of orogenic wedges. *Journal of Metamorphic Geology* 21, 123-141.
- Goffé, B., Schwartz, S., Lardeaux, J.-M. & Bousquet, R. (2004): Metamorphic structure of the Western and Ligurian Alps. In: Oberhänsli, R. (Ed): Explanatory note to the map «Metamorphic structure of the Alps». *Mitteilungen der Österreichischen Mineralogischen Gesellschaft* 149, 125-144.
- Gouzu, C., Itaya, T., Hyodo, H. & Matsuda, T. (2006): Excess ⁴⁰Ar-free phengite in ultrahigh-pressure metamorphic rocks from the Lago di Cignana area, Western Alps. *Lithos* 92, 418-430.
- Grew, E.S. (1974): Carbonaceous material in some metamorphic rocks of New England and other areas. *Journal of Geology* 82, 50-73.
- Guedes, A., Noronha, F. & Prieto, A. C. (2005): Characterisation of dispersed organic matter from lower Palaeozoic metasedimentary rocks by organic petrography, X-ray diffraction and micro-Raman spectroscopy analyses. *International Journal of Coal Geology* 62, 237-249.
- Handy, M. & Oberhänsli, R. (2004): Age map of the metamorphic structure of the Alps - tectonic interpretation and outstanding problems. In: Oberhänsli, R. et al. (Eds): Explanatory note to the map «Metamorphic structure of the Alps». *Mitteilungen der Österreichischen Mineralogischen Gesellschaft* 149, 201-226.
- Hauy, R.-J. (1822): *Traité de minéralogie*. Seconde édition, revue, corrigée et considérablement augmentée par l'auteur. Bachelier et Huzard, Paris.
- Hébert, R. & Ballèvre, M. (1993): Petrology of staurotide-bearing metapelites from the Cadomian belt, northern Brittany (France): constraints on low-pressure metamorphism. *Bulletin de la Société géologique de France* 164, 215-228.
- Heinrich, C.A. (1982): Kyanite-eclogite to amphibolite facies evolution of hydrous mafic and pelitic rocks, Adula-nappe, Central Alps. *Contributions to Mineralogy and Petrology* 81, 30-38.
- Heinrich, C.A. (1986): Eclogite facies regional metamorphism of hydrous mafic rock in the Central Alpine Adula Nappe. *Journal of Petrology* 27, 123-154.
- Henry, C. (1990): L'unité à coesite du massif de Dora maira dans son cadre pétrologique et structural (Alpes occidentales, Italie), Unpub. PhD thesis Université Paris VI.
- Henry, P., Le Pichon, X. & Goffé, B. (1997): Kinematic, thermal and petrological model of the Himalayas: constraints related to metamorphism within the underthrust Indian crust and topographic elevation. *Tectonophysics* 273, 31-56.
- Herwartz, D., Münker, C., Scherer, E.E., Nagel, T.J., Pleuger, J. & Froitzheim, N. (2008): Lu-Hf garnet geochronology of eclogites from the Balma Unit (Pennine Alps): implications for Alpine paleotectonic reconstructions. In: Froitzheim, N. & Schmid, S.M. (Eds): *Orogenic processes in the Alpine collision zone*. *Swiss Journal of Geosciences* 101(Suppl), S173-S189.
- Hess, J.C. & Lippolt, H.J. (1994): Compilation of K-Ar measurements on HD-B1 standard biotite, 1994 status report. Phanerozoic time scale, Bull. Liaisons Inform. IUGS Subcomm. Geochronol., 122, Paris.
- Hitz, L. (1995): The 3D crustal structure of the Alps of eastern Switzerland and western Austria interpreted from a network of deep-seismic profiles. *Tectonophysics* 248, 71-96.
- Hitz, L. (1996): The deep structure of the Engadine Window: Evidence from deep seismic data. *Eclogae geologicae Helvetiae* 89, 657-675.
- Hitz, L. & Pfiffner, O.A. (1997): Geologic interpretation of the seismic profiles of the Eastern Traverse (lines E1 - E3, E7 - E9): eastern Swiss Alps. In: Pfiffner et al. (Eds.): *Deep Structure of the Swiss Alps - Results of NRP 20*, Birkhäuser, Basel, 73-100.
- Höck, V. (1974): Coexisting phengite, paragonite and margarite in metasediments of mittlere Hohe-Tauern, Austria. *Contributions to Mineralogy and Petrology* 43, 261-273.
- Höck, V. (1980): Distribution maps of minerals of the Alpine metamorphism in the Penninic Tauern window, Austria. *Mitteilungen Österreichische Geologische Gesellschaft*, 71/72, 119-127.

- Hoefs, J. & Frey, M. (1976): The isotopic composition of carbonaceous matter in a metamorphic profile from the Swiss Alps. *Geochimica et Cosmochimica Acta* 40, 945-951.
- Hsü, K.J. & Briegel, U. (1991): *Geologie der Schweiz – Ein Lehrbuch für den Einstieg, und eine Auseinandersetzung mit den Experten*. Birkhäuser, Basel, 219 pp.
- Huerta, A.D., Royden, L.H. & Hodges, K.V. (1998): The thermal structure of collisional orogens as a response to accretion, erosion, and radiogenic heating. *Journal of Geophysical Research Solid Earth* 103, 15287-15302.
- Hunziker, J.C. (1974): Rb-Sr and K-Ar age determination and the Alpine history of the Western Alps. *Memoire degli Istituti di Geologia e Mineralogia dell'Università di Padova* 31, 1-54.
- Hunziker, J.C., Frey, M., Clauer, N., Dallmeyer, R.D., Friedrichsen, H., Flehmig, W., Hochstrasser, K., Roggwiler, P. & Schwander, H. (1986): The evolution of illite to muscovite: mineralogical and isotopic data from the Glarus Alps, Switzerland. *Contributions to Mineralogy and Petrology* 92, 157-180.
- Hunziker, J.C., Desmons, J. & Hurford, A.J. (1992): Thirty-two years of geochronological work in the Central and Western Alps: a review on seven maps, *Mémoires de Géologie de l'Université Lausanne*.
- Hunziker, P. (2003): The stability of tri-octahedral Fe²⁺-Mg-Al-chlorite. A combined experimental and theoretical study. Unpub. PhD thesis, Universität Basel. 162 pp.
- Hurford, A.J. (1986): Cooling and uplift patterns in the Lepontine Alps, south-central Switzerland and an age of vertical movement on the Insubric fault line. *Contributions to Mineralogy and Petrology* 92, 413-427.
- Hurford, A.J. (1990): Standardization of fission track dating calibration: recommendation by the Fission Track Working Group of the IUGS Subcommittee on Geochronology. *Chemical Geology* 80, 171-178.
- Irouschek, A. (1983): *Mineralogie und Petrographie von Metapeliten der Simano-Decke unter besonderer Berücksichtigung Cordierit-führender Gesteine zwischen Alpe Sponda und Biasca*. Unpub. PhD thesis Universität Basel.
- Ishizuka, O. (1998): Vertical and horizontal variations of the fast neutron flux in a single irradiation capsule and their significance in the laser-heating ⁴⁰Ar/³⁹Ar analysis: Case study for the hydraulic rabbit facility of the JMTR reactor, Japan. *Geochemical Journal* 32, 243-252.
- Ishizuka, O., Yuasa, M. & Uto, K. (2002): Evidence of porphyry copper-type hydrothermal activity from a submerged remnant back-arc volcano of the Izu-Bonin arc - Implications for the volcanotectonic history of back-arc seamounts. *Earth and Planetary Science Letters* 198, 381-399.
- Itaya, T. (1981): Carbonaceous material in pelitic schists of the Sanbagawa metamorphic belt in central Shikoku, Japan. *Lithos* 14, 215-224.
- Jäger, E., Niggli, E. & Wenk, E. (1967): Rb-Sr Altersbestimmungen an Glimmern der Zentralalpen. *Beiträge zur Geologischen Karte der Schweiz - NF 134*, 67 pp.
- Jamieson, R.A., Beaumont, C., Fullsack, P. & Lee, B. (1998): Barrovian regional metamorphism: where's the heat? In: Treloar, P.J. & O'Brian, P.J. (Eds.): *What drives metamorphism and metamorphic reactions?* Geological Society Special Publications 138, 23-51.
- Janots, E., Negro, F., Brunet, F., Goffé, B., Engi, M. & Bouybaouene, M.L., (2006): Evolution of the REE mineralogy in HP-LT metapelites of the Sebti complex, Rif, Morocco: Monazite stability and geochronology. *Lithos* 87, 214-234.
- Janots, E., Engi, M., Berger, A., Rubatto, D. & Gregory, C. (2007): Texture, chemistry and age of monazite and allanite in the northern Central Alps. *Geophysical Research Abstracts* 9, EGU2007-A-08582.
- Janots, E., Engi, M., Berger, A., Allaz, J., Schwarz, J.O. & Spandler, C. (2008): Prograde metamorphic sequence of REE minerals in pelitic rocks of the Central Alps: implications for allanite-monazite-xenotime phase relations from 250 to 610 °C. *Journal of Metamorphic Geology* 26, 509-526.
- Janots, E., Engi, M., Rubatto, D., Berger, A., Gregory, C. & Rahn, M.K. (2009): Metamorphic rates in collisional orogeny from in situ allanite and monazite dating. *Geology* 37, 11-14.
- Jenny, H., Frischknecht, G. & Kopp, J. (1923): *Geologie der Adula*. Beiträge zur Geologischen Karte der Schweiz NF 51, 123 pp.

- Jolivet, L., Faccenna, C., Goffé, B., Mattei, M., Rossetti, F., Brunet, C., Storti, F., Funicello, R., Cadet, J.-P., d'Agostino, N. & Parra, T. (1998a): Midcrustal shear zones in postorogenic extension: Example from the northern Tyrrhenian Sea. *Journal of Geophysical Research* 103, 12123-12161.
- Jolivet, L., Goffé, B., Bousquet, R., Oberhänsli, R. & Michard, A. (1998b): Detachments in high-pressure mountain belts, Tethyan examples. *Earth and Planetary Science Letters* 160, 31-47.
- Jullien, M. & Goffé, B. (1993): Occurrences de cookeite et de pyrophyllite dans les schistes du Dauphinois (Isère, France): Conséquences sur la répartition du métamorphisme dans les zones externes alpines. *Schweizerische Mineralogische und Petrographische Mitteilungen* 73, 357-363.
- Jung, W. (1963): Die mesozoischen Sedimente am Südostrand des Gotthard-Massivs (zwischen Plaun la Greina und Versam). *Eclogae geologicae Helvetiae* 56, 653-754.
- Keller, F. (1968): Mineralparagenesen und Geologie der Campo Tencia-Pizzo Forno-Gebirgsgruppe. Beiträge zur Geologischen Karte der Schweiz NF 135, 71 pp.
- Keller, L.M., Hess, M., Fügenschuh, B. & Schmid, S.M. (2005a): Structural and metamorphic evolution of the Camughera - Moncucco, Antrona and Monte Rosa units southwest of the Simplon line, Western Alps. *Eclogae geologicae Helvetiae* 98, 19-49.
- Keller, L.M., Abart, R., Schmid, S.M. & De Capitani, C. (2005b): Phase relations and chemical composition of phengite and paragonite in pelitic schists during decompression: a case study from the Monte Rosa nappe and Camughera-Moncucco unit, Western Alps. *Journal of Petrology* 46, 2145-2166.
- Keller, L.M., De Capitani, C. & Abart, R. (2005c): A quaternary solution model for white micas based on natural coexisting phengite-paragonite pairs. *Journal of Petrology* 46, 2129-2144.
- Keller, L.M., Fügenschuh, B., Hess, M., Schneider, B. & Schmid, S.M. (2006): Simplon fault zone in the Western and Central Alps: Mechanism of Neogene faulting and folding revisited. *Geology* 34, 317-320.
- Kelley, S.P., Arnaud, N.O. & Turner, S.P. (1994): High spatial resolution $^{40}\text{Ar}/^{39}\text{Ar}$ investigations using an ultra-violet laser probe extraction technique. *Geochimica et Cosmochimica Acta* 58, 3519-3525.
- Kligfield, R., Hunziker, J., Dallmeyer, R.D. & Schamel, S. (1986): Dating of deformation phases using K-Ar and $^{40}\text{Ar}/^{39}\text{Ar}$ techniques - Results from the Northern Apennines. *Journal of Structural Geology* 8, 781-798.
- Köppel, V., Günthert, A. & Grünenfelder, M. (1981): Patterns of U-Pb zircon and monazite ages in polymetamorphic units of the Swiss Central Alps. *Schweizerische Mineralogische und Petrographische Mitteilungen* 61, 97-119.
- Kohn, M.J. & Spear, F.S. (1993): Phase equilibria of margarite-bearing schists and chloritoid-hornblende rocks from Western New Hampshire, USA. *Journal of Petrology* 34, 631-651.
- Koller, F. & Höck, V. (1987): Mesozoic ophiolites in the Eastern Alps. In: Malpas, J. et al. (Eds): *Ophiolites, oceanic crustal analogues, Proceedings of the Symposium "TROODOS 1987"*, 253-263.
- Koons, P.O. & Thompson, A.B. (1985): Non-mafic rocks in the greenschist, blueschist and eclogite facies. *Chemical Geology* 50, 3-30.
- Kribek, B., Hrabal, J., Landais, P. & Hladikova, J. (1994): The association of poorly ordered graphite, coke and bitumens in greenschist facies rocks of the Ponikla Group, Lugicum, Czech Republic: the result of graphitization of various types of carbonaceous matter. *Journal of Metamorphic Geology* 12, 493-503.
- Kuhn, B.K., Reusser, E., Powell, R. & Günther, D. (2005): Metamorphic evolution of calc-schists in the Central Alps, Switzerland. *Schweizerische Mineralogische und Petrographische Mitteilungen* 85, 175-190.
- Kupferschmid, C. (1977): Geologie auf der Lugnezer Seite der Piz Aul-Gruppe. *Eclogae geologicae Helvetiae* 70, 1-58.
- Kurz, W., Neubauer, F. & Unzog, W. (1999): Evolution of Alpine eclogites in the Eastern Alps: implications for Alpine geodynamics. *Physics and Chemistry of the Earth, part A: Solid Earth And Geodesy* 24, 667-674.
- Lagabriele, Y. & Lemoine, M. (1997): Alpine, Corsican and Apennine ophiolites: the slow-spreading ridge model. *Comptes Rendus de l'Academie des Sciences - Series IIA - Earth and Planetary Science*, 325, 909-920.

- Lammerer, B. & Weger, M. (1998): Footwall uplift in an orogenic wedge: the Tauern Window in the Eastern Alps of Europe. *Tectonophysics* 285, 213-230.
- Landis, C.A. (1971): Graphitization of dispersed carbonaceous material in metamorphic rocks. *Contributions to Mineralogy and Petrology* 30, 34-45.
- Lanphere, M.A. & Baadsgaard, H. (2001): Precise K-Ar, $^{40}\text{Ar}/^{39}\text{Ar}$, Rb-Sr and U/Pb mineral ages from the 27.5 Ma Fish Canyon Tuff reference standard. *Chemical Geology* 175, 653-671.
- Lapen, T.J., Johnson, C.M., Baumgartner, L.P., Dal Piaz, G.V., Skora, S. & Beard, B.L. (2007): Coupling of oceanic and continental crust during Eocene eclogite-facies metamorphism: evidence from the Monte Rosa nappe, Western Alps. *Contributions to Mineralogy and Petrology* 153, 139-157.
- Lardeaux, J.M., Schwartz, S., Tricart, P., Paul, A., Guillot, S., Bethoux, N. & Masson, F. (2006): A crustal-scale cross-section of the south-western Alps combining geophysical and geological imagery. *Terra Nova* 18, 412-422.
- Large, D.J., Christy, A.G. & Fallick, A.E. (1994): Poorly crystalline carbonaceous matter in high grade metasediments: implications for graphitisation and metamorphic fluid composition. *Contributions to Mineralogy and Petrology* 116, 108-116.
- Le Bayon, B., Pitra, P., Ballèvre, M. & Bohn, M. (2006): Reconstructing P-T paths during continental collision using multi-stage garnet (Gran Paradiso nappe, Western Alps). *Journal of Metamorphic Geology* 24, 477-496.
- Le Pichon, X., Bergerat, F. & Roulet, M.-J. (1988): Plate kinematics and tectonics leading to the Alpine belt formation: A new analysis. In: Clark, S.P. et al., (Eds): *Processes in continental lithospheric deformation*. Geological Society of America Special Paper 218, 111-131.
- Lee, Y.J. (2004): The second order Raman spectroscopy in carbon crystallinity. *Journal of Nuclear Materials* 325, 174-179.
- Lefèvre, R. & Michard, A. (1965): La jadéite dans le métamorphisme alpin, à propos des gisements de type nouveau, de la bande d'Acceglio (Alpes cottiennes, Italie). *Bulletin de la Société française de Minéralogie et de Cristallographie* LXXXVIII, 664-677.
- Leikine, M., Kienast, J.-R., Eltchaninoff-Lancelot, C. & Triboulet, S. (1983): Le métamorphisme polyphasé des unités dauphinoises entre Belledonne et Mont-Blanc (Alpes occidentales). Relation avec les épisodes de déformation. *Bulletin de la Société géologique de France* XXV, 575-587.
- Leimser, W.M. & Purtscheller, F. (1980): Beiträge zur Metamorphose von Metavulkaniten im Pennin des Engadiner Fensters. *Mitteilungen Österreichische Geologische Gesellschaft* 71/72, 129-137.
- Leloup, P.H., Arnaud, N., Sobel, E.R. & Lacassin, R. (2005): Alpine thermal and structural evolution of the highest external crystalline massif: The Mont Blanc. *Tectonics* 24, TC4002. doi: 10.1029/2004tc001676.
- Lemoine, M. & Tricart, P. (1986): Les schistes lustrés piémontais des Alpes Occidentales: Approches stratigraphique, structurale et sédimentologique. *Eclogae geologicae Helvetiae* 79, 271-294.
- Leoni, L., Marroni, M., Sartori, F. & Tamponi, M. (1996): Metamorphic grade in the metapelites of the Internal Liguride Units (Northern Apennines, Italy). *European Journal of Mineralogy* 8, 35-50.
- Lespade, P., Marchand, A., Couzi, M. & Cruege, F. (1984): Caractérisation de matériaux carbonés par microspectroscopie Raman. *Carbon* 22, 375-385.
- Liati, A. & Froitzheim, N. (2006): Assessing the Valais Ocean, Western Alps: U-Pb SHRIMP zircon geochronology of eclogite in the Balma unit, on top of the Monte Rosa nappe. *European Journal of Mineralogy* 18, 299-308.
- Liati, A., Froitzheim, N. & Fanning, C.M. (2005): Jurassic ophiolites within the Valais domain of the Western and Central Alps: geochronological evidence for re-rifting of oceanic crust. *Contributions to Mineralogy and Petrology* 149, 446-461.
- Lihou, J.C. & Allen, P.A. (1996): Importance of inherited rift margin structures in the early North Alpine Foreland Basin, Switzerland. *Basin Research* 8, 425-442.
- Livi, K.J.T., Ferry, J.M., Veblen, D.R., Frey, M. & Connolly, J.A.D. (2002): Reactions and physical conditions during metamorphism of Liassic aluminous black shales and marls in central Switzerland. *European Journal of Mineralogy* 14, 647-672.
- Löw, S. (1987): Die tektono-metamorphe Entwicklung der nördlichen Adula-Decke. *Beiträge zur Geologischen Karte der Schweiz* NF 161, 84 pp.

- Maluski, H. & Monié, P. (1988): $^{40}\text{Ar}/^{39}\text{Ar}$ laser-probe multidating inside single biotites of a Variscan orthogneiss (Pinet Massif Central, France). *Chemical Geology* 73, 245-263.
- Mancktelow, N.S. (1992): Neogene lateral extension during convergence in the Central Alps: evidence from interrelated faulting and backfolding around the Simplonpass (Switzerland). *Tectonophysics* 215, 295-317.
- Mancktelow, N.S. & Pavlis, T.L. (1994): Fold-fault relationships in low-angle detachment systems. *Tectonics* 13, 668-685.
- Marquer, D. & Gapais, D. (1985): Les massifs cristallins externes sur une transversale Guttannen-Val Bedretto (Alpes centrales): structure et histoire cinématique. *Comptes Rendues de l'Académie des Sciences de Paris* 301, 543-546.
- Marquer, D., Challandes, N. & Baudin, T. (1996): Shear zone patterns and strain distribution at the scale of a Penninic nappe: The Suretta nappe (eastern Swiss Alps). *Journal of Structural Geology* 18, 753-764.
- Massonne, H.-J. (1995): Experimental and petrogenetic study of UHPM. In: Coleman, R.G. & Wang, X. (Eds): *Ultra-high pressure metamorphism*. Cambridge University Press, 159-181.
- Massonne, H.-J. & Schreyer, W. (1987): Phengite geobarometry based on the limiting assemblage with K-feldspar, phlogopite and quartz. *Contributions to Mineralogy and Petrology* 96, 212-224.
- Massonne, H.-J. & Szpurka, Z. (1997): Thermodynamic properties of white micas on the basis of high-pressure experiments in the systems $\text{K}_2\text{O}-\text{MgO}-\text{Al}_2\text{O}_3-\text{SiO}_2-\text{H}_2\text{O}$ and $\text{K}_2\text{O}-\text{FeO}-\text{Al}_2\text{O}_3-\text{SiO}_2-\text{H}_2\text{O}$. *Lithos* 41, 229-250.
- Massonne, H.-J. & O'Brien, P.J. (2003): The Bohemian Massif and the NW Himalaya. In: Carson, C.J. & Compagnoni, R. (Eds): *Ultrahigh Pressure Metamorphism*. Eötvös University Press, Budapest, 145-187.
- Matile, L. & Widmer, T.W. (1993): Contact-metamorphism of siliceous dolomites marls and pelites in the SE contact aureole of the Bruffione intrusion (SE Adamello, N Italy). *Schweizerische Mineralogische und Petrographische Mitteilungen* 73, 53-67.
- Mayerat Demarne, A.-M. (1994): Analyse structurale de la zone frontale de la nappe de Tambo (Pennique, Grisons, Suisse). *Beiträge zur Geologischen Karte der Schweiz NF 165*, 68 pp.
- McDade, P. & Harley, S.L. (2001): A petrogenetic grid for aluminous granulite facies metapelites in the KFMASH system. *Journal of Metamorphic Geology* 19, 45-60.
- McDougall, I. & Harrison, T.M. (1999): *Geochronology and thermochronology by the $^{40}\text{Ar}/^{39}\text{Ar}$ method*. Oxford University Press, New York and Oxford, 269 pp.
- Mercogli, I., Biino, G.G. & Abrecht, J. (1994): The lithostratigraphy of the pre-Mesozoic basement of the Gotthard massif - a review. *Schweizerische Mineralogische und Petrographische Mitteilungen* 74, 29-40.
- Merle, O., Cobbold, P.R. & Schmid, S.M. (1989): Tertiary kinematics in the Lepontine Alps. In: Coward, M.P. et al. (Eds.): *Alpine Tectonics*. Geological Society Special Publications 45, 113-134.
- Meyre, C., De Capitani, C. & Partzsch, J.H. (1997): A ternary solid solution model for omphacite and its application to geothermobarometry of eclogites from the Middle Adula nappe (Central Alps, Switzerland). *Journal of Metamorphic Geology* 15, 687-700.
- Michard, A., Chopin, C. & Henry, C. (1993): Compression versus extension in the exhumation of the Dora-Maira coesite-bearing unit, Western Alps, Italy. *Tectonophysics* 221, 173-193.
- Michalski, I. & Soom, M. (1990): The Alpine thermo-tectonic evolution of the Aar and Gotthard massifs, central Switzerland: Fission track ages on zircon and apatite and K-Ar mica ages. *Schweizerische Mineralogische und Petrographische Mitteilungen* 70, 373-387.
- Miller, C., Konzett, J., Tiepolo, M., Armstrong, R.A. & Thöni, M. (2007): Jadeite-gneiss from the Eclogite Zone, Tauern Window, Eastern Alps, Austria: Metamorphic, geochemical and zircon record of a sedimentary protolith. *Lithos* 93, 68-88.
- Milnes, A.G. (1974): Structure of the Pennine zone (Central Alps) - a new working hypothesis. *Geological Society of America Bulletin* 85, 1727-1732.
- Milnes, A.G. (1976): Strukturelle Probleme im Bereich der Schweizer Geotraverse - das Lukmanier-Massiv. *Schweizerische Mineralogische und Petrographische Mitteilungen* 56, 615-618.

- Milnes, A.G. & Schmutz, H.-U. (1978): Structure and history of the Suretta nappe (Pennine zone, Central Alps) - a field study. *Eclogae geologicae Helvetiae* 71, 19-33.
- Molli, G., Conti, P., Giorgetti, G., Meccheri, M. & Oesterling, N. (2000a): Microfabric study on the deformational and thermal history of the Alpi Apuane marbles (Carrara marbles), Italy. *Journal of Structural Geology* 22, 1809-1825.
- Molli, G., Giorgetti, G. & Meccheri, M. (2000b): Structural and petrological constraints on the tectono-metamorphic evolution of the Massa Unit (Alpi Apuane, NW Tuscany, Italy). *Geological Journal* 35, 251-264.
- Molli, G., Tribuzio, R. & Marquer, D. (2006): Deformation and metamorphism at the eastern border of the Tenda Massif (NE Corsica): a record of subduction and exhumation of continental crust. *Journal of Structural Geology* 28, 1748-1766.
- Monié, P. (1990): Preservation of Hercynian $^{40}\text{Ar}/^{39}\text{Ar}$ ages through high-pressure low-temperature Alpine metamorphism in the Western Alps. *European Journal of Mineralogy* 2, 343-361.
- Nabholz, W.K. (1945): Geologie der Bündnerschiefergebirge zwischen Rheinwald, Valser- und Safiental. *Eclogae geologicae Helvetiae* 38, 1-119.
- Nagel, T. (2002): Metamorphic and structural history of the southern Adula nappe (Graubünden, Switzerland). Unpub. PhD thesis, Universität Basel. 103 pp.
- Nagel, T. (2008): Tertiary subduction, collision, and exhumation recorded in the Adula nappe, central Alps. In S. Siegesmund et al. (Eds.): *Tectonic Aspects of the Alpine-Dinaride-Carpathian system*. Geological Society Special Publications 298, 365-392.
- Nagel, T., de Capitani, C., Frey, M., Froitzheim, N., Stünitz, H. & Schmid, S.M. (2002a): Structural and metamorphic evolution during rapid exhumation in the Lepontine dome (southern Simano and Adula nappes, Central Alps, Switzerland). *Eclogae geologicae Helvetiae* 95, 301-321.
- Nagel, T., de Capitani, C. & Frey, M. (2002b): Isograds and P-T evolution in the eastern Lepontine Alps (Graubünden, Switzerland). *Journal of Metamorphic Geology* 20, 309-324.
- Nänny, P. (1948): Zur Geologie der Prättigauschiefer zwischen Rhätikon und Plessur. *Mitteilungen aus dem Geologischen Institut der Eidgenössischen Technischen Hochschule und der Universität Zürich* 30, 127 pp.
- Nasdala, L., Smith, D.C., Kaindl, R. & Ziemann, M.A. (2004): Raman spectroscopy: analytical perspectives in mineralogical research. In: A. Beran & E. Libowitzky (Eds.): *Spectroscopic Methods in Mineralogy*. EMU Notes in Mineralogy 6, European Mineralogical Union, Eötvös University Press, Budapest, 281-343.
- Negro, F., Beyssac, O., Goffé, B., Saddiqi, O. & Bouybaouène, M.L. (2006): Thermal structure of the Alboran Domain in the Rif (northern Morocco) and the Western Betics (southern Spain). Constraints from Raman spectroscopy of carbonaceous material. *Journal of Metamorphic Geology* 24, 309-327.
- Nemanich, R.J. & Solin, S.A. (1979): First- and second-order Raman scattering from finite-size crystals of graphite. *Physical Review B* 20, 392-401.
- Neubauer, F., Genser, J., Kurz, W. & Wang, X. (1999): Exhumation of the Tauern window, Eastern Alps. *Physics and Chemistry of the Earth, part A: Solid Earth and Geodesy* 24, 675-680.
- Niggli, E. (1970): Alpine Metamorphose und alpine Gebirgsbildung. *Fortschritte der Mineralogie* 47, 16-26.
- Niggli, E. & Niggli, C. (1965): Karten der Verbreitung einiger Mineralien der alpidischen Metamorphose in den Schweizer Alpen (Stilpnomelan, Alkali-Amphibol, Chloritoid, Staurolith, Disthen, Sillimanit). *Eclogae geologicae Helvetiae* 58, 335-368.
- Niggli, E. & Zwart, H.J. (1973): Metamorphic Map of the Alps, scale 1:1'000'000. Subcommission for the Cartography of the Metamorphic Belts of the World. Sheet 17 of the Metamorphic Map of Europe. Leiden/UNESCO, Paris.
- Niggli, P., Preiswerk, H., Grütter, O., Bossard, L. & Kündig, E. (1936): Geologische Beschreibung der Tessiner Alpen zwischen Maggia und Bleniothal. *Beiträge zur Geologischen Karte der Schweiz NF* 71, 190 pp.
- Nimis, P. & Trommsdorff, V. (2001): Revised thermobarometry of Alpe Arami and other garnet peridotites from the Central Alps. *Journal of Petrology* 42, 103-115.

- Nover, G., Stoll, J.B. & von der Gönna, J. (2005): Promotion of graphite formation by tectonic stress - a laboratory experiment. *Geophysical Journal International* 160, 1059-1067.
- Oberhänsli, R. (1977): Natriumamphibol-führende metamorphe basische Gesteine aus den Bündnerschiefern Graubündens. Unpub. PhD thesis, ETH Zürich. 152 pp.
- Oberhänsli, R. (1978): Chemische Untersuchungen an Glaukophan-führenden basischen Gesteinen aus den Bündnerschiefern Graubündens. *Schweizerische Mineralogische und Petrographische Mitteilungen* 58, 139-156.
- Oberhänsli, R. (1994): Subducted and obducted ophiolites of the Central Alps: Paleotectonic implications deduced by their distribution and metamorphic overprint. *Lithos* 33, 109-118.
- Oberhänsli, R., Goffé, B. & Bousquet, R. (1995): Record of a HP-LT metamorphic evolution in the Valais zone: Geodynamic implications. In: Lombardo, B. (Ed.): *Studies on metamorphic rocks and minerals of the western Alps. A Volume in Memory of Ugo Pognante*. Bolletino Museo Regionale di Scienze Naturali, Torino, 13, 221-239.
- Oberhänsli, R., Partzsch, J., Candan, O. & Cetinkaplan, M. (2001): First occurrence of Fe-Mg-carpholite documenting a high-pressure metamorphism in metasediments of the Lycian Nappes, SW Turkey. *International Journal of Earth Sciences* 89, 867-873.
- Oberhänsli, R., Bousquet, R. & Goffé, B. (2003): Comment to «Chloritoid composition and formation in the eastern Central Alps: a comparison between Penninic and Helvetic occurrences» by M. Rahn, M. Steinmann & M. Frey. *Schweizerische Mineralogische und Petrographische Mitteilungen* 83, 341-344.
- Oberhänsli, R., Bousquet, R., Engi, M., Goffé, B., Gosso, G., Handy, M., Höck, V., Koller, F., Lardeaux, J.-M., Polino, R., Rossi, P., Schuster, R., Schwartz, S. & Spalla, M.I. (2004): Metamorphic structure of the Alps. In: Oberhänsli, R. (Ed.): *Explanatory note to the map «Metamorphic structure of the Alps, 1:1'000'000»*, Commission for the Geological Map of the World, Paris. *Mitteilungen der Österreichischen Mineralogischen Gesellschaft*, 149.
- Okuyama-Kusunose, Y. & Itaya, T. (1987): Metamorphism of carbonaceous material in the Tono contact aureole, Kitakami Mountains, Japan. *Journal of Metamorphic Geology* 5, 121-139.
- Parra, T., Vidal, O. & Agard, P. (2002a): A thermodynamic model for Fe-Mg dioctahedral K white micas using data from phase-equilibrium experiments and natural pelitic assemblages. *Contributions to Mineralogy and Petrology* 143, 706-732.
- Parra, T., Vidal, O. & Jolivet, L. (2002b): Relation between the intensity of deformation and retrogression in blueschist metapelites of Tinos Island (Greece) evidenced by chlorite-mica local equilibria. *Lithos* 63, 41-66.
- Partzsch, J.H. (1998): The tectono-metamorphic evolution of the middle Adula nappe, Central Alps, Switzerland. Unpub. PhD Thesis, Universität Basel, 142 pp.
- Pasteris, J.D. (1989): In situ analysis in geological thin-sections by Laser Raman microprobe microspectroscopy: a cautionary note. *Applied Spectroscopy* 43, 567-570.
- Pasteris, J.D. & Wopenka, B. (1991): Raman-spectra of graphite as indicators of degree of metamorphism. *Canadian Mineralogist* 29, 1-9.
- Pattison, D.R.M., Spear, F.S., Debuhr, C.L., Cheney, J.T. & Guidotti, C.V. (2002): Thermodynamic modelling of the reaction muscovite + cordierite Al_2SiO_5 + biotite + quartz + H_2O : constraints from natural assemblages and implications for the metapelitic petrogenetic grid. *Journal of Metamorphic Geology* 20, 99-118.
- Peacock, S.M. (1996): Thermal and petrologic structure of subduction zones. In: Bebout G.E. et al. (Eds.): *Subduction from Top to Bottom*. American Geophysical Union, Washington D.C., 119-133.
- Pesquera, A. & Velasco, F. (1988): Metamorphism of the Paleozoic Cinco Villas massif (Basque Pyrenees) - Illite crystallinity and graphitization degree. *Mineralogical Magazine* 52, 615-625.
- Petrova, T.V., Ferreiro Mählmann, R., Stern, W.B. & Frey, M. (2002): Application of combustion and DTA-TGA analysis to the study of metamorphic organic matter. *Schweizerische Mineralogische und Petrographische Mitteilungen* 82, 33-53.
- Pfiffner, O.A. (1977): Tektonische Untersuchungen im Infrahelvetikum der Ostschweiz. *Mitteilungen aus dem Geologischen Institut der Eidgenössischen Technischen Hochschule und der Universität Zürich* 217, 432 pp.

- Pfiffner, O.A., Sahli, S. & Stäubli, M. (1997): Compression and uplift of the external massifs in the Helvetic zone. In: Pfiffner, O.A. et al. (Eds.): *Deep Structure of the Swiss Alps - Results of NRP 20*, Birkhäuser, Basel, 139-153.
- Pfiffner, O.A., Ellis, S. & Beaumont, C. (2000): Collision tectonics in the Swiss Alps: Insight from geodynamic modeling. *Tectonics* 19, 1065-1094.
- Philippot, P., Blichert-Toft, J., Perchuk, A., Costa, S. & Gerasimov, V. (2001): Lu-Hf and Ar-Ar chronometry supports extreme rate of subduction zone metamorphism deduced from geospeedometry. *Tectonophysics* 342, 23-38.
- Platt, J.P. (1986): Dynamics of orogenic wedges and the uplift of high-pressure metamorphic rocks. *Geological Society of America Bulletin* 97, 1037-1053.
- Platt, J.P. (1993): Exhumation of high-pressure rocks: a review of concepts and processes. *Terra Nova* 5, 119-133.
- Pleuger, J., Hundenborn, R., Kremer, K., Babinka, S., Kurz, W., Jansen, E. & Froitzheim, N. (2003): Structural evolution of Adula nappe, Misox zone, and Tambo nappe in the San Bernardino area: Constraints for the exhumation of the Adula eclogites. *Mitteilungen der Österreichischen Geologischen Gesellschaft* 94 (2001), 99-122.
- Pleuger, J., Froitzheim, N. & Jansen, E. (2005): Folded continental and oceanic nappes on the southern side of Monte Rosa (western Alps, Italy): Anatomy of a double collision suture. *Tectonics* 24, TC4013. doi: 10.1029/2004tc001737.
- Pleuger, J., Nagel, T.J., Walter, J.M., Jansen, E. & Froitzheim, N. (2008): On the role and importance of orogen-parallel and -perpendicular extension, transcurrent shearing, and backthrusting in the Monte Rosa nappe and the Southern Steep Belt of the Alps (Penninic zone, Switzerland and Italy). In: Siegesmund, S. et al. (Eds.): *Tectonic Aspects of the Alpine-Dinaride-Carpathian system*. Geological Society Special Publications 298, 251-280.
- Polino, R., Dal Piaz, G.V. & Gosso, G. (1990): The alpine cretaceous orogeny : an accretionary wedge model based on integrated stratigraphic, petrologic and radiometric data. In: Roure, F. et al. (Eds.): *Deep structure of the Alps*. Mémoire de la Société géologique de France, Paris, 345-367.
- Preiswerk, H. (1918): *Geologische Beschreibung der Lepontinischen Alpen*. Zweiter Teil: Oberes Tessin und Maggiagebiet. Beiträge zur Geologischen Karte der Schweiz 26, 81pp.
- Probst, P. (1980): Die Bündnerschiefer des nördlichen Penninikums zwischen Valser Tal und Passo di San Giacomo. Beiträge zur Geologischen Karte der Schweiz - NF 153, 64 pp.
- Proyer, A. (2003): Metamorphism of pelites in NKFMAASH a new petrogenetic grid with implications for the preservation of high-pressure mineral assemblages during exhumation. *Journal of Metamorphic Geology* 21, 493-509.
- Purdy, J.W. & Jäger, E. (1976): K-Ar ages on rock-forming minerals from the Central Alps. *Memorie degli Istituti di geologia e mineralogia dell'Università di Padova* 30, 32 pp.
- Quinn, A.W. & Glass, H.D. (1958): Rank of coal and metamorphic grade of rocks of Narragansett basin of Rhode Island. *Economic Geology* 53, 563-576.
- Rahl, J.M., Anderson, K.M., Brandon, M.T. & Fassoulas, C. (2005): Raman spectroscopic carbonaceous material thermometry of low-grade metamorphic rocks: Calibration and application to tectonic exhumation in Crete, Greece. *Earth and Planetary Science Letters* 240, 339-354.
- Rahn, M.K., Steinmann, M. & Frey, M. (2003): Chloritoid composition and formation in the eastern Central Alps: a comparison between Penninic and Helvetic occurrences. *Schweizerische Mineralogische und Petrographische Mitteilungen* 82, 409-426.
- Rantitsch, G., Grogger, W., Teichert, C., Ebner, F., Hofer, C., Maurer, E.M., Schaffer, B. & Toth, M. (2004): Conversion of carbonaceous material to graphite within the Greywacke Zone of the Eastern Alps. *International Journal of Earth Sciences* 93, 959-973.
- Ratschbacher, L., Dingeldeya, C., Miller, C., Hacker, B.R. & McWilliams, M.O. (2004): Formation, subduction, and exhumation of Penninic oceanic crust in the Eastern Alps: time constraints from $^{40}\text{Ar}/^{39}\text{Ar}$ geochronology. *Tectonophysics* 394, 155-170.
- Rimmelé, G., Jolivet, L., Oberhänsli, R. & Goffé, B. (2003a): Deformation history of the high-pressure Lycian Nappes and implications for tectonic evolution of SW Turkey. *Tectonics* 22, doi:10.1029/2001TC901041.

- Rimmelé, G., Oberhänsli, R., Goffé, B., Jolivet, L., Candan, O. & Cetinkaplan, M. (2003b): First evidence of high-pressure metamorphism in the "Cover Series" of the southern Menderes Massif. Tectonic and metamorphic implications for the evolution of SW Turkey. *Lithos* 71, 19-46.
- Rimmelé, G., Parra, T., Goffé, B., Oberhänsli, R., Jolivet, L. & Candan, O. (2005): Exhumation paths of high-pressure-low-temperature metamorphic rocks from the Lycian Nappes and the Menderes Massif (SW Turkey): a multi-equilibrium approach. *Journal of Petrology* 46, 641-669.
- Ring, U. (1992): The Alpine geodynamic evolution of Penninic nappes in the eastern Central Alps: geothermobarometric and kinematic data. *Journal of Metamorphic Geology* 10, 33-53.
- Robyr, M., Vonlanthen, P., Baumgartner, L.P. & Grobety, B. (2007): Growth mechanism of snowball garnets from the Lukmanier Pass area (Central Alps, Switzerland): a combined mCT/EPMA/EBSD study. *Terra Nova* 19, 240-244.
- Rolland, Y., Lardeaux, J.M., Guillot, S. & Nicollet, C. (2000): Extension syn-convergence, poinçonnement vertical et unités métamorphiques contrastées en bordure ouest du Grand Paradis (Alpes Franco-Italiennes). *Geodinamica Acta* 13, 133-148.
- Roselle, G.T. & Engi, M. (2002): Ultra high pressure (UHP) terrains: Lessons from thermal modeling. *American Journal of Science* 302, 410-441.
- Roselle, G.T., Thüning, M. & Engi, M. (2002): MELONPIT: A finite element code for simulating tectonic mass movement and heat flow within subduction zones. *American Journal of Science* 302, 381-409.
- Rossetti, F., Faccenna, C., Jolivet, L., Funiciello, R., Tecce, F. & Brunet, C. (1999): Syn- versus post-orogenic extension: the case study of Giglio Island (Northern Tyrrhenian Sea, Italy). *Tectonophysics* 304, 71-93.
- Rossetti, F., Faccenna, C., Jolivet, L., Funiciello, R., Goffé, B., Tecce, F., Brunet, C., Monié, P. & Vidal, O. (2001): Structural signature and exhumation P-T-t path of the Gorgona blueschist sequence (Tuscan archipelago, Italy). *Ophioliti* 26, 175-186.
- Roure, F., Heitzmann, P. & Polino, R. (1990): Deep structure of the Alps. *Mémoires de la société géologique de France*, Paris.
- Rütti, R., Maxelon, M. & Mancktelow, N.S. (2005): Structure and kinematics of the northern Simano Nappe, Central Alps, Switzerland. *Eclogae geologicae Helveticae* 98, 63-81.
- Rütti, R., Marquer, D. & Thompson, A.B. (2008): Tertiary tectono-metamorphic evolution of the European margin during Alpine collision: Example of the Leventina Nappe (Central Alps, Switzerland). In: Froitzheim, N. & Schmid, S.M. (Eds): *Orogenic processes in the Alpine collision zone*. *Swiss Journal of Geosciences* 101(Suppl), S157-S172.
- Santini, L. (1992): Geochemistry and geochronology of the basic rocks of the Penninic nappes of East-Central Alps (Switzerland). Unpub. PhD thesis, Université de Lausanne. 150 pp.
- Saliot, P. (1979): La jadéite dans les Alpes françaises. *Bulletin de la Société française de Minéralogie et de Cristallographie* 102, 391-401.
- Scaillet, S. (1996): Excess ^{40}Ar transport scale and mechanism in high-pressure phengites: A case study from an eclogitized metabasite of the Dora Maira nappe, Western Alps. *Geochimica et Cosmochimica Acta* 60, 1075-1090.
- Schaer, J.-P. (1959): Géologie de la partie septentrionale de l'éventail de Bagnes (entre le Val d'Hérémence et le Val de Bagnes, Valais, Suisse). *Archives des Sciences (Genève)* 12, 473-620.
- Schmid, S.M. & Kissling, E. (2000): The arc of the Western Alps in the light of new data on deep crustal structure. *Tectonics* 19, 62-85.
- Schmid, S.M., Zingg, A. & Handy, M. (1987): The kinematics of movements along the Insubric line and the emplacement of the Ivrea zone. *Tectonophysics* 135, 47-66.
- Schmid, S.M., Rück, P. & Schreurs, G. (1990): The significance of the Schams nappes for the reconstruction of the paleotectonic and orogenic evolution of the Penninic zone along the NFP-20 East traverse (Grisons, eastern Switzerland). In: Roure, F. et al. (Eds.): *Deep structure of the Alps*, *Mémoire de la Société de France*, Paris, 156, 263-287.
- Schmid, S.M., Pfiffner, O.A., Froitzheim, N., Schönborn, G. & Kissling, E. (1996): Geophysical-geological transect and tectonic evolution of the Swiss-Italian Alps. *Tectonics* 15, 1036-1064.

- Schmid, S.M., Pfiffner, O.A., Schönborn, G., Froitzheim, N. & Kissling, E. (1997a): Integrated cross section and tectonic evolution of the Alps along the Eastern Traverse. In: Pfiffner, O.A. et al. (Eds.): Deep Structure of the Swiss Alps - Results of NRP 20, Birkhäuser, Basel, 289-304.
- Schmid, S.M., Pfiffner, O.A. & Schreurs, G. (1997b): Rifting and collision in the Penninic zone of eastern Switzerland. In: Pfiffner, O.A. et al. (Eds.): Deep Structure of the Swiss Alps - Results of NRP 20, Birkhäuser, Basel, 160-185.
- Schmid, S.M., Fügenschuh, B., Kissling, E. & Schuster, R. (2004): Tectonic map and overall architecture of the Alpine orogen. *Eclogae geologicae Helveticae* 97, 93-117.
- Schmid, S.M., Bernoulli, D., Fügenschuh, B., Matenco, L., Schefer, S., Schuster, R., Tischler, M. & Ustaszewski, K. (2008): The Alpine-Carpathian-Dinaridic orogenic system: correlation and evolution of tectonic units. *Swiss Journal of Geosciences* 101, 139-183.
- Schmidt, C. & Preiswerk, H. (1908): Geologische Karte der Simplongruppe mit Profilen und Erläuterungen. *Beiträge zur Geologischen Karte der Schweiz* 26.
- Schmitz, S., Möller, A., Wilke, M., Malzer, W., Kanngiesser, B., Bousquet, R., Berger, A. & Schefer, S. (*in press*): 3D synchrotron radiation x-ray fluorescence (SRXRF) chemical U-Th-Pb dating of monazite. *European Journal of Mineralogy*, *in press*.
- Schreurs, G. (1993): Structural analysis of the Schams nappes and adjacent tectonic units: implications for the orogenic evolution of the Pennine zone in eastern Switzerland. *Bulletin de la Société Géologique de France* 164, 415-435.
- Schwartz, S., Lardeaux, J.-M. & Tricart, P. (2000): La zone d'Acceglio (Alpes cottiennes): un nouvel exemple de croûte continentale éclogitisée dans les Alpes occidentales. *Comptes Rendus de l'Académie des Sciences Paris* 320, 859-866.
- Scrocca, D., Doglioni, C. & Innocenti, F. (2003): Constraints for an interpretation of the Italian geodynamics: a review. *Memorie Descrittive della Carta Geologica d'Italia LXII*, 15-46.
- Selverstone, J. (1985): Petrological constraints on imbrication metamorphism and uplift in the SW Tauern Window, Eastern Alps. *Tectonics* 4, 687-704.
- Selverstone, J. & Spear, F.S. (1985): Metamorphic P-T paths from pelitic schists and greenstones from the south-west Tauern Window. *Journal of Metamorphic Geology* 3, 439-465.
- Selverstone, J., Spear, F.S., Franz, G. & Morteani, G. (1984): High-pressure metamorphism in the SW Tauern Window, Austria: P-T paths from hornblende-kyanite-staurolite schists. *Journal of Petrology* 25, 501-531.
- Sherlock, S. & Kelley, S. (2002): Excess argon evolution in HP-LT rocks: a UVLAMP study of phengite and K-free minerals, NW Turkey. *Chemical Geology* 182, 619-636.
- Spear, F.S. (1993): Metamorphic phase equilibria and pressure-temperature-time paths. Mineralogical Society of America, Washington, D. C.
- Spear, F.S. & Selverstone, J. (1983): Quantitative P-T paths from zoned minerals: Theory and tectonic applications. *Contributions to Mineralogy and Petrology* 83, 348-357.
- Spear, F.S. & Cheney, J. (1989): A petrogenetic grid for pelitic schists in the system SiO₂-Al₂O₃-FeO-MgO-K₂O-H₂O. *Contributions to Mineralogy and Petrology* 101, 149-164.
- Spear, F.S. & Markussen, J.C. (1997): Mineral zoning, P-T-X-M phase relations, and metamorphic evolution of some Adirondack granulites, New York. *Journal of Petrology* 38, 757-783.
- Spear, F.S., Kohn, M.J., Florence, F.P. & Menard, T. (1991): A model for garnet and plagioclase growth in pelitic schists: implications for thermobarometry and P-T path determinations. *Journal of Metamorphic Geology* 8, 683-696.
- Spicher, A. (1980): Tektonische Karte der Schweiz, 1:500'000. Schweizerische Geologische Kommission, Bern.
- Stampfli, G.M. (1993): Le Briançonnais: terrain exotique dans les Alpes? *Eclogae geologicae Helveticae* 86, 1-45.
- Stampfli, G.M., Mosar, J., Marquer, D., Marchant, R., Baudin, T. & Borel, G. (1998): Subduction and obduction processes in the Swiss Alps. In: Vauchez, A. & Meissner, R. (Eds): Continents and their mantle root. *Tectonophysics* 296, 159-204.
- Staub, R. (1926): Geologische Karte des Avers, 1:50'000. *Beiträge zur geologischen Karte der Schweiz, Geologische Spezialkarte Nr. 97*.

- Steck, A. (1984): Structures de deformations tertiaires dans les Alpes centrales (transversale Aar-Simplon-Ossola). *Eclogae geologicae Helvetiae* 77, 55-100.
- Steck, A. (1990): Une carte des zones de cisaillement ductile des Alpes Centrales. *Eclogae geologicae Helvetiae* 83, 603-627.
- Steck, A. & Hunziker, J.C. (1994): The Tertiary structural and thermal evolution of the Central Alps – Compressional and extensional structures in an orogenic belt. *Tectonophysics* 238, 229-254.
- Steiger, R.H. (1962): Petrographie und Geologie des südlichen Gotthardmassivs zwischen St. Gotthard- und Lukmanierpass. *Schweizerische Mineralogische und Petrographische Mitteilungen* 64, 381-577.
- Steinmann, M. (1994a): Die nordpenninischen Bündnerschiefer der Zentralalpen Graubündens: Tektonik, Stratigraphie und Beckenentwicklung. Unpublished PhD Thesis, ETH Zürich, 220 pp.
- Steinmann, M. (1994b): Ein Beckenmodell für das Nordpenninikum der Ostschweiz. *Jahrbuch der Geologischen Bundesanstalt* 137, 675-721.
- Steinmann, M. & Stille, P. (1999): Geochemical evidence for the nature of the crust beneath the eastern North Penninic basin of the Mesozoic Tethys ocean. *Geologische Rundschau* 87, 633-643.
- Streckeisen, A., Wenk, E. & Frey, M. (1974): Steep isogradic surface in Simplon area. *Contributions to Mineralogy and Petrology* 47, 81-95.
- Strohbach, H.E. (1965): Der mittlere Abschnitt der Tambodecke samt seiner mesozoischen Unterlage und Bedeutung. *Mitteilungen aus dem Geologischen Institut der Eidgenössischen Technischen Hochschule und der Universität Zürich* 38, 171 pp.
- Suchy, V., Frey, M. & Wolf, M. (1997): Vitrinite reflectance and shear-induced graphitization in orogenic belts: A case study from the Kandersteg area, Helvetic Alps, Switzerland. *International Journal of Coal Geology* 34, 1-20.
- Sudo, M., Uto, K., Anno, K., Ishizuka, O. & Uchiumi, S. (1998): SORI93 biotite: A new mineral standard for K-Ar dating. *Geochemical Journal* 32, 49-58.
- Tagami, T. & Shimada, C. (1996): Natural long-term annealing of the fission-track system around a granitic pluton. *Journal of Geophysical Research* 101, 8245-8255.
- Teichmüller, M. (1987): Organic material and very low-grade metamorphism. In M. Frey (Ed): *Low temperature metamorphism*. Blacky, Glasgow and London. 114-161.
- Teutsch, R. (1982): Alpine Metamorphose der Misoxer-Zone (Bündnerschiefer, Metabasite und granitische Gneise). Unpub. PhD thesis, Universität Bern. 172 pp.
- Thakur, V.C. (1971): The structural and metamorphic history of the Mesozoic and pre-Mesozoic basement rocks of the Molare region, Ticino, Switzerland. Unpublished PhD Thesis, Imperial college of London, 229 pp.
- Thakur, V.C. (1973): Events in the Alpine deformation and metamorphism in the northern Pennine zone and southern Gotthard massif regions, Switzerland. *Geologische Rundschau* 62, 549-563.
- Theye, T., Seidel, E. & Vidal, O. (1992): Carpholite, sudoite and chloritoid in low-grade high-pressure metapelites from Crete and the Peloponnese, Greece. *European Journal of Mineralogy* 4, 487-507.
- Theye, T., Reinhardt, J., Goffé, B., Jolivet, L. & Brunet, C. (1997): Ferro- and magnesio-carpholite from the Monte Argentario (Italy): First evidence for high-pressure metamorphism of the metasedimentary Verrucano sequence, and significance for P-T path reconstruction. *European Journal of Mineralogy* 9, 859-873.
- Thoenen, A. (1989): A comparative study of garnet-biotite geothermometers. Unpub. PhD thesis, Universität Basel. 118 pp.
- Thompson, P.H. (1976): Isograd patterns and pressure-temperature distributions during regional metamorphism. *Contributions to Mineralogy and Petrology* 57, 277-295.
- Thöni, M. (2006): Dating eclogite-facies metamorphism in the Eastern Alps - approaches, results, interpretations: a review. *Mineralogy and Petrology* 88, 123-148.
- Thüring, M. (1990): Geologie um den Hennensädel im hinteren Valsertal (GR). Unpub. Diploma thesis, Universität Basel. 127 pp.

- Tinkham, D.K. & Ghent, E.D. (2005): Estimating P-T conditions of garnet growth with isochemical phase-diagram sections and the problem of effective bulk-composition. *Canadian Mineralogist* 43, 35-50.
- Todd, C.S. & Engi, M. (1997): Metamorphic field gradients in the Central Alps. *Journal of Metamorphic Geology* 15, 513-530.
- Tribuzio, R. & Giacomini, F. (2002): Blueschist facies metamorphism of peralkaline rhyolites from the Tenda crystalline massif (northern Corsica): evidence for involvement in the Alpine subduction event? *Journal of Metamorphic Geology* 20, 513-526.
- Tricart, P. (1984): From passive margin to continental collision: a tectonic scenario for the Western Alps. *American Journal of Science* 284, 97-120.
- Trommsdorff, V. (1966): Progressive Metamorphose kieseliger Karbonatgesteine in den Zentralalpen zwischen Bernina und Simplon. *Schweizerische Mineralogische und Petrographische Mitteilungen* 46, 431-460.
- Trommsdorff, V. (1990): Metamorphism and tectonics in the Central Alps: The Alpine lithospheric mélange of Cima Lunga and Adula. *Memorie della Societa Geologica Italiana* 45, 39-49.
- Trotet, F., Goffé, B., Vidal, O. & Jolivet, L. (2006): Evidence of retrograde Mg-carpholite in the Phyllite-Quartzite nappe of Peloponnese from thermobarometric modelisation - geodynamic implications. *Geodinamica Acta* 19, 323-343.
- Trümpy, R. (1960): Paleotectonic evolution of the Central and Western Alps. *Geological Society of America Bulletin* 71, 843-908.
- Trümpy, R. (1980): *Geology of Switzerland – a guide-book. Part A: An outline of the Geology of Switzerland.* Wepf, Basel, 104 pp.
- Tuinstra, F. & Koenig, J.L. (1970): Raman spectrum of graphite. *Journal of Chemical Physics* 53, 1126-1130.
- Uhr, A. (Unpublished): *Geologische Untersuchungen im Gebiet des Piz Terri (Kt. Tessin und Graubünden).* Textmanuskript, hinterlegt beim BWG, Bern-Ittigen.
- Uto, K., Ishizuka, O., Matsumoto, A., Kamioka, H. & Togashi, S. (1997): Laser-heating $^{40}\text{Ar}/^{39}\text{Ar}$ dating system of the Geological Survey of Japan: System outline and preliminary results. *Bulletin of the Geological Survey of Japan* 48, 23-46.
- Van der Plaas, L., Hügi, T., Mladeck, M.H. & Niggli, E. (1958): Chloritoid vom Hennensädel südlich Vals (nördliche Aduladecke). *Schweizerische Mineralogische und Petrographische Mitteilungen* 38, 237-246.
- Venturini, G. (1995): *Geology, Geochemistry and Geochronology of the inner central Sesia Zone (Western Alps).* Unpub. PhD thesis Université Lausanne.
- Verdoya, M., Chiozzi, P. & Pasquale, V. (2001): Heat-producing radionuclides in metamorphic rocks of the Briançonnais-Piedmont Zone. *Eclogae geologicae Helvetiae* 94, 213-219.
- Vernon, A.J., van der Beek, P.A., Sinclair, H.D. & Rahn, M.K. (2008): Increase in late Neogene denudation of the European Alps confirmed by analysis of a fission-track thermochronology database. *Earth and Planetary Science Letters* 270, 316-329.
- Vidal, O. & Theye, T. (1996): Comment on "Petrology of Fe-Mg-carpholite-bearing metasediments from northeast Oman". *Journal of Metamorphic Geology* 14, 381-386.
- Vidal, O. & Parra, T. (2002): Exhumation paths of high-pressure metapelites obtained from local equilibria for chlorite-phengite assemblages. *Geological Journal* 35, 139-161.
- Vidal, O., Goffé, B. & Theye, T. (1992): Experimental study of the stability of sudoite and magnesio-carpholite and calculation of a new petrogenetic grid for the system $\text{FeO-MgO-Al}_2\text{O}_3\text{-SiO}_2\text{-H}_2\text{O}$. *Journal of Metamorphic Geology* 10, 603-614.
- Vidal, O., Theye, T. & Chopin, C. (1994): Experimental study of chloritoid stability at high pressure and various $f\text{O}_2$ conditions. *Contributions to Mineralogy and Petrology* 118, 256-270.
- Vidal, O., Parra, T. & Trotet, F. (2001): A thermodynamic model for Fe-Mg aluminous chlorite using data from phase equilibrium experiments and natural pelitic assemblages in the 100-600°C, 1-25 kbar range. *American Journal of Science* 301, 557-592.
- Villa, I.M. (1998): Isotopic closure. *Terra Nova* 10, 42-47.

- Villa, I.M. (2006): From nanometer to megameter: Isotopes, atomic scale processes, and continent-scale tectonic models. *Lithos* 87, 155-173.
- Voll, G. (1976): Structural Studies of the Valser Rhine Valley and the Lukmanier Region and their Importance for the nappe Structure of the Central Swiss Alps. *Schweizerische Mineralogische und Petrographische Mitteilungen* 56, 619-626.
- von Blanckenburg, F. (1992): Combined high-precision chronometry and geochemical tracing using accessory minerals: applied to the Central-Alpine Bergell intrusion (central Europe). *Chemical Geology* 100, 19-40.
- von Blanckenburg, F. & Davies, J.H. (1995): Slab breakoff: A model for syncollisional magmatism and tectonics in the Alps. *Tectonics* 14, 120-131.
- Wada, H., Tomita, T., Matsuura, K., Iuchi, K., Ito, M. & Morikiyo, T. (1994): Graphitization of carbonaceous matter during metamorphism with references to carbonate and pelitic rocks of contact and regional metamorphisms, Japan. *Contributions to Mineralogy and Petrology* 118, 217-228.
- Waldhauser, F., Kissling, E., Ansorge, J. & Mueller, S. (1998): Three-dimensional interface modelling with two-dimensional seismic data: the Alpine crust-mantle boundary. *Geophysical Journal International* 135, 264-278.
- Wang, A., Dhamelincourt, P., Dubessy, J., Guerard, D., Landais, P. & Lelaurain, M. (1989): Characterization of graphite alteration in an uranium deposit by micro-Raman spectroscopy, X-RAY diffraction, Transmission Electron Microscopy and Scanning Electron Microscopy. *Carbon* 27, 209-218.
- Wang, P. & Spear, F.S. (1991): A field and theoretical analysis of garnet + chlorite + chloritoid + biotite assemblages from the tri-state (MA, CT, NY) area, USA. *Contributions to Mineralogy and Petrology* 106, 217-235.
- Weh, M. & Froitzheim, N. (2001): Penninic cover nappes in the Prättigau half-window (Eastern Switzerland): Structure and tectonic evolution. *Eclogae geologicae Helveticae* 94, 237-252.
- Wei, C.J. & Holland, T.J.B. (2003): Phase relations in high-pressure metapelites in the system KFMASH ($K_2O-FeO-MgO-Al_2O_3-SiO_2-H_2O$) with application to natural rocks. *Contributions to Mineralogy and Petrology* 301, 301-315.
- Wei, C.J. & Powell, R. (2004): Calculated phase relations in high-pressure metapelites in the system NKFASH ($Na_2O-K_2O-FeO-MgO-Al_2O_3-SiO_2-H_2O$). *Journal of Petrology* 45, 183-202.
- Wei, C.J., Powell, R. & Clarke, G.L. (2004): Calculated phase equilibria for low- and medium-pressure metapelites in the KFMASH and KMnFMASH systems. *Journal of Metamorphic Geology* 22, 495-508.
- Wenk, E. (1962): Plagioklas als Indexmineral in den Zentralalpen. *Schweizerische Mineralogische und Petrographische Mitteilungen* 42, 139-152.
- Wenk, E. (1970): Zur Regionalmetamorphose und Ultrametamorphose im Lepontin. *Fortschritte der Mineralogie* 47, 34-51.
- Wheeler, J. (1991): Structural evolution of a subducted continental sliver - the northern Dora Maira massif, Italian Alps. *Journal of the Geological Society* 148, 1101-1113.
- Wiederkehr, M. (2004): Strukturelle und metamorphe Entwicklung der Metasedimente am Kontakt Briançonnais - Piemont-Liguria, Val Madris, Avers/GR. Unpublished Diploma Thesis, Universität Basel. 145 pp.
- Wiederkehr, M., Bousquet, R., Ziemann, M. A., Schmid, S. M. & Berger, A., 2007. Thermal structure of the Valaisan and Ultra-Helvetian sedimentary units of the northern Lepontine dome – consequences regarding the tectono-metamorphic evolution. *Geophysical Research Abstracts* 9, EGU2007-A-05981.
- Wiederkehr, M., Bousquet, R., Schmid, S.M. & Berger, A. (2008): From subduction to collision: Thermal overprint of HP/LT meta-sediments in the north-eastern Lepontine Dome (Swiss Alps) and consequences regarding the tectono-metamorphic evolution of the Alpine orogenic wedge. In: Froitzheim, N. & Schmid, S.M. (Eds): *Orogenic processes in the Alpine collision zone*. *Swiss Journal of Geosciences* 101(Suppl), S127-S155.
- Wiederkehr, M., Bousquet, R., Sudo, M., Berger, A. & Schmid, S.M. (*submitted, a*): Tracing the geodynamic evolution of polymetamorphic metasediments by $^{40}Ar/^{39}Ar$ investigations on white mica and biotite (NE Lepontine, Swiss Central Alps). *submitted to Tectonics*.

- Wiederkehr, M., Bousquet, R., Ziemann, M.A., Berger, A. & Schmid, S.M. (*submitted, b*): Raman spectroscopy of carbonaceous material in metasediments at the margin of the Lepontine dome (Swiss Central Alps): 3-D assessment of peak-metamorphic conditions. *submitted to Contributions to Mineralogy and Petrology*.
- Wiederkehr, M., Bousquet, R., Schmid, S.M. & Berger, A. (*in preparation*): Interference between an earlier HP/LT and a later Barrow-type event: Metamorphic evolution and geodynamic implications. *in preparation*.
- Wijbrans, J.R. & McDougall, I. (1986): $^{40}\text{Ar}/^{39}\text{Ar}$ dating of white micas from an Alpine high-pressure metamorphic belt on Naxos (Greece) - the resetting of the argon isotopic system. *Contributions to Mineralogy and Petrology* 93, 187-194.
- Wopenka, B. & Pasteris, J.D. (1993): Structural characterization of kerogens to granulite-facies graphite - Applicability of Raman microprobe spectroscopy. *American Mineralogist* 78, 533-557.
- Wyss, R. & Isler, A. (2007): Blatt 1234 Vals - Geologischer Atlas der Schweiz 1:25'000, Erläuterungen 121, 78 pp.
- Yardley, B.W.D. (1989): An introduction to metamorphic petrology. Longman, New York.
- Yui, T.F., Huang, E. & Xu, J. (1996): Raman spectrum of carbonaceous material: A possible metamorphic grade indicator for low-grade metamorphic rocks. *Journal of Metamorphic Geology* 14, 115-124.
- Zeh, A. (2001): Inference of a detailed P-T path from P-T pseudosections using metapelitic rocks of variable composition from a single outcrop, Shackleton Range, Antarctica. *Journal of Metamorphic Geology* 19, 329-350.
- Ziegler, W. (1956): Geologische Studien in den Flyschgebieten des Oberhalbsteins (Graubünden). *Eclogae geologicae Helveticae* 49, 1-78.
- Zimmermann, R., Hammerschmidt, K. & Franz, G. (1994): Eocene high pressure metamorphism in the Penninic units of the Tauern Window (Eastern Alps): evidence from ^{40}Ar - ^{39}Ar dating and petrological investigations. *Contributions to Mineralogy and Petrology* 117, 175-186.
- Zulbati, F. (2008): Structural and metamorphic evolution of the phengite-bearing schists of the northern Adula Nappe (Central Alps, Switzerland). *Geological Journal* 43, 33-57.
- Zwart, H.J. (1973): Metamorphic map of Europe, scale 1:2'500'000. Subcommittee of Cartography of the Metamorphic Belts of the World, Leiden / UNESCO, Paris.
- Zwart, H.J., Sobolev, V.S. & Niggli, E. (1978): Metamorphic map of Europe, scale 1:2'500'000. Explanatory text. Subcommittee of Cartography of the Metamorphic Belts of the World, Leiden / UNESCO, Paris.

Curriculum Vitae

Michael Wiederkehr

Personal Details

Date of birth: 31.10.1977
Place of birth: Dagmersellen/LU
Marital status: single
Citizenship: Swiss

Professional Address:

Departement für Geowissenschaften
Mineralogisch-Petrographisches Institut
Universität Basel
Bernoullistrasse 30
4056 Basel
Tel: 061 267 36 28
Email: m.wiederkehr@unibas.ch

Home Address:

Jungstrasse 23
4056 Basel
Tel: 061 321 41 78

Education

- Nov. 2004 – 1. April 2009: PhD in Earth Sciences (joint study/co-tutelle between the Universities of Basel/Switzerland and Potsdam/Germany)
“From subduction to collision - a combined metamorphic, structural and geochronological study of polymetamorphic metasediments at the NE edge of the Lepontine dome (Swiss Central Alps)”
Supervisors: Prof. S.M. Schmid, Prof. R. Bousquet & PD A. Berger
- Oct. 2004: Diploma in Earth Sciences
Diploma thesis: **“Strukturelle und metamorphe Entwicklung am Kontakt Briançonnais and Piemont-Liguria, Val Madris, Avers/GR”**
Diploma mapping: **“Geologische Karte des Val Madris, Kontakt zwischen der Suretta-Decke und den Avers-Bündnerschiefer”**
Supervisors: Prof. R. Bousquet & PD H. Stünitz
- Oct. 1997 – Oct. 2004: Studies in Earth Sciences, Geophysics, Geography, Meteorology, Soil Sciences and Astronomy at the Universities of Basel (Switzerland), Freiburg i.Brsg. (Germany) und ETH Zürich (Switzerland)
- Aug. 1992 – Feb. 1997: Gymnasium Solothurn and Matura Typus E (Emphasizes Economy)

